NASA-

THEORETICAL AND EXPERIMENTAL STUDIES OF HIGH-TEMPERATURE GAS TRANSPORT PROPERTIES

Prepared by

RESEARCH AND ADVANCED DEVELOPMENT DIVISION
AVCO CORPORATION
Wilmington, Massachusetts

FINAL REPORT
(11 May 1964 through 10 May 1965)

GPO PRICE $ _____

CFSTI PRICE(S) $ _____

Hard copy (HC) 5.00

Microfiche (MF) 1.00

ff 653 July 65

Technical Report
RAD-TR-65-7
Contract NASw-916

10 May 1965

Prepared for

NATIONAL AERONAUTICS AND SPACE ADMINISTRATION
RESEARCH DIVISION
OFFICE OF ADVANCED RESEARCH AND TECHNOLOGY
Washington, D. C.

FACILITY FORM 602

N67 13538 (ACCESSION NUMBER)

(THRU)

172 (PAGES)

1 (CODE)

CR-80649 (NASA CR OR TMX OR AD NUMBER)

25 (CATEGORY)

NASA-

This document consists of 178 pages,
151 copies, Series A

THEORETICAL AND EXPERIMENTAL STUDIES OF HIGH-TEMPERATURE GAS TRANSPORT PROPERTIES

Prepared by

RESEARCH AND ADVANCED DEVELOPMENT DIVISION
AVCO CORPORATION
Wilmington, Massachusetts

FINAL REPORT
(11 May 1964 through 10 May 1965)

Technical Report
RAD-TR-65-7
Contract NASw-916

10 May 1965

Prepared for

NATIONAL AERONAUTICS AND SPACE ADMINISTRATION
RESEARCH DIVISION
OFFICE OF ADVANCED RESEARCH AND TECHNOLOGY
Washington, D. C.

CONTENTS

I. Introduction 1

II. Experimental Determination of Electrical and Thermal Conductivities in a Laminar Electric Arc Column 4

- A. Background 4
- B. Experimental Apparatus 6
- C. Spectroscopic Techniques 10
- D. Experimental Observations 17
- E. Analysis of Experimental Observations 29
- F. Conclusions and Recommendations 52

III. Heitler-London Interaction Potentials and Resonant Charge Exchange Cross Sections for $N-N^+$ and $O-O^+$ Collisions 55

- A. Introduction 55
- B. Unperturbed Wavefunctions for the Atom-Ion System 58
- C. General Equations for the Interaction Energies 67
- D. Spin Dependence of the Potentials for $N-N^+$ and $O-O^+$ 71
- E. Reduction of the Matrix Elements for $N-N^+$ and $O-O^+$ to Standard One- and Two-Electron Integrals 75
- F. Evaluation of the Basic Molecular Integrals 89
- G. The $N-N^+$ and $O-O^+$ Interaction Potentials 118
- H. Charge Exchange and Diffusion Cross Sections for N^+ in N and O^+ in O 125

IV. References 132

Appendixes

- A. Explicit Solution of the Elenbaas-Heller Equations for the Transport Properties 139
- B. Analytic Curvefits to Arc Temperature Distributions 146
- C. The Two-Run Method of Analyzing Wall-Stabilized Arc Data to Obtain Transport Properties 150
- D. The Effect of Paired Electrons on the Spin Dependence of the Potentials 156
- E. Explicit Formulas for the Two-Center Overlap, Kinetic-Energy, and Hybrid Integrals for $N-N^+$ and $O-O^+$ 161
- F. A Relation among the Functions $C_{\alpha\beta}^{\gamma\delta\epsilon}$ 167

ILLUSTRATIONS

Figure 1 Diagram of the Constricted Arc Unit 7

2 Photograph of the Argon Arc at 60 Amperes, Atmospheric Pressure 9

3 Diagram of Optical System 11

4 Absolute Intensity of the Argon Atom Line ArI 4158.59 as a Function of Temperature at a Pressure of 1 Atmosphere . 14

5 Absolute Line Intensity versus Temperature for Three Atomic Nitrogen Lines 15

6 Effect of Errors in Spectrographic Measurements on Temperature Based on the Argon Atom Line 16

7 Absolute Intensity of a 1-A Argon Continuum Band Centered at 4285A as a Function of Temperature at Atmospheric Pressure 18

8 Absolute Intensity of a 1-A Nitrogen Continuum Band Centered at 4955A as a Function of Temperature at Atmospheric Pressure 19

9 Effect of Errors in Spectrographic Measurements upon Temperature Measurement in Argon Using a 1-A Continuum Band Centered at 4285A 20

10 Typical Integrated Intensity Distribution Measured in the Constricted Arc 22

11 Radial Intensity Distribution Obtained from Integrated Intensity Distribution 23

12 Radial Temperature Distributions for 30-, 50, and 80-Ampere Argon Arcs 25

13 Radial Temperature Distributions for 40-, 60-, and 100-Ampere Argon Arcs 26

14 Radial Temperature Distributions for 40-, 60-, and 100-Ampere Nitrogen Arcs 27

ILLUSTRATIONS (Cont'd)

Figure 15 Radial Temperature Distributions for 50-, 80-, and 150-Ampere Nitrogen Arcs 28

16 Circuit for Measuring Voltage Gradients in the Nitrogen Arc Column 30

17 Total Infrared, Visible, and Near-Ultraviolet Radiation of Argon at Atmospheric Pressure 34

18 Theoretical Electrical Conductivity of Argon 35

19 Thermal Conductivity of Argon from the Calculated-Current Energy Balance Method 37

20 Comparison of Present Results with Those of a Previous Investigation of the Thermal Conductivity of Argon 38

21 Thermal Conductivity of Argon from the Measured-Current Energy Balance Method..... 39

22 Thermal Conductivity of Argon from the Two-Run Method.. 41

23 Electrical Conductivity of Argon from the Two-Run Method. 43

24 Theoretical Electrical Conductivity of Nitrogen 44

25 The Thermal Conductivity of Nitrogen as Determined by Maecker under the Assumption that Radiative Losses are Negligible 45

26 Thermal Conductivity of Nitrogen from the Calculated-Current Energy Balance Method using the Measured Radiative Loss 47

27 Measured and Measured-plus-Calculated Values of the Total Radiation of Nitrogen at Atmospheric Pressure 48

28 Thermal Conductivity of Nitrogen Determined from the Data of Maecker with the Inclusion of Calculated and Measured Radiative Losses 50

29 Thermal Conductivity of Nitrogen from the Calculated-Current Method with the Inclusion of Calculated and Measured Radiative Losses 51

ILLUSTRATIONS (Cont'd)

Figure 30 Percentage of Radiated Power, Based upon the Sum of Calculated and Measured Radiation, as a Function of the Axis Temperature of the Nitrogen Arc 53

31 Two-center Overlap and Kinetic-Energy Integrals for $N-N^+$ 106

32 Two-Center Overlap and Kinetic-Energy Integrals for $O-O^+$.107

33 Hybrid Integrals for $N-N^+$ 109

34 Hybrid Integrals for $O-O^+$ 110

35 Interaction Potentials between Ground-State N and N^+ 122

36 Interaction Potentials between Ground-State O and O^+ 123

37 Theoretical Relationship between Charge-Exchange Cross Section and Collision Velocity 126

38 Resonant Charge-Exchange Cross Section for $N-N^+$ Collisions.....128

39 Resonant Charge-Exchange Cross Section for $O-O^+$ Collisions 129

40 Diffusion Collision Integrals for N^+ in N and O^+ in O 131

C-1 Thermal Conductivity Calculated by the Two-Run Method from Numerical Solutions of the Elenbaas-Heller Equation ..153

C-2 Electrical Conductivity Calculated by the Two-Run Method from Numerical Solutions of the Elenbaas-Heller Equation ..154

TABLES

Table I — Parmeters in the Analytic Hartree-Fock Wavefunctions for the Ground-States of N, N^+, O, and O^+ (from reference 48) .. 59

II — Hartree-Fock Wavefunctions for the Ground States of Atoms and Ions Having an Unfilled p-Shell 62

III — One-Electron Wavefunctions for the N-N^+ and O-O^+ Interactions 76

IV — Expansion Coefficients $c_{a_i}^{(t)}$ for the Transformed Positive Ion Wavefunctions 92

V — Multipole Expansion Coefficients for the Coulomb Integral .. 98

VI — Multipole Moments for the N-N^+ and O-O^+ Interactions 101

VII — Expansion Coefficients c_{s_i} for the Wavefunction ψ_s 101

B-1 — Correspondence between Form of Curvefit and Type of Plot Yielding a Linear Correlation of the Data 148

B-2 — Analytic Curvefits to the Experimental Temperature Distributions in Argon 149

C-1 — Summary of Cases for Test of the Two-Run Method on Numerical Solutions of the Elenbaas-Heller Equation 155

PREFACE

This document is the final report on Contract NASw-916 between the National Aeronautics and Space Administration and the Research and Advanced Development Division of Avco Corporation. The objectives of the contract were

1. to calculate resonant atom-ion charge-exchange cross sections as functions of the relative collision velocity for nitrogen and oxygen; and

2. to determine the thermal and electrical conductivity coefficients as functions of temperature for argon and nitrogen, from spectroscopic and electrical measurements on a laminar electric-arc column.

The program was carried out under the sponsorship of the Research Division, Office of Advanced Research and Technology, National Aeronautics and Space Administration, under the technical supervision of Alfred Gessow, Chief of the Physics of Fluids Program. The Avco/RAD project director was Dr. Stewart Bennett. Dr. W. L. Bade and Mr. James Morris were project engineers. Dr. C. F. Knopp carried out the experimental investigations. Dr. Jerrold M. Yos performed the theoretical calculations of charge exchange and derived the explicit solution of the Elenbaas-Heller equations for the thermal and electrical conductivity.

The key suggestion that far-ultraviolet radiation might play an important role in constricted arc columns was made independently by A. Gessow of NASA and Prof. H. A. Bethe of Cornell University, an Avco consultant.

I. INTRODUCTION

This report presents the results obtained during the first year of a NASA-supported program of research on high-temperature gas transport properties. The program emphasizes gas species which are present under thermally dissociated and/or ionized conditions in the atmospheres of Earth, Venus, and Mars. During this first year, the program has included two lines of effort:

1. Establishment of a wall-stabilized arc as a standard tool for experimental determination of thermal conductivity and certain other transport properties, and investigation of high-temperautre argon and nitrogen by this method.

2. Development of a technique for calculating interaction potentials between atoms and/or atomic ions from their analytic Hartree-Fock wavefunctions, and application of this technique to determination of the charge-exchange cross sections for the systems $N-N^+$ and $O-O^+$.

The use of cylindrical wall-stabilized arcs for determining high-temperature transport properties was originated by Maecker[1], who used this technique to obtain thermal conductivity values for nitrogen at atmospheric pressure and temperatures from 5000 to 15,500°K. At the higher temperatures in this range, Maecker's experimental values are about ten times higher than those obtained from the best available theoretical calculations[2] of thermal conductivity for equilibrium nitrogen. Moreover, at these higher temperatures, the experimental conductivity is an apparent function of arc current. This finding indicates the presence of an energy transport mechanism which has not been allowed for properly in the analysis of the data. One of the objectives of the present program is to elucidate the reasons for these discrepancies and to obtain correct and reasonably accurate values for the high-temperature thermal conductivity of nitrogen.

In a more recent application of the wall-stabilized arc technique, Knopp[3] has measured the thermal conductivity of argon from 9000 to 12,000°K using an apparatus with a transparent quartz constrictor. Knopp's data agree reasonably well with theoretical calculations[4] for argon.

The present investigation has included studies of both argon and nitrogen. In the case of argon, a considerable experimental effort was required to reduce the "bulging" of the arc column into the gap between the constrictors. The experimental data for argon have been analyzed for thermal conductivity by three methods, all based upon the energy equation for an optically thin, cylindrically symmetric arc column (Elenbaas - Heller equation). The thermal conductivity values obtained for argon are within about 40 percent of the theoretical predictions, but discrepancies between the results of the different methods suggest the presence of some systematic errors in the data. A study of

literature data on the absorption coefficient of argon in the vacuum ultraviolet has now led to the conclusion that the argon arc column emits a significant amount of radiation in that wavelength region, and is relatively opaque to such radiation. The effects of emission and absorption of this radiation may account, in large part, for the apparent discrepancies among the experimental results and between them and the theoretical predictions.

In the case of nitrogen, the experimental results obtained in the present investigation are similar to those reported by Maecker. If they are interpreted using the Elenbaas - Heller equation, assuming that the only radiative contribution to the energy balance is that given by the observed radiation in the infrared, visible, and near ultraviolet, then the thermal conductivity values obtained are much higher than theoretical predictions, and show a significant dependence on arc current. However, available calculations of the absorption coefficient of high-temperature nitrogen in the far-ultraviolet indicate the emission of very large amounts of radiation in that region. Inclusion of this vacuum ultraviolet radiation in the assumed radiative loss largely eliminates the dependence of thermal conductivity on current, and brings the experimental values down into approximate agreement with theory.

Neither the argon nor the nitrogen arc column is optically thin in the important far-ultraviolet regions of wavelength. Thus, correct analysis of wall-stabilized arc data for thermal conductivity requires a study of solutions of the Elenbaas-Heller equation with nongrey radiative transfer terms. This presumably difficult problem has not yet been investigated. Consequently, the thermal conductivity values reported for argon and nitrogen are not considered to be definitive.

Details of the wall-stabilized arc investigations carried out under the present program are reported in section II.

Resonant charge-exchange processes, in which an electron is transferred from an atom to a postive ion of the same species (e.g., $N+N^{+} \longrightarrow N^{+}+N$), play an important role in determining the thermal conductivity of a gas at temperatures where it is partially ionized. One of the chief mechanisms for transporting energy through such a gas is ionization of neutral atoms at a higher temperature, diffusion of the resulting ions and electrons to regions of lower temperature, and recombination with thermal release of the energy of ionization. In calculations of transport properties, the term corresponding to this process is called the "reaction conductivity" for ionization. Charge exchange between the diffusing ions and neutral atoms which they encounter impedes the transport of energy by this mechanism. In atmospheric-pressure nitrogen at temperatures of about 12,000 to 16,000°K, the ionization reaction is a major component of the thermal conductivity, and its magnitude is strongly dependent on the charge-exchange cross section.

The resonant charge-exhange cross section for oxygen has been measured by Stebbings, Smith, and Ehrhardt[5]. No measurements are available at present for nitrogen. The most recent calculation of these cross sections for nitrogen and oxygen is that of Knof, Mason, and Vanderslice[6]. Their results are based upon use of a semiempirical valence bond method to generate the interaction potential curves for nine unobserved states of N_2^+ or O_2^+ from extrapolations of spectroscopically determined curves for three states. In the case of oxygen, their results agree well with the experimental values of Stebbings, et al[5].

In the present investigation, resonant charge-exchange cross sections for nitrogen and oxygen are obtained from quantum mechanical calculations which do not make use of spectroscopic data for N_2^+ and O_2^+. The results for oxygen are in excellent agreement with the experimental data of Stebbings, et al. These calculations are performed by a method which is completely independent of, and probably more accurate than, that employed by Knof, et al. The method developed under the present program is also applicable to cases in which insufficient spectroscopic information is available to permit carrying out a semiempirical valence bond calculation.

Details of this theoretical study of interaction potentials and charge-exchange cross sections are reported in section III.

II. EXPERIMENTAL DETERMINATION OF ELECTRICAL AND THERMAL CONDUCTIVITIES IN A LAMINAR ELECTRIC ARC COLUMN

A. BACKGROUND

Most previous experimental work on the transport properties of hot gases has been performed in shock tubes. Although shock tubes provide a well-defined geometry, the short duration of the test time available in these devices imposes serious limitations upon the measurement of transport properties. For example, the measurement of thermal conductivity by shock tube techniques relies upon the accuracy and response capabilities of heat transfer gauges. A further source of error is inherent in the analytical prediction of the temperature and pressure of the test gas. The use of a wall-stabilized arc to generate a steady state, stable, high-temperature gas column obviates these restrictions. It has been demonstrated by numerous authors[7] that equilibrium can be achieved in arc columns over a wide range of operating conditions. For these reasons, the wall-stabilized arc appears particularly well-suited to the experimental determination of transport properties.

The basic idea of the experimental technique discussed in the present section is to heat a gas by operating an electric arc in it, to determine its temperature distribution spectroscopically, and to obtain its thermal conductivity by analyzing the energy production, loss, and transport processes occurring in it. The spectroscopic determination of the temperature distribution and the analysis of the data to yield transport properties are feasible only if the heated gas has such a high degree of symmetry that all relevant quantities are functions of only a single spatial coordinate. This condition may be achieved by confining an arc-generated plasma within a long, small-diameter,* electrically nonconducting tube with strongly cooled walls. The wall cooling produces a thermal boundary layer in the gas which confines the high-temperature region of the flow to the center of the tube and forces the temperature distribution to have cylindrical symmetry. This experimental arrangement is commonly referred to as a wall-stabilized or constricted arc.

In cylindrical coordinates, the ordinary energy equation of fluid dynamics,[8] with addition of Joule heating and radiative loss terms, is

$$\rho\left[\frac{\partial\epsilon}{\partial t} + V_r\frac{\partial\epsilon}{\partial r} + \frac{V_\theta}{r}\frac{\partial\epsilon}{\partial\theta} + V_z\frac{\partial\epsilon}{\partial z} + p\frac{\partial(1/\rho)}{\partial t} + pV_r\frac{\partial(1/\rho)}{\partial r} + \frac{V_\theta}{r}\frac{\partial(1/\rho)}{\partial\theta} + pV_z\frac{\partial(1/\rho)}{\partial z}\right]$$

$$= (\vec{j}\cdot\vec{E}) + \frac{1}{r}\frac{\partial}{\partial r}\left(rK\frac{\partial T}{\partial r}\right) + \frac{1}{r^2}\frac{\partial}{\partial\theta}\left(K\frac{\partial T}{\partial\theta}\right) + \frac{\partial}{\partial z}\left(K\frac{\partial T}{\partial z}\right) + \Phi - P_{rad} \qquad (1)$$

*The diameter is small compared with the length of the tube, but much larger than capillary size.

where

ρ	=	mass density
ϵ	=	internal energy per unit mass
V_i	=	i^{th} component of the velocity
p	=	pressure
$\vec{j}$	=	current density
$\vec{E}$	=	electric field vector
K	=	thermal conductivity
Φ	=	viscous dissipation term
P_{rad}	=	radiative loss term (optically thin approximation)

In the wall-stabilized arc used in this study and described in detail below, a small, continuous flow of gas is introduced into a small plenum chamber and bled from the chamber into the arc column proper. As a result, the flow has only an axial component of velocity in the region in which measurements are performed, and none of the important quantities depend upon θ. Thus,

$$\frac{\partial}{\partial t} = 0$$

$$\frac{\partial}{\partial \theta} = 0$$

$$V_\theta = 0 \qquad (2)$$

$$V_r = 0$$

Equation (1) may therefore be written as

$$\rho V_z \frac{\partial \epsilon}{\partial z} + \rho p V_z \frac{\partial (1/\rho)}{\partial z} = (\vec{j} \cdot \vec{E}) + \frac{1}{r} \frac{\partial}{\partial r}\left(r K \frac{\partial T}{\partial r}\right) + \frac{\partial}{\partial z}\left(K \frac{\partial T}{\partial z}\right) + \Phi - P_{rad} \qquad (3)$$

With the additional assumptions

$$(\vec{j} \cdot \vec{E}) = \sigma E^2 >> \Phi$$

$$p \simeq \text{constant} \qquad (4)$$

$$\partial T / \partial z \simeq 0,$$

equation (3) can be further simplified to the form

$$\sigma E^2 + \frac{1}{r}\frac{d}{dr}\left(r K \frac{dT}{dr}\right) - P_{rad} = 0. \tag{5}$$

This relation, frequently referred to as the Elenbaas-Heller equation, is used to describe the energy transport in the arc column.

The description of radiative effects by a simple volumetric loss term P_{rad}, as in equations (1), (3), and (5), implies the assumption that the arc column is optically thin to its own thermal radiation in all regions and at all important wavelengths. If this assumption is not made, then the radiative contributions to the energy equation must be treated by the methods of the theory of transfer, and equation (5) becomes an integro-differential equation.

If the Elenbaas-Heller equation (5) is valid, it can be used to obtain transport-property values from experimental data on a wall-stabilized arc. In equation (5), the voltage gradient E, the temperature distribution function $T(r)$, and the radiative power loss $P_{rad}(T)$ are all measurable quantities. If the electrical conductivity $\sigma(T)$ is a known function, then the thermal conductivity $K(T)$ can be calculated from (5) by a quadrature. Details of this procedure are presented below in section IIE. Of course, this approach based upon the assumption of known $\sigma(T)$ is somewhat objectionable, because σ is really another transport property. However, it is demonstrated in appendix A that, if the optically thin Elenbaas-Heller equation (5) is valid, both the thermal conductivity and the electrical conductivity are uniquely determined as functions of temperature by the experimental data for any pair of arc runs with different axis temperatures.

Section B describes the experimental apparatus. The principal experimental technique is the use of spectroscopic diagnostics to ascertain the radial temperature distribution in the arc column. Details of the spectroscopic methods employed and a critical evaluation of the applicability of these methods are given in section C. Section D presents observations on argon and nitrogen. Section E describes the methods used to analyze the data for transport properties, and presents the results obtained for these two gases. Finally, section F summarizes the chief findings of the program to date and presents conclusions.

B. EXPERIMENTAL APPARATUS

The wall-stabilized arc facility used in this program is shown schematically in figure 1. This arc is capable of sustaining an axis temperature of 14,000°K in nitrogen or oxygen with an arc diameter of 4.8 mm and a current of 150 amperes. The arc column is confined within a series of water-cooled, copper constrictors electrically insulated from one another by molded silicone rubber gaskets. The gaskets are pierced for observation windows so that the arc column may be observed between any two constrictors or between the electrodes and a constrictor. The width of each constrictor is 8 mm. The distance between adjacent constrictors

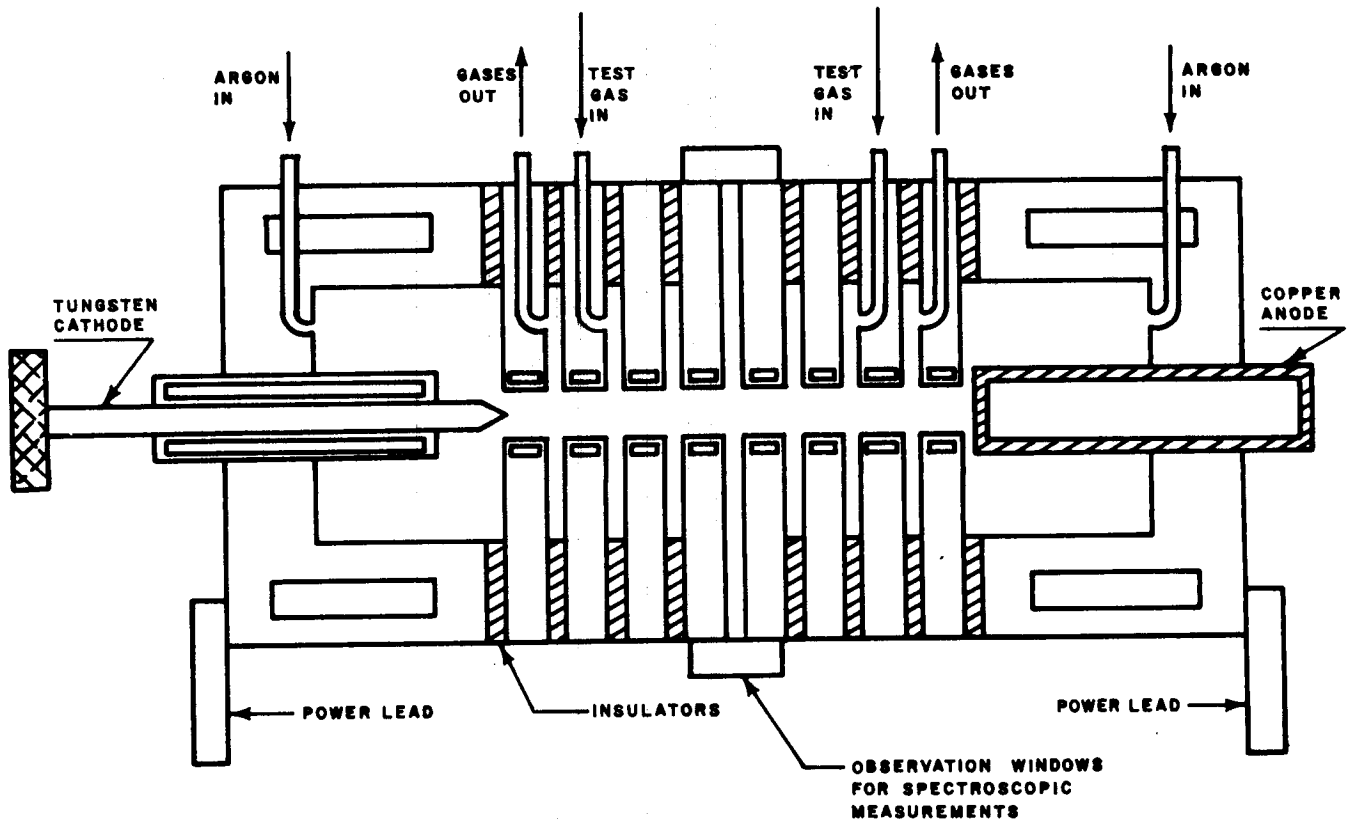

NOTE: SHADED AREAS INDICATE WATER COOLING PASSAGES

64-3213

Figure 1 DIAGRAM OF THE CONSTRICTED ARC UNIT

is 1.25 mm, except in the case of the two constrictors between which the spectroscopic measurements are normally made. These have a separation of 0.25 mm. The observation window for spectroscopic measurements is made of schlieren quality sapphire, while the other observation windows are fused silica.

The constrictors, electrode housings, and windows of the wall-stabilized arc are made gas-tight with the insulating gaskets. The various gas inlets and exits are metered with flow gauges and regulating valves which are used to control the pressure and flow rates within the arc column. This arrangement allows the option of choosing any flow rate, ranging from stagnation to full flow through the observation chamber. When experiments are conducted on gases other than those of the inert series, the electrodes are blanketed with argon. The flow rates of argon and the test gas are balanced so that no argon is observed spectroscopically in the test region, but the electrodes remain immersed in argon.

Power for the arc is supplied by 84 truck batteries arranged in 4 banks of 21 batteries. These banks may be used in series or parallel combinations to obtain open circuit voltages of 252, 504, or 1008 volts. The batteries are charged by a three-phase rectifier on the 220-volt ac service line.

Gross adjustments to the arc current are made with two variable, air-cooled ballast resistors, each capable of carrying 200 amperes. Fine adjustment and regulation of the arc current is accomplished by a water-cooled stainless steel tube with a sliding contact. Regulation is provided by a potentiometric reading of the difference in voltage across a precision shunt in the arc power lead and a pre-set reference voltage. The voltage difference is displayed upon a rotating beam galvanometer. As the beam swings to pre-set limits, photoconductive cells actuate the sliding contact on the stainless steel tubing. Using this system, it is possible to maintain constant arc current to within ±0.001 ampere. A photograph of the arc operating in argon at atmospheric pressure and a current of 60 amperes is shown in figure 2.

A 0.75-meter, f/10 grating monochrometer employing a Czerny-Turner mounting is used to obtain the spectroscopic measurements necessary for the determination of radial temperature distributions within the arc column. This instrument, which was constructed in our laboratory, has a reciprocal linear dispersion of 10.8 A/mm in the first order at 4000A. The radiation detector is an RCA type 1P21 or EMI type 6255B photomultiplier. The photomultiplier power supply has 0.01-percent regulation and ripple suppression. The photomultiplier signal is measured and amplified by a pico-ammeter having a linearity of 2 percent. The output signal of the amplifier is digitized and, along with the gain of the amplification system, punched onto computer cards in a semiautomatic manner.

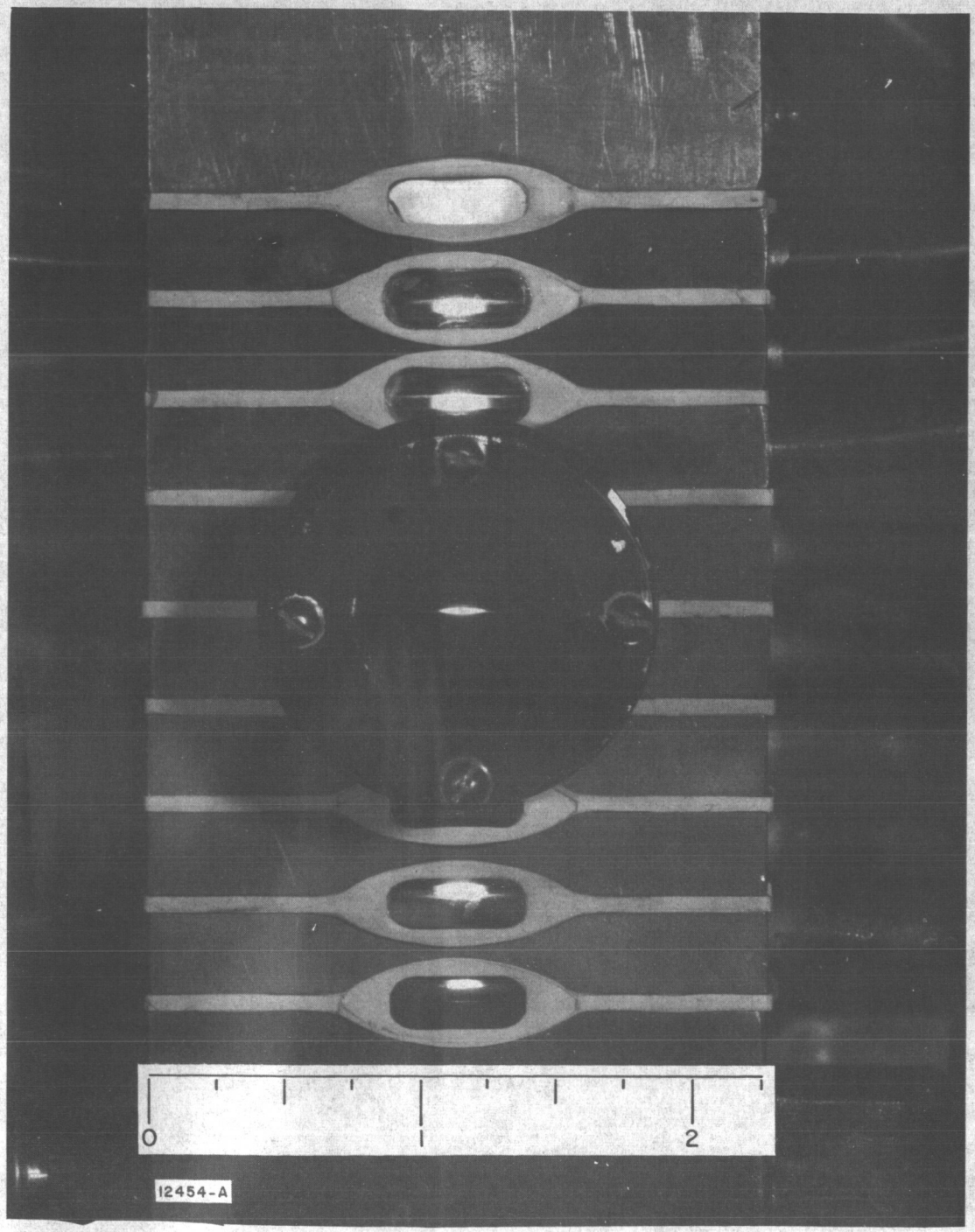

Figure 2 PHOTOGRAPH OF THE ARGON ARC AT 60 AMPERES, ATMOSPHERIC PRESSURE

Figure 3 depicts the optical system used to obtain the integrated intensity distribution* of a spectral line or continuum band. The image of the arc column is focused upon the entrance slit of the monochrometer by the imaging lens. This lens is apertured to alleviate distortion and to provide a large depth of field. The f-number of the optical system is approximately f/70, providing a depth of field sufficient to ensure that both the front and back of the arc column are in focus when the lens is focused on the axis of the arc column.

The arc column is imaged upon the entrance slit of the monochrometer in such a way that the axis of the arc is parallel to the entrance slit. Spatial resolution is accomplished by the use of a 25-micron entrance slit combined with a 0.65-mm slit placed in the same plane and perpendicular to the entrance slit. Based upon the effective slit widths and the magnification of the optical system, this arrangement provides an effective spatial resolution of approximately 0.2 mm along the axis of the column and approximately 0.05 mm perpendicular to the axis.

Calibration of the electronic and optical systems is provided by an NBS tungsten standard lamp located at the same position as that normally occupied by the arc facility.

C. SPECTROSCOPIC TECHNIQUES

The basic variable determined experimentally in this study is the temperature of the plasma column. At the temperatures and pressures of interest, probe or microwave techniques are of little value. Emission spectroscopy, however, is a powerful diagnostic tool for the conditions encountered in high pressure arc columns.

The basic fact underlying all spectroscopic measurements of temperature is that the measured quantity (radiation intensity) is determined by two variables of state of the plasma (temperature and number density of the radiating species):

$$I_i = I_i\,(n_i, T) \tag{6}$$

where I_i is the radiation intensity emanating from the number density n_i of particles of type i at a temperature T. Thus, to obtain T from a measurement of I_i, the dependence of n_i upon T must be known. For a gas in equilibrium at a given pressure, the species number densities are determined as functions of temperature by the laws of statistical thermodynamics.[9,10] In general, solution of this problem requires computer solution of a series of mass action (Saha) equations

* The basic quantity measured in these experiments is the sum of intensity contributions, in a certain small wavelength interval, from gas elements lying along a rectilinear optical path through the arc column. The optical path is at right angles to the arc axis, but in general does not pass through the axis. The sum of intensity contributions, considered as a function of the perpendicular distance from the arc axis to the optical path, is briefly termed the "integrated intensity."

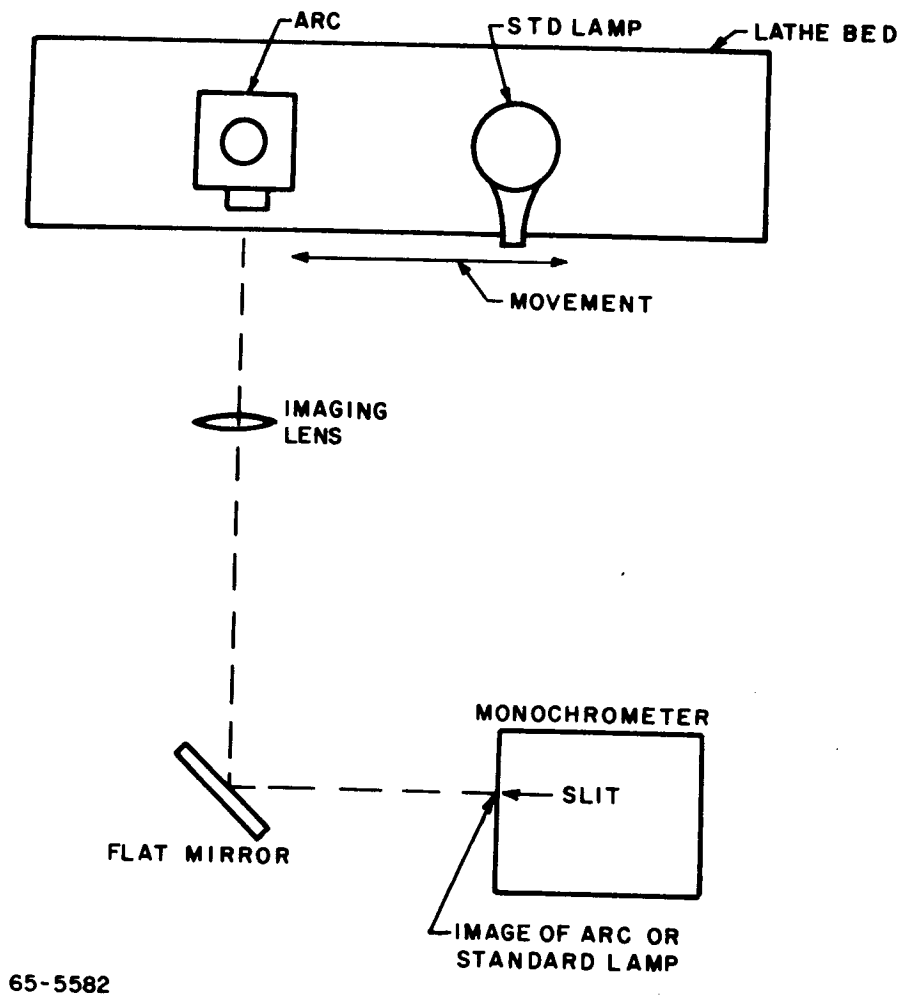

Figure 3 DIAGRAM OF OPTICAL SYSTEM

coupled with Dalton's law of partial pressures and the assumption of charge neutrality. When this thermodynamic relation between n_i and T is taken into account, equation (6) reduces to

$$I_i \approx I_i\ (T), \tag{7}$$

and a measurement of I_i then determines the value of the temperature T.

The radiation emanating from the plasma produced in a wall-stabilized arc consists of a discrete spectrum superposed upon a background of continuous radiation. Both line and continuum radiation may be used to determine the temperature of the gas.

The absolute radiant intensity of a spectral line which is emitted spontaneously in all directions by a unit volume of the plasma is proportional to the spontaneous transition probability A_n^m for a transition from the upper energy state m to the lower energy state n; to the number of atoms, n_m, in the upper state; and to the energy of the light quanta, $h\nu_{mn}$ (ν_{mn} = frequency of emitted light). It is customary to speak of radiant intensity per unit solid angle, so that the intensity per unit volume per steradian of a spectral line is given by

$$I_{mn} = \frac{1}{4\pi} A_n^m h \nu_{mn} n_m \tag{8}$$

In an equilibrium situation, the distribution of electrons in the various energy levels of the atom is given by the Boltzmann distribution, so that the absolute intensity of a spectral line emanating from a homogeneous unit volume is found to be

$$I_{mn} = \frac{1}{4\pi} \frac{A_n^m h \nu_{mn} n_a g_m}{Q_a} \exp\ (-E_m/kT) \tag{9}$$

where Q_a is the partition function of the atom, g_m is the degeneracy of the mth energy level, n_a is the total number of atoms per unit volume, and E_m is the energy of the mth level. Equation (9) may be applied when the radiating volume is optically thin and the number of exciting collisions is large compared with the number of emissions. These conditions are well satisfied in the visible region of the spectrum for the operating conditions and gases employed in the experiments reported here.

Equation (9) shows that in order to determine temperature from the intensity of a spectral line it is necessary to have prior knowledge of the transition probability, the partition function, and the number density of emitters as a function of temperature. It is also necessary to know the upper energy level of the line being emitted.

Transition probabilities for nitrogen and argon have been determined experimentally by several authors. The most recent and probably the most accurate investigation of argon transition probabilities was conducted by Olsen,[11] whose data have been used in this investigation. The experimental transition probabilities available for nitrogen show a great deal more scatter than those for argon. Following a suggestion of Solarski and Wiese,[12] the nitrogen transition probabilities calculated by Bates and Damgaard[13] have been employed. These calculated transition probabilities are quite close to the mean of the available experimental data. The upper energy levels of both argon and nitrogen were taken from the data compiled by Moore.[14]

Partition functions and number densities of the various components of high-temperature argon and nitrogen were taken from the tables of Drellishak, et al.[9, 10] These data were used in calculations of line and continuum intensities as functions of temperature.

Figure 4 shows the dependence of the absolute intensity of the 4158.59-A ArI line on temperature at a pressure of one atmosphere. The upper energy levels of the principal argon lines differ by only a small amount, so that figure 4 is representative of the temperature dependence of the visible and near-infrared argon lines. Theoretical intensity versus temperature curves for selected atomic nitrogen lines are shown in figure 5.

The effect of an error in the measured intensity upon the calculated temperature is shown in figure 6 for the 4158.59-A ArI line. The errors shown in this figure are typical of those to be expected with any argon line in the visible or near-infrared. Because of the similarity of ionization energies of argon and nitrogen, figure 6 is also representative of the errors to be expected when using any of the three nitrogen lines given in figure 5. The insensitivity of temperature to errors in intensity makes absolute intensity measurements of spectral lines a powerful method for determining temperature.

An alternate method of spectroscopic temperature measurement is provided by continuum radiation. Continuum radiation is emitted by a hot gas through two mechanisms: free-free or Bremsstrahlung radiation, and radiative recombination processes which give rise to a free-bound continuum. Since radiant energy is additive, the total continuum radiation is the sum of these two processes and a separate measurement of each cannot be obtained experimentally.

Since the continuum radiation immediately adjacent to a spectral line must be measured in order to separate the line from the background, it is advantageous to use the continuum radiation as a technique for measuring temperature. Use of the continuum has the advantage of requiring only one measurement of the intensity of the gas at a given wavelength, rather than the two needed in the case of a spectral line.

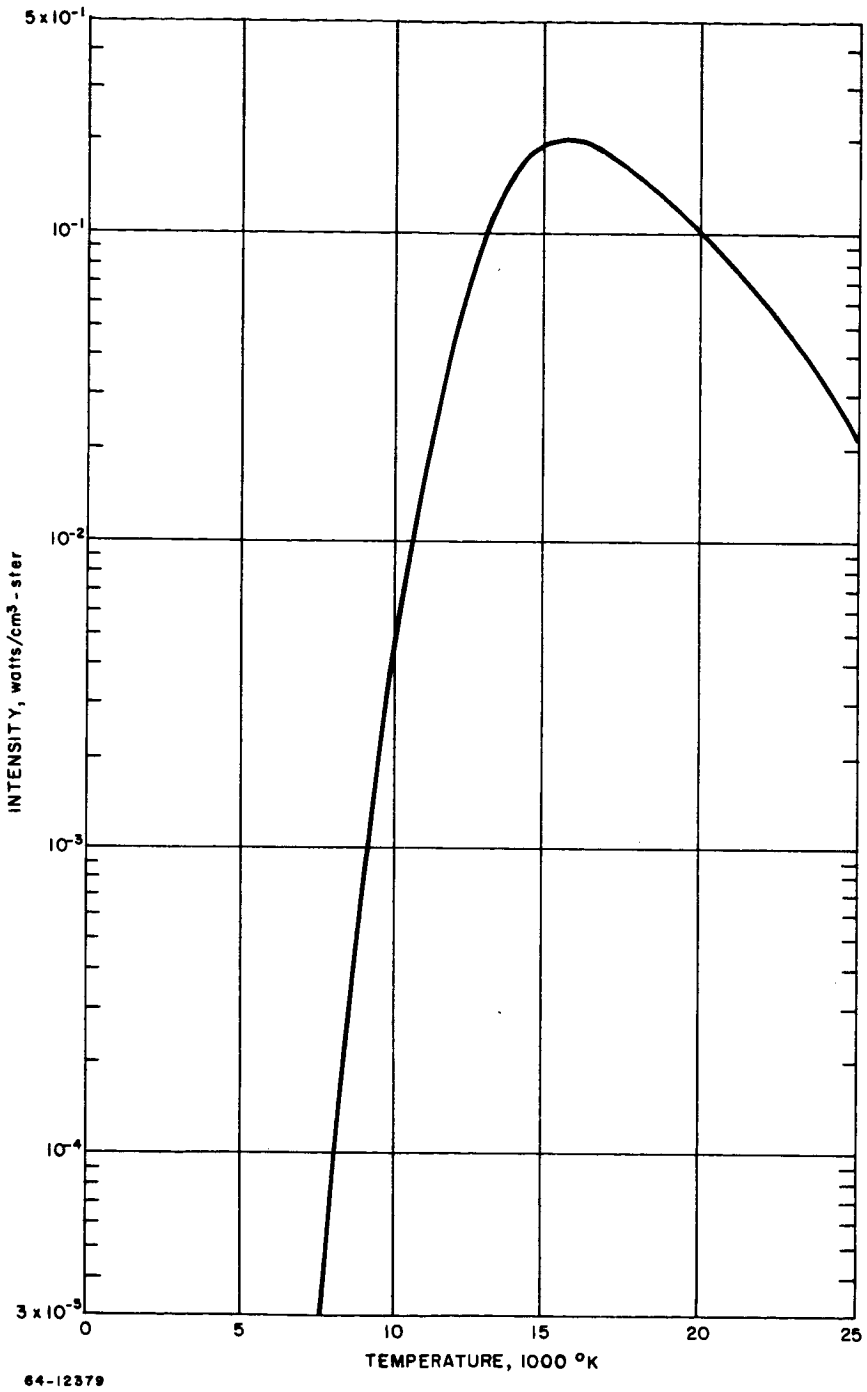

Figure 4 ABSOLUTE INTENSITY OF THE ARGON ATOM LINE ArI 4158.59 AS A FUNCTION OF TEMPERATURE AT A PRESSURE OF 1 ATMOSPHERE

64-3349

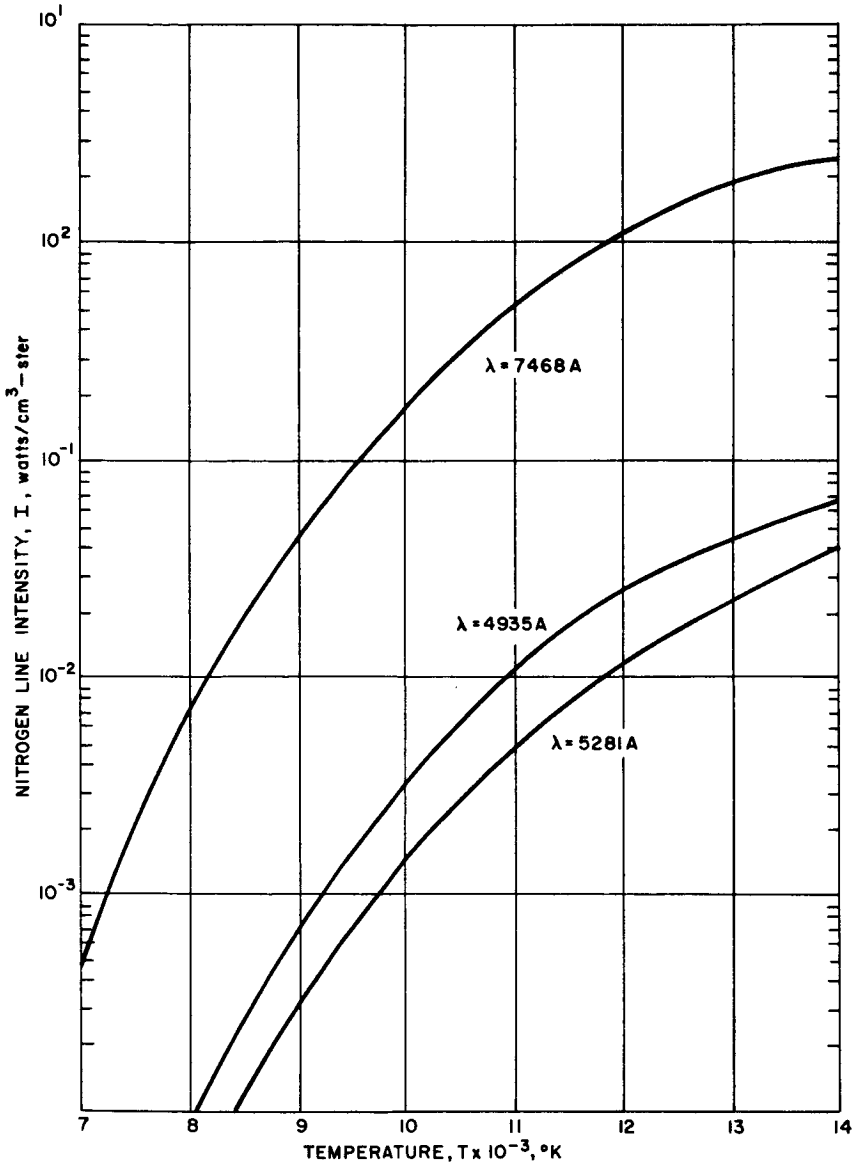

64-3349

Figure 5 ABSOLUTE LINE INTENSITY VERSUS TEMPERATURE FOR THREE ATOMIC NITROGEN LINES

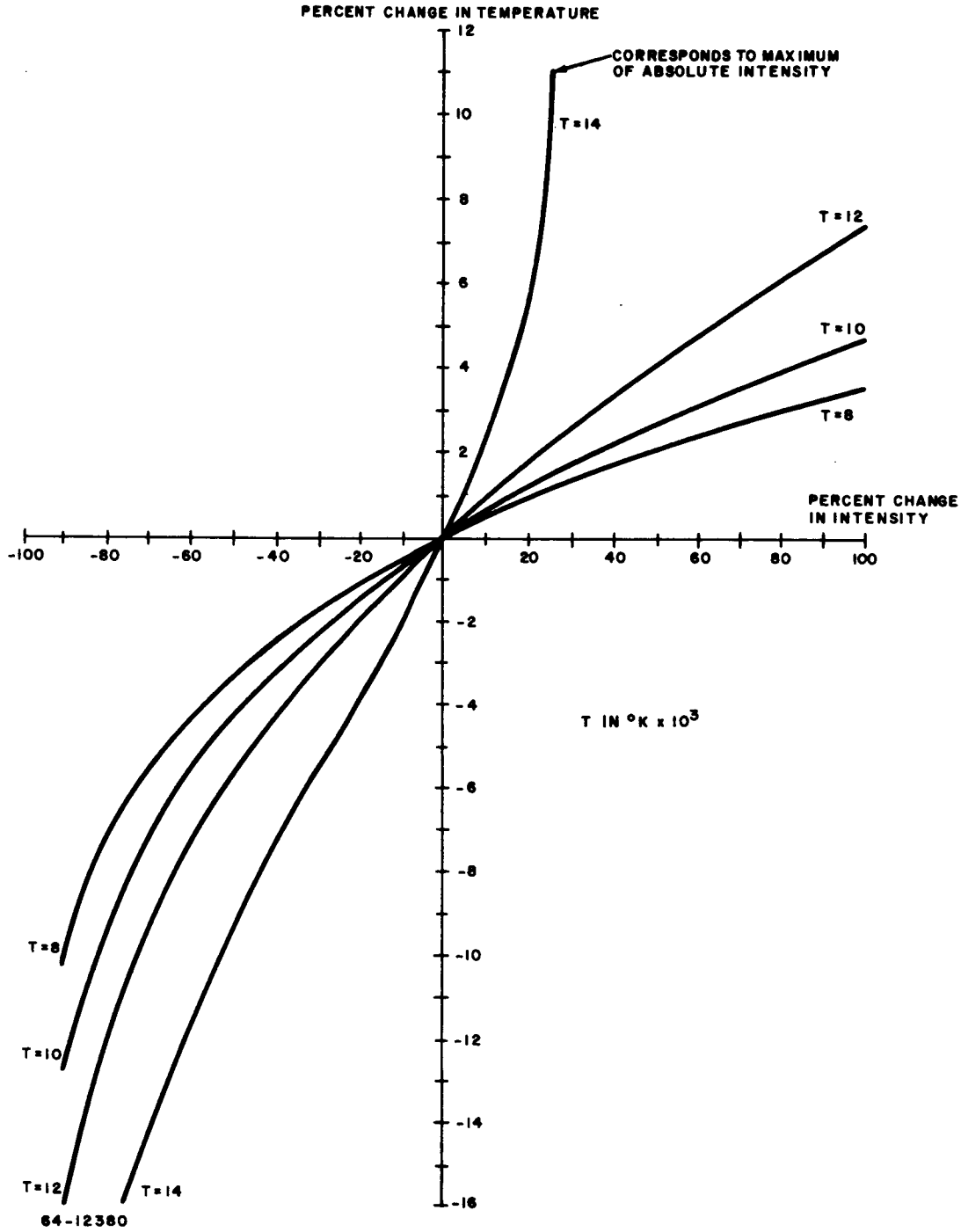

Figure 6 EFFECT OF ERRORS IN SPECTROGRAPHIC MEASUREMENTS ON TEMPERATURE BASED ON THE ARGON ATOM LINE

Theoretical calculations of absolute continuum intensity are not on as firm a footing as those for line radiation. The Kramers-Unsöld expression,

$$I = 5.41 \times 10^{-46} \frac{\overline{Z^2}\, n_e\, n_{it}}{T^{1/2}} \quad (\mathrm{W/cm^3 - ster\text{-}sec}) \tag{10}$$

where

$$\overline{Z^2} = \frac{\Sigma_i\ i^2\, n_i}{n_{it}} = \frac{\Sigma_i\ i^2\, n_i}{\Sigma_i\ n_i}$$

and n_e is the electron density, gives the correct functional dependence for the argon continuum radiation throughout the temperature range examined, and for the nitrogen continuum for temperatures above approximately 9,000°K. The absolute magnitude given by this expression is in error by varying amounts, depending upon the gas. Consequently, the continuum bands used for temperature measurements were calibrated with lines of known transition probability. Figure 7 shows, for argon, the absolute intensity of a 1A continuum band centered at 4285A. Similarly, for nitrogen, figure 8 depicts the intensity of a 1A continuum band centered at 4955A. The effect upon the measured temperature of errors in spectrographic measurements is shown in figure 9 for argon. As in the case of absolute line measurements, the error curves for nitrogen are quite similar. It will be appreciated from figure 9 that the determination of temperature from measurements of absolute continuum intensity is insensitive to experimental errors in the temperature range covered to date.

D. EXPERIMENTAL OBSERVATIONS

The objective of the experimental measurements has been to determine the thermodynamic state of the gas as a function of the radial coordinate of the column, and to use this measured state to determine the thermal and electrical conductivities as functions of temperature. The general approach in the spectrographic investigation has been to determine the temperature from absolute line and continuum measurements. The remaining information necessary for a solution of the Elenbaas-Heller equation (5) is obtained from measurements of the applied electric field strength in the column, the arc current, and the volumetric radiative losses.

The integrated intensity distribution of the arc column is obtained by translating the image of the column across the entrance slit of the monochrometer. In taking measurements, the arc is moved an incremental distance and stopped, and the intensity is then measured. The amplification of the photomultiplier signal is automatically optimized for each measurement. This technique is considered to be superior to continuously scanning the image of the arc column, since it allows reliable measurements to be obtained for intensities varying by as much as a factor of 10^3, a considerably wider range than can be measured successfully

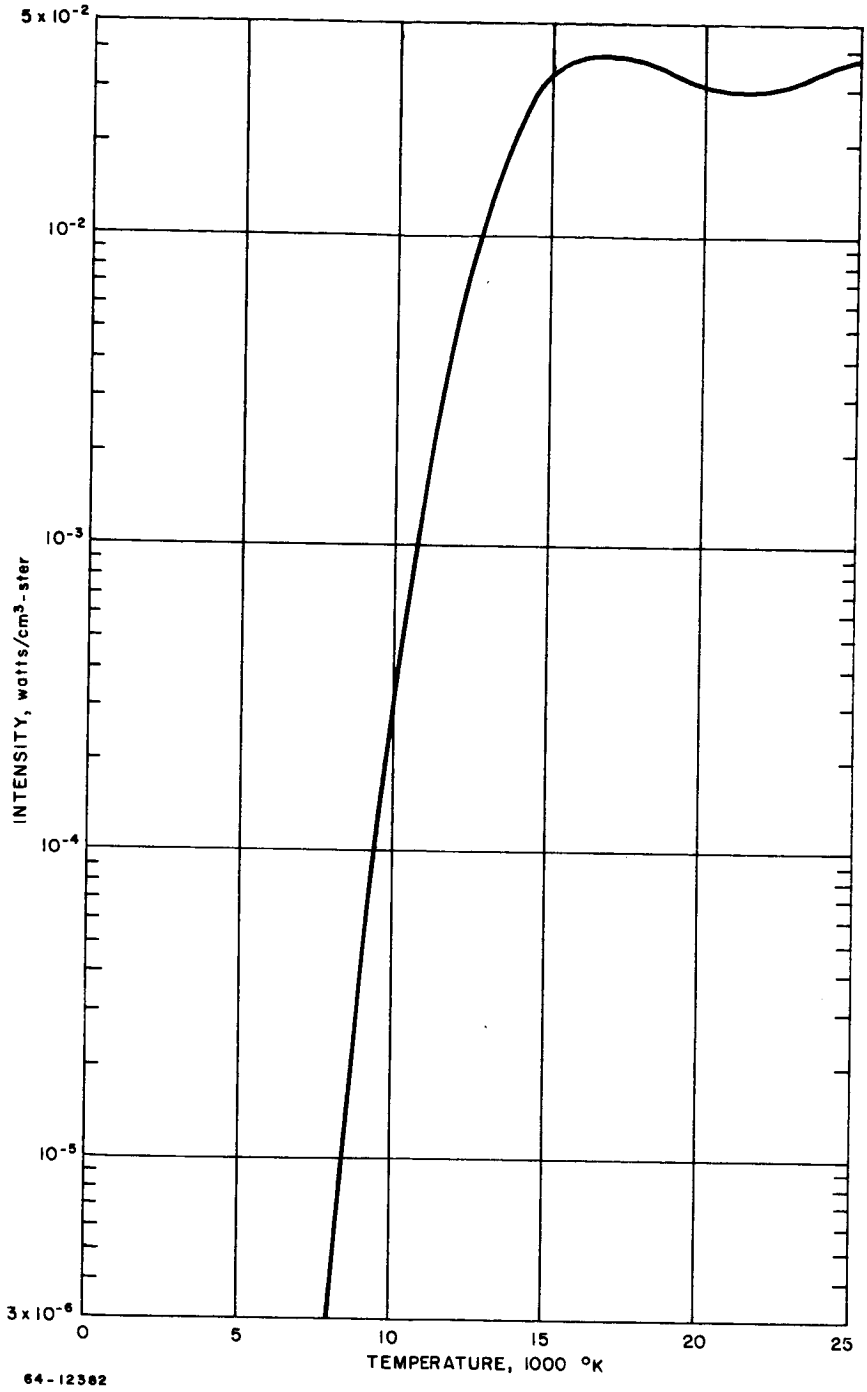

Figure 7 ABSOLUTE INTENSITY OF A 1-A ARGON CONTINUUM BAND CENTERED AT 4285A AS A FUNCTION OF TEMPERATURE AT ATMOSPHERIC PRESSURE

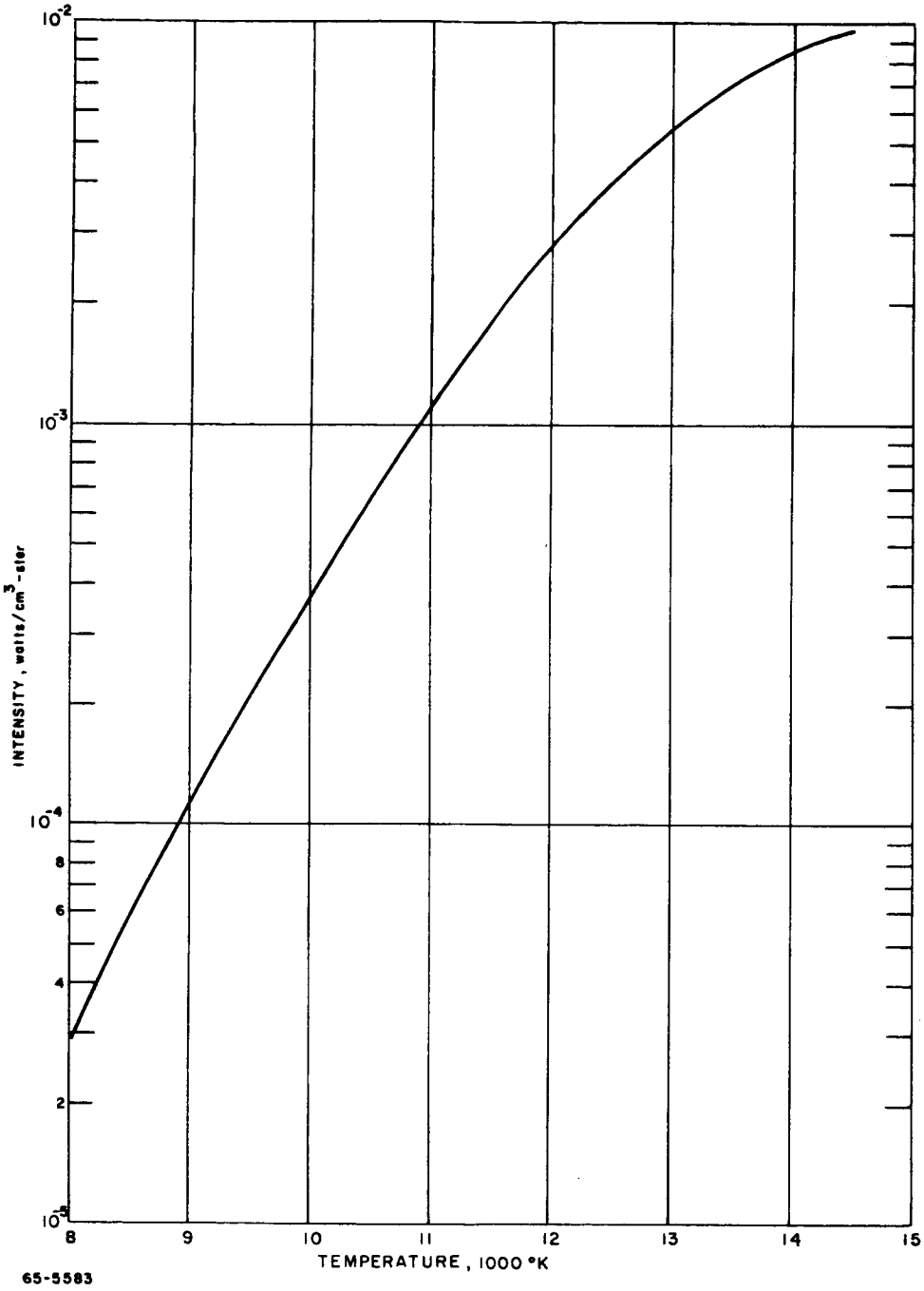

Figure 8 ABSOLUTE INTENSITY OF A 1-A NITROGEN CONTINUUM BAND CENTERED AT 4955A AS A FUNCTION OF TEMPERATURE AT ATMOSPHERIC PRESSURE

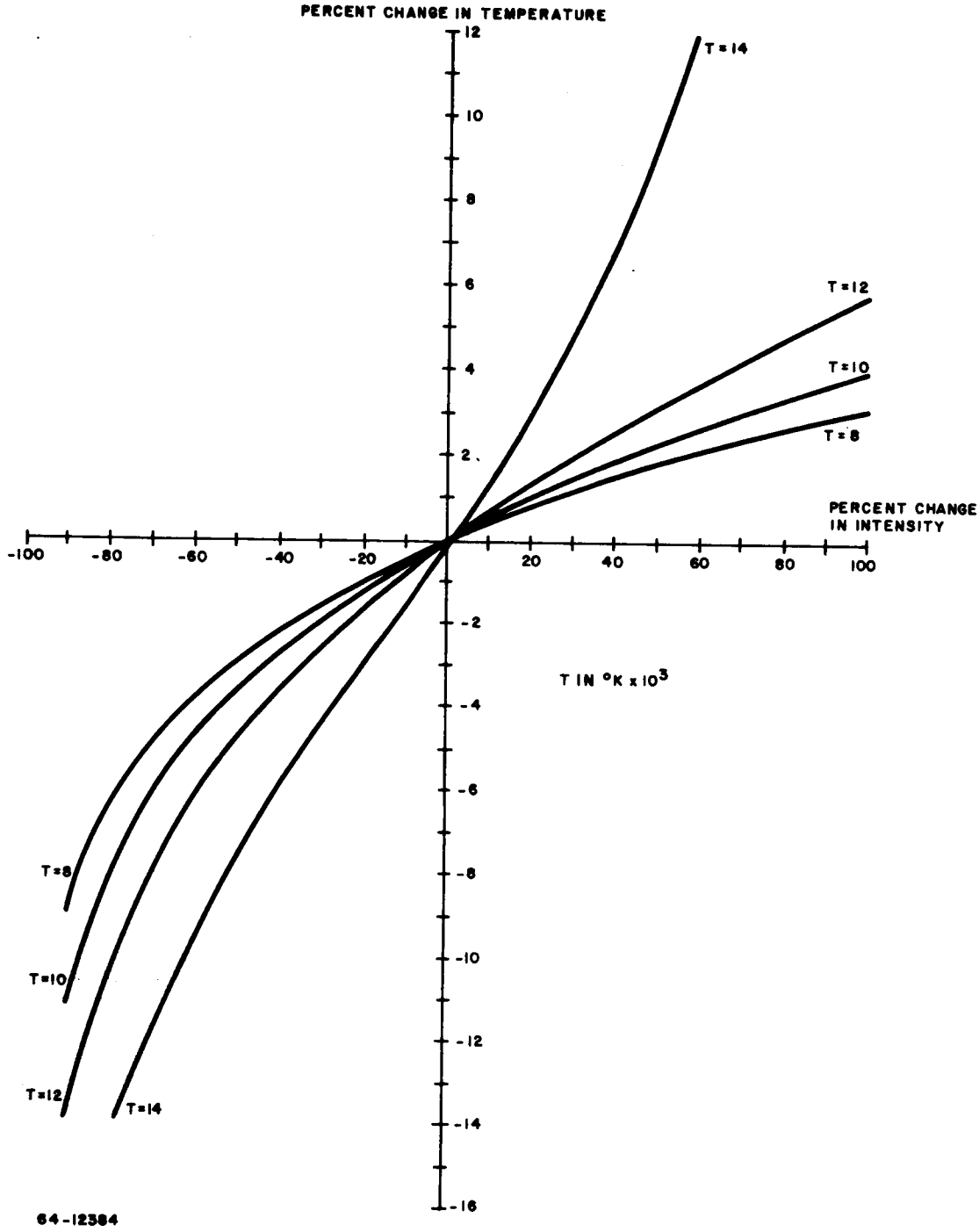

Figure 9 EFFECT OF ERRORS IN SPECTROGRAPHIC MEASUREMENTS UPON TEMPERATURE MEASUREMENT IN ARGON USING A 1-A CONTINUUM BAND CENTERED AT 4285A

by a continuous scan. The relative position of the arc column is controlled by a drive motor and a dial indicator. The centerline of the column is determined by taking intensity measurements at incremental distances across the entire arc diameter, plotting the signals obtained, and folding the plot so that the curves to the right and left of the center are mirror images. In actual practice, this operation is performed by machine calculation. Figure 10 shows the results of the centering routine. In this figure, points from both right and left of the center line are plotted.

The integrated intensity distribution is converted to a radial intensity distribution by an inversion of the Abel integral equation. Implicit in the solution of this equation is a process of numerical differentiation. In the technique used, the differentiation is performed by curvefitting a region of the integrated intensity distribution to obtain smooth derivatives. This is similar to the method employed by Barr.[15] As is characteristic of numerical differentiation, derivatives at the end points of the curve tend to be unreliable. The accuracy of the inversion technique has been checked by inverting numerically a function which could be inverted analytically. It was found that the numerical technique gave excellent results except at the first three inverted points. As the inversion starts at the outer edge of the integrated intensity distribution and works inward, the error due to numerical methods occurs at the outer edge of the radial intensity distribution. The error inherent in numerical differentiation is aggravated by the shape of the integrated intensity distribution. At the periphery of the arc column, the gradient of the integrated intensity is extremely large, the intensity changing by an order of magnitude or more within 5 percent of the projected radius. Consequently, inversion of the integrated intensity distribution using, say, 20 increments across the projected radius tends to decrease the gradient and produce artificially high inverted values at the outer edge. Greater resolution at the outer edge of the distribution is obtained by using a finer mesh for the numerical inversion. At present, a fifty-zone inversion is used. This is a sufficient number of zones to give good results for large gradients. Figure 11 shows the radial intensity distribution obtained from the integrated intensity distribution of figure 10.

In the initial experiments with argon, it was found that the arc column was rather severely distorted in the region between constrictors. The distortion appeared as a "bulge" in the luminous column. Such bulging is a significant deviation from the cylindrical symmetry required for the validity of the Elenbaas-Heller equation and determination of transport properties. This type of problem is particularly disturbing since the distortion of the column occurs at the same location at which measurements are taken. Qualitative observations indicated that bulging of the arc column was much more severe for argon than for nitrogen or oxygen. For this reason the argon arc column was examined in detail; it was felt that an experimental solution to the bulging of the argon column would allow measurements in nitrogen and oxygen to be made with confidence.

It was found that the apparent bulging of the argon column could be eliminated for currents up to at least 100 amperes (axis temperature of 13,700°K) by

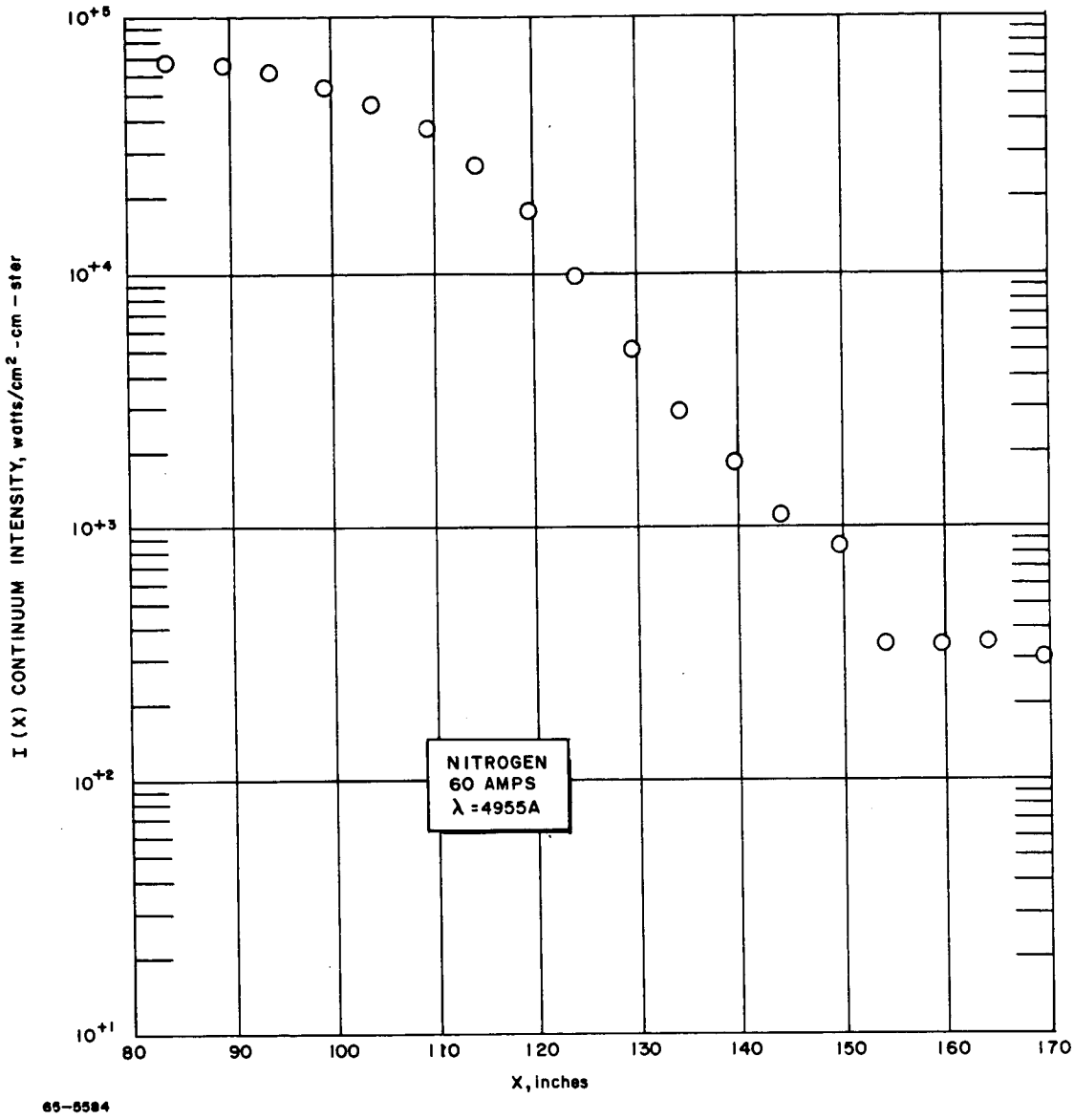

Figure 10 TYPICAL INTEGRATED INTENSITY DISTRIBUTION MEASURED IN THE CONSTRICTED ARC

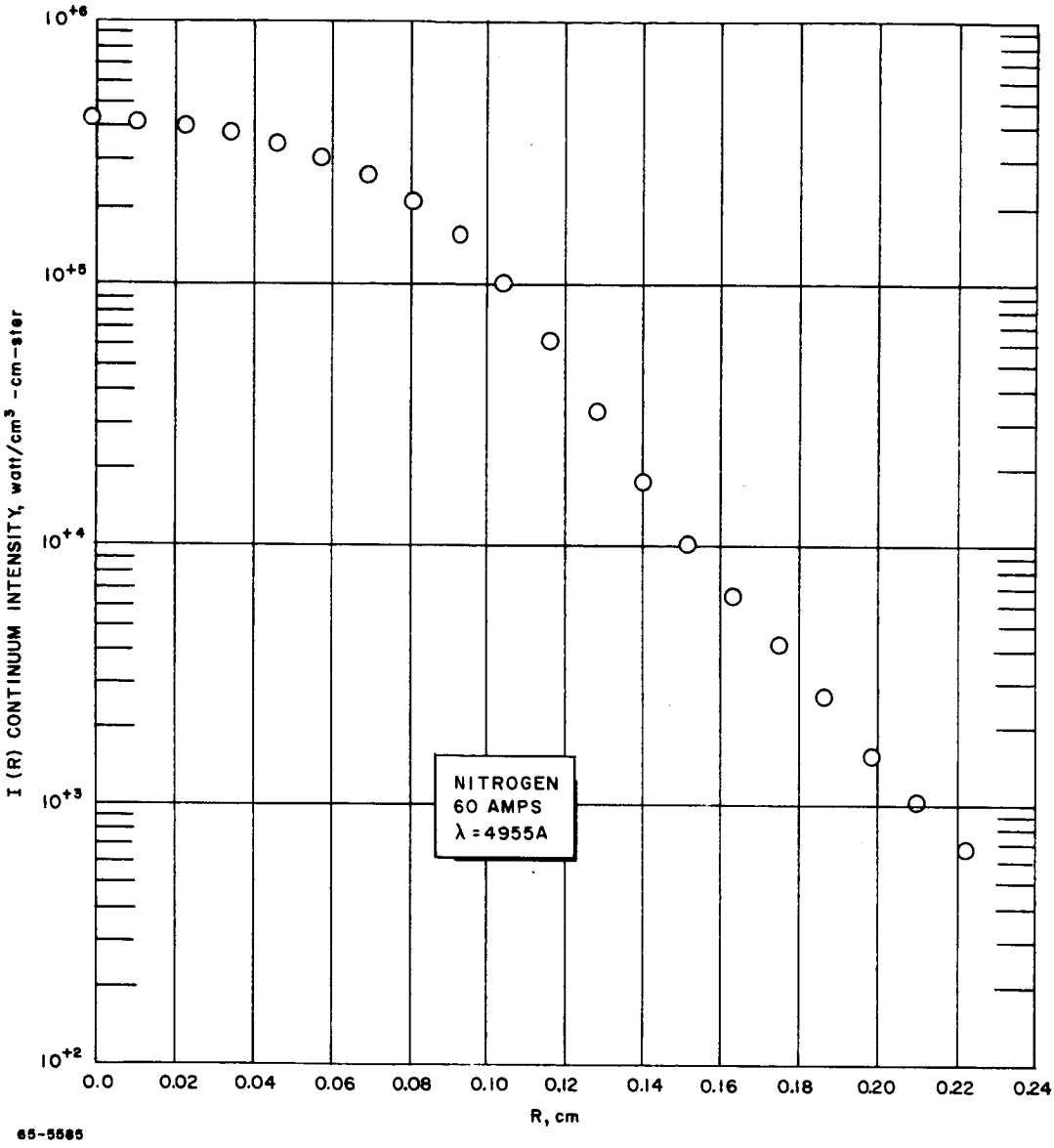

Figure 11 RADIAL INTENSITY DISTRIBUTION OBTAINED FROM INTEGRATED INTENSITY DISTRIBUTION

reducing the width of the gap between constrictors to 5 percent of the channel diameter and by reducing the gas flow rate to 10^{-3} gm/sec.

With procedures for obtaining approximate cylindrical symmetry of the arc column thus established, the main effort was directed toward determination of transport properties for argon and nitrogen. Temperatures in the arc column were determined on the basis of absolute intensity measurements of continuum radiation, the nitrogen and argon continuum radiation having been calibrated previously against spectral lines. Integrated intensity distribitions were obtained in argon for a continuum band at 4285A at arc currents of 30, 40, 50, 60, 80, and 100 amperes, and in nitrogen for a continuum band at 4955A at currents of 40, 50, 60, 80, 100, and 150 amperes. In each case a level of scattered light was evident at the outer periphery of the arc column. An example of this can be seen in figure 10, where the scattered light is manifested as a region of constant intensity at the outer edge of the distribution. In order to approximate the true course of the integrated intensity distribution, a correction was made for the scattered light. Figures 12 and 13 show the radial temperature distributions obtained for argon, and figures 14 and 15 those for nitrogen.

The temperature profiles in the region from 1,000°K to 5,000°K were calculated from the conductive energy flux to the walls and the classical thermal conductivity. At 5,000° K the internal excitation of argon atoms is low enough that the thermal conductivity given by Amdur and Mason[16] is applicable. For nitrogen, the situation is not quite as favorable, although the thermal conductivity at 5,000°K is sufficiently well-known to permit reasonably accurate temperature profiles to be constructed. The values of Yos[17] were used for nitrogen. The dotted portions of the temperature profiles represent interpolation between the calculated and measured portions of the profiles. Neither the calculated nor the interpolated portions were used to obtain thermal conductivity.

The dissimilarity in temperature profiles between argon and nitrogen is due to the presence, in the thermal conductivity curve for nitrogen, of the reaction conductivity peak corresponding to dissociation. The inflection point in the nitrogen profiles corresponds to this extremum in the thermal conductivity.

It is estimated that the uncertainty in the intensity of the NBS standard lamp is approximately ±5 percent. The uncertainty in the detection and recording system is estimated to be ±2 percent. For line radiation, the uncertainty in the transition probabilities and the ratio of number density to partition function is estimated to be ±8 percent. For the continuum radiation, it is reasonable to expect the same sort of uncertainty in the product of the constant determined from calibration of continuum with line radiation, the ion density, and the electron density. It can be seen from figure 6 that a ±15-percent uncertainty in the absolute line intensity produces a ±1.5-percent uncertainty in the temperature at 12,000°K. Analogously, figure 9 shows that the uncertainty to be expected in the temperature determined from absolute continuum intensity is ±1 percent at 12,000°K.

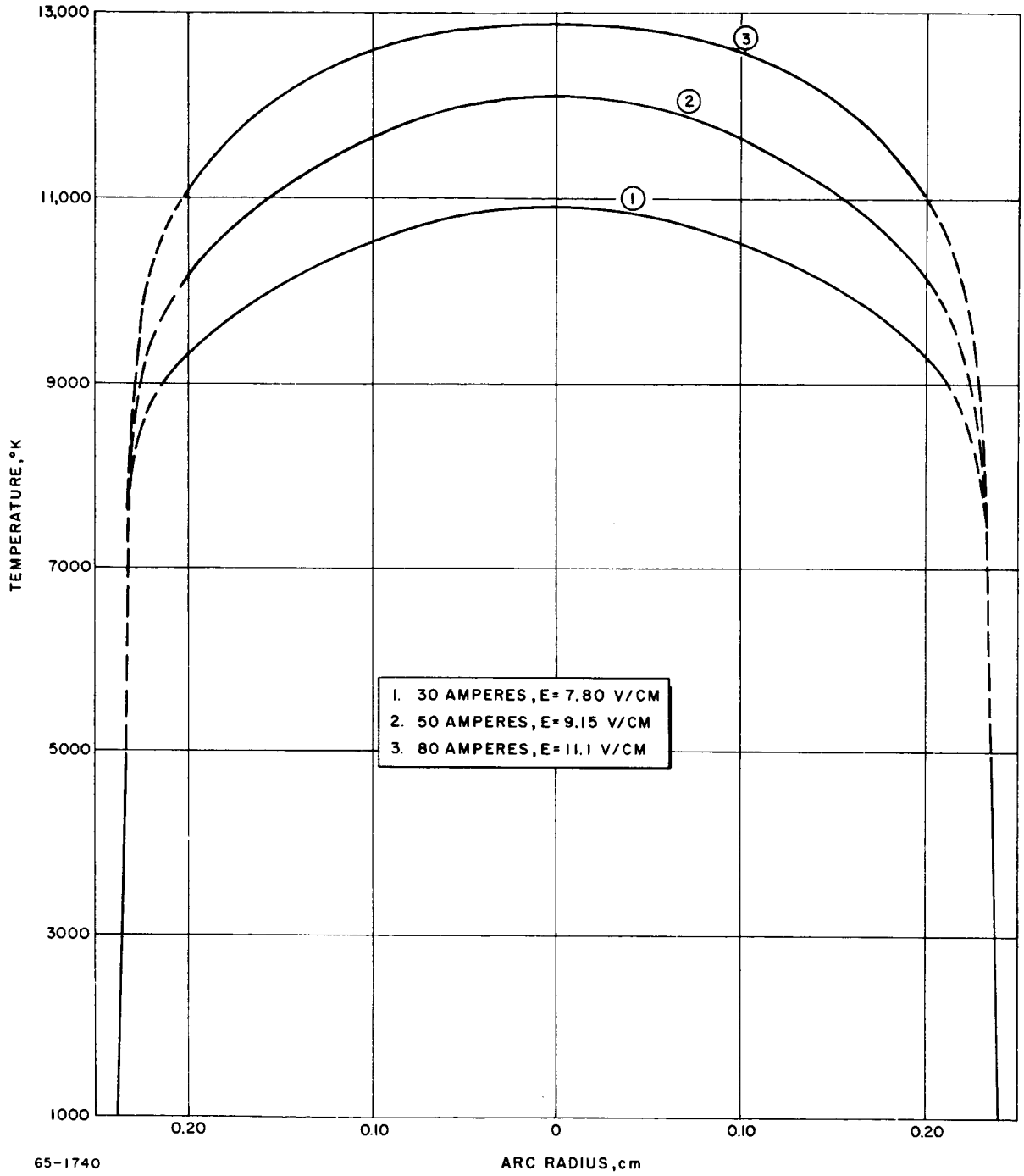

Figure 12 RADIAL TEMPERATURE DISTRIBUTIONS FOR 30, 50, AND 80 AMPERE ARGON ARCS

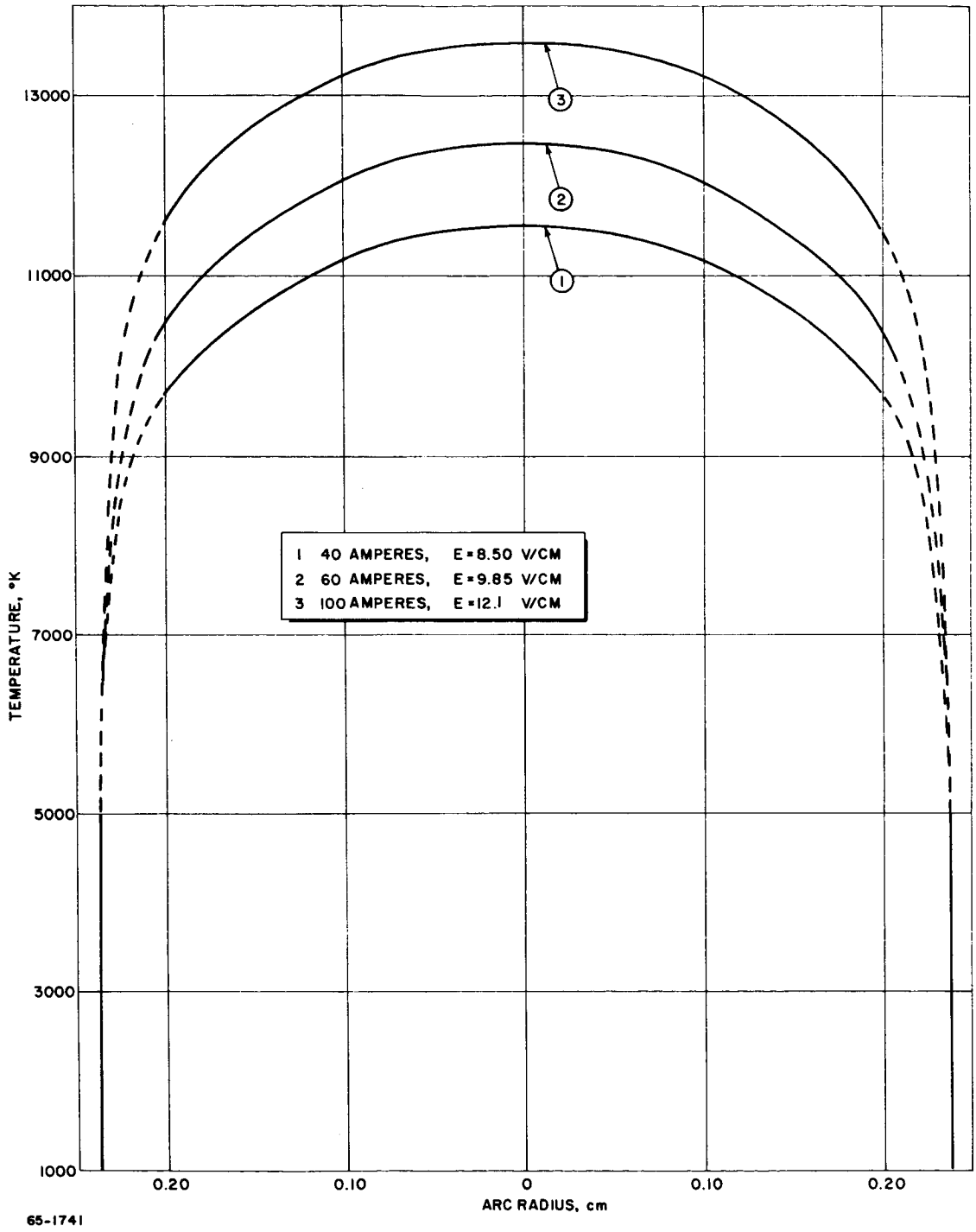

Figure 13 RADIAL TEMPERATURE DISTRIBUTIONS FOR 40-, 60-, AND 100-AMPERE ARGON ARCS

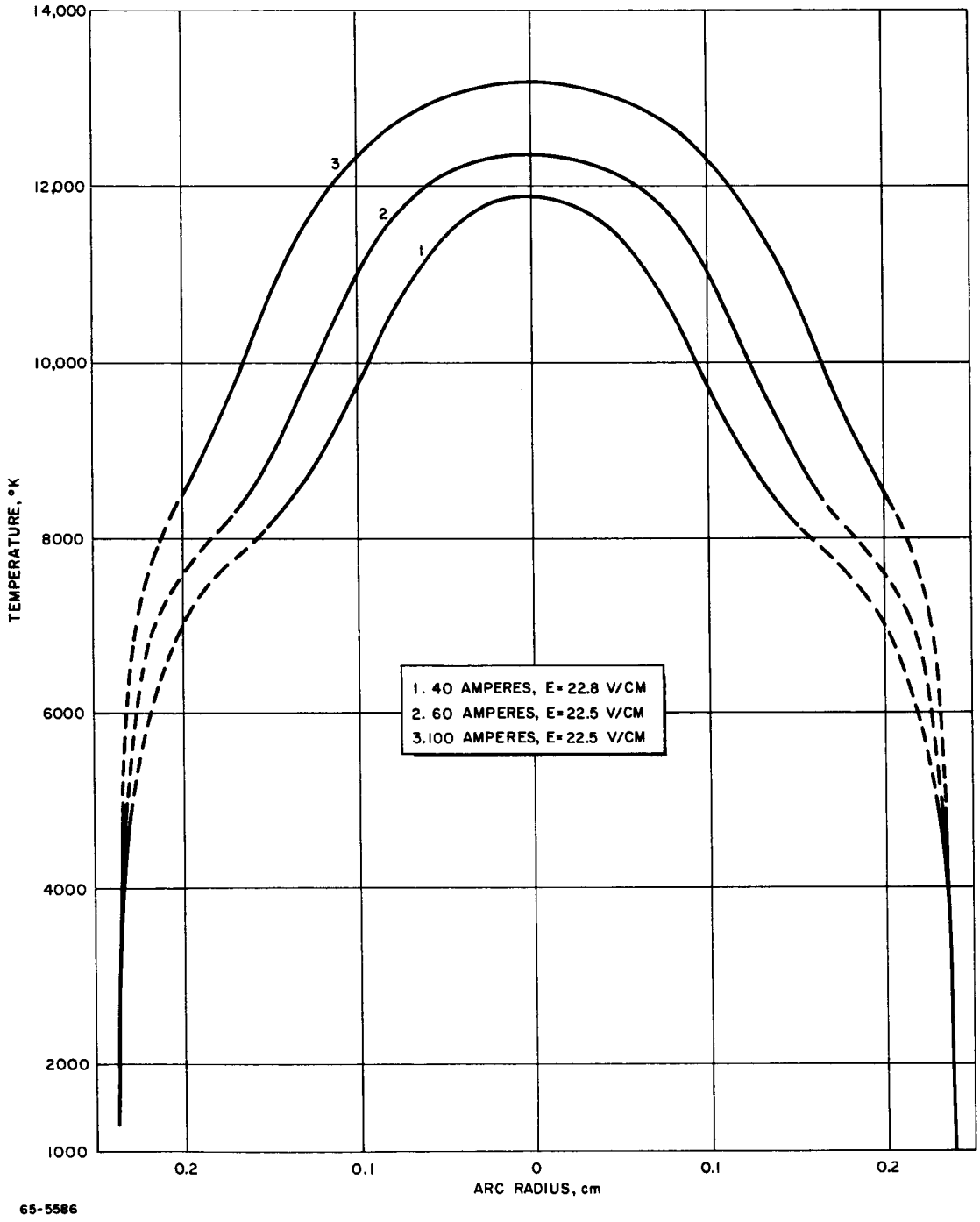

Figure 14 RADIAL TEMPERATURE DISTRIBUTIONS FOR 40-, 60-, AND 100-AMPERE NITROGEN ARCS

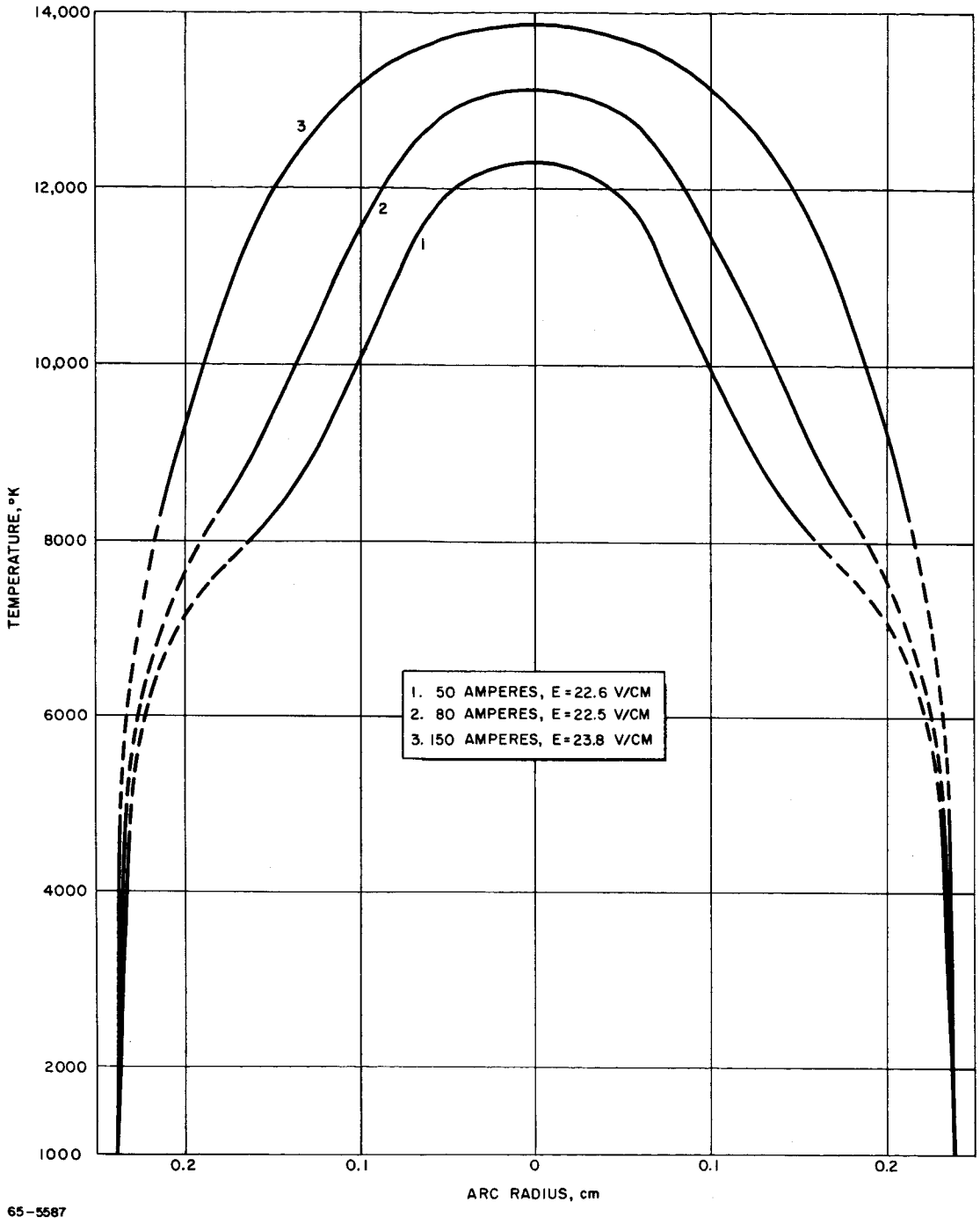

Figure 15 RADIAL TEMPERATURE DISTRIBUTIONS FOR 50-, 80-, AND 150-AMPERE NITROGEN ARCS

The column voltage gradient necessary for the solution of the Elenbaas-Heller equation was obtained in two ways. For argon, voltage gradients were obtained by decreasing the inter-electrode spacing by a known distance and determining, for a constant arc current, the decrease in arc voltage. For a homogeneous arc column, i.e., electrodes not blanketed in a gas different from that being investigated, this method gives the voltage gradient to a high degree of precision. In the case of nitrogen, it is necessary to blanket the electrodes in argon, and this method cannot be used. Voltage gradients in the nitrogen arc were measured using the circuit shown in figure 16. In this circuit, which has been used to advantage by several other investigators,[18-20] the constrictors at each end of the column of test gas serve as probes. A small amount of current is supplied to the arc at these constrictors. Although this current is small, it is much larger than the current drawn by the voltmeter, so that the effect of the contact resistance of the probes, even if it is extremely high, is negligible. Consequently, the voltmeter reads the true voltage difference across the constrictors. An electrometer with an impedence of 10^{14} ohms was used in the determination of the voltage gradients in both argon and nitrogen.

The electric field associated with each of the arc currents used for argon and nitrogen is given in the temperature-profile plots, figures 12, 13, 14, and 15.

E. ANALYSIS OF EXPERIMENTAL OBSERVATIONS

1. Methods of Analysis

Solution of the Elenbaas-Heller equation,

$$\sigma E^2 + \frac{1}{r} \frac{d}{dr} \left(r K \frac{dT}{dr} \right) - P_{rad} = 0, \tag{5}$$

for thermal conductivity, K, requires that the radial temperature gradient be known as a function of radius. In the present program, temperature gradients have been determined both by graphical analysis and by differentiating analytical curvefits to the experimental temperature distributions. The method used for curvefitting temperature distributions is described in appendix B.

In the graphical analysis, the slope of the radial temperature distribution at a given radius is found by first determining the normal to the curve. The normal is determined by placing a half-silvered mirror, mounted perpendicular to the plane of the paper, on the temperature profile at the point where the derivative is to be evaluated. The mirror is rotated until the image of the curve and the curve itself coincide. A line is then drawn along the face of the mirror at that point. It is then a simple matter to evaluate the slope of the curve graphically.

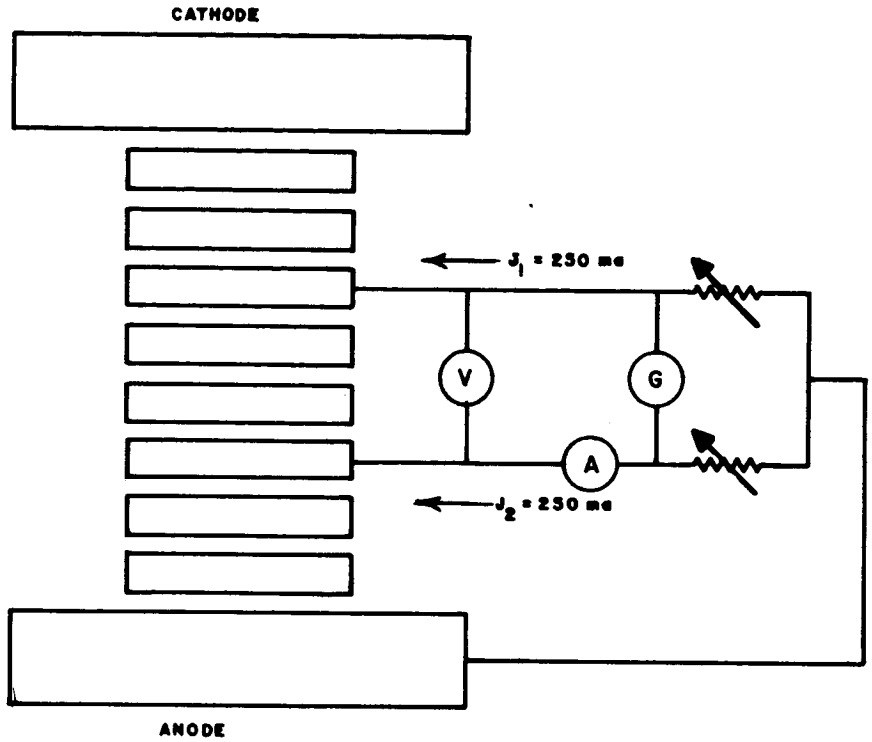

65-5566

Figure 16 CIRCUIT FOR MEASURING VOLTAGE GRADIENTS IN THE NITROGEN ARC COLUMN

An estimate of the accuracy of this technique has been obtained by comparing the analytically and graphically evaluated slopes of a parabola. The minimum error in the graphical technique occurred at slopes in the neighborhood of 1 and was approximately 2 percent. Larger errors occurred at larger and smaller slopes, rising to 7 percent at a slope of 0.05. To reduce the effect of such errors, which appear to be random, a smooth curve passing through the origin at zero radius is fitted by eye to graphically determined slopes of the temperature distribution. In view of the accuracy obtained in the case of the parabola, it is estimated that the radial temperature gradients are accurate to 5 percent or better. The agreement between the radial temperature gradients determined by graphical analysis and by curve-fitting the radial temperature distribution is quite good. In most cases the two methods agree to better than 5 percent.

The thermal conductivity is calculated from the data using three different methods for solution of the Elenbaas-Heller equation (5). Two of these methods are based upon an energy balance applied to a cylindrical control volume within the arc column. These two energy-balance methods differ in their techniques for estimating the electrical current through the control volume, which is responsible for the production of heat in the volume. The "calculated-current" method estimates this current from the experimental temperature distribution and theoretical electrical conductivity of the gas, using Ohm's law. The "measured-current" method, on the other hand, estimates the current through the control volume from the measured total current by subtracting an estimate of the current outside the control volume. Both of these methods provide thermal conductivity as a function of temperature from the data of each arc run, but these results are more or less dependent upon the assumed theoretical electrical conductivity. In contrast, the "two-run" method discussed in appendix C yields both thermal and electrical conductivity without the use of assumed values for the electrical conductivity.

In the calculated-current method, the Elenbaas-Heller equation (5) is integrated once and solved for the thermal conductivity of the gas at the radial distance r' from the column axis,

$$(K)_{r'} = -\frac{\int_0^{r'} (E^2 \sigma - P_{rad})\, r\, dr}{(r\, dT/dr)_{r'}} \tag{10}$$

This equation is equivalent to the statement that the heat conducted out across a cylindrical surface of radius r' is equal to the heat generated inside the surface by Joule heating, less the heat lost from inside the surface by radiation.

Since the radial temperature distribution is known, equation (10) determines the thermal conductivity at the temperature associated with r', if the electrical conductivity σ and radiative power loss P_{rad} are known as functions of temperature.

In the measured-current method, the thermal conductivity is again calculated essentially from equation (10), but the integral over σ in the numerator is expressed in terms of the total current using Ohm's law:

$$I = 2\pi E \int_0^R \sigma r dr = 2\pi E \left[\int_0^{r'} \sigma r dr + \int_{r'}^R \sigma r dr \right] , \tag{11}$$

where R denotes the arc column radius and I the total current. Elimination of the integral of σr from 0 to r' between (10) and (11) gives the thermal conductivity formula of the measured-current method,

$$(K)_{r'} = - \frac{EI - 2\pi E^2 \int_{r'}^R \sigma r dr - 2\pi \int_0^{r'} P_{rad} r dr}{2\pi (r\, dT/dr)_{r'}} \tag{12}$$

At fairly large values of r', where the temperature is relatively low, the integral over σ in (12), which represents the power dissipated at radii larger than r', becomes small in comparison with the total arc power per unit length, EI. In such regions, (12) is quite insensitive to errors in the assumed electrical conductivity function $\sigma(T)$. Thus, (12) is preferable to (10) for evaluating thermal conductivity in the outer part of the experimental temperature distribution. On the other hand, (10) is preferable to (12) at points relatively near the column axis.

The two-run method, discussed in appendix C, is based on an explicit solution of equations (5) and (11) for the thermal and electrical conductivities, K and σ. The solution, presented in appendix A, requires knowledge of the voltage gradients and temperature distributions for two arc runs with different axial temperatures. The advantage of the two-run method over the two energy-balance methods described above is that it does not call for a priori knowledge of the electrical conductivity σ. The disadvantages are that it is more sensitive to errors in the data, and that it requires knowledge of the thermal conductivity at an initial temperature. This second disadvantage is not too serious, however, because the initial temperature can be relatively low, and the thermal conductivity at relatively low temperatures can be determined by the measured-current energy balance method without relying heavily on the theoretical electrical conductivity.

All three of these methods are faulty in that they are based on the energy equation in the Elenbaas-Heller form (5), which assumes that the arc column is optically thin to its own thermal radiation. As shown below, this assumption is not valid for the arc column in either argon or nitrogen at atmospheric pressure.

2. Argon Results

The three methods outlined above have been employed to analyze the data obtained from the several arc runs in argon. The amount of energy radiated from the arc per unit volume in the infrared, visible, and near-ultraviolet has been determined as a function of temperature, by relating the profile of measured radiated power to the temperature profile at the same arc conditions. A Perkin-Elmer thermocouple calibrated with an NBS standard lamp was used for the total radiation detector. This detector is gray from about 2500A to beyond 6 microns, the wavelength at which the sapphire observation window cuts off. The undetected radiation at wavelengths greater than 6 microns is estimated to be about 15 percent of the total detected radiation. Figure 17 shows the results obtained for argon, corrected for undetected radiation in the far-infrared by multiplication with the factor 1.15.

Calculations based upon the absorption cross section measurements by Samson[21] indicate that there is a significant amount of radiation at wavelengths below 2500A from the free-bound continuum of argon. At 14,000°K this radiation is about equal to the total measured radiation shown in figure 17. At this temperature, however, the absorption coefficient for the free-bound transition is 7 cm^{-1}, which corresponds to an e-folding path length of 1.4 mm. At lower temperatures, the absorption coefficient is considerably larger. Consequently, the ultraviolet radiation is essentially totally absorbed and then re-radiated, even in the central core of the column. Under these circumstances, it is not permissible to include the ultraviolet radiation in the radiative term of the Elenbaas-Heller equation. In order to treat the problem rigorously, the Elenbaas-Heller equation should be reformulated to include nongrey radiative transfer, a difficult problem to solve in cylindrical coordinates. Unfortunately, the Rosseland approximation is inapplicable, since the argon also radiates strongly at wavelengths in the infrared, visible, and near-ultraviolet to which the arc column is essentially transparent. In the absence of any satisfactory procedure for including the far-ultraviolet radiation in the analysis of the problem, the argon data have been treated using the "optically thin" Elenbaas-Heller equation (5) with a radiative loss term P_{rad} based upon the infrared, visible, and near-ultraviolet data shown in figure 17. In other words, the far-ultraviolet radiation has been ignored in the analysis of the data, with consequences which are discussed below.

The electrical conductivity used in the determination of the thermal conductivity of argon from the calculated-current and measured-current methods is shown in figure 18. This calculation by Yos[17] agrees well with calculations made by Cann.[22]

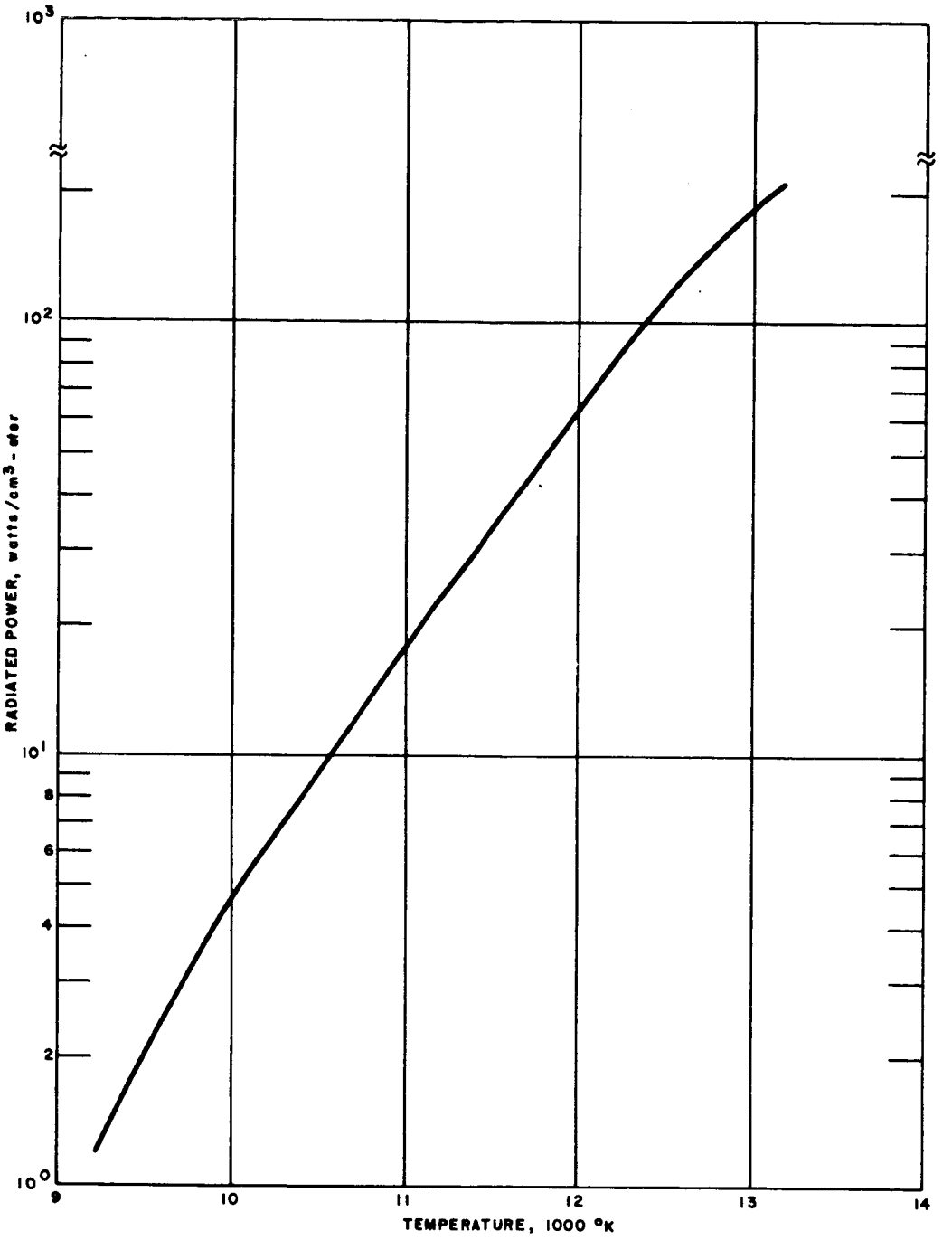

64-12385

Figure 17 TOTAL INFRARED, VISIBLE, AND NEAR-ULTRAVIOLET RADIATION OF ARGON AT ATMOSPHERIC PRESSURE

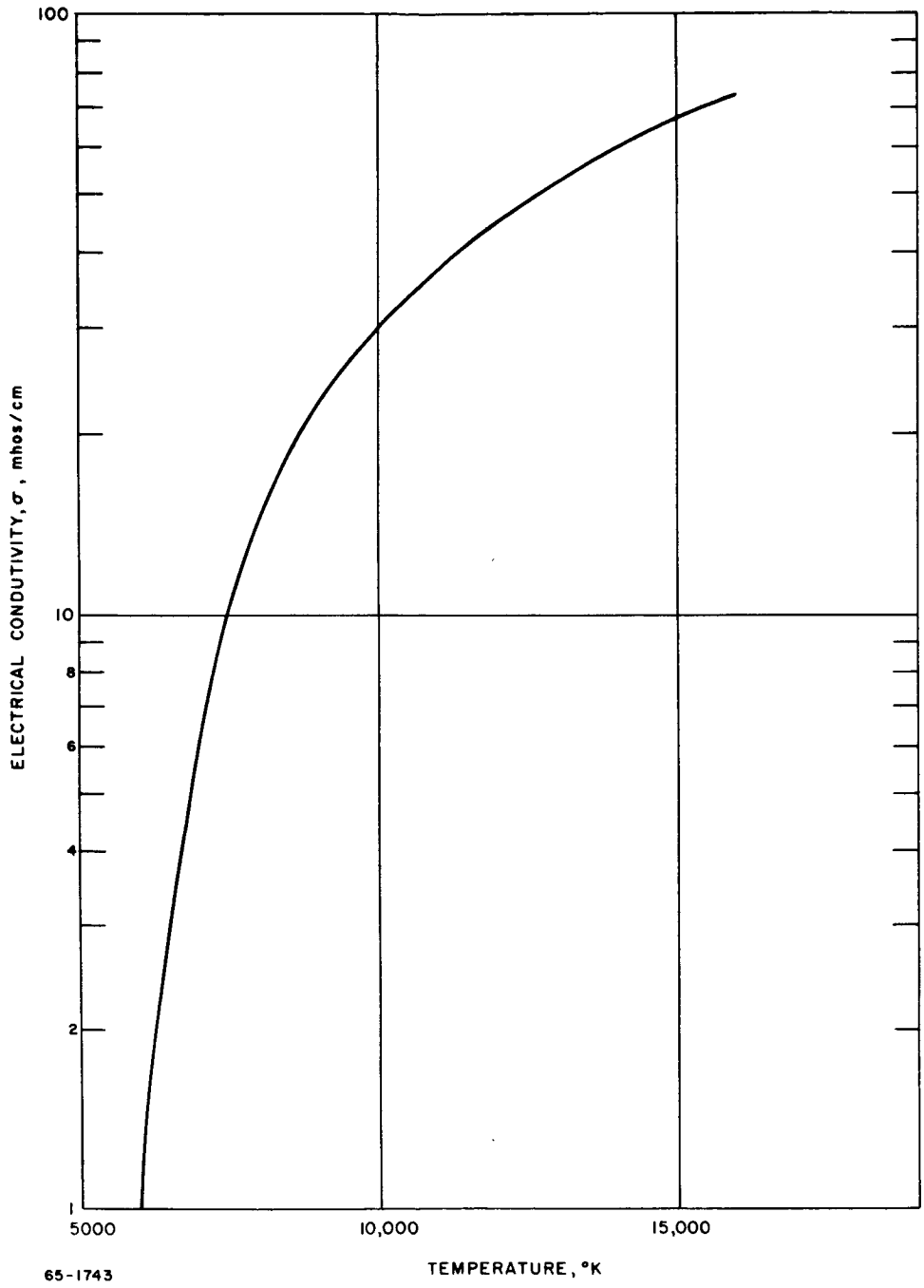

Figure 18 THEORETICAL ELECTRICAL CONDUCTIVITY OF ARGON

The thermal conductivity values obtained by the calculated-current method using the electrical conductivity of figure 18 and the radiated power given in figure 17 are represented by the points in figure 19. This figure also shows Yos's theoretical conductivity and a dashed curve representing the results of analyzing the data using the measured-current method discussed above; these results are presented more fully in figure 21. At the higher temperatures of each arc run, the thermal conductivity from the calculated-current method exhibits a downward trend. This behavior possibly results from the difficulty of obtaining accurate derivatives of the temperature profile at positions close to the axis of the arc or from inaccuracy of the Abel inversion near the axis.

It was estimated above that the overall uncertainty in the measurement of the absolute intensity distribution of the arc column is approximately ±15 percent. At 14,000°K, the maximum temperature achieved, this gives rise to a ±2-percent error in temperature. At lower temperatures the error is much less. Random errors in the voltage gradient are approximately ±2 percent. As indicated above, the radial temperature gradients are estimated to be accurate to ±7 percent near the center line of the temperature profiles and as accurate as ±2 percent elsewhere. On the basis of these uncertainties, the expected random error in the thermal conductivity values ranges from ±8 percent to ±13 percent, the larger error occurring at the higher temperatures of each profile (near the center line of the profile). To these errors must be added the unknown systematic errors due to uncertainty in the electrical conductivity values used and effects of the neglected far-ultraviolet radiation.

Figure 20 compares the thermal conductivity of argon as measured in this investigation with the results of Knopp.[3] The data of reference 3 were obtained using a non-segmented constricted arc which was known to be cylindrically symmetric. The two sets of data agree to within the limits of experimental error. The relatively good agreement between the sets of experimental results shown in figure 20, and the approximate agreement of these data with theory, indicates that it is possible to obtain reliable measurements of transport phenomena using the segmented constricted arc.

Figure 21 shows values of the thermal conductivity of argon calculated from the same experimental data (figures 12 and 13), the same assumed radiative loss (figure 17), and the same theoretical electrical conductivity function (figure 18), using the measured-current energy balance method. As discussed above in part 1 of the present section, this method is similar to the calculated-current method upon which the results of figure 19 are based, but differs from it in that the theoretical electrical conductivity $\sigma(T)$ is used for temperatures lower than that at which thermal conductivity is being calculated, rather than for higher temperatures. When applied at the lower temperatures in the experimental distribution, this approach has the advantage of being less sensitive than the calculated-current method to errors

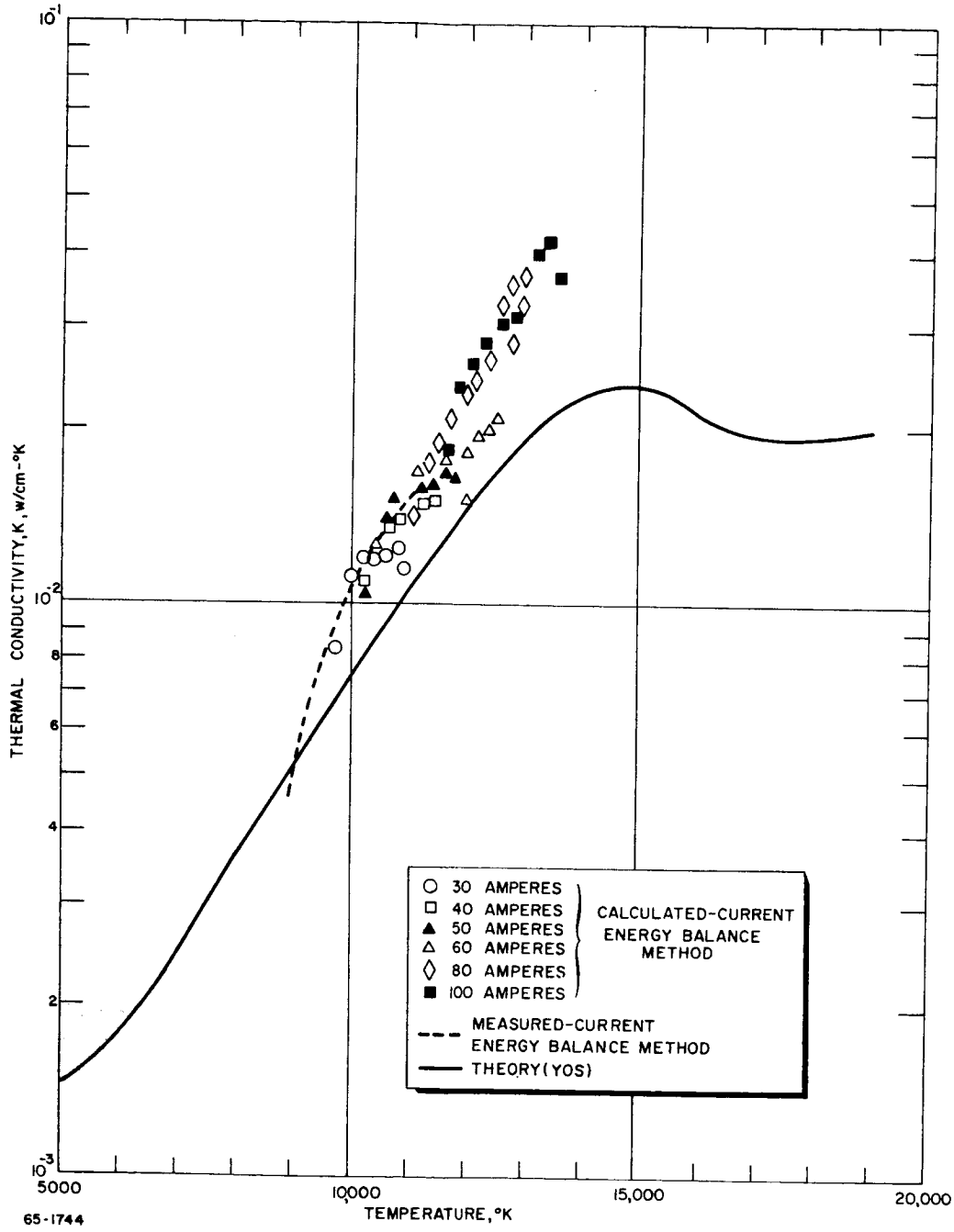

Figure 19 THERMAL CONDUCTIVITY OF ARGON FROM THE CALCULATED-CURRENT ENERGY BALANCE METHOD

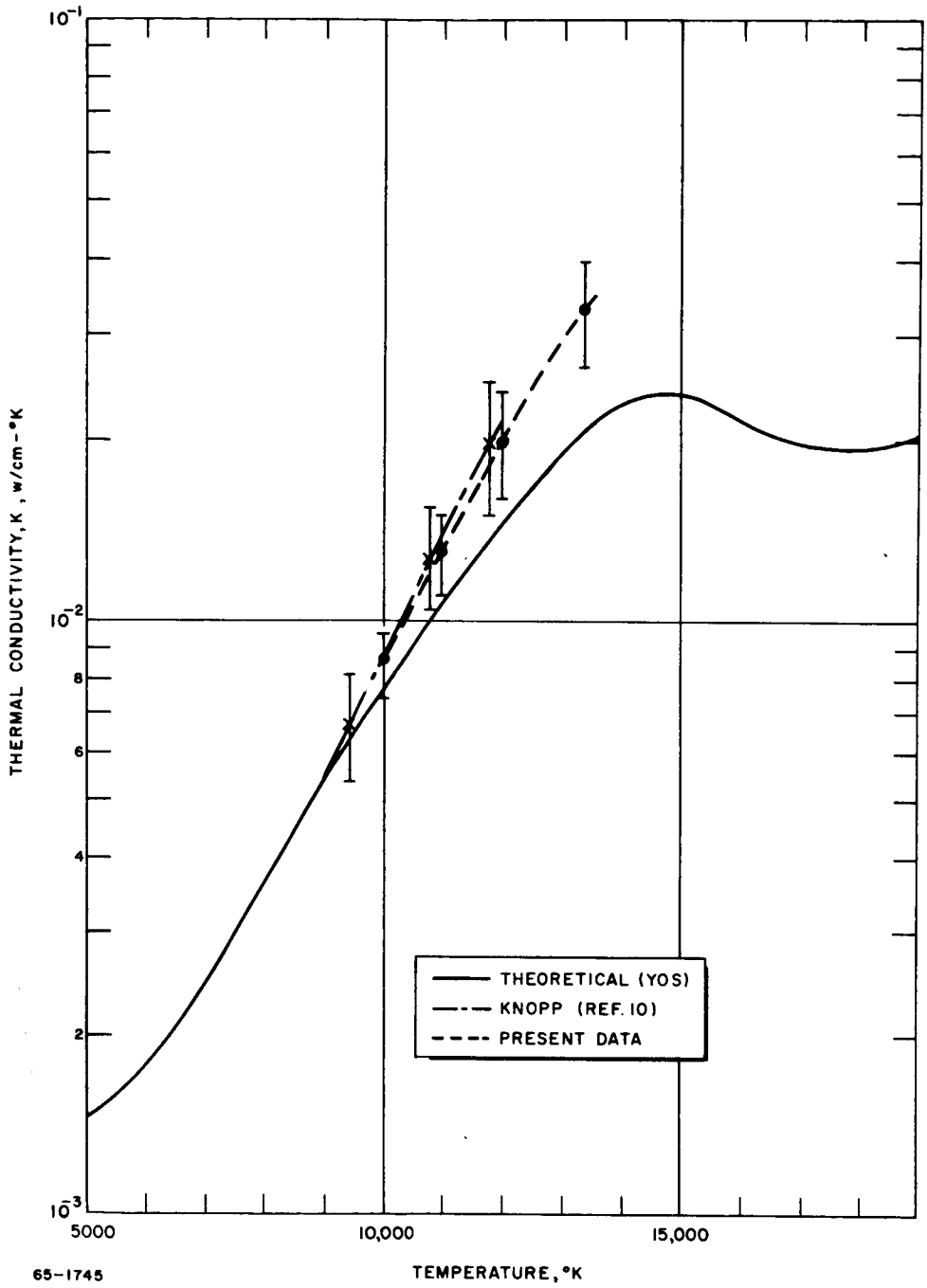

Figure 20 COMPARISON OF PRESENT RESULTS WITH THOSE OF A PREVIOUS INVESTIGATION OF THE THERMAL CONDUCTIVITY OF ARGON

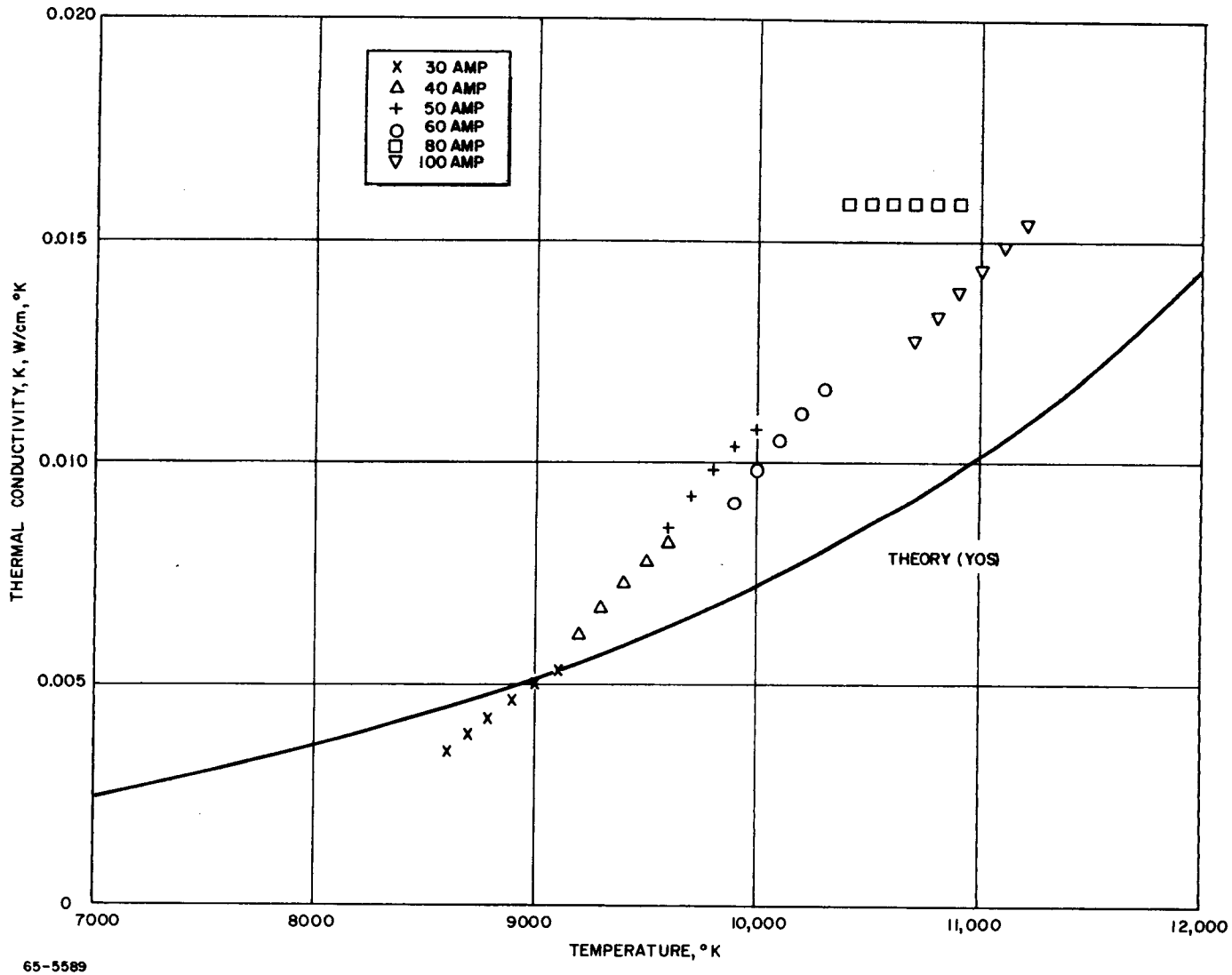

Figure 21 THERMAL CONDUCTIVITY OF ARGON FROM THE MEASURED-CURRENT ENERGY BALANCE METHOD

in the assumed theoretical electrical conductivity function. In the case of argon, at the lowest temperature for which the gradient dT/dr is determined with reasonable accuracy by the experimental data, the correction for current flow at larger radii is only 8 to 10 percent of the total current. Since the theoretical electrical conductivity affects only this relatively small correction, moderate errors in $\sigma(T)$ cannot have a major effect upon the calculation.

The temperature range shown in figure 21 for each arc current is that extending from the third Abel inversion point above the bottom of the experimental distribution up to the temperature at which the correction for current flow at larger radii is 20 percent of the total current. The points thus plotted follow a rather clearly defined locus which crosses the curve representing Yos's theoretical calculations at 9000°K and rises above it for higher temperatures. At 11,000°K, the thermal conductivity obtained by the measured-current energy-balance method is about 50 percent higher than the corresponding theoretical value. As already shown in figure 19, the results obtained by the measured-current method agree well with those of the calculated-current method in the temperature range where the two sets of results overlap.

The results presented in figure 21 have been used to select initial values of thermal conductivity, $K(T_o)$, for use in an analysis of the argon data by the two-run method. The thermal conductivity values resulting from this analysis are shown in figure 22. The various symbols appearing in this figure represent the eleven usable* pairwise combinations of the six different arc currents for which data are available. The filled-in symbols denote the combinations in which the two arc currents and axial temperatures differ by the largest factors. For these pairs of runs, random errors should be amplified least by the differencing procedures inherent in the two-run method. The open circle, square, triangle, and nabla represent pairs of runs with smaller differences in arc current, and would be expected to have intermediate sensitivity to random errors. The plus, times, and asterisk denote combinations with the smallest relative difference in arc current and the greatest sensitivity to random errors. The dashed line in figure 22 is the locus of assumed $K(T_o)$ values, based upon figure 21. The sequence of points representing the $K(T)$ values for each combination of arc currents always begins on this line. Essentially, the two-run method determines only the temperature dependence of $K(T)$, not the absolute value.

Figure 22 shows that the temperature dependence of $K(T)$ as indicated by the two-run analysis does not agree with that of the $K(T_o)$ values determined by the energy-balance method (figure 21). The points representing the results of the two-run calculation for each combination of arc runs tend to follow a horizontal trend (constant thermal conductivity) instead of rising with increasing temperature.

*In the four remaining combinations, the two temperature distributions do not overlap sufficiently to permit execution of the two-run analysis.

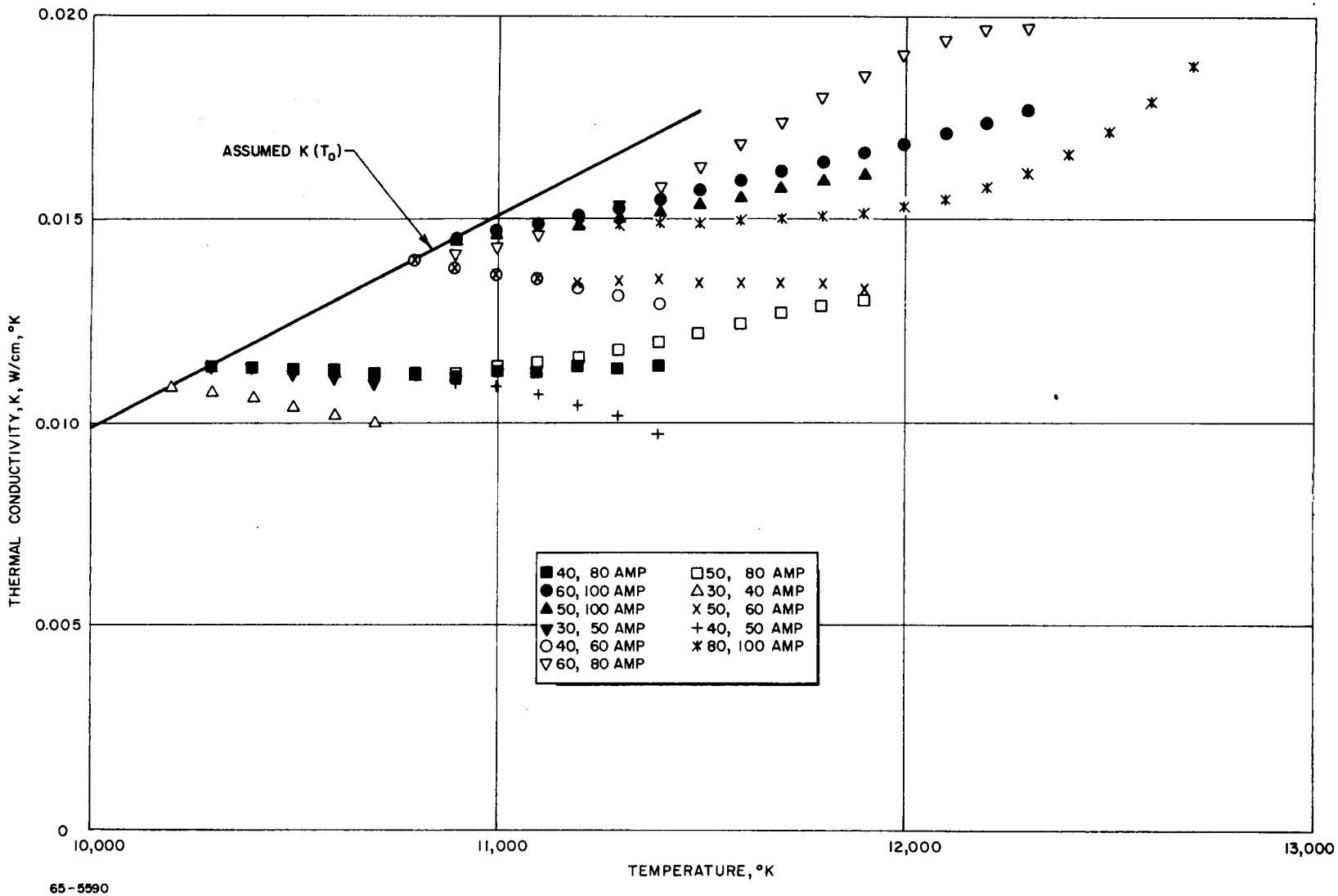

65-5590

Figure 22 THERMAL CONDUCTIVITY OF ARGON FROM THE TWO-RUN METHOD

Figure 23 shows the electrical conductivity values obtained from the two-run analysis of the argon data. In the case of σ, the absolute value as well as the temperature dependence is given by the calculation. The results from the various combinations of runs agree reasonably well, although there is considerable scatter because σ depends upon the second derivatives of the temperature distributions. On the average, the values are slightly lower than the dashed line representing Yos's theoretical calculations of electrical conductivity for equilibrium argon at one-atmosphere pressure. The approximate agreement with the theoretical curve is probably fortuitous.

The discrepancies between the results obtained by analyzing the argon data using the two-run method (figure 22) and the energy-balance methods (figures 19, 21) are attributed to the neglect of far-ultraviolet radiation and radiative transfer effects. The emission and reabsorption of argon recombination radiation provides an additional mechanism, not included in equation (5), for transporting energy outward through the arc column. The energy-balance methods, equations (10) and (12), credit this additional transport of energy to heat conduction, and thus yield effective conductivity values larger than the true thermal conductivity. Similarly, the two-run method, also based on the optically thin Elenbaas-Heller equation (5), yields unrealistic results when applied to the experimental temperature distributions, which are actually affected by the radiative transfer processes occurring in the far-ultraviolet.

Since the transport property results for argon (presented in figures 19, 21, 22, and 23) have been obtained from the experimental data without treating the effects of far-ultraviolet radiative transfer, these results cannot be considered definitive. The discrepancies between the experimental and theoretical values of thermal conductivity may be due, in part or in whole, to these neglected radiative effects.

3. Nitrogen Results

The calculated-current method has been employed to analyze the data from the nitrogen arc runs for which temperature profiles are shown in figures 14 and 15. Burhorn[23] and Maecker[24] have reported thermal conductivity data for nitrogen at temperatures up to 15,500°K. In order to compare the results obtained in this investigation with those of Maecker, the electrical conductivity assumed by Maecker in his analysis was used. Figure 24 shows the electrical conductivity of nitrogen as calculated by Maecker and by Yos.[11] The difference between the two is clearly not appreciable for temperatures between 9,000°K and 15,500°K.

In his work, Maecker considered that the radiative heat loss from nitrogen could be neglected compared with the energy flux due to thermal conductivity. Maecker's experimental results are shown in figure 25 along with the

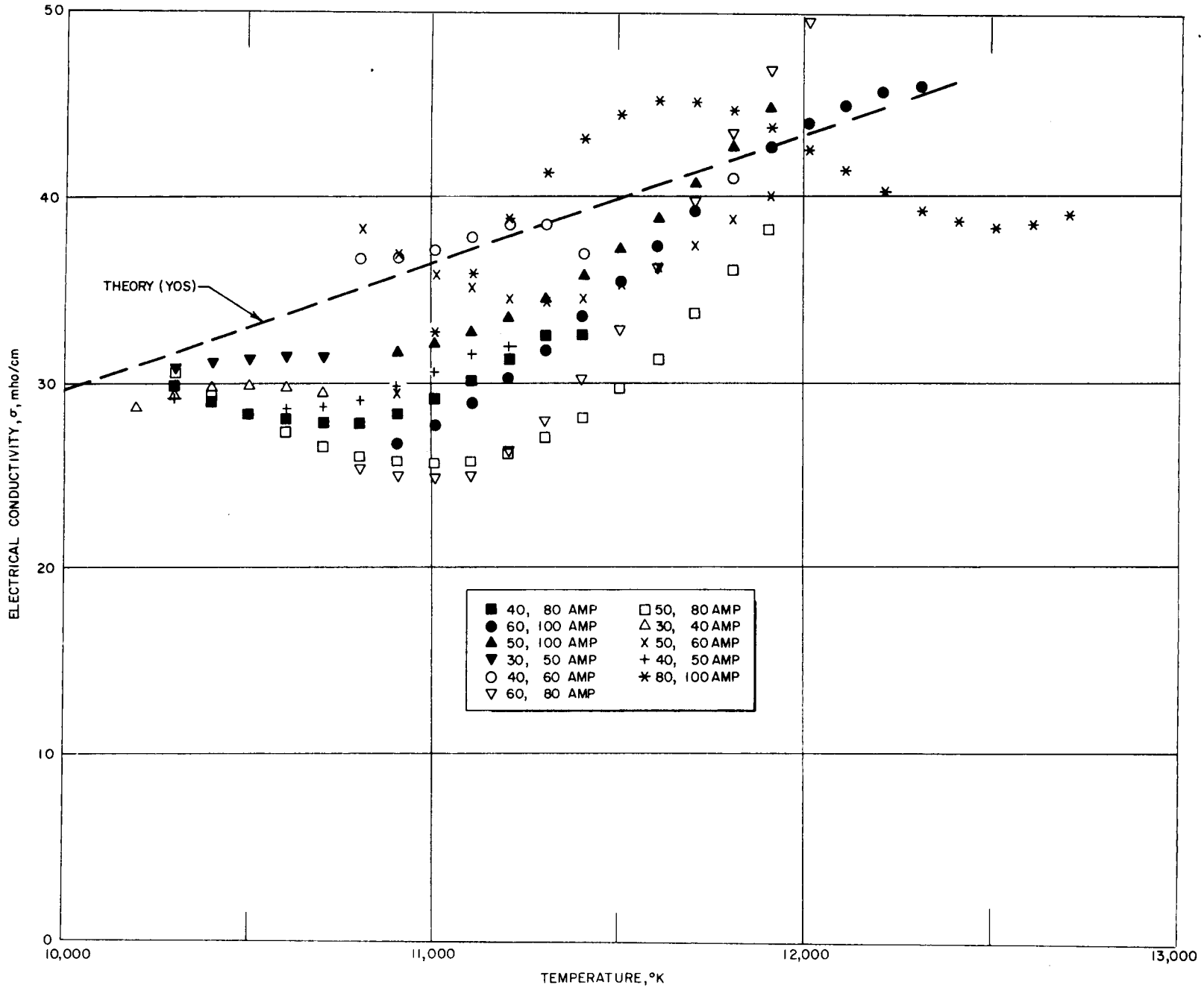

65-5591

Figure 23 ELECTRICAL CONDUCTIVITY OF ARGON FROM THE TWO-RUN METHOD

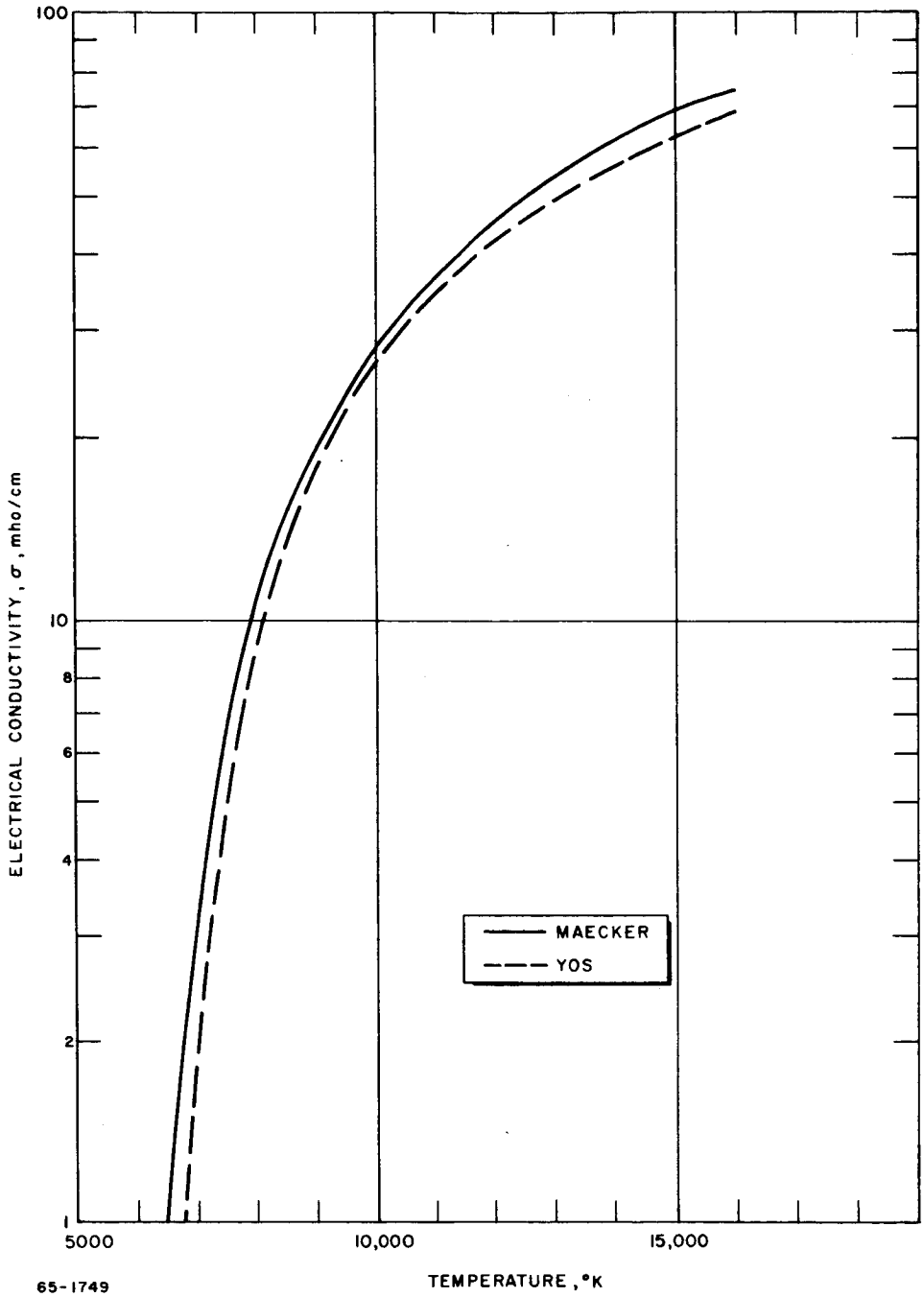

Figure 24 THEORETICAL ELECTRICAL CONDUCTIVITY OF NITROGEN

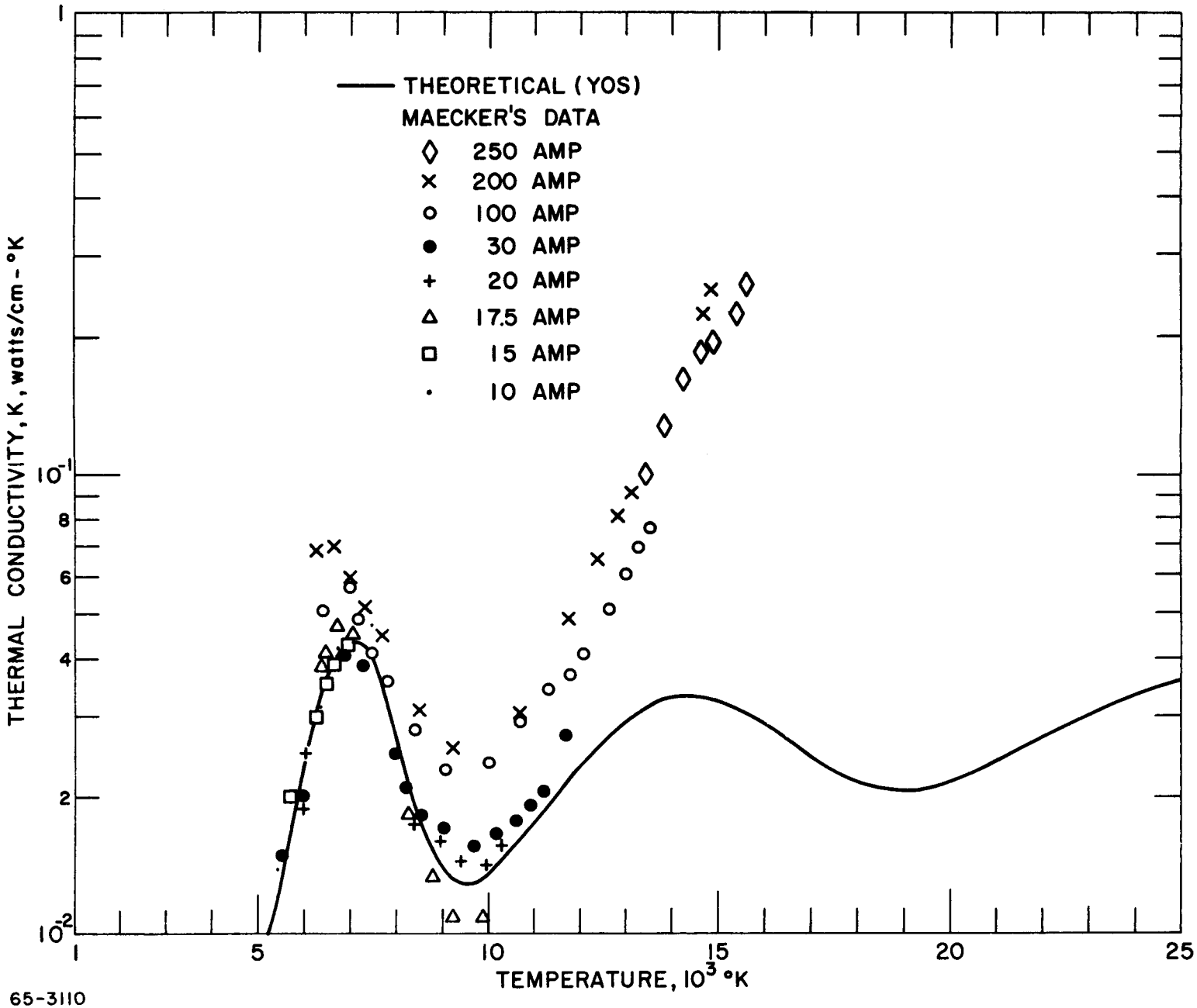

Figure 25 THE THERMAL CONDUCTIVITY OF NITROGEN AS DETERMINED BY MAECKER UNDER THE ASSUMPTION THAT RADIATIVE LOSSES ARE NEGLIGIBLE

theoretical thermal conductivity computed by Yos.* Apart from the large discrepancy between experimental and theoretical values, the most disturbing aspect of the experimental results is the apparent dependence of the thermal conductivity upon arc current, since the true conductivity is a property of the gas and not of the apparatus.

Figure 26 shows the thermal conductivity obtained from the measured temperature profiles and voltage gradients of the present investigation, given in figures 14 and 15, using the calculated-current method. Values of the radiative term used in the solution of the Elenbaas-Heller equation are shown by the solid line in figure 27. These data were measured in the same manner as the radiation data for argon, and for the same wavelength interval, i.e., 2500A to 6 microns. The electrical conductivity given by Maecker was used. It can be seen that the thermal conductivity results exhibit the same sort of dependence upon arc current as those of Maecker, and indeed are in good agreement with the values obtained by Maecker.

There is available a considerable amount of information suggesting that the power radiated from nitrogen at temperatures of 10,000°K to 20,000°K contains a large contribution from the far-ultraviolet at wavelengths below 2500A. Stewart and Pyatt[25] have calculated the continuous and discrete absorption coefficients as functions of temperature, density, and frequency for nitrogen among other light elements. Their results for a temperature of 1.5 ev (17,400°K) and a pressure of about 1 atmosphere show a giant absorption edge near 1100A. The absorption coefficient for wavelengths below this edge is about two orders of magnitude higher than that in the visible region of the spectrum. Correspondingly, nitrogen at typical arc temperatures in excess of 10,000°K would be expected to show intense emission at wavelengths less than 1100A. This conclusion is strengthened by recent experimental data of Allen, Textoris and Wilson,[26] obtained using a tungsten photoelectric gauge which is most sensitive below 1100A. These authors found that air at 9,500°K and about 1/4-atm pressure is nearly black over path lengths of 2 to 5 cm in the wavelength range to which the gauge responded.

The calculations of Stewart and Pyatt are based upon a hydrogenic approximation for the free-bound oscillator strengths. This approximation is of questionable accuracy. Burgess and Seaton[27] have calculated the free-bound absorption cross section for nitrogen using the quantum defect method and a coulombic field. Their results, which are believed to be more accurate than those obtained from the hydrogenic approximation, have been used to estimate the power radiated by nitrogen in the ultraviolet as a function of temperature and pressure. In estimating the ultraviolet radiation,

*The theoretical values presented by Maecker [24] are in relatively good agreement with his experimental results. However, these theoretical results did not include the effect of charge exchange, which has subsequently been shown to be of considerable importance.

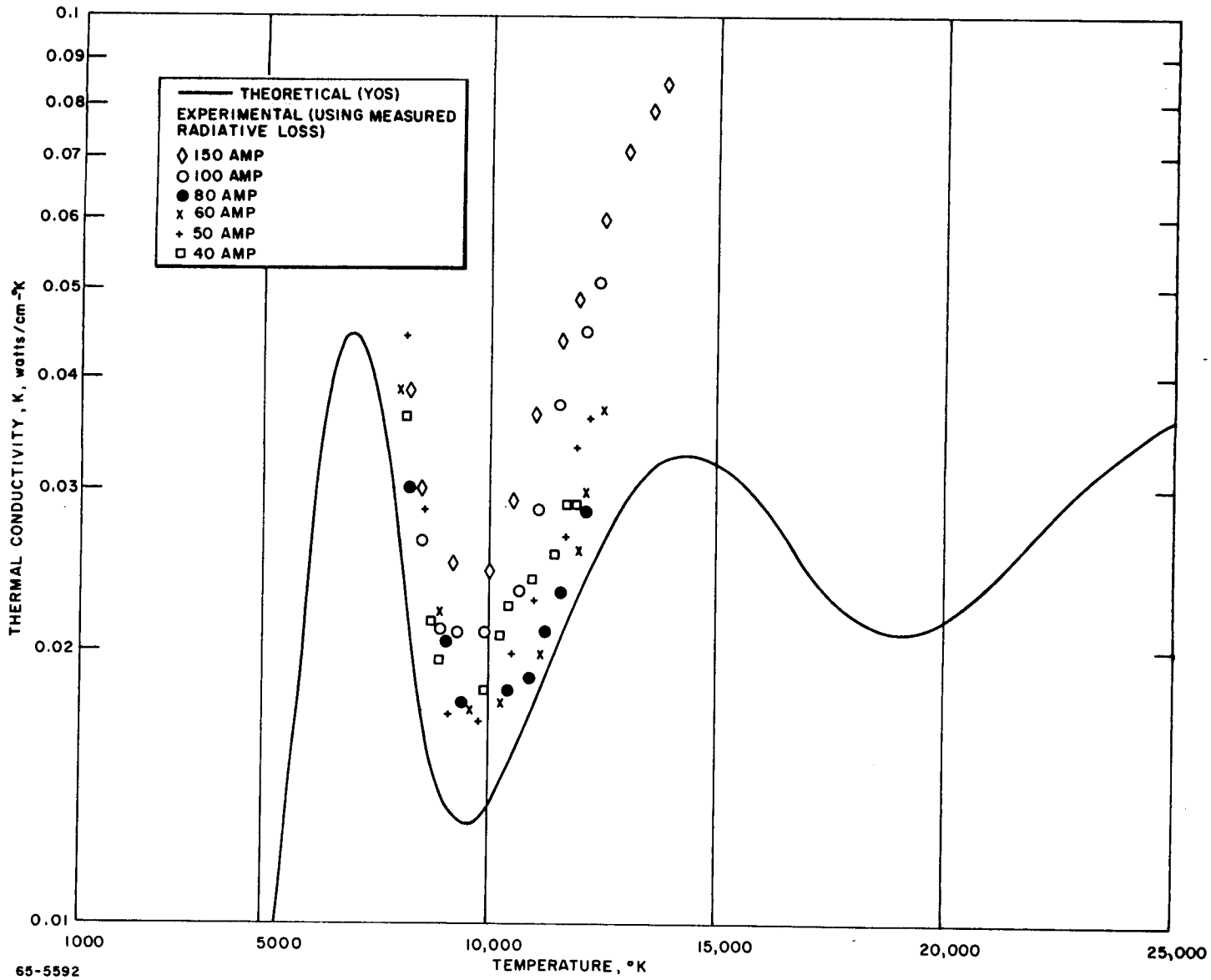

Figure 26 THERMAL CONDUCTIVITY OF NITROGEN FROM THE CALCULATED-CURRENT ENERGY BALANCE METHOD USING THE MEASURED RADIATIVE LOSS

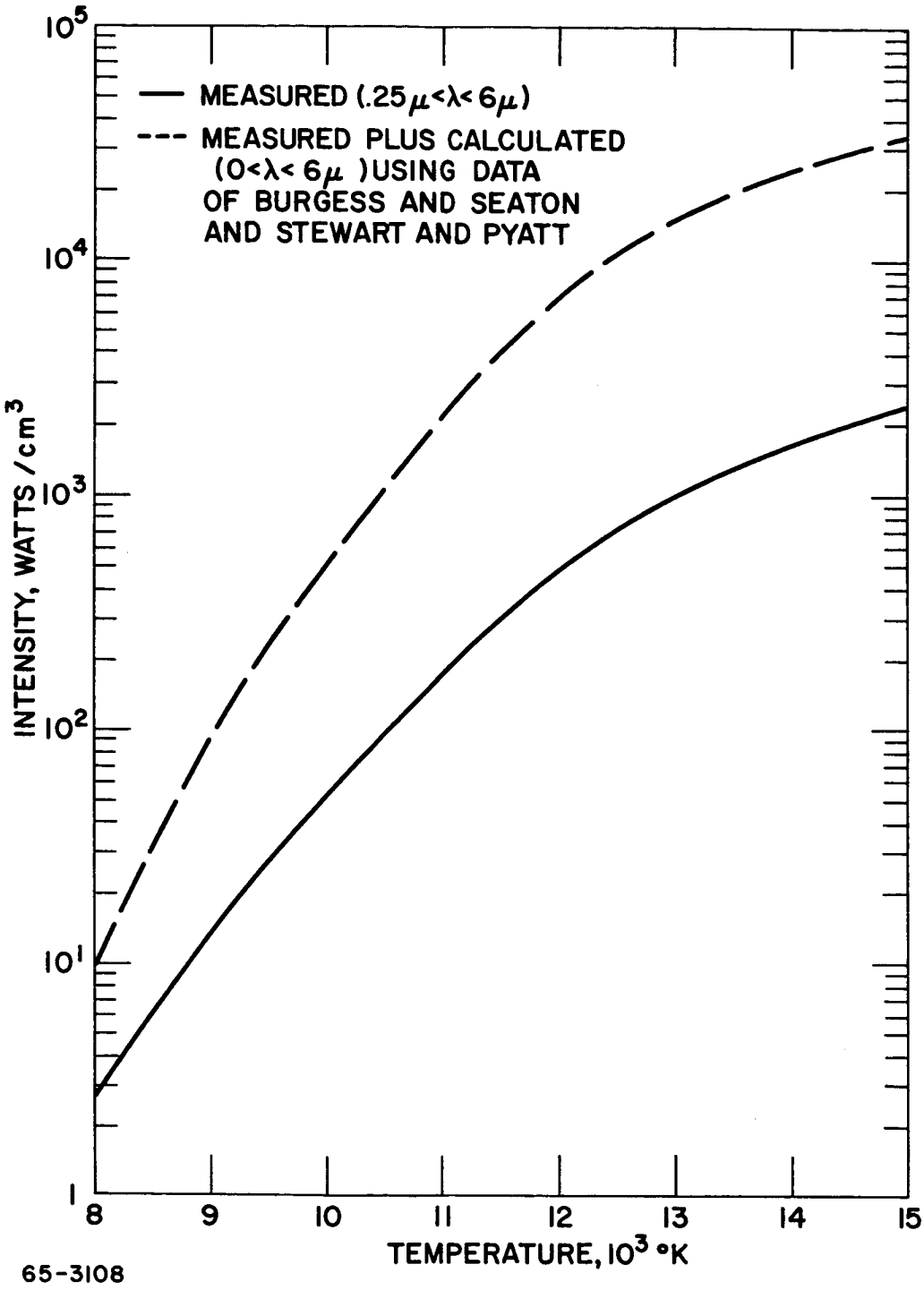

Figure 27 MEASURED AND MEASURED-PLUS-CALCULATED VALUES OF THE TOTAL RADIATION OF NITROGEN AT ATMOSPHERIC PRESSURE

it is important to include line radiation. An estimate of the contribution from lines was obtained by comparing the values given by Stewart and Pyatt for continuous and discrete absorption coefficients. These authors predict that the line radiation is approximately three times greater than continuum radiation at 1 atm for the temperatures and wavelength interval of interest.

The sum of radiated power calculated from the absolute magnitude of the far-ultraviolet continuum radiation predicted by Burgess and Seaton, the relative contribution of the line radiation given by Stewart and Pyatt, and the experimentally determined infrared, visible, and near-ultraviolet radiation is shown by the dashed curve in figure 27. Using this estimate of radiation with the electrical conductivity and temperature profiles given by Maecker,[24] the experimental data of Maecker have been reanalyzed by the calculated-current method, assuming the arc column to be optically thin.* Figure 28 shows the results obtained by thus including the ultraviolet radiation in the analysis of Maecker's data. Shown in the same figure are the results reported by Maecker and the theoretical values predicted by Yos. The change in the experimental results is most dramatic. Not only do the reanalyzed data agree more closely with the theoretical predictions, but also the strong current dependence of the data has been removed.

Figure 29 shows the thermal conductivity data obtained for nitrogen in this investigation using the radiated power given by the dashed curve of figure 27 and the calculated-current method, again assuming the column to be optically thin. It will be noted that the current dependence of the data of figure 29 is negligible. The excellent agreement between the theoretical and experimental values is probably somewhat fortuitous, particularly in view of the uncertainty in the calculation of the ultraviolet radiation. Below 9,000°K, the data do not show as good agreement with theory as Maecker's do, because molecular band structure becomes superimposed upon the continuum, so that use of continuum radiation measurements to determine temperature becomes questionable below this temperature.

The experimental uncertainties in the nitrogen data are approximately the same as those in the argon data, except for that in the electric field. The measurements of the voltage gradient in nitrogen exhibited more scatter than did the measurements in argon. Consequently, it is felt that random errors in the nitrogen voltage gradients produce an uncertainty of ±4 percent. An error analysis similar to that given for argon then indicates that random errors in the measurements of thermal conductivity for nitrogen should range from ±12 percent to ±17 percent, the larger value pertaining to temperatures above 13,000°K and below 9000°K. In addition, the measurements are affected by systematic errors of undetermined magnitude resulting from uncertainties in the theoretical electrical conductivity and the

*The Stewart-Pyatt and Burgess-Seaton calculations indicate that the fully dissociated portion of an arc column in nitrogen is fairly transparent to the far-ultraviolet radiation. However, this radiation is strongly absorbed in the surrounding region of molecular nitrogen.

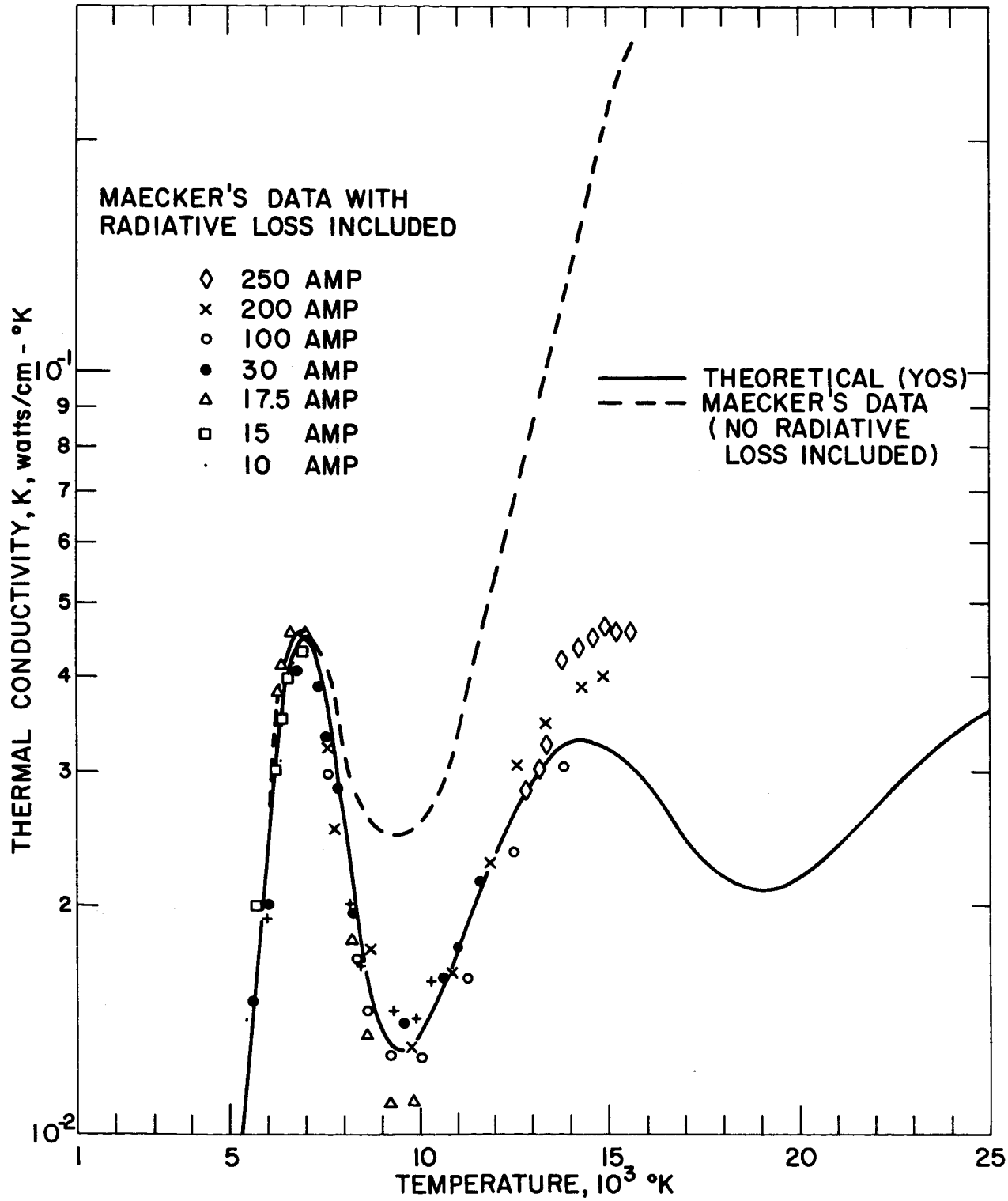

65-3109

Figure 28 THERMAL CONDUCTIVITY OF NITROGEN DETERMINED FROM THE DATA OF MAECKER WITH THE INCLUSION OF CALCULATED AND MEASURED RADIATIVE LOSSES

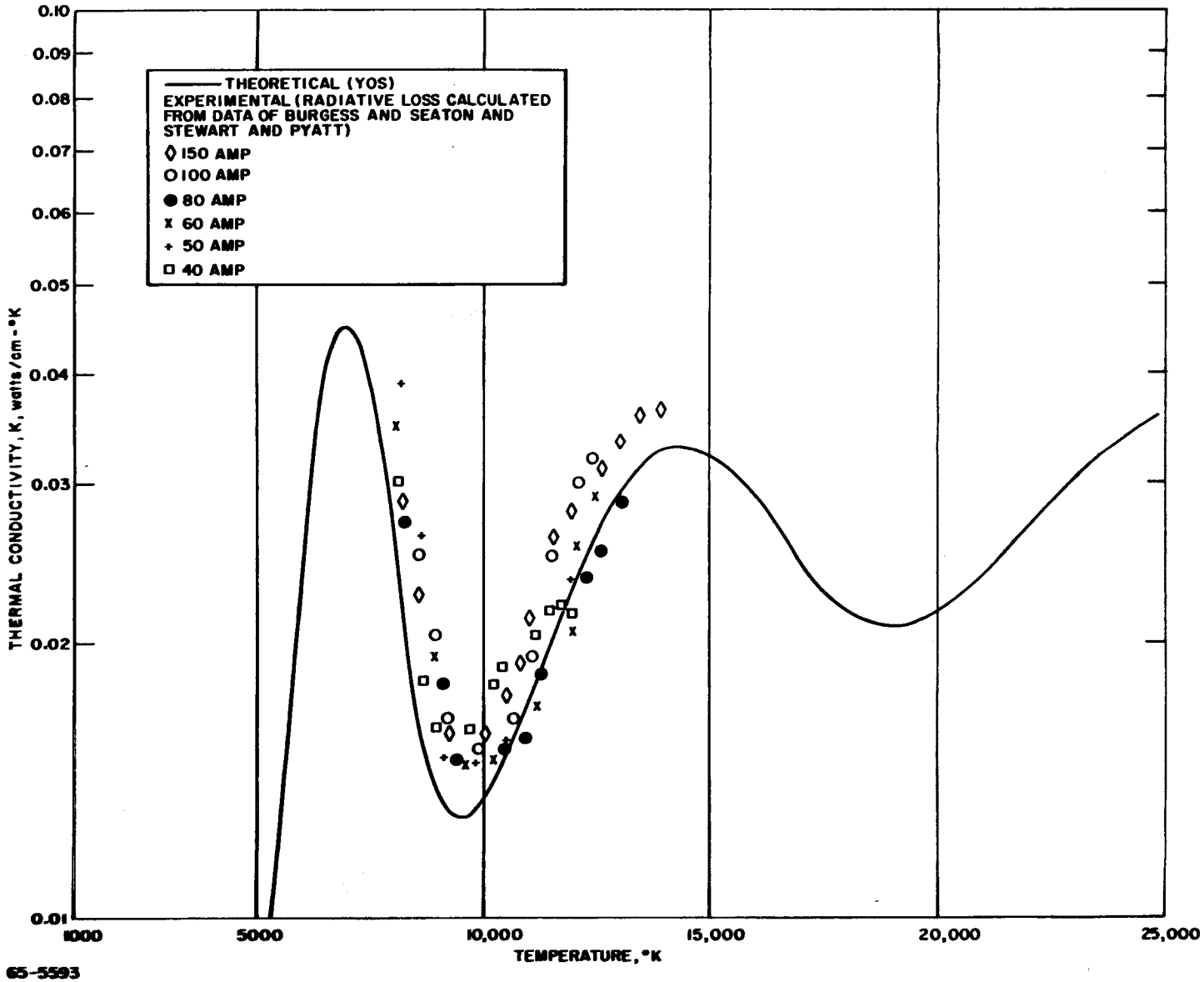

65-5593

Figure 29 THERMAL CONDUCTIVITY OF NITROGEN FROM THE CALCULATED-CURRENT METHOD WITH THE INCLUSION OF CALCULATED AND MEASURED RADIATIVE LOSSES

calculated far-ultraviolet radiation, and from possible effects of reabsorption of the ultraviolet radiation within the arc column.

Because of the uncertainty in the estimated ultraviolet radiation and the neglect of reabsorption of this radiation within the arc column, the thermal conductivity values presented in figure 29 cannot be regarded as definitive. However, it appears highly probable that the discrepancies exhibited in figures 25 and 26 are largely attributable to neglect of far-ultraviolet radiation in the data analysis. The great importance of this ultraviolet radiation poses a serious problem in the experimental determination of thermal conductivity. As shown in figure 30, at temperatures approaching 15,000°K the radiated power including the far-ultraviolet is a substantial fraction of the total arc power. The power radiated from the high-temperature region near the axis is an even larger fraction of the power produced by electrical dissipation in the same region. Thus, near the axis the power carried by heat conduction is a relatively small difference between two large terms, and these terms must be determined very precisely to obtain thermal conductivity values of useful accuracy. A possible solution to this problem would be to perform the experiments at somewhat reduced pressures, where the radiative loss would be less important.

F. CONCLUSIONS AND RECOMMENDATIONS

The following are the most important conclusions resulting from the first year of this program on transport property determinations using wall-stabilized arcs.

1. An electric arc operating in a constricting tube of segmented design, such as that used in the investigations reported above, is cylindrically symmetric to a sufficiently close approximation that data obtained from it can, in principle, be analyzed to determine transport properties.

2. The Elenbaas-Heller Equation in its usual "optically thin" form (5) is not applicable to arc columns at one atmosphere in argon and nitrogen (and probably in many other gases), because the arc plasma radiates substantial power at wavelengths in the far-ultraviolet to which at least some portions of the arc column are relatively opaque. To formulate this process properly, the energy equation for a cylindrical arc column must be written with the radiative contributions represented by transfer integrals instead of the simple volumetric loss term appearing in (5).

3. Therefore, the analysis of wall-stabilized arc data to obtain transport properties should be based on an energy equation with "transfer" treatment of the radiation, in place of equation (5). The formulation of such an equation and its solution for $K(T)$ in terms of $\sigma(T)$ and the experimental quantities do not appear prohibitively difficult, and should be attempted in the near future. Once these problems have been solved, the argon and nitrogen

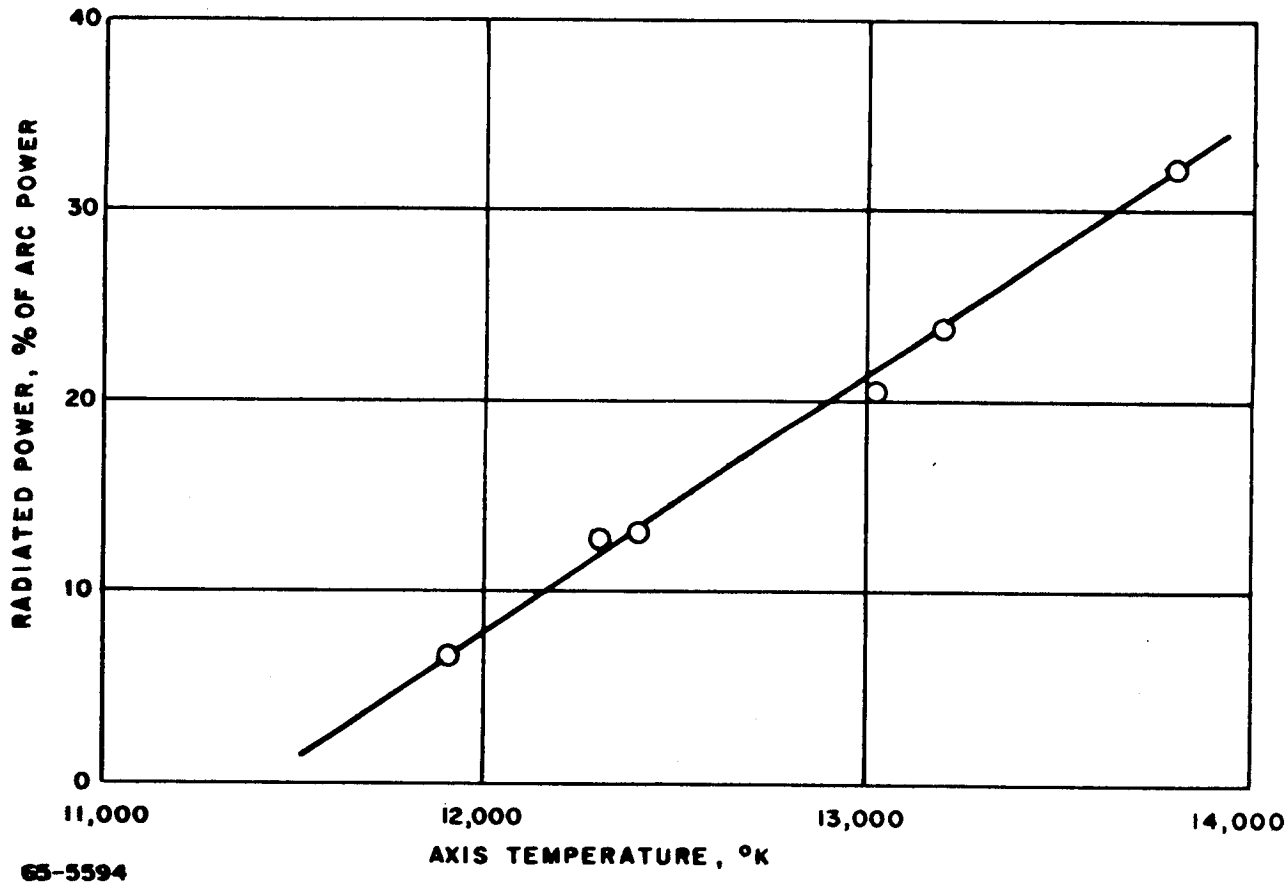

Figure 30 PERCENTAGE OF RADIATED POWER, BASED UPON THE SUM OF CALCULATED AND MEASURED RADIATION, AS A FUNCTION OF THE AXIS TEMPERATURE OF THE NITROGEN ARC

experimental data reported above should be reanalyzed to obtain the true thermal conductivity.

4. In addition, an attempt should be made to carry through an analysis similar to that presented in appendix A (upon which the two-run method is based) for an arc column with radiative transfer in the vacuum ultraviolet.

5. One obstacle to definitive analysis of arc data for the transport properties will be deficiencies in the available information on the optical properties of gases in the far-ultraviolet. Further theoretical and especially experimental study of these properties appears warranted.

6. Since energy transport by emission and reabsorption of far-ultraviolet radiation is several times as important as heat conduction in the nitrogen arc at high temperatures, the possible importance of this mechanism in various technological applications, such as heat shield design for space vehicles, should be examined.

III. HEITLER - LONDON INTERACTION POTENTIALS AND RESONANT CHARGE EXCHANGE CROSS SECTIONS FOR $N-N^+$ AND $O-O^+$ COLLISIONS

A. INTRODUCTION

The diffusion of atomic nitrogen and oxygen ions with respect to their parent atoms is important in a number of problems both in connection with the basic structure of the atmosphere[28-30] and with the performance of high-velocity re-entry vehicles in the atmosphere.[31] For example, at temperatures around 10,000 to 15,000°K, where air is fully dissociated and partially ionized, one finds that the ionization energy carried by the diffusion of atomic ions can represent a significant fraction of the total heat transfer in the gas,[2] and this effect must therefore be taken into account in the design of very high speed re-entry vehicles. Because of the difficulties involved in the experimental determination of thermal conductivities in this temperature region (see section II), engineering calculations in this regime must rely heavily on theoretical calculations of the thermal conductivity, based on independently determined values of the N^+ and O^+ diffusion coefficients.

Because of the very large cross sections for resonant charge exchange between an ion and its parent atom, it is this process which largely determines the rate of diffusion of the N^+ and O^+ ions in most circumstances.[32, 33] A number of approximate calculations of the $N-N^+$ and $O-O^+$ charge exchange cross sections have been given in the literature,[2, 6, 33, 34] and recently the $O-O^+$ cross section has been determined experimentally by a crossed beam technique.[5]

Unfortunately, the calculations do not agree well among themselves or with experiment, differences between the various determinations of the cross-sections ranging from about 50 percent to better than a factor of 3 (see figures 38 and 39.)* In order to attempt to clear up these discrepancies and provide a more reliable value for this important quantity, we have therefore undertaken the present, more detailed calculation of the $N-N^+$ and $O-O^+$ charge-exchange cross sections.

For the ion energies which are of importance for the study of diffusion in atmospheric gases (say about 0.1 to 10 ev), it is generally acknowledged that the semi-classical impact parameter approximation gives a quite accurate description of the charge exchange process.[32-36] In this approximation, the motion of the colliding nuclei is treated classically and the probability P_{ex} of charge exchange during any collision is calculated from the relation

*Note that the interaction potentials and charge exchange cross sections reported in reference 6 do not appear to be consistent with each other. It is not clear which of these values was intended by the authors, and hence both the cross sections reported in reference 6 and the cross sections calculated from the reported interaction potentials have been shown in figures 38 and 39.

$$P_{ex} = \sin^2 \int_{-\infty}^{\infty} \frac{\Delta E}{2\hbar} \, dt \tag{13}$$

where $\Delta E = \Delta E(R)$ is the difference in energy between the symmetric and anti-symmetric electronic states of the system for a fixed internuclear separation R, and the integral is evaluated along the classical trajectory of the nuclear motion. The cross section Q_{ex} for charge exchange is then found by integrating equation (13) over all collisions having a given energy, according to the classical formula

$$Q_{ex} = 2\pi \int_{0}^{\infty} P_{ex} \, b \, db, \tag{14}$$

where b is the classical impact parameter for the collision. For non-closed-shell atoms and ions, equations (13) and (14) are applied separately to each possible angular momentum state of the interacting atoms, and the total charge exchange cross section is then found by averaging the partial cross sections (14) over all angular momentum states.[37]

In order to calculate Q_{ex} from equations (13) and (14) it is evidently necessary to know the energy difference ΔE occuring in equation (13) as a function of R, and it is the determination of this quantity which ordinarily accounts for the major part of the work in any actual calculation of Q_{ex}. Although equations (13) and (14) involve the value of ΔE at all internuclear separations R, a simple consideration of the nature of the solutions shows that in fact the value of Q_{ex} calculated from (13) and (14) is only sensitive to values of ΔE in the neighborhood of the critical impact parameter b_c for which the argument $\int_{-\infty}^{\infty} (\Delta E/2\hbar)\, dt$ in equation (13) is of the order of $\pi/4$.[32-37] Thus, for calculations of Q_{ex}, it is only necessary to know the value of ΔE accurately for separations R in the neighborhood of this critical value. An approximate integration of equation (13) shows that the value of ΔE at the critical separation is approximately (see equation (117b) below)

$$(\Delta E)_c \approx \frac{\hbar v}{2} \sqrt{\frac{\pi}{2\rho b_c}} = 0.057 \frac{1}{\sqrt{\rho b_c}} \sqrt{\frac{E}{M}} \text{ ev} \tag{15}$$

where $\frac{1}{\rho} = -\frac{1}{\Delta E}\frac{d\Delta E}{dr}$ is the logarithmic derivative of ΔE evaluated at the critical impact parameter b_c, E is the energy of the impinging ion in ev, M is the atomic weight, and the distances ρ and b_c are measured in Å. For reasonable values

of the parameters ρ and b_c, equation (15) gives a critical energy difference $(\Delta E)_c \approx 0.01$ ev for ion energies $E \sim 1$ ev. This is a rather small interaction energy compared to molecular binding energies ($\sim$5 to 10 ev) and thus corresponds to a rather large separation between the interacting atom and ion.

For the relatively large internuclear separations of interest in the present work, the interaction between an atom and ion may be divided essentially into two components: the exchange force, which arises from the overlapping of the electronic charge clouds, and the London-van der Waals polarization force, which arises from the long-range electrical interactions between the two particles.[38, 39] Although the polarization force contributes a large part of the total interaction energy at these separations, it is essentially the same for the symmetric and antisymmetric states and so makes only a small contribution to the energy difference ΔE between the states.[33, 38] Thus the problem of calculating resonant charge exchange cross sections from equations (13) and (14) reduces essentially to that of obtaining reasonably accurate estimates of the exchange force between an atom and ion at rather large internuclear separations. There is very little quantitative information on the exchange force at such separations available in the literature,[38] and the uncertainty in the values used for this force has apparently been the major source of error in previous calculations of Q_{ex}.[2, 6, 33, 34]

In the present work, the interaction energies for the N-N^+ and O-O^+ systems have been calculated by means of the Heitler-London method,[40, 41] in which the interaction is treated as a perturbation of the isolated atom and ion at infinite separation. Although this was one of the first methods developed for the treatment of intermolecular forces,[40] it has been used only rarely in the subsequent literature, and then in most cases only for rather simple systems.[38, 41-46] The reason for this neglect is not altogether clear, but it appears to be mainly because the primary interest has been in obtaining potentials for diatomic molecules near the equilibrium separation, where the Heitler-London method gives rather poor results.[41] For the very much weaker interactions of interest in the present work, however, one might expect the Heitler-London method to be considerably better, since it is basically a large R approximation; and this theoretical expectation is borne out by the limited data presently available on the exchange force at large internuclear separations.[38] In the case of H_2^+, for example, where the exact potentials are known from theory,[47] one finds that the energy difference ΔE calculated from the simple Heitler-London treatment differs by only about 10 percent from the exact theoretical value over the range of separations of interest for the charge exchange problem. It thus appears that the Heitler-London approach to the calculation of interatomic potentials may offer a promising technique for the study of the exchange force between atoms at large internuclear separations, and that a re-examination of the method in this connection would be desirable.

In the present report, a generalized version of the Heitler- London method is developed which is applicable to any pair of atoms and/or atomic ions, with

either open or closed electronic shells, and this method is then applied to calculate all the Heitler-London interaction potentials between the ground-state atoms and ions for the systems N-N^+ and O-O^+. In this calculation, analytic Hartree-Fock wave functions from the literature are used for the unperturbed atom and ion,[48] and the results are carried only to first order in the expansion parameter $e^{-\zeta R}$, where ζ is one of the orbital exponents in the atomic wavefunction. The interaction potentials calculated in this way are then substituted into equations (13) and (14) to obtain the total charge exchange cross sections Q_{ex} and the diffusion cross sections $\bar{\Omega}^{(1,1)}$ for the N-N^+ and O-O^+ systems.

B. UNPERTURBED WAVEFUNCTIONS FOR THE ATOM-ION SYSTEM

1. Atomic Wavefunctions

Before discussing the unperturbed wavefunctions for the interacting system, let us first review briefly the properties of the Hartree-Fock atomic wavefunctions which will be required in the calculations.* The (restricted) Hartree-Fock wavefunctions for an isolated atom are in the form of sums of Slater determinants of one-electron wavefunctions. Each one-electron function ψ_i is taken to be a product of a radial wavefunction R, a spherical harmonic Y, and a spin function χ,

$$\psi_i(\vec{r}) = R_{n_i l_i}(r)\, Y_{l_i m_{l_i}}(\theta,\phi)\, \chi_{m_{s_i}}(\sigma).$$

$$= u_i(\vec{r})\, \chi_{m_{s_i}}(\sigma) \tag{16}$$

where $u(\vec{r}) \equiv R(r)\, Y(\theta,\phi)$ denotes the spatial part of the wavefunction. Each wavefunction ψ_i is identified by the four quantum numbers, n, l, m_l, and m_s, indicating the principal quantum number, the orbital angular momentum, the z-component of the orbital angular momentum, and the z-component of the spin, respectively. Two wavefunctions having the same values of n and l are said to belong to the same shell; all wavefunctions in the same shell are assumed to have the same radial part $R = R_{nl}(r)$. In the present work, it will be assumed that the $R_{nl}(r)$ are of the form

$$R_{n_i l_i}(r) = \sum_{j=0}^{N_i} c_{ij}\, r^{n_{ij}-1}\, e^{-\zeta_{ij} r}, \tag{17}$$

where the n_{ij} are integers greater than or equal to l_i+1, N_i is an integer, and the constants c_{ij} and ζ_{ij} are chosen to give a good approximation to the true Hartree-Fock functions. Values of these constants for the atoms and ions of interest in the present work have been calculated recently by a number of authors;[48, 50-53] for the present work we have used the values of Clementi given in table I.

*This information is taken mainly from reference 49, and the reader is referred to that work for further details.

TABLE I

PARAMETERS IN THE ANALYTIC HARTREE-FOCK WAVEFUNCTIONS FOR THE GROUND-STATES OF N, N^+, O, AND O^+ (FROM REFERENCE 48)

Species	i	n_{s_i}	ζ_{s_i}	c_{1s_i}	c_{2s_i}	n_{p_i}	ζ_{p_i}	c_{2p_i}
N	1	1	6.4730	30.5402	-7.01724	2	1.1937	0.534425
	2	1	10.970	4.60058	-0.72449	2	1.7124	2.14388
	3	2	1.5937	-0.00263	2.21838	2	3.0112	5.10224
	4	2	2.6295	0.05204	6.64907	2	7.1018	2.09829
	5	2	5.5731	1.50537	-7.87483			
N^+	1	1	6.38207	29.8110	-6.38248	2	1.44588	0.642802
	2	1	10.6536	5.34258	-1.83256	2	1.93941	3.73057
	3	2	1.79832	-0.01337	2.78752	2	3.40192	5.00108
	4	2	2.50239	0.07309	6.01234	2	7.79579	1.75366
	5	2	6.38917	0.50995	-10.91376			
O	1	1	7.6063	39.2169	-9.28733	2	1.1536	0.270232
	2	1	13.224	3.95292	-0.50105	2	1.7960	2.87509
	3	2	1.8792	0.00073	3.49860	2	3.4379	8.44957
	4	2	3.1441	0.04655	10.0411	2	7.9070	3.03487
	5	2	6.3783	4.19038	-12.3872			
O^+	1	1	7.47803	38.1978	-9.69320	2	1.67702	1.16971
	2	1	12.6307	4.98180	-0.50363	2	2.23780	4.56034
	3	2	2.07323	-0.00879	4.53590	2	3.82447	7.91973
	4	2	3.10090	0.09287	9.24941	2	8.58105	2.65757
	5	2	6.37277	2.13681	-11.2772			

gives an antisymmetric function of N electrons in which one-electron is in each of the one-electron states ψ_i (though of course one cannot say which electron is in any given state). From the definition, one sees that if two of the one-electron states are the same, the corresponding Slater determinant (equation 19) will be zero, since it will have two rows the same. Hence, there cannot be more than one-electron in any state or more than $2(2l + 1)$ electrons in any shell. A shell containing the maximum possible number of electrons is called a closed shell.

Two Slater determinants are said to belong to the same configuration if they have the same number of electrons in each shell. The configuration is generally indicated by placing the number of electrons in each shell as an exponent to the shell symbol; thus $1s^2\ 2s^2\ 2p^3$ would indicate a configuration having two electrons in states with $n = 1$, $l = 0$, two electrons in states with $n = 2$, $l = 0$ and three electrons in states with $n = 2$, $l = 1$. The different Slater determinants within a given configuration are then distinguished by indicating the values of m_l and m_s for the individual electrons. In this connection it is, of course, only necessary to specify the values of m_l and m_s for the electrons in unfilled shells, since the values for the electrons in closed shells are always the same. Following Slater, we indicate the one-electron wavefunctions by $m_l^{\pm}$, where $\pm$ indicates the sign of m_s, and indicate the Slater determinant formed from given electronic states by enclosing the symbols for those states in parentheses. In order to make the sign of the determinant definite, we specify that the symbols for the different states should be written in the same order in which the corresponding wavefunctions occur in the Slater determinant, and that the closed shells should always be taken in the same order. As an example of the notation, the Slater determinant belonging to the $1s^2\ 2s^2\ 2p^3$ configuration and having the quantum numbers $m_l = 1$, $m_s = 1/2$; $m_l = -1$, $m_s = 1/2$ and $m_l = 0$, $m_s = -1/2$, respectively, for the three 2p electrons would be denoted by the symbol $(1^+, -1^+, 0^-)$.

The Hartree-Fock wavefunctions for an atom are formed by taking linear combinations of Slater determinants belonging to a single configuration in such a way that the resulting wavefunctions are eigen-functions of the orbital angular momentum and spin operators for the atom as a whole. These wavefunctions are thus identified by the four quantum numbers L, S, M_L, and M_S, indicating the total orbital angular momentum, the total spin angular momentum, the z-component of the orbital angular momentum, and the z-component of the spin, respectively. Methods for finding the proper linear combinations of Slater determinants are described by Slater in chapter 20 of reference 49; the results for a good many cases are tabulated in appendix 24 of reference 49. Using Slater's methods and results, we have calculated table II, which gives the proper Hartree-Fock wavefunctions for the ground-states of atoms and ions having an unfilled p-shell. Since closed shells do not affect the results given in table II, we have specified only the unfilled shells in compiling the table.

The spherical harmonics Y_{lm} in equation (16) are given by the general formula

$$Y_{lm}(\theta, \phi) = (-1)^{(m+|m|)/2} \sqrt{\frac{(2l+1)(l-|m|)!}{4\pi(l+|m|)!}} \; P_l^{|m|}(\cos\theta) e^{im\phi} \quad (18a)$$

where the $P_l^{|m|}(\cos\theta)$ are the usual associated Legendre functions; in our work we shall be dealing only with s and p electrons (i.e., electrons with $l = 0$ and 1, respectively), so that Y_{lm} takes on one of the four following forms:

$$Y_{00} = \frac{1}{\sqrt{4\pi}}$$

$$Y_{11} = -\frac{1}{\sqrt{4\pi}} \sqrt{\frac{3}{2}} \sin\theta \; e^{i\phi}$$

$$Y_{10} = \frac{1}{\sqrt{4\pi}} \sqrt{3} \cos\theta$$

$$Y_{1,-1} = \frac{1}{\sqrt{4\pi}} \sqrt{\frac{3}{2}} \sin\theta \; e^{-i\phi} \quad (18b)$$

The spin quantum number m_s in equation (16) may take on two possible values, $m_s = \pm 1/2$, corresponding to the two possible spin states of an electron, either "up" or "down."

For a given set of one-electron wavefunctions ψ_i ($i = 1, 2, \ldots N$) the Slater determinant

$$\psi(\vec{r}_1, \vec{r}_2, \ldots, \vec{r}_N) \equiv \frac{1}{\sqrt{N!}} \; |\psi_i(\vec{r}_j)|$$

$$\equiv \frac{1}{\sqrt{N!}} \begin{vmatrix} \psi_1(\vec{r}_1) & \cdots & \psi_1(\vec{r}_N) \\ \vdots & & \vdots \\ \psi_N(\vec{r}_1) & \cdots & \psi_N(\vec{r}_N) \end{vmatrix} \quad (19)$$

TABLE II

HARTREE-FOCK WAVEFUNCTIONS FOR THE GROUND STATES OF ATOMS AND IONS HAVING AN UNFILLED p-SHELL

Species	Configuration	Ground-State	L	S	M_L	M_S	Hartree-Fock Wavefunction, ψ
C^+	np^1	^2P	1	$\frac{1}{2}$	1	$\frac{1}{2}$	(1^+)
					1	$-\frac{1}{2}$	(1^-)
					0	$\frac{1}{2}$	(0^+)
					0	$-\frac{1}{2}$	(0^-)
					-1	$\frac{1}{2}$	(-1^+)
					-1	$-\frac{1}{2}$	(-1^-)
C, N^+	np^2	^3P	1	1	1	1	$(1^+, 0^+)$
					1	0	$\frac{1}{\sqrt{2}}[(1^-, 0^+) + (1^+, 0^-)]$
					1	-1	$(1^-, 0^-)$
					0	1	$(1^+, -1^+)$
					0	0	$\frac{1}{\sqrt{2}}[(1^-, -1^+) + (1^+, -1^-)]$
					0	-1	$(1^-, -1^-)$
					-1	1	$(0^+, -1^+)$
					-1	0	$\frac{1}{\sqrt{2}}[(0^-, -1^+) + (0^+, -1^-)]$
					-1	-1	$(0^-, -1^-)$
N, O^+	np^3	^4S	0	$\frac{3}{2}$	0	$\frac{3}{2}$	$(1^+, 0^+, -1^+)$
					0	$\frac{1}{2}$	$\frac{1}{\sqrt{3}}[(1^-, 0^+, -1^+) + (1^+, 0^-, -1^+) + (1^+, 0^+, -1^-)]$
					0	$-\frac{1}{2}$	$\frac{1}{\sqrt{3}}[(1^-, 0^-, -1^+) + (1^-, 0^+, -1^-) + (1^+, 0^-, -1^-)]$
					0	$-\frac{3}{2}$	$(1^-, 0^-, -1^-)$
O	np^4	^3P	1	1	1	1	$(1^+, 0^+, -1^+, 1^-)$
					1	0	$\frac{1}{\sqrt{2}}[(1^+, 0^+, -1^-, 1^-) + (1^+, 0^-, -1^+, 1^-)]$
					1	-1	$(1^+, 0^-, -1^-, 1^-)$
					0	1	$(0^+, -1^+, 1^+, 0^-)$
					0	0	$\frac{1}{\sqrt{2}}[(0^+, -1^+, 1^-, 0^-) + (0^+, -1^-, 1^+, 0^-)]$
					0	-1	$(0^+, -1^-, 1^-, 0^-)$
					-1	1	$(-1^+, 1^+, 0^+, -1^-)$
					-1	0	$\frac{1}{\sqrt{2}}[(-1^+, 1^+, 0^-, -1^-) + (-1^+, 1^-, 0^+, -1^-)]$
					-1	-1	$(-1^+, 1^-, 0^-, -1^-)$
	np^5	^2P	1	$\frac{1}{2}$	1	$\frac{1}{2}$	$(1^+, 1^-, 0^+, 0^-, -1^+)$
					1	$-\frac{1}{2}$	$(1^+, 1^-, 0^+, 0^-, -1^-)$
					0	$\frac{1}{2}$	$(-1^+, -1^-, 1^+, 1^-, 0^+)$
					0	$-\frac{1}{2}$	$(-1^+, -1^-, 1^+, 1^-, 0^-)$
					-1	$\frac{1}{2}$	$(0^+, 0^-, -1^+, -1^-, 1^+)$
					-1	$-\frac{1}{2}$	$(0^+, 0^-, -1^+, -1^-, 1^-)$

Table II is complete in the sense that it gives the proper linear combinations of Slater determinants for all the ground-state wavefunctions of the listed configurations. In the case of the configurations np^2, np^3, and np^4; however, there are also other linear combinations of Slater determinants of the same configuration which have different values of the quantum numbers L and S, and which are not listed in table II. These linear combinations correspond to low-lying excited states of the atom or ion. For example, the nitrogen atom has low lying ^2D and ^2P excited states at 2.38 and 3.65 ev above the ground level, respectively, which have the same electronic configuration as the ground-state; whereas, the other excited states, which correspond to different configurations, all have energies greater than 10 ev.

2. Unperturbed Wavefunctions for the Ion-Atom Pair

The Hartree-Fock wavefunctions for the isolated atoms and ions which have been described in the previous section must now be combined to obtain the unperturbed wavefunctions for the ion-atom system. There are various ways of choosing these unperturbed functions; however, the calculation of the interaction energies is greatly simplified if we choose them so as to satisfy the various symmetries of the system, as described, for example, by Herzberg.[54]

The classification of the wavefunctions according to symmetry and the conventional designation for each of the symmetry types is also given by Herzberg.[54] The various symmetry types which result from the interaction of any pair of atoms or ions in given states of the isolated system can be found readily by the Wigner-Witmer rules.[55] The unperturbed wavefunctions corresponding to each of these symmetry types can then be found by the general procedure to be described below.

Let us designate the two nuclei of the ion-atom system as A and B and choose the z-axis of the coordinate system along the internuclear axis. We then form the product wavefunctions $\psi_A(M_{L_A}, M_{S_A})\,\psi_B^+(M_{L_B}, M_{S_B})$ and $\psi_A^+(M_{L_A}, M_{S_A})\psi_B(M_{L_B}, M_{S_B})$, where ψ and ψ^+ designate the ground-state Hartree-Fock wavefunctions for the neutral atom and ion, respectively, and the subscripts A and B indicate wavefunctions centered on the nuclei A and B, respectively. In the product $\psi_A\psi_B^+$ it is assumed that ψ_A depends on the first N electronic coordinates $\vec{r}_1$ through $\vec{r}_N$ while ψ_B^+ depends on the remaining coordinates $\vec{r}_{N+1}$ through $\vec{r}_{2N-1}$, where N is the number of electrons in the neutral atom. Similarly, in the product $\psi_A^+\psi_B$, ψ_A^+ depends on the first N-1 electrons and ψ_B on the remaining N. Thus, the sets of product functions $\psi_A\psi_B^+$ and $\psi_A^+\psi_B$ are each orthonormal but are not properly antisymmetrized in the electronic coordinates.

We now wish to form wavefunctions of the proper symmetry types from the basic product functions introduced above. First of all, we note that the product functions $\psi_A \psi_B^+$ and $\psi_A^+ \psi_B$ are already eigen-functions of the z-component of the orbital angular momentum, with the eigen-value[55]

$$M_L = M_{L_A} + M_{L_B} , \tag{20}$$

so that it is not necessary to introduce any further symmetrization with respect to this operator.

The problem of determining the proper eigen-functions for the spin operator of the system represents a special case of the general problem of determining the eigen-functions for an arbitary angular momentum vector $\vec{J}$ which results from the coupling of two other angular momentum vectors $\vec{J}_1$ and $\vec{J}_2$. This problem has been solved in general, and it is found that if ψ_{JM} represents a simultaneous eigen-function of the operators J^2 and J_z having the eigen-values J and M, then it can be represented by a formula of the form[56]

$$\psi_{JM} = \sum_{M_1, M_2}^{(M_1 + M_2 = M)} C(M_1, M_2; J, M)\, \psi(J_1, M_1; J_2, M_2) , \tag{21}$$

where the $\psi(J_1, M_1; J_2, M_2)$ are simultaneous eigen-functions for the component vectors and the sum extends only over those values of M_1 and M_2 such that $M_1 + M_2 = M$; the coefficients $C(M_1, M_2; J, M)$ are known as Clebsch-Gordan coefficients. A general formula for these coefficients, as well as tables of values for all cases of interest to us, is given in Slater's book[56] (equation (20-29) and table 20-5) so that equation (21) gives an explicit formula for the eigen-functions ψ_{JM} in term of the eigen-functions $\psi(J_1, M_1; J_2, M_2)$ for the components. Applying this formula to the present case, we obtain the eigen-functions for the total electronic spin in the general form

$$\Psi_A(S, M_S; M_{L_A} M_{L_B}) = \sum_{M_{S_A}, M_{S_B}}^{(M_{S_A} + M_{S_B} = M_S)} C(M_{S_A}, M_{S_B}; S, M_S)\, \psi_A(M_{L_A}, M_{S_A})\, \psi_B^+(M_{L_B}, M_{S_B}) \tag{22a}$$

$$\Psi_B(S, M_S; M_{L_A}, M_{L_B}) = \sum_{M_{S_A}, M_{S_B}}^{(M_{S_A} + M_{S_B} = M_S)} C(M_{S_A}, M_{S_B}; S, M_S)\, \psi_A^+(M_{L_A}, M_{S_A})\, \psi_B(M_{L_B}, M_{S_B}) \tag{22b}$$

where the quantum numbers S and M_S indicate, respectively, the total electronic spin and its z-component for the ion-atom pair; the Clebsch-Gordan coefficients $C(M_{S_A}, M_{S_B}; S, M_S)$ can be evaluated readily in specific cases from table 20-5 of reference 56.

In order to satisfy the Pauli principle for the combined ion-atom system, it is now necessary to antisymmetrize equation (22) in all the electronic coordinates. Remembering that the Hartree-Fock wavefunctions, ψ and ψ^+ for the isolated atoms and ions are simply linear combinations of Slater determinants involving the electrons within the individual atom or ion, we see that equation (22) has the form of a sum of terms, each of which is the product of two Slater determinants times a coefficient which can be determined from table II and the values of the Clebsch-Gordan coefficients in equation (22). Now it can be shown without too much difficulty that the result of antisymmetrizing the product of two Slater determinants which do not contain any electrons in common is simply to give a new Slater determinant which is made up by taking all the one-electron wavefunctions from the two original determinants in the same order in which they originally occurred, and combining them into one large Slater determinant involving all the electrons from both the original determinants. Thus, equation (22) can still be used to describe the antisymmetrized wavefunctions for the system, if one simply replaces each product of Slater determinants which occurs in the equation by the corresponding combined Slater determinant for the whole system. We note that, since the one-electron orbitals on the two centers A and B are in general not orthogonal, the Slater determinants for the combined system will generally not be properly normalized and the antisymmetrized wave functions (22a) and (22b) will thus no longer form orthonormal sets, except insofar as required by their symmetry properties.

As the final step in obtaining unperturbed wavefunctions having the proper symmetry properties, we now take account of the reflection symmetries of the system. Since in our work we are dealing with systems in which the two nuclei have the same charge, the wavefunctions will have the g, u symmetry arising from reflection in a plane perpendicular to the nuclear axis.[55] The proper unperturbed wavefunctions for the system are thus of the form[55]

$$\Psi_{g,u} = \frac{1}{\sqrt{2}}\left[\Psi_A (S, M_S; M_{L_A}, M_{L_B}) \pm \Psi_B (S, M_S; M_{L_B}, M_{L_A})\right] \tag{23}$$

where the antisymmetrized wavefunctions Ψ_A and Ψ_B are given by equation (22), and represent, respectively, situations in which atom A is neutral and B is ionized and in which B is neutral and A is ionized. We note in passing that it is the splitting $\Delta E \equiv |E_g - E_u|$ between the g and u states given by equation (23) which is responsible for the phenomenon of resonant charge exchange, and which forms the main objective of the present investigation. In the event that $M_L = 0$ and $M_{L_A} = -M_{L_B} \neq 0$, then it is also necessary to consider the ± symmetry arising from reflections of the wavefunctions in a plane containing the internuclear axis.[55] This symmetry then leads to unperturbed wavefunctions for the system of the form[55]

$$\Psi^{\pm}_{g,u} = \frac{1}{\sqrt{2}}\left[\Psi_{g,u}(S, M_S; M_{L_A}, -M_{L_A}) \pm \Psi_{g,u}(S, M_S; -M_{L_A}, M_{L_A})\right] \tag{24}$$

where one must of course use either all Ψ_g's or all Ψ_u's in evaluating the equation. The final symmetrization (24) will not be required in the present work however, since one readily sees from table II and equation (20) that the case $M_L = 0$, $M_{L_A} \neq 0$ does not arise for the $N-N^+$ and $O-O^+$ systems considered here.

3. Comparison with Valence Bond Theory

It is of interest to compare the Heitler-London wavefunctions obtained in the previous section with those given by simple valence bond theory.[57] Both types of wavefunctions are constructed as linear combinations of Slater determinants which are made up from the one-electron wavefunctions of the ground-state configurations of the separated atoms, and in both cases these linear combinations are chosen to have the proper symmetry types as indicated by the Wigner-Witmer rules. Thus if we consider the set of all wavefunctions of a given symmetry type which can arise from the interaction of atoms in the ground-state or in the low-lying excited states of the same configuration as the ground state, then the valence-bond wavefunctions will all be linear combinations of the Heitler-London wavefunctions, and conversely. However the individual wavefunctions within these sets are chosen in different ways in the two methods, and in general will not be the same.

The difference between the two types of wavefunctions is a result of the way in which electron correlations are treated in the two methods. Thus, in the Heitler-London method one chooses wavefunctions in which there is a definite correlation between the spins of the electrons within each atom, but the correlation between electrons in different atoms is arbitary; whereas, in the valence-bond method one choses wavefunctions in which the electrons

in corresponding orbitals of the two atoms are correlated, but in which there is no definite correlation between the electrons in a given atom. There is no reason to expect that these two procedures should yield the same sets of basis wavefunctions, and in fact one finds that in general they do not. This point has recently been discussed in detail by Mulliken[58] for the case of the $^5\Sigma_g^+$ states of N_2. As another example, we note that the valence-bond wavefunctions obtained by Knof, et al.,[6] for the sextet states of the $N-N^+$ and $O-O^+$ interactions are the same as would be obtained by the Heitler-London method, while those for the doublet and quartet states are different.

In general we expect that at large internuclear separations, where the interaction energy between the atoms is small, the correlations within the individual atoms will be dominant and the wavefunctions obtained by the present method will be appropriate unperturbed functions; while, at small internuclear separations the correlations between atoms will be dominant and the valence-bond wavefunctions will be applicable. In general, one might expect the transition between these two types of wave functions to occur when the energy associated with the spin correlations between atoms is comparable to that associated with the correlations within the individual atoms, i.e., when the interaction energy is comparable to the separation in energy between the ground-state and the low-lying excited states of the isolated atoms. Since this latter energy is of the order of 1 or 2 ev, whereas the interaction energies of interest for the charge exchange problem are only a few hundredths of an ev (equation 15), it appears that the Heitler-London wavefunctions of equation (24), which arise from the ground states of the separated atoms, are the appropriate ones to use here, and that the interaction with the low-lying excited states of the same configuration, which is assumed in the valence-bond wavefunctions will be small.

C. GENERAL EQUATIONS FOR THE INTERACTION ENERGIES

1. The Heitler-London Equations

In the general Heitler-London formulation of molecular theory, the energy levels E of the system are given by the solutions of the determinantal equation[59]

$$| H_{ij} - E\, S_{ij} | = 0 \tag{25}$$

with the matrix elements S_{ij} and H_{ij} defined by

$$S_{ij} \equiv \int \Psi_i^* \; \Psi_j^* \; d^\nu \vec{r}$$

$$H_{ij} \equiv \int \Psi_i^* \; H \; \Psi_j \; d^\nu \vec{r} \tag{26}$$

Here Ψ_i and Ψ_j are the unperturbed wavefunctions for the system, and the Hamiltonian H is given in atomic units (distance measured in Bohr radii $\equiv \hbar^2/\mu e^2 = 0.529$ Å, energies in atomic units $= \mu e^4/\hbar^2 = 27.2$ ev) by

$$H = -\frac{1}{2}\sum_{i=1}^{\nu} \nabla_i^2 - \sum_{i=1}^{\nu} \frac{Z_A}{r_{iA}} - \sum_{i=1}^{\nu} \frac{Z_B}{r_{iB}} + \frac{Z_A Z_B}{r_{AB}} + \sum_{1 \le i < j \le \nu} \frac{1}{r_{ij}} \tag{27}$$

where ν is the total number of electrons in the system, Z_A and Z_B are the nuclear charges in units of e, $\vec{r}_A$ and $\vec{r}_B$ are the position vectors of the two nuclei, the $\vec{r}_i$ are the position vectors of the electrons, and as usual $r_{ij} \equiv |\vec{r}_i - \vec{r}_j|$. For the present work, we have $Z_A = Z_B = Z = N$ and $\nu = 2N-1$, with N=7 for nitrogen and N=8 for oxygen. Equation (25) is greatly simplified if one uses the unperturbed wavefunctions for the system obtained in the previous section, since the matrix elements (26) between wavefunctions of different symmetry type will vanish. Thus in the case of $N-N^+$ and $O-O^+$, for example, one finds from the Wigner-Witmer rules that there is only one wavefunction of each symmetry type, so that all nondiagonal components of equation (25) vanish, and it becomes simply

$$E = H_{ii}/S_{ii} \ . \tag{28}$$

Substituting the unperturbed wavefunctions from equation (23) into equation (26) and defining

$$O_{AA} \equiv \int \Psi_A^* \ O \ \Psi_A \ d^\nu \vec{r} \equiv \int \Psi_B^* \ O \ \Psi_B \ d^\nu \vec{r}$$

$$O_{AB} \equiv \int \Psi_A^* \ O \ \Psi_B \ d^\nu \vec{r} \equiv \int \Psi_B^* \ O \ \Psi_A \ d^\nu \vec{r} \ , \tag{29}$$

where the operator O may represent either H or the identity, we find that $O_{ii} = O_{AA} \pm O_{AB}$ and equation (28) reduces further to the form

$$E = \frac{H_{AA} \pm H_{AB}}{S_{AA} \pm S_{AB}} \ . \tag{30}$$

2. Simplification of the Matrix Elements

According to the antisymmetrized version of equation (22) the wavefunctions Ψ_A and Ψ_B occurring in the matrix elements (29) are linear combinations of Slater determinants. In the evaluation of the integrals, we may eliminate the Slater determinants occurring in the second factor in the usual way[60] to reduce equation (29) to a sum over permutations of the form

$$O_{XY} = \sum_{(r)} (-1)^r \int F_X^* (r_1, r_2, \ldots, r_{2N-1})\, O\, F_Y (1, 2, \ldots, 2N-1)\, d^{\nu}\vec{r} \tag{31}$$

where the subscripts X and Y indicate either A or B and $F_X(\vec{r}_1, \vec{r}_2, \ldots, \vec{r}_{2N-1})$ is simply the function which results if we replace each Slater determinant in Ψ_X by the product of its diagonal elements. We note that equation (22) may also be interpreted as an equation for F_X if we simply replace the wavefunctions ψ_X and $\psi_Y{}^+$ in equation (22) by the corresponding functions f_X and $f_Y{}^+$ which result when the Slater determinants in ψ_X and $\psi_Y{}^+$ are replaced by their diagonal elements. The functions f_X and $f_Y{}^+$ may then be found directly from table II.

It is possible to make a considerable simplification in equation (31) by noting that, for all cases shown in table II, the orbital part of the wavefunction depends only on the quantum number M_L, while the spin part depends only on M_S. Thus we may factor f_X into orbital and spin parts

$$f_{X, M_L M_S} (\vec{r}, \sigma) = U_{X, M_L} (\vec{r})\; g_{M_S} (\sigma) \tag{32}$$

were σ is the spin coordinate and $\vec{r}$ is now assumed to include only the spatial coordinates. Substituting equation (32) into equation (22) we obtain the equation for F in the form

$$F_A (S, M_S;\, M_{L_A}, M_{L_B}) = U_{A, M_{L_A}} (1, 2, \ldots, N)\; U^+_{B, M_{L_B}} (N+1, \ldots, 2N-1)$$

$$\cdot\; G_{S, M_S} (1, 2, \ldots, N;\, N+1, \ldots, 2N-1)$$

$$F_B (S, M_S;\, M_{L_A}, M_{L_B}) = U^+_{A, M_{L_A}} (1, 2, \ldots, N-1)\; U_{B, M_{L_B}} (N, \ldots, 2N-1)$$

$$\cdot\; G_{S, M_S} (N, N+1, \ldots, 2N-1;\, 1, 2, \ldots, N-1) \tag{33}$$

where the spin-function G is defined by

$$G_{S, M_S} (1, 2, \ldots, N;\, N+1, \ldots, 2N-1)$$

$$= \sum_{M_{S_A}, M_{S_B}} C (M_{S_A}, M_{S_B};\, S, M_S)\; g_{M_{S_A}} (1, 2, \ldots, N)\; g^+_{M_{S_B}} (N+1, \ldots, 2N-1) \tag{34}$$

With the expression (33) for F, we see that equation (31) for the matrix elements can be factored into orbital and spin parts to give

$$O_{AA} = \sum_{(\tau)} (-1)^{\tau} a_S(\tau) \int U^*_{A, M_{L_A}}(\tau_1, \ldots, \tau_N)\, U^{+*}_{B, M_{L_B}}(\tau_{N+1}, \ldots, \tau_{2N-1})$$

$$\cdot\ O\, U_{A, M_{L_A}}(1, \ldots, N)\, U^{+}_{B, M_{L_B}}(N+1, \ldots, 2N-1)\, d\vec{r} \tag{35a}$$

$$O_{AB} = \sum_{(\tau)} (-1)^{\tau} b_S(\tau) \int U^{+*}_{A, M_{L_B}}(\tau_1, \ldots, \tau_{N-1})\, U^{*}_{B, M_{L_A}}(\tau_N, \ldots, \tau_{2N-1})$$

$$\cdot\ O\, U_{A, M_{L_A}}(1, \ldots, N)\, U^{+}_{B, M_{L_B}}(N+1, \ldots, 2N-1)\, d\vec{r} \tag{35b}$$

where the sum is over all permutations τ of the integers 1 through 2N-1 and the spin dependent factors a_S and b_S are given by

$$a_S(\tau) = \sum_{\text{spins}} G_{S, M_S}(\tau_1, \tau_2, \ldots \tau_N;\ \tau_{N+1}, \ldots, \tau_{2N-1})$$

$$\cdot\ G_{S, M_S}(1, 2, \ldots, N;\ N+1, \ldots, 2N-1)$$

$$b_S(\tau) = \sum_{\text{spins}} G_{S, M_S}(\tau_N, \tau_{N+1}, \ldots, \tau_{2N-1};\ \tau_1, \ldots, \tau_{N-1})$$

$$\cdot\ G_{S, M_S}(1, 2, \ldots, N;\ N+1, \ldots, 2N-1) \tag{36}$$

We note that a_S and b_S cannot depend on M_S since the interaction energies must be independent of the direction of the spin vector.

Equations (34) through (36) furnish explicit equations for the required matrix elements O_{AA} and O_{BB} in terms of the orbital and spin factors U and g defined by equation (32). Since these factors can be evaluated directly from table II, we see that it is unnecessary to go through the intermediate step of actually constructing the unperturbed wavefunctions for the system, as described in section B above.

A further important simplification in the calculation of the matrix elements (35) can be made if we introduce the approximation mentioned in the introduction of considering only the lowest order terms in $e^{-\zeta R}$, where $R = r_{AB}$ is the internuclear separation and ζ may be any one of the orbital exponents ζ_i occurring in equation (17). It can be readily shown from the form of equation (35) that each electron which is exchanged between the nuclei A and B will give a factor of $e^{-\zeta R}$ in the integrals, so that the approximation of neglecting higher powers of $e^{-\zeta R}$ in equation (35) implies that we need only consider permutations in which no more than one electron is exchanged between the two nuclei. For the matrix elements O_{AA}, we note that the number of electrons on each nucleus is the same for the initial and final states, so that the number of electrons exchanged between the nuclei is always even. Thus, within the present approximation we need only consider permutations r in which all the electrons remain on the same nucleus in evaluating the matrix elements O_{AA}. Similarly, we see that for the elements O_{AB} the number of electrons exchanged is always odd and we need consider only permutations r in which just one electron is exchanged in evaluating the matrix elements.

It has been pointed out by Slater[61] that the neglect of multiple exchange terms is a very poor approximation at ordinary internuclear separations, since these terms are actually proportional to powers of $\nu e^{-\zeta R}$, where ν is the total number of electrons in the system. However, the approximation will of course become better at larger separations, and it appears likely that it will give at least a reasonable first approximation to the matrix elements at the very large separations of interest in the present work. In the present work we have therefore considered only terms of first order in $e^{-\zeta R}$, as described in the preceding paragraph, in order to see the dominant behavior of the potential curves at large R. The contributions resulting from the higher order terms will be investigated in the future, and will be included as a correction to the present results if this appears necessary.

D. SPIN DEPENDENCE OF THE POTENTIALS FOR $N-N^+$ and $O-O^+$

We now wish to evaluate the spin dependent factors $a_S(r)$ and $b_S(r)$ in equation (35) for the interactions between N and N^+ and between O and O^+ in their ground states. From the Wigner-Witmer rules we find that the $N-N^+$ and $O-O^+$ interactions both give rise to states of the following 12 symmetry types;

$$^2\Sigma^+_{u,g}\,,\ ^4\Sigma^+_{u,g}\,,\ ^6\Sigma^+_{u,g}\,,\ ^2\Pi_{u,g}\,,\ ^4\Pi_{u,g}\,,\ ^6\Pi_{u,g}\,, \tag{37}$$

so that the spin quantum number S in equation (35) takes on the three possible values S = 1/2, 3/2, and 5/2. From table II we can immediately write down the

values for the spin factors g and g^+ in equation (32) for the ground-state species N, N^+, O, and O^+ as follows:

$$\overset{N}{g}_{M_S}(1,2,..,7) = \overset{O^+}{g}_{M_S}(1,2,...,7) = \alpha(1)\,\beta(2)\,\alpha(3)\,\beta(4)\,\overset{3/2}{h}_{M_S}(5,6,7)$$

$$\overset{N^+}{g}_{M_S}(1,2,...6) = \alpha(1)\,\beta(2)\,\alpha(3)\,\beta(4)\,\overset{1}{h}_{M_S}(5,6)$$

$$\overset{O}{g}_{M_S}(1,2,...,8) = \alpha(1)\,\beta(2)\,\alpha(3)\,\beta(4)\,\alpha(5)\,\beta(8)\,\overset{1}{h}_{M_S}(6,7) \tag{38a}$$

where the factors $\overset{S}{h}_{M_S}$ are defined by

$$\overset{3/2}{h}_{3/2}(1,2,3) = \alpha(1)\,\alpha(2)\,\alpha(3)$$

$$\overset{3/2}{h}_{1/2}(1,2,3) = \frac{1}{\sqrt{3}}[\beta(1)\,\alpha(2)\,\alpha(3) + \alpha(1)\,\beta(2)\,\alpha(3) + \alpha(1)\,\alpha(2)\,\beta(3)]$$

$$\overset{3/2}{h}_{-1/2}(1,2,3) = \frac{1}{\sqrt{3}}[\beta(1)\,\beta(2)\,\alpha(3) + \beta(1)\,\alpha(2)\,\beta(3) + \alpha(1)\,\beta(2)\,\beta(3)]$$

$$\overset{3/2}{h}_{-3/2}(1,2,3) = \beta(1)\,\beta(2)\,\beta(3)$$

$$\overset{1}{h}_{1}(1,2) = \alpha(1)\,\alpha(2)$$

$$\overset{1}{h}_{0}(1,2) = \frac{1}{\sqrt{2}}[\alpha(1)\,\beta(2) + \beta(1)\,\alpha(2)]$$

$$\overset{1}{h}_{-1}(1,2) = \beta(1)\,\beta(2) \tag{38b}$$

In these equations α and β are the usual one-electron spin functions for $m_S = +1/2$ and $m_S = -1/2$, respectively. The initial factor $\alpha(1)\,\beta(2)\,\alpha(3)\,\beta(4)$, of course, comes from the closed 1s and 2s shells, while the factor for the p shell is obtained simply by rewriting the formula in table II with the orbital symbols replaced by the appropriate spin functions α or β. The quantities a_S and b_S can now be calculated explicity from equations (34), (36), and (38), using values of the Clebsch-Gordan coefficients from reference 56. For the present approximation, a_S only needs to be evaluated for permutations in which no electron is exchanged between the nuclei A and B and b_S for permutations in which just one electron is exchanged.

Let us consider first the case in which only the unpaired electrons (i.e., the electrons in the argument of $h^{S}_{M_S}$) are permuted, while the paired electrons are all held fixed. One sees from equation (38) that in all cases the spin functions g_{M_S} are symetric in the spins of the unpaired electrons, and hence the functions G defined by equation (34) are also symmetric under any permutations of the unpaired electrons within one atom. It then follows readily from equation (36) that, for permutations which involve only the unpaired electrons, the values of $a_S(\tau)$ and $b_S(\tau)$ depend only on the number of electrons exchanged between the atoms. Thus a_S and b_S are independent of τ for all permutations of interest here, and, using equation (36), we may write them in terms of a typical permutation as

$$a_S(\tau) = a_S^{(0)} = \sum_{\text{spins}} [G_{SM_S}(1, 2, \ldots N; N+1, \ldots, 2N-1)]^2$$

$$b_S(\tau) = b_S^{(1)} = \sum_{\text{spins}} G_{SM_S}(N+1, \ldots, 2N-1, N; 1, \ldots, N-1) \cdot G_{SM_S}(1, \ldots, N; N+1, \ldots, 2N-1) \tag{39}$$

It is now a straightforward calculation to evaluate these expressions using equations (34) and (38) and the usual orthonormality relations for the spin functions α and β. One finds in this way that

$$a_S^{(0)} = 1 \qquad \text{for all } S$$

$$b_S^{(1)} = \begin{cases} 1 & \text{for } S = \frac{5}{2} \\ -\frac{2}{3} & \text{for } S = \frac{3}{2} \\ \frac{1}{3} & \text{for } S = \frac{1}{2} \end{cases} \tag{40}$$

for both the $N-N^+$ and $O-O^+$ interactions.

The analysis becomes more complex when one considers permutations which involve paired electrons as well as unpaired electrons, but as might be expected the conclusions remain essentially the same. The details of the analysis for the case of a general permutation are given in appendix D. From this analysis, one finds that for a general permutation τ in which no electrons are exchanged between the nuclei, the equation for $a_S(\tau)$ may be reduced to the product of a

factor which depends only on the permutation τ (and not on S), and the spin-dependent factor $a_S^{(0)}$ of equation (39). Similarly, for a permutation τ in which one-electron is exchanged, $b_S(\tau)$ reduces to a function of τ only times the spin-dependent factor $b_S^{(1)}$ of equation (39). It thus follows that, in the approximation in which we neglect multiple exchange, the spin dependence can be completely factored out of the matrix elements (35), so that the matrix elements for any spin state can be expressed in terms of the elements for one spin state, S = 5/2 say, and the spin dependent factors $a_S^{(0)}$ and $b_S^{(1)}$ given by equation (40); i.e.,

$$O_{AA}(S) = a_S^{(0)} \; O_{AA}^{(5/2)} = O_{AA}^{(5/2)}$$

$$O_{AB}(S) = b_S^{(1)} \; O_{AB}^{(5/2)} \quad .$$

Substituing this result in equation (30) and remembering that O_{AB} is of order $e^{-\zeta R}$, so that we may expand in powers of O_{AB} and neglect higher order terms, we obtain the expression for the $N-N^+$ and $O-O^+$ interaction energies in the form

$$E_{S,\,M_L} = W_0^{(M_L)} \pm b_S^{(1)} \; W_1^{(M_L)} \quad , \tag{41}$$

where the quantities

$$W_0^{(M_L)} = H_{AA}/S_{AA}$$

and

$$W_1^{(M_L)} = \frac{1}{S_{AA}} \left(H_{AB} - S_{AB} \; W_0^{(M_L)} \right) \tag{42}$$

are to be evaluated for the sextet states (i.e., for S = 5/2), and the spin dependent factors $b_S^{(1)}$ are given by equation (40).

When we compare equation (41) for the $N-N^+$ and $O-O^+$ potential curves with the results obtained by Knof, Mason and Vanderslice,[6] we see that the predicted relationship among the states at large internuclear separations is altogether different from that found by Knof, et al. There are two main reasons for this discrepancy. First, the exchange integrals J of reference 6, which we have here assumed to be negligible at large internuclear separations, have been empirically estimated by Knof, et al., to be quite large. These integrals do not affect the charge-exchange cross section significantly, so that their value is not really relevent to the main objective of the present work; however, it appears to us that the experimantal evidence for the values given in reference 6 is quite inconclusive, and that probably these integrals actually drop off considerably faster at large R than has been estimated by Knof, et al. However, this is still an open question.

The second difference between our results and those of reference 6 is that the valence-bond wavefunctions used in that work give a spin factor $b_S^{(1)} = 1$ in all cases; whereas, we obtain the values given by equation (40). Thus, the splitting between the g and u states obtained by Knof, et al., is independent of spin, whereas in our results the splitting is considerably greater for the higher spin-states. This difference is evidently due to the different wavefunctions used in the two calculations, as discussed in section B.3 above.

E. REDUCTION OF THE MATRIX ELEMENTS FOR N-N$^+$ AND O-O$^+$ TO STANDARD ONE-AND TWO-ELECTRON INTEGRALS

1. The Evaluation of the Wavefunctions for N-N$^+$ and O-O$^+$

We now turn to the problem of evaluating the integrals over the spatial coordinates in the matrix elements of equation (35). We have only considered the case of the N-N$^+$ and O-O$^+$ systems in carrying out these calculations here; however, the general procedure which we use should also be applicable to interactions between other pairs of atoms and atomic ions with only minor modifications.

According to the results of the preceding section, it is only necessary to evaluate the matrix elements of equation (35) for one spin-state of the system. For this purpose, we choose the sextet state $S = 5/2$, $M_S = 5/2$, since for this case the wavefunctions Ψ_A and Ψ_B in equation (22) become especially simple, and in fact reduce to a single Slater determinant, which can be written down immediately by reference to Table II and equation (22). In order to facilitate the evaulation of the matrix elements, it proves to be convenient to change the order in which the one-electron wavefunctions occur in the wavefunctions Ψ_A and Ψ_B of equation (22), so that the extra orbital on the atom will always be called ψ_N, where N is again the number of electrons on the atom (N=7 for nitrogen and 8 for oxygen). This will at most change the sign of the quantity $\mathbb{W}_1$ in equation (41), and since $\mathbb{W}_1$ enters into the energy equation with a $\pm$ sign, the final formula (41) for the interaction energies will not be changed. We therefore write the wavefunctions (22) for the sextet states in the form

$$\Psi_A = \frac{1}{\sqrt{(2N-1)!}} \, |\psi_i(j)|, \qquad \Psi_B = \frac{1}{\sqrt{(2N-1)!}} \, |\psi_i'(j)| \tag{43}$$

where the one-electron wavefunctions ψ_i and ψ_i' are given in table III

In table III we follow the usual convention of designating the 2p orbitals with $m_l = 0$ by 2σ and those with $m_l = \pm 1$ by $2\pi^{\pm}$. The spin state is designated by the subscript α or β and the nucleus upon which the wavefunction is centered by the subscript A or B. The wavefunctions having the superscript + are the one-electron wavefunctions for the ion, and those without the superscript are for the neutral atom.

TABLE IIIa

ONE-ELECTRON WAVEFUNCTIONS FOR THE N-N$^+$ INTERACTION

Ψ_A	ψ_1	ψ_2	ψ_3	ψ_4	ψ_5	ψ_6	ψ_7	ψ_8	ψ_9	ψ_{10}	ψ_{11}	ψ_{12}	ψ_{13}
$^6\Sigma$	$\psi_{1s\alpha A}$	$\psi_{1s\beta A}$	$\psi_{2s\alpha A}$	$\psi_{2s\beta A}$	$\psi_{2\pi^+\alpha A}$	$\psi_{2\pi^-\alpha A}$	$\psi_{2\sigma\alpha A}$	$\psi^+_{1s\alpha B}$	$\psi^+_{1s\beta B}$	$\psi^+_{2s\alpha B}$	$\psi^+_{2s\beta B}$	$\psi^+_{2\pi^+\alpha B}$	$\psi^+_{2\pi^-\alpha B}$
$^6\Pi$	$\psi_{1s\alpha A}$	$\psi_{1s\beta A}$	$\psi_{2s\alpha A}$	$\psi_{2s\beta A}$	$\psi_{2\pi^+\alpha A}$	$\psi_{2\sigma\alpha A}$	$\psi_{2\pi^-\alpha A}$	$\psi^+_{1s\alpha B}$	$\psi^+_{1s\beta B}$	$\psi^+_{2s\alpha B}$	$\psi^+_{2s\beta B}$	$\psi^+_{2\pi^+\alpha B}$	$\psi^+_{2\sigma\alpha B}$
Ψ_B	ψ_1'	ψ_2'	ψ_3'	ψ_4'	ψ_5'	ψ_6'	ψ_7'	ψ_8'	ψ_9'	ψ_{10}'	ψ_{11}'	ψ_{12}'	ψ_{13}'
$^6\Sigma$	$\psi^+_{1s\alpha A}$	$\psi^+_{1s\beta A}$	$\psi^+_{2s\alpha A}$	$\psi^+_{2s\beta A}$	$\psi^+_{2\pi^+\alpha A}$	$\psi^+_{2\pi^-\alpha A}$	$\psi_{2\sigma\alpha B}$	$\psi_{1s\alpha B}$	$\psi_{1s\beta B}$	$\psi_{2s\alpha B}$	$\psi_{2s\beta B}$	$\psi_{2\pi^+\alpha B}$	$\psi_{2\pi^-\alpha B}$
$^6\Pi$	$\psi^+_{1s\alpha A}$	$\psi^+_{1s\beta A}$	$\psi^+_{2s\alpha A}$	$\psi^+_{2s\beta A}$	$\psi^+_{2\pi^+\alpha A}$	$\psi^+_{2\sigma\alpha A}$	$\psi_{2\pi^-\alpha B}$	$\psi_{1s\alpha B}$	$\psi_{1s\beta B}$	$\psi_{2s\alpha B}$	$\psi_{2s\beta B}$	$\psi_{2\pi^+\alpha B}$	$\psi_{2\sigma\alpha B}$

TABLE IIIb

ONE-ELECTRON WAVEFUNCTIONS FOR THE O-O$^+$ INTERACTION

Ψ_A	ψ_1	ψ_2	ψ_3	ψ_4	ψ_5	ψ_6	ψ_7	ψ_8	ψ_9	ψ_{10}	ψ_{11}	ψ_{12}	ψ_{13}	ψ_{14}	ψ_{15}
$^6\Sigma$	$\psi_{1s\alpha A}$	$\psi_{1s\beta A}$	$\psi_{2s\alpha A}$	$\psi_{2s\beta A}$	$\psi_{2\pi^+\alpha A}$	$\psi_{2\sigma\alpha A}$	$\psi_{2\pi^-\alpha A}$	$\psi_{2\sigma\beta A}$	$\psi^+_{1s\alpha B}$	$\psi^+_{1s\beta B}$	$\psi^+_{2s\alpha B}$	$\psi^+_{2s\beta B}$	$\psi^+_{2\pi^+\alpha B}$	$\psi^+_{2\sigma\alpha B}$	$\psi^+_{2\pi^-\alpha B}$
$^6\Pi$	$\psi_{1s\alpha A}$	$\psi_{1s\beta A}$	$\psi_{2s\alpha A}$	$\psi_{2s\beta A}$	$\psi_{2\pi^+\alpha A}$	$\psi_{2\sigma\alpha A}$	$\psi_{2\pi^-\alpha A}$	$\psi_{2\pi^+\beta A}$	$\psi^+_{1s\alpha B}$	$\psi^+_{1s\beta B}$	$\psi^+_{2s\alpha B}$	$\psi^+_{2s\beta B}$	$\psi^+_{2\pi^+\alpha B}$	$\psi^+_{2\sigma\alpha B}$	$\psi^+_{2\pi^-\alpha B}$
Ψ_B	ψ_1'	ψ_2'	ψ_3'	ψ_4'	ψ_5'	ψ_6'	ψ_7'	ψ_8'	ψ_9'	ψ_{10}'	ψ_{11}'	ψ_{12}'	ψ_{13}'	ψ_{14}'	ψ_{15}'
$^6\Sigma$	$\psi^+_{1s\alpha A}$	$\psi^+_{1s\beta A}$	$\psi^+_{2s\alpha A}$	$\psi^+_{2s\beta A}$	$\psi^+_{2\pi^+\alpha A}$	$\psi^+_{2\sigma\alpha A}$	$\psi^+_{2\pi^-\alpha A}$	$\psi_{2\sigma\beta B}$	$\psi_{1s\alpha B}$	$\psi_{1s\beta B}$	$\psi_{2s\alpha B}$	$\psi_{2s\beta B}$	$\psi_{2\pi^+\alpha B}$	$\psi_{2\sigma\alpha B}$	$\psi_{2\pi^-\alpha B}$
$^6\Pi$	$\psi^+_{1s\alpha A}$	$\psi^+_{1s\beta A}$	$\psi^+_{2s\alpha A}$	$\psi^+_{2s\beta A}$	$\psi^+_{2\pi^+\alpha A}$	$\psi^+_{2\sigma\alpha A}$	$\psi^+_{2\pi^-\alpha A}$	$\psi_{2\pi^+\beta B}$	$\psi_{1s\alpha B}$	$\psi_{1s\beta B}$	$\psi_{2s\alpha B}$	$\psi_{2s\beta B}$	$\psi_{2\pi^+\alpha B}$	$\psi_{2\sigma\alpha B}$	$\psi_{2\pi^-\alpha B}$

2. The Integrals S_{AA} and H_{AA}

For the wavefunctions (43), equation (29) for O_{AA} reduces to the simple form

$$O_{AA} = \sum_{(\tau)} (-1)^{\tau} \int \prod_{i=1}^{\nu} \psi_i^* (\tau_i) \; O \; \prod_{i=1}^{\nu} \psi_i (i) \; d^{\nu} \vec{r} \; , \tag{44}$$

where the one-electron wavefunctions ψ_i through ψ_N are on nucleus A, ψ_{N+1} through ψ_ν are on nucleus B, $\nu \equiv 2N-1$, and for the present approximation we consider only permutations τ which do not interchange any electrons between the two atoms. Since the one-electron wavefunctions ψ_i (equation 16) within a given atom are assumed to form an orthonormal set, we see immediately that to this approximation the overlap integral

$$S_{AA} = 1 \; . \tag{45}$$

To evaluate the matrix element H_{AA} it is convenient to write the Hamiltonian for the system (equation 27) in the form

$$H = H_A + H_B^+ + H' \tag{46a}$$

where

$$H_A = -\frac{1}{2} \sum_{i=1}^{N} \nabla_i^2 - \sum_{i=1}^{N} \frac{Z}{r_{iA}} + \sum_{1 \leq i < j \leq N} \frac{1}{r_{ij}}$$

$$H_B^+ = -\frac{1}{2} \sum_{j=N+1}^{\nu} \nabla_j^2 - \sum_{j=N+1}^{\nu} \frac{Z}{r_{jB}} + \sum_{N+1 \leq i < j \leq \nu} \frac{1}{r_{ij}}$$

are the Hamiltonians of the isolated atom and ion, respectively, and

$$H' = \frac{Z^2}{r_{AB}} - \sum_{i=1}^{N} \frac{Z}{r_{iB}} - \sum_{j=N+1}^{\nu} \frac{Z}{r_{jA}} + \sum_{i=1}^{N} \sum_{j=N+1}^{\nu} \frac{1}{r_{ij}} \tag{46b}$$

may be thought of as the perturbation term. In the approximation of neglecting electron exchange between the atoms,

$$\sum_{(r)} (-1)^r \int \prod_{i=1}^{\nu} \psi_i^* (r_i) (H_A + H_B^+) \prod_{i=1}^{\nu} \psi_i(i) \, d^\nu \vec{r} = E_0 + E_0^+ \equiv H_0 \tag{47}$$

where E_0 and E_0^+ are the Hartree-Fock energies of the isolated atom and ion, respectively.

The terms in H' in equation (46) each involve at most one-electron in a given atom, so that any permutation of the electrons within one atom will always give a factor in the integral of the form $\int \psi_i^* (\vec{r}) \psi_j (\vec{r}) d\vec{r}$ with $i \neq j$, and this factor is zero because of the orthogonality of the one-electron wave-functions within each atom. We therefore only need to consider the diagonal terms in evaluating the matrix element of H' and equation (44) for H_{AA} may be written simply as

$$H_{AA} = H_0 + Q_0 \tag{48}$$

where the term

$$Q_0 \equiv \int \prod_{i=1}^{\nu} \psi_i^* (i) \, H' \prod_{i=1}^{\nu} \psi_i (1) \, d^\nu \vec{r}$$

$$= \left[\frac{Z^2}{r_{AB}} - \int \frac{Z}{r_{1B}} \sum_{i=1}^{N} \psi_i^* (1) \, \psi_i (1) \, d\vec{r}_1 \right] +$$

$$- \int \left[\sum_{j=N+1}^{\nu} \psi_j^* (2) \, \psi_j (2) \right] \left[\frac{Z}{r_{2A}} - \int \frac{1}{r_{12}} \sum_{i=1}^{N} \psi_i^* (1) \, \psi_i (1) \, d\vec{r}_1 \right] d\vec{r}_2 \tag{49}$$

may be recognized as simply the electrostatic interaction energy between the charge distributions on the atom and ion.

3. Transformed Wavefunctions for the Positive Ion

The calculation of the matrix elements O_{AB} is complicated somewhat by the fact that the one-electron wavefunctions for the atom and ion are slightly different (see table I), so that we can no longer use the condition that $\int \psi_i'(\vec{r})\, \psi_j(\vec{r})\, d\vec{r} = \delta_{ij}$ to eliminate terms in the matrix elements arising from permutations of the electrons within one atom. This difficulty can be avoided, however, by a simple transformation of the one-electron wavefunctions ψ_i. In general, we see that if $\psi_i^{(0)}$ represents any set of one-electron wavefunctions and

$$\psi_i^{(t)} = \sum_k c_{ik}\, \psi_k^{(0)} \tag{50}$$

represents some linear transformation of these wavefunctions, then the Slater determinant formed from the $\psi_i^{(t)}$ is related to that formed from the $\psi_i^{(0)}$ by the simple formula

$$\frac{1}{\sqrt{\nu!}} \left| \psi_i^{(t)}(j) \right| \equiv \frac{1}{\sqrt{\nu!}} \left| \sum_k c_{ik}\, \psi_k^{(0)}(j) \right| = \frac{1}{\sqrt{\nu!}} \left| c_{ik} \right| \cdot \left| \psi_k^{(0)}(j) \right| \tag{51}$$

Thus the Slater determinant of the transformed one-electron wavefunctions will be the same as that of the original wavefunctions, except for the constant multiplying factor $|c_{ik}|$.

We now wish to apply the general transformation defined by equation (50) to generate a new set of one-electron wavefunctions for the ion which will be orthogonal to the corresponding set for the atom, i.e., will satisfy the condition

$$\int \psi_{iA}^{+(t)*}(\vec{r})\, \psi_{jA}(\vec{r})\, d\vec{r} = \delta_{ij} \quad \text{for } 1 \le i \le N-1,\ 1 \le j \le N \tag{52}$$

where the $\psi_{iA}^{+(t)}$ are assumed to be related to the original positive-ion wavefunctions ψ_{kA}^{+} by a linear transformation

$$\psi_{iA}^{+(t)} = \sum_{k=1}^{N-1} c_{ik}^{+} \psi_{kA}^{+} \qquad \text{for } 1 \leq i \leq N-1 \quad . \tag{53}$$

Substituting equation (53) into equation (52) gives an equation for the coefficients c_{ik}^{+} in the form

$$\sum_{k=1}^{N-1} c_{ik}^{+} s_{kj}^{(0)} = \delta_{ij} \qquad \text{for } 1 \leq i, j \leq N-1 \tag{54}$$

where

$$s_{kj}^{(0)} \equiv \int \psi_{kA}^{+*} \psi_{jA} \, d\vec{r} \qquad \text{for } 1 \leq k \leq N-1, \; 1 \leq j \leq N \tag{55}$$

and we have omitted the case $j = N$ in equation (41) since it is automatically satisfied for the wavefunctions of table III because of their symmetry properties.

Now, since the positive ion wavefunctions ψ_k^{+} differ only slightly from the corresponding atomic wavefunctions ψ_k and since the determinant $\left| \int \psi_{kA}^{*} \psi_{jA} \, d\vec{r} \right| = 1$, it appears reasonable to expect, and this will be verified later by direct numerical computation, that for the present problem, the determinant of equation (55)

$$D \equiv |s_{kj}^{(0)}| \neq 0 \qquad 1 \leq k, j \leq N-1 \tag{56}$$

It then follows from equation (54) that the transformation defined by equations (52) and (53) exists and that in fact the coefficient matrix c_{ik}^{+} of the transformation is just the inverse of the matrix $(s_{kj}^{(0)})$.

If we now define the transformed wavefunctions $\Psi_A^{(t)}$ and $\Psi_B^{(t)}$ as the result of replacing the positive-ion wavefunctions by the transformed positive-ion wavefunctions (53) everywhere in equation (43), then it follows from equation (51) that

$$\Psi_A^{(t)} = |c_{ik}^{+}| \, \Psi_A = \frac{1}{D} \Psi_A \tag{57a}$$

and similarly

$$\Psi_B^{(t)} = \frac{1}{D} \Psi_B \tag{57b}$$

where D is, of course, the quantity defined in equation (56). Introducing (57) into equation (29), we find that in terms of the transformed wavefunctions $\Psi_A^{(t)}$ and $\Psi_B^{(t)}$ the matrix element O_{AB} becomes

$$O_{AB} = D^2 \int \Psi_B^{(t)*} \; O \, \Psi_A^{(t)} \; d^\nu \vec{r} \tag{58}$$

With this expression for the matrix elements, we see that the desired orthonormality condition (52) will be satisfied for all permutations within a given atom, so that the simplifications which resulted from the use of orthonormal orbitals in the preceding section will also be obtained in evaluating equation (58).

In our subsequent work the superscript (t) on the transformed wavefunctions will generally be omitted in order to simplify the notation; however it should be understood that the transformed positive-ion wavefunctions $\psi_k^{+(t)}$ are always to be used in place of the original Hartree-Fock wavefunctions ψ_k^+ in evaluating matrix elements of the form O_{AB}.

4. The Integrals S_{AB} and H_{AB}

When the Slater determinants in equation (58) are expanded as before, the matrix element O_{AB} becomes

$$O_{AB} = D^2 \sum_{(\tau)} (-1)^\tau \int \prod_{i=1}^{\nu} \psi_i'^{\,*}(\tau_i) \; O \prod_{i=1}^{\nu} \psi_i(i) \cdot d^\nu \vec{r} \tag{59}$$

where the sum is to be taken only over permutations τ in which just one electron is exchanged between the two nuclei. From the definition of the one-electron wavefunctions in table III*, we see that this means that we consider only those permutations in which $N-1$ of the N electrons 1 through N go into the orbitals ψ_1' through ψ_{N-1}' while the remaining electrons go into the remaining orbitals ψ_N' through ψ_{2N-1}'.

To evaluate the overlap integral S_{AB} we note that according to equation (52) any permutation τ in which an electron is transferred from one orbital

* As stated in the previous section, the positive ion wavefunctions indicated in table III are of course to be interpreted here, and throughout this section, as the transformed positive-ion wavefunctions of equation (53).

to another orbital on the same nucleus will give a vanishing contribution to the matrix element (59). This implies that the exchanged electron must occupy the odd orbital ψ_N for both the initial and final states, since otherwise the electron which was in the odd orbital would have to drop down into another orbital on the same nucleus; and it further implies that the electrons which are not exchanged must remain in the same orbitals. Thus all permutations in equation (59) will vanish except for the diagonal term, and we obtain simply

$$S_{AB} = D^2 \, s_{NN} \tag{60}$$

where we define in general

$$s_{ij} = \int \psi_i'^{*} \, \psi_j \, d\vec{r} \tag{61}$$

We see that the factor s_{NN} in this equation is just the usual overlap integral which is obtained in the one-electron theory of charge exchange[62] while D^2 represents a correction factor to this theory which results from the readjustment of the remaining electrons in the atom when the exchange occurs.

We now turn to the evaluation of the matrix element H_{AB} which results when the Hamiltonian of equation (27) is substituted into equation (59). Since each term in the Hamiltonian depends on at most two electrons, it follows from equation (52) that any permutation in which more than two electrons are transferred from one orbital to another orbital on the same atom will give a vanishing contribution to H_{AB}. Since for the permutations which we are considering only one electron is transferred from an orbital on one atom to an orbital on the other atom, we see that altogether no more than three electrons can be transferred from one orbital to another, and hence only permutations involving three or fewer electrons give a nonzero contribution to the matrix element H_{AB}. The only permutations which need to be considered in evaluating equation (59) are thus the identity permutation, the permutations $(i\,j)$ in which two electrons are interchanged, and the permutations (i, j, k) in which three electrons are permuted cyclicly.

In carrying out the sum over permutations in equation (59), it is convenient to divide the permutations into groups according to the orbitals occupied by the exchanged electron in the initial and final states. For this purpose we shall designate those permutations in which the exchanged electron always occupies the odd orbital ψ_N as group I; those in which it occupies the odd orbital on atom B but not on atom A as group II, those in which it occupies the odd orbital on A but not on B as group II'; and those in which it does not occupy the odd orbital on either atom as group III. From

table III we see that the group I permutations correspond to permutations of the electronic coordinates in equation (59) for which electron N remains the same, electrons 1 through $N-1$ are permuted among themselves and electrons $N+1$ through $2N-1$ are permuted among themselves; the group II permutations correspond to those in which electrons 1 through N are permuted among themselves and electrons $N+1$ through $2N-1$ among themselves, except that those permutations in which electron N remains the same are excluded, and the group II permutations correspond to those in which electrons 1 through $N-1$ are permuted among themselves and electrons N through $2N-1$ among themselves, except that again the case where electron N remains the same is excluded; the remaining permutations in equation (59) which are not included in any of the above groups of course fall into group III. The total matrix element H_{AB} will then be the sum of contributions from the permutations in each of these groups, as indicated by the equation

$$H_{AB} = H_{AB}^{I} + H_{AB}^{II} + H_{AB}^{II'} + H_{AB}^{III} \tag{62}$$

Let us consider first the group III permutations, for which the exchanged electron is not in the odd orbital ψ_N in either atom. We see that these permutations must always involve at least three electrons; the electron N which is initially in the odd orbital ψ_N on nucleus A and drops down to some other orbital on A after the exchange, the electron j which is initially in an ortibal on B and moves up into the odd orbital ψ_N' after the exchange, and the exchanged electron i. It then follows from the discussion above that the only non-vanishing group III permutations are the cyclic permutations $N \to i \to j \to N$, with $1 \leq i \leq N-1$ and $N+1 \leq j \leq 2N-1$, and that these permutations give a non-zero contribution to the matrix element only for those terms in the Hamiltonian which depend on both electrons N and j. Thus the total contribution to the matrix element H_{AB} from group III permutations is

$$H_{AB}^{III} = D^2 \sum_{i=1}^{N-1} \sum_{j=N+1}^{2N-1} \iiint \psi_i'^*(N)\, \psi_j'^*(i)\, \psi_N'^*(j) \frac{1}{r_{Nj}} \psi_i(i)\, \psi_j(j)\, \psi_N(N)\, d\vec{r}_i\, d\vec{r}_j\, d\vec{r}_N$$

$$= D^2 \sum_{i=1}^{N-1} \sum_{j=N+1}^{2N-1} s_{ji} \iint \psi_i'^*(1)\, \psi_N'^*(2) \frac{1}{r_{12}} \psi_N(1)\, \psi_j(2)\, d\vec{r}_1\, d\vec{r}_2 \tag{63}$$

where s_{ij} is the quantity defined by equation (61).

For the group II permutations, one sees readily from the discussion above that the only nonvanishing contributions to H_{AB} come from the transpositions (Ni) of two electrons and the cyclic permutations $N \to i \to j \to N$ of three electrons, where i and j lie in the range $1 \leq i, j \leq N-1$ and $i \neq j$, and further that these permutations give nonzero contributions only for those terms in the Hamiltonian involving electron N. The total contribution to H_{AB} from group II permutations thus becomes

$$
\begin{aligned}
H_{AB}^{II} = D^2 \Bigg\{ & -\sum_{i=1}^{N-1} \iint \psi_i'^*(N)\, \psi_N'^*(i) \left[-\frac{1}{2} \nabla_N^2 - \frac{Z}{r_{NA}} - \frac{Z}{r_{NB}} + \frac{1}{r_{iN}} \right] \psi_i(i)\, \psi_N(N)\, d\vec{r}_i\, d\vec{r}_N \\
& - \sum_{i=1}^{N-1} \sum_{j=1\,(N \neq j \neq i)}^{2N-1} \iiint \psi_i'^*(N)\, \psi_N'^*(i)\, \psi_j'^*(j) \frac{1}{r_{jN}} \psi_i(i)\, \psi_N(N)\, \psi_j(j)\, d\vec{r}_i\, d\vec{r}_N\, d\vec{r}_j + \\
& + \sum_{i=1}^{N-1} \sum_{j=1\,(j \neq i)}^{N-1} \iiint \psi_i'^*(N)\, \psi_j'^*(i)\, \psi_N'^*(j) \frac{1}{r_{iN}} \psi_i(i)\, \psi_N(N)\, \psi_j(j)\, d\vec{r}_i\, d\vec{r}_N\, d\vec{r}_j \Bigg\}
\end{aligned}
$$

$$
\begin{aligned}
= D^2 \Bigg\{ & \int \left(\sum_{i=1}^{N-1} s_{Ni}\, \psi_i'^*(1) \right) \left(\frac{1}{2} \nabla_1^2 + \frac{N}{r_{1A}} + \frac{N}{r_{1B}} \right) \psi_N(1)\, d\vec{r}_1 + \\
& - \iint \left(\sum_{i=1}^{N-1} s_{Ni}\, \psi_i'^*(1) \right) \left(\sum_{j=N+1}^{2N-1} \psi_j'^*(2) \frac{1}{r_{12}} \psi_j(2) \right) \psi_N(1)\, d\vec{r}_1\, d\vec{r}_2 + \\
& - \sum_{i=1}^{N-1} \iint \psi_i'^*(1)\, \psi_N'^*(2) \frac{1}{r_{12}} \psi_N(1)\, \psi_i(2)\, d\vec{r}_1\, d\vec{r}_2 + \\
& - \sum_{i=1}^{N-1} \sum_{j=1}^{N-1} s_{Ni} \iint \psi_i'^*(1)\, \psi_j'^*(2) \frac{1}{r_{12}} \psi_N(1)\, \psi_j(2)\, d\vec{r}_1\, d\vec{r}_2 + \\
& + \sum_{i=1}^{N-1} \sum_{j=1}^{N-1} s_{Ni} \iint \psi_i'^*(1)\, \psi_j'^*(2) \frac{1}{r_{12}} \psi_j(1)\, \psi_N(2)\, d\vec{r}_1\, d\vec{r}_2 \Bigg\}
\end{aligned}
\qquad (64)
$$

where we have made use of equations (52) and (61) to simplify the results.

There are a number of further simplifications which can be made in equation (64), when we take account of the explicit form of the wavefunctions ψ_i and ψ_i', as given in table III. Considering first the last two integrals in equation (64), we note that these integrals contain only wavefunctions centered on nucleus A. General formulas for the evaluation of this type of integral are given by Slater[63], and one finds from his results that these integrals will vanish unless the wavefunctions ψ_i' and ψ_N have the same quantum numbers m_s and m_l, and in addition the sum of the quantum numbers l is even. We see from table III that this condition cannot be satisfied for the present case, and hence the last two integrals in equation (64) vanish. Further, one finds from the results in reference 63 that the matrix elements of ∇_1^2 and $\frac{1}{r_{1A}}$ in the first term of equation (64) will always vanish for the wavefunctions ψ_i given in table III, so that equation (64) reduces to the form

$$H_{AB}^{II} = D^2 \left\{ \int \left(\sum_{i=1}^{N-1} s_{Ni}\, \psi_i'^{*}(1) \right) \Phi(1)\, \psi_N(1)\, d\vec{r}_1 + \right.$$

$$\left. - \sum_{i=1}^{N-1} \iint \psi_i'^{*}(1)\, \psi_N'^{*}(2)\, \frac{1}{r_{12}}\, \psi_N(1)\, \psi_i(2)\, d\vec{r}_1\, d\vec{r}_2 \right\} \tag{65a}$$

where we have defined

$$\Phi(1) \equiv \frac{N}{r_{1B}} - \int \sum_{j=N+1}^{2N-1} \psi_j'^{*}(2)\, \frac{1}{r_{12}}\, \psi_j(2)\, d\vec{r}_2 \; . \tag{65b}$$

As a final simplification of equation (65), we note that the overlap integral s_{ij} (61) vanishes unless ψ_i' and ψ_j have the same values of the quantum numbers m_l and m_s. It thus follows from table III that for Π-states $s_{Ni} = 0$ for all $i \neq N$, and the first term in (65) vanishes identically. This is not true for Σ-states however, so that for the general case both terms in equation (65) must be retained.

Because of the symmetry between the initial and final states of the system one finds that the group II' permutations give a contribution to the matrix element H_{AB} identical to that from the group II permutations, so that we obtain simply

$$H_{AB}^{II'} = H_{AB}^{II} \tag{66}$$

The contribution of the group I permutations to the matrix element H_{AB} can be most conveniently calculated by writing the Hamiltonian (equation 27) in the form

$$H = H_A^+ + H_B^+ + H_{int} + H_{ex} \tag{67a}$$

where

$$H_A^+ = -\frac{1}{2}\sum_{i=1}^{N-1} \nabla_i^2 - \sum_{i=1}^{N-1} \frac{Z}{r_{Ai}} + \sum_{1\le i<j\le N-1} \frac{1}{r_{ij}}$$

$$H_B^+ = -\frac{1}{2}\sum_{i=N+1}^{2N-1} \nabla_i^2 - \sum_{i=N+1}^{2N-1} \frac{Z}{r_{Bi}} + \sum_{N+1\le i<j\le 2N-1} \frac{1}{r_{ij}}$$

$$H_{int} = \frac{Z^2}{r_{AB}} - \sum_{i=N+1}^{2N-1} \frac{Z}{r_{Ai}} - \sum_{i=1}^{N-1} \frac{Z}{r_{Bi}} + \sum_{i=1}^{N-1}\sum_{j=N+1}^{2N-1} \frac{1}{r_{ij}} \tag{67b}$$

and

$$H_{ex} = -\frac{1}{2}\nabla_N^2 - \frac{Z}{r_{NA}} - \frac{Z}{r_{NB}} + \sum_{i=1}^{N-1} \frac{1}{r_{iN}} + \sum_{i=N+1}^{2N-1} \frac{1}{r_{iN}} .$$

Here H_A^+ and H_B^+ are the Hamiltonians for the positive ion centered on nuclei A and B, respectively, H_{int} is the Hamiltonian for the interaction between these two ions and H_{ex} is the additional contribution to H due to the exchanged electron.

Let us consider first the contribution to the matrix elements arising from the terms H_A^+ and H_B^+ in equation (67). From symmetry we see that the contributions from these two terms must be the same. Since as we pointed out above group I contains only permutations of electrons 1 through N−1 among themselves and of N+1 through 2N−1 among themselves, the matrix elements for H_A^+ and H_B^+ factor to give

$$(H_A^+ + H_B^+)^I_{AB} = D^2 \sum_{(r \epsilon I)} (-1)^r \iint \prod_{i=1}^{2N-1} \psi_i'^*(r_i)\,(H_A^+ + H_B^+) \prod_{i=1}^{2N-1} \psi_i(i)\, d^{2N-1}\vec{r}$$

$$= 2D^2 s_{NN} \sum_{(r)} (-1)^r \iint \prod_{i=1}^{N-1} \psi_i'^*(r_i) H_A^+ \prod_{i=1}^{N-1} \psi_i(i)\, d^{N-1}\vec{r}$$

where the sum is now over all permutations of the integers 1 through N-1. In view of the orthogonality relation (52), we see that this term is quite analogous to the matrix elements obtained in evaluating the Hartree-Fock energies of atomic systems[64] except that the wavefunctions ψ_i and ψ_i' would be identical in the latter problem. This makes little difference for the analysis however, and by applying the methods used for atomic systems one readily finds that

$$(H_A^+ + H_B^+)^I_{AB} \equiv s_{NN} D^2 H_0'$$

$$= 2D^2 \; {}_{NN} \left\{ -\sum_{i=1}^{N-1} \int \psi_i'^*(1) \left(\frac{1}{2} \nabla_1^2 + \frac{N}{r_{1A}} \right) \psi_i(1)\, d\vec{r}_1 + \right.$$

$$\left. + \sum_{1 \le i < j \le N-1} \int [\psi_i'^*(1)\psi_j'^*(2) - \psi_j'^*(1)\psi_i'^*(2)] \frac{1}{r_{12}} \psi_i(1)\psi_j(2)\, d\vec{r}_1\, d\vec{r}_2 \right\} \quad (68)$$

where we have introduced the separation-independent quantity H_0' in equation (68) in analogy with the similar quantity H_0 found in equation (47). One notes that if the difference between the atomic and ionic wavefunctions were neglected, then H_0' would be simply equal to twice the ground-state energy E_0^+ of the isolated ion, and $H_0' - H_0$ would be just the ionization energy.

To evaluate the matrix elements of the quantities H_{int} and H_{ex} in equation (67) for the group I permutations, we note that each term in these operators contains at most one electron in each of the ranges $1 \le i \le N-1$ and $N+1 \le j \le 2N-1$. It then follows from equation (52) that any permutation of electrons within either of these ranges will give a zero contribution to the matrix elements. Thus the only group I permutation

which gives a nonvanishing contribution to the matrix elements is the identity permutation, and we obtain the result that

$$H^{I}_{AB} = D^2 \left\{ H_0' \, s_{NN} + \left[N\Phi(A) - \int \sum_{i=1}^{N-1} \psi_i'^{*}(1)\, \Phi(1)\, \psi_i(1)\, d\vec{r}_1 \right] s_{NN} + \right.$$

$$\left. + \int \psi_N'^{*}(1) \left[-\frac{1}{2} \nabla_1^2 - 2\Phi(1) \right] \psi_N(1)\, d\vec{r}_1 \right\} \tag{69}$$

where $\Phi(1)$ is defined by equation (65b) and $\Phi(A)$ is the value of $\Phi(1)$ for $\vec{r}_1 = \vec{r}_A$.

The expressions for the matrix elements given by equations (45), (48), (60), (62), (63), (65), (66), and (69) of the present section may now be substituted into equations (41) and (42) to obtain an explicit formula for the interaction energies of the $N-N^+$ and $O-O^+$ systems. Taking the zero of energy equal to the energy H_0 of the atom and ion at infinite separation, the formula becomes

$$E_{S,M_l} = Q_0 \pm b_S^{(1)} \, W_1^{(M_l)}$$

$$= \pm \, b_S^{(1)} D^2 \left\{ (H_0' - H_0)\, s_{NN} - \frac{1}{2} \int \psi_N'^{*}(1)\, \nabla_1^2 \psi_N(1)\, d\vec{r}_1 + \right.$$

$$+ \left[N\Phi(A) - \int \sum_{i=1}^{N-1} \psi_i'^{*}(1)\, \Phi(1)\, \psi_i(1)\, d\vec{r}_1 - Q_0 \right] s_{NN}$$

$$+ 2 \sum_{i=1}^{N-1} s_{Ni} \int \psi_i'^{*}(1)\, \Phi(1)\, \psi_N(1)\, d\vec{r}_1 +$$

$$+ \sum_{i=1}^{N-1} \sum_{j=N+1}^{2N-1} s_{ji} \iint \psi_i'^{*}(1)\, \psi_N'^{*}(2)\, \frac{1}{r_{12}}\, \psi_N(1)\, \psi_j(2)\, d\vec{r}_1\, d\vec{r}_2 \; +$$

$$- 2 \int \psi_N'^{*}(1)\, \Phi(1)\, \psi_N(1)\, d\vec{r}_1 \; +$$

$$\left. - 2 \sum_{i=1}^{N-1} \iint \psi_i'^{*}(1)\, \psi_N'^{*}(2)\, \frac{1}{r_{12}}\, \psi_N(1)\, \psi_i(2)\, d\vec{r}_1\, d\vec{r}_2 \right\} + Q_0 \qquad (70)$$

where $N = 7$ for nitrogen and 8 for oxygen, $b_S^{(1)}$ is given by equation (40), Q_0 by equation (49), D by equations (55) and (56), s_{ij} by equation (61), Φ by equation (65b), H_0' by equation (68), and H_0 can be obtained from the Hartree-Fock calculations for the isolated atoms.[48]

The one-electron wavefunctions ψ_i and ψ_i' are defined in table III, where it is understood that the original Hartree-Fock wavefunctions are to be used for the positive ion in evaluating the terms H_0, Q_0, and D in equation (70), while the transformed wavefunctions (53) are to be used in evaluating all the other terms.

F. EVALUATION OF THE BASIC MOLECULAR INTEGRALS

1. Classification of the Basic One- and Two-Electron Integrals

Equation (70) for the interaction energy is given in terms of certain integrals over the coordinates of one or two electrons. A detailed examination of the form of these integrals shows that they are all of one or another of the following standard types:[65]

a. One-Center Integrals

1) Overlap integrals, $\int \psi_{iA}^{*}\, \psi_{jA}\, d\vec{r}$,

2) Kinetic energy integrals, $\int \psi_{iA}^{*}\, \nabla^2\, \psi_{jA}\, d\vec{r}$

3) Nuclear attraction integrals, $\int \psi_{iA}^{*} \frac{1}{r_A} \psi_{jA} \, d\vec{r}$

4) 2-electron integrals, $\int \psi_{iA}^{*}(1) \psi_{jA}^{*}(2) \frac{1}{r_{12}} \psi_{kA}(1) \psi_{tA}(2) \, d\vec{r}_1 \, d\vec{r}_2$

b. Two-Center Integrals

1) Overlap integrals, $\int \psi_{iA}^{*} \psi_{jB} \, d\vec{r}$

2) Kinetic energy integrals, $\int \psi_{iA}^{*} \nabla^2 \psi_{jB} \, d\vec{r}$

3) Nuclear attraction integrals of two types

a) Coulomb integrals, $\int \psi_{iA}^{*} \frac{1}{r_B} \psi_{jA} \, d\vec{r}$

b) Resonance integrals, $\int \psi_{iA}^{*} \frac{1}{r_A} \psi_{jB} \, d\vec{r}$

4) 2-electron integrals of two types

a) Coulomb integrals, $\int \psi_{iA}^{*}(1) \psi_{jB}^{*}(2) \frac{1}{r_{12}} \psi_{kA}(1) \psi_{tB}(2) \, d\vec{r}_1 \, d\vec{r}_2$

for which one electron is always on nucleus A and the other is always on nucleus B

b) Ionic or hybrid integrals, $\int \psi_{iA}^{*}(1) \psi_{jA}^{*}(2) \frac{1}{r_{12}} \psi_{kA}(1) \psi_{tB}(2) \, d\vec{r}_1 \, d\vec{r}_2$,

for which one electron remains always on the same nucleus while the other electron is exchanged.

There is also a third type of two-electron integral which does not occur in our formulas, and which will therefore not need to be considered here. namely the exchange integral

$$\iint \psi^*_{iB}(1)\psi^*_{jA}(2)\frac{1}{r_{12}}\psi_{kA}(1)\psi_{tB}(2)\, d\vec{r}_1\, d\vec{r}_2$$ in which both electrons are exchanged.

Specifically, we see from equation (70) and the table of wavefunctions III that the first term in the braces in equation (70) consists of a sum of one-center integrals times a two-center overlap integral, the second term is a two-center kinetic energy integral, the terms in the second, third, and fourth lines each consist of a coulomb integral times a two-center overlap integral, while the terms in the final two lines are hybrid or ionic integrals. These various types of integrals have all been studied extensively in the literature[63, 65-69] and they can all be evaluated in closed form for wavefunctions of the form used here (equations 16 and 17). The evaluation of each of the integrals is discussed individually below.

2. The Transformed Positive-Ion Wavefunctions and the Electron Readjustment Integral, D^2

Let us consider first the one-center overlap integrals $s^{(0)}_{kj}$ which are defined in equation (55) and are required in calculating the transformed positive-ion wavefunctions of equation (53). For wavefunctions of the form given by equations (16) and (17), these integrals can be carried out immediately by using the orthogonality properties of the spherical harmonics and evaluating the radial integrals in terms of the Γ-function to obtain the general formula

$$\int \psi^*_\alpha \psi_\beta\, d\vec{r} = \delta_{l_\alpha l_\beta}\delta_{m_{l_\alpha} m_{l_\beta}}\delta_{m_{s_\alpha} m_{s_\beta}} \int_0^\infty R_\alpha R_\beta r^2\, dr$$

$$= \delta_{l_\alpha l_\beta}\delta_{m_{l_\alpha} m_{l_\beta}}\delta_{m_{s_\alpha} m_{s_\beta}} \sum_{i=1}^{N_\alpha}\sum_{j=1}^{N_\beta} \frac{c_{\alpha_i} c_{\beta_j} (n_{\alpha_i} + n_{\beta_j})!}{(\zeta_{\alpha_i} + \zeta_{\beta_j})^{n_{\alpha_i} + n_{\beta_j} + 1}} \tag{71}$$

The values of the $s^{(0)}_{kj}$ for nitrogen and oxygen were calculated from this formula using the wavefunction parameters given in table I, and the results were then substituted into equations (53) and (54) to obtain the transformed N^+ and 0^+ wavefunctions given in table IV. Since the only non-zero

TABLE IV

EXPANSION COEFFICIENTS $c_{\alpha_i}^{(t)}$ FOR THE TRANSFORMED POSITIVE ION WAVEFUNCTIONS

	N^+			O^+		
	$c_{1s_i}^{(t)}$	$c_{2s_i}^{(t)}$	$c_{2p_i}^{(t)}$	$c_{1s_i}^{(t)}$	$c_{2s_i}^{(t)}$	$c_{2p_i}^{(t)}$
1	29.8050	-6.42817	0.647845	38.1921	-9.73085	1.17995
2	5.34086	-1.84260	3.75984	4.98150	-0.50735	4.60027
3	-0.01076	2.79505	5.04031	-0.00613	4.54300	7.98906
4	0.07872	6.02848	1.76741	0.09829	9.26383	2.68083
5	0.49973	-10.94368		2.13020	-11.2961	

off-diagonal elements $s_{kj}^{(0)}$ in this case were those between the 1s and 2s wavefunctions of the same spin, it was in effect only necessary here to invert a two-by-two matrix in order to determine the transformation coefficients c_{ik}^{+} in equation (53).

The calculated values of the $s_{kj}^{(0)}$ were also used to evaluate the determinant D^2 which occurs in equation (70) and which presumably takes account of the effects on the interaction potential produced by the readjustment of the remaining electrons in the system when one electron is transferred from the atom to the ion. In terms of the non-zero $s_{kj}^{(0)}$, it was found that for nitrogen

$$D^2 = (s_{1s,1s}\, s_{2s,2s} - s_{1s,2s}\, s_{2s,1s})^4\, s_{2p,2p}^4 = 0.95884 \tag{72a}$$

and for oxygen

$$D^2 = (s_{1s,1s}\, s_{2s,2s} - s_{1s,2s}\, s_{2s,1s})^4\, s_{2p,2p}^6 = 0.94316 \tag{72b}$$

Thus, as might have been expected, we see that electron readjustment has only a relatively small effect on the interaction potentials.

3. The One-Center Integrals

One sees from table III that the quantity H_0', defined by equation (68), contains only wavefunctions centered on a single nucleus, and is thus independent of the internuclear separation, R. Explicit formulas for the various integrals occurring in equation (68) in terms of the radial wavefunctions $R_{nl}(r)$ are given in Slater's book on atomic theory.[63] Substituting in equation (68) from table III and equations (13-5), (13-6), (13-18), and (13-19) of reference 63, we obtain the formula for H_0' in the form

$$\begin{aligned} H_0' = 2\Big\{ & 2T(1s) + 2T(2s) + (N-5)\,T(2p) - N\,[2V(1s) + 2V(2s) + (N-5)\,V(2p)] \\ & + F^0(1s,1s) + 2\,[2F^0(1s,2s) - G^0(1s,2s)] + F^0(2s,2s) + \\ & + (N-5)\left[2F^0(1s,2p) + 2F^0(2s,2p) - \frac{1}{3}G^1(1s,2p) - \frac{1}{3}G^1(2s,2p)\right] \\ & + a\left[F^0(2p,2p) - \frac{1}{5}F^2(2p,2p)\right]\Big\} \end{aligned} \tag{73}$$

where again $N = Z$ is the nuclear charge, $(N-5)$ is, of course, the number of p-electrons on the ion, the coefficient a is 1 for nitrogen and 3 for oxygen, and the radial integrals T, V, F^l and G^l are defined by the formulas

$$T(\alpha) \equiv \frac{1}{2} \int_0^\infty \frac{d}{dr} \left[R_\alpha^+(r)/r^{l_\alpha} \right] \frac{d}{dr} \left[R_\alpha(r)/r^{l_\alpha} \right] r^{2l_\alpha+2} \, dr$$

$$V(\alpha) \equiv \int_0^\infty R_\alpha^+(r) \, R_\alpha(r) \, r \, dr$$

$$F^l(\alpha, \beta) \equiv J^l(\alpha, \alpha; \beta, \beta)$$

$$G^l(\alpha, \beta) \equiv J^l(\alpha, \beta; \beta, \alpha)$$

$$J^l(\alpha, \beta; \gamma, \delta) \equiv \int_0^\infty \int_0^\infty R_\alpha^+(r_1) R_\beta(r_1) R_\gamma^+(r_2) R_\delta(r_2) I_l(r_1, r_2) \, r_1^2 \, r_2^2 \, dr_1 \, dr_2$$

and

$$I_l(r_1, r_2) \equiv r_1^l / r_2^{l+1} \quad \text{for} \quad r_1 \leq r_2$$

$$\equiv r_2^l / r_1^{l+1} \quad \text{for} \quad r_1 \geq r_2 \; . \tag{74}$$

For the radial wavefunctions of equation (17), the one-electron integrals $T(\alpha)$ and $V(\alpha)$ can be readily evaluated by direct integration of the defining equations, using the same procedure as for the one-center overlap integrals (equation 71), to give the general formulas

$$T(\alpha) = \sum_{i=1}^{N_\alpha} \sum_{j=1}^{N_\alpha^+} \frac{c_{\alpha_i} c_{\alpha_j}^+ (n_{\alpha_i} + n_{\alpha_j}^+ - 2)!}{(\zeta_{\alpha_i} + \zeta_{\alpha_j}^+)^{n_{\alpha_i} + n_{\alpha_j}^+ + 1}}$$

$$\times \left[l_\alpha (l_\alpha + 1) (\zeta_{\alpha_i} + \zeta_{\alpha_j}^+)^2 - (n_{\alpha_j}^+ \zeta_{\alpha_i} - n_{\alpha_i} \zeta_{\alpha_j}^+)^2 + n_{\alpha_j}^+ \zeta_{\alpha_i}^2 + n_{\alpha_i} \zeta_{\alpha_j}^{+2} \right]$$

$$V(a) = \sum_{i=1}^{N_a} \sum_{j=1}^{N_a^+} \frac{c_{a_i} c_{a_j}^+ (n_{a_i} + n_{a_j}^+ - 1)!}{(\zeta_{a_i} + \zeta_{a_j}^+)^{(n_{a_i} + n_{a_j}^+)}} \tag{75}$$

To evaluate the two-electron integrals J^l we introduce the auxiliary function

$$K_{mnl}(x, y) \equiv \int_0^\infty \int_0^\infty r_1^m r_2^n \; e^{-x r_1} \; e^{-y r_2} \; I_l(r_1, r_2) \, dr_1 \, dr_2 \quad \text{for } m,n > l+1 \tag{76}$$

so that equation (74) for J^l becomes

$$J^l(a, \beta; \gamma, \delta) = \sum_{i=1}^{N_a^+} \sum_{j=1}^{N_\beta} \sum_{k=1}^{N_\gamma^+} \sum_{m=1}^{N_\delta} c_{a_i}^+ c_{\beta_j} c_{\gamma_k}^+ c_{\delta_m} K_{n_{a_i}^+ + n_{\beta_j}, \, n_{\gamma_k}^+ + n_{\delta_m}, \, l} (\zeta_{a_i}^+ + \zeta_{\beta_j}, \zeta_{\gamma_k}^+ + \zeta_{\delta_m}) \tag{77}$$

The K's are then calculated from the formula

$$K_{mnl}(x, y) = \frac{(m+n-1)!}{xy(x+y)^{m+n-1}} \left\{ 1 + \sum_{k=1}^{m-l-1} \frac{(m-l-1)!\,(n+l)!}{(m-l-1-k)!\,(m+l+k)!} \left(\frac{y}{x}\right)^k \right.$$

$$\left. + \sum_{k=1}^{n-l-1} \frac{(n-l-1)!\,(m+l)!}{(n-l-1-k)!\,(m+l+k)!} \left(\frac{x}{y}\right)^k \right\} \quad \text{for } m, n \geq l+1. \tag{78}$$

Equation (78) can be readily verified by induction on m and n; to do this equation (76) is integrated directly for the case $m = n = l + 1$ to establish the base of the induction, and higher values of m and n are then obtained by differentiation of equations (76) and (78) with respect to x and y.

Equations (75), (77), and (78) were programmed for digital computation and the results of these programs were used to calculate the value of H_0' from equation (73). As a check, these programs were also used to calculate the Hartree-Fock energy H_0 of the isolated atoms and ions, giving agreement to six significant figures with Clementi's results.[48]

The values of H_0' calculated from equations (73) through (78) for the wavefunctions of tables I and IV were

$$H_0' = -107.76970 \qquad \text{for nitrogen}$$

and

$$H_0' = -148.73342 \qquad \text{for oxygen,} \tag{79a}$$

or, combining with the values of H_0 from Clementi's calculation,[48]

$$H_0' - H_0 = 0.51918 \text{ atomic units} = 14.12 \text{ ev for nitrogen}$$

and

$$H_0' - H_0 = 0.44860 \text{ atomic units} = 12.20 \text{ ev for oxygen.} \tag{79b}$$

As expected, these values are approximately equal to the ionization potentials of the atoms, i.e. 14.54 ev and 13.6 ev respectively for nitrogen and oxygen.

4. The Coulomb Integrals

The Coulomb integrals which occur in lines two, three, and four of equation (70), are all of the general form

$$Q(i, k; j, t) \equiv \iint \psi_{iA}^*(1)\, \psi_{jB}^*(2)\, (1/r_{12})\, \psi_{kA}(1)\, \psi_{tB}(2)\, d\vec{r}_1\, d\vec{r}_2 \tag{80}$$

in which electron 1 remains always on nucleus A and electron 2 always on nucleus B. It is readily shown[66] that this expression represents the Coulomb interaction between the electronic charge distributions $\psi_{iA}^* \psi_{kA}$ on nucleus A and $\psi_{kB}^* \psi_{tB}$ on nucleus B. For the wavefunctions given by equations (16) and (17), it consists simply of a long-range multipole interaction term plus a term in $e^{-2\zeta R}$ which arises from the overlap of the charge distributions in the two atoms. Since the latter term is of the same order as the multiple electron exchange terms which have been neglected in the present calculation, we can omit it and consider only the multipole term in calculating Q. Thus for the present approximation Q can be expanded in terms of the multipole moments of the charge distributions $\psi_{iA}^* \psi_{kA}$ and $\psi_{jB}^* \psi_{tB}$ giving the result that

$$Q(i,k;j,t) = \delta_{m_{s_i} m_{s_k}} \delta_{m_{s_j} m_{s_t}} \sum_{m,n} \frac{g_{mn}(i,k;j,t)}{R^{m+n+1}} q_{ik}^{(m)} q_{tj}^{(n)} \tag{81a}$$

where

$$q_{\alpha\beta}^{(m)} = \int_0^\infty R_\alpha(r) R_\beta(r) r^{2+m} dr \tag{81b}$$

is proportional to the mth multipole moment of the charge distribution $\psi_\alpha^* \psi_\beta$ and the coefficients g_{mn} depend only on the angular part of the wavefunctions. For the cases required here, the g_{mn} can be readily evaluated by comparison with the explicit formulas for the Coulomb integrals which have been calculated by Roothaan for a number of special cases,[66] and in this way we have obtained the values given in table V. The coefficients g_{mn} for other combinations of s and p electrons can be obtained from the values given in table V by applying the following symmetry relations, which are readily derived from the defining equations (16), (17), (80), and (81):

$$g_{mn}(i,k;j,t) = g_{mn}(k,i;t,j) = g_{nm}(j,t;i,k) = g_{mn}(i^*,k^*;j^*,t^*) = g_{mn}(k,i;j,t) \tag{82a}$$

$$g_{mn}(i,k;j,t) = 0 \qquad \text{for } m_{l_i} - m_{l_k} \neq m_{l_t} - m_{l_j} \tag{82b}$$

In these equations, m_{l_i}, m_{l_k}, m_{l_j}, and m_{l_t} are the azimuthal quantum numbers of the states i, k, j, and t, respectively, the transformation* of the wavefunctions simply interchanges π^+ and π^-, and the last equality in (82a) holds only when ψ_i and ψ_k have the same value for the azimuthal quantum number m_l.

The one-electron Coulomb integral

$$Q^0(i,k) \equiv \int \psi_{iA}^*(1) \frac{1}{r_{1B}} \psi_{kA}(1) d\vec{r}_1 \tag{83}$$

is simply a special case of equation (80) in which the charge distribution $\psi^* \psi$ on nucleus B is replaced by a point charge at the nuclear center. The multipole expansion of equation (83) follows immediately when one notes that all multipoles are zero for a point charge except for the zero-order term which is just the total charge on the system, equal to one unit. Thus the expansion (81a) becomes

TABLE V

MULTIPOLE EXPANSION COEFFICIENTS g_{mn} FOR THE COULOMB INTEGRAL*

Integral	g_{00}	g_{01}	g_{02}	g_{10}	g_{11}	g_{12}	g_{20}	g_{21}	g_{22}
$Q(s, s; s, s)$	1								
$Q(s, s; s, \sigma)$		$\frac{1}{\sqrt{3}}$							
$Q(s, \sigma; s, \sigma)$					$\frac{2}{3}$				
$Q(s, s; \sigma, \sigma)$	1		$\frac{2}{5}$						
$Q(s, \sigma; \sigma, \sigma)$				$\frac{1}{\sqrt{3}}$		$\frac{2\sqrt{3}}{5}$			
$Q(\sigma, \sigma; \sigma, \sigma)$	1		$\frac{2}{5}$				$\frac{2}{5}$		$\frac{24}{25}$
$Q(s, s; \pi^+, \pi^+)$	1		$-\frac{1}{5}$						
$Q(s, \pi^+; \pi^+, s) = Q(s, \pi^+; s, \pi^-)$					$\frac{1}{3}$				
$Q(s, \sigma; \pi^+, \pi^+)$				$\frac{1}{\sqrt{3}}$		$-\frac{\sqrt{3}}{5}$			
$Q(s, \pi^+; \pi^+, \sigma) = Q(s; \pi^+; \sigma, \pi^-)$						$\frac{\sqrt{3}}{5}$			
$Q(\sigma, \sigma; \pi^+, \pi^+)$	1		$-\frac{1}{5}$				$\frac{2}{5}$		$-\frac{12}{25}$
$Q(\sigma, \pi^+; \pi^+, \sigma) = Q(\sigma, \pi^+; \sigma, \pi^-)$									$\frac{12}{25}$
$Q(\pi^+, \pi^+; \pi^+, \pi^+) = Q(\pi^+, \pi^+; \pi^-, \pi^-)$	1		$-\frac{1}{5}$				$-\frac{1}{5}$		$\frac{6}{25}$
$Q(\pi^+, \pi^-; \pi^-, \pi^+)$									$\frac{6}{25}$

*Coefficients not indicated are equal to 0.

$$Q^0(i,k) = \delta_{m_{s_i} m_{s_k}} \sum_m \frac{g_{m0}(i,k;s,s)}{R^{m+1}} \quad q_{ik}^{(m)} \tag{84}$$

When equations (81) and (84) are substituted into the expression for the interaction potentials (equation 70), and the results simplified by the use of the orthonormality condition (52), we find that lines two, three, and four of equation (70) reduce to the form

$$E^{(Q)} = \left(\frac{1}{R} + \frac{2}{5}\frac{q_0}{R^3} + \frac{4}{5}\frac{q}{R^3} + \frac{24}{25}\frac{q^2}{R^5}\right) S(2\sigma, 2\sigma) + \frac{24}{25}\frac{q^2}{R^5} S(2\pi^+, 2\pi^+)$$

$$+ \frac{2}{\sqrt{3}}\frac{1}{R^2}\left(1 + \frac{6}{5}\frac{q}{R^2}\right) [d_1 S(1s, 2\sigma) + d_2 S(2s, 2\sigma)]$$

$$+ \frac{2}{3R^3}[d_1^2 S(1s,1s) + 2 d_1 d_2 S(1s,2s) + d_2^2 S(2s,2s)] \quad \text{for } \Sigma - \text{states,}$$

and

$$E^{(Q)} = \left(\frac{1}{R} - \frac{1}{5}\frac{q_0}{R^3} - \frac{2}{5}\frac{q}{R^3} + \frac{12}{25}\frac{q^2}{R^5}\right) S(2\pi^+, 2\pi^+) + \frac{12}{25}\frac{q^2}{R^5} S(2\sigma, 2\sigma)$$

$$+ \frac{2\sqrt{3}}{5}\frac{q}{R^4} [d_1 S(1s, 2\sigma) + d_2 S(2s, 2\sigma)]$$

$$+ \frac{1}{3R^3}[d_1^2 S(1s,1s) + 2 d_1 d_2 S(1s,2s) + d_2^2 S(2s,2s)] \quad \text{for } \Pi - \text{states}, \tag{85}$$

where q_0 is proportional to the quadrupole moment of the atom and is given by

$$q_0 = 0 \qquad \text{for nitrogen}$$

$$q_0 = \int_0^\infty (R_{2p})^2 r^4 \, dr \qquad \text{for oxygen,} \tag{86a}$$

q is related to the quadrupole moment of the ionic core and is given by

$$q = \int_0^\infty R_{2p}^+ \; R_{2p} \; r^4 \, dr \qquad \text{for nitrogen}$$

$$q = 0 \qquad \text{for oxygen,} \tag{86b}$$

the dipole moments d_1 and d_2 are given by

$$d_1 = \int_0^\infty R_{1s}^+ \; R_{2p} \; r^3 \, dr$$

$$d_2 = \int_0^\infty R_{2s}^+ \; R_{2p} \; r^3 \, dr \tag{86c}$$

for both nitrogen and oxygen, and the two-center overlap integrals $S(\alpha, \beta)$ are defined by the relation

$$S(\alpha, \beta) \equiv \int u_{\alpha A}^* \; u_{\beta B} \; d\vec{r} \tag{87}$$

where $u \equiv R(r) \; Y(\theta, \phi)$ is the spatial part of the one-electron wavefunction ψ given by equation (16).

Equation (85) can be further simplified by introducing the new wavefunctions

$$u_s \equiv d_1 \, u_{1s} + d_2 \, u_{2s}$$

$$= \left(\sum_{i=1}^{5} c_{s_i} \, r^{n_{s_i} - 1} \, e^{-\zeta_{s_i} r} \right) Y_{00} \, (\theta, \phi) \tag{88a}$$

where the coefficients c_{s_i} are given by

$$c_{s_i} = d_1 \, c_{1s_i} + d_2 \, c_{2s_i} \tag{88b}$$

Substituting equation (88a) into equation (85), we obtain the final formula for the Coulomb integrals in the form

$$E^{(Q)} = \left(\frac{1}{R} + \frac{2}{5}\frac{q_0}{R^3} + \frac{4}{5}\frac{q}{R^3} + \frac{24}{25}\frac{q^2}{R^5}\right) S(2\sigma, 2\sigma) + \frac{24}{25}\frac{q^2}{R^5} S(2\pi^+, 2\pi^+)$$

$$+ \frac{2}{\sqrt{3}}\frac{1}{R^2}\left(1 + \frac{6}{5}\frac{q}{R^2}\right) S(s, 2\sigma) + \frac{2}{3R^3} S(s, s) \qquad \text{for } \Sigma - \text{states}$$

$$E^{(Q)} = \left(\frac{1}{R} - \frac{1}{5}\frac{q_0}{R^3} - \frac{2}{5}\frac{q}{R^3} + \frac{12}{25}\frac{q^2}{R^5}\right) S(2\pi^+, 2\pi^+) + \frac{12}{25}\frac{q^2}{R^5} S(2\sigma, 2\sigma)$$

$$+ \frac{2\sqrt{3}}{5}\frac{q}{R^4} S(s, 2\sigma) + \frac{1}{3R^3} S(s, s) \qquad \text{for } \Pi - \text{states} \tag{89}$$

For the radial wavefunctions (17), the integral (81b) for the multipole moments $q^{(m)}_{\alpha\beta}$ can be evaluated by the same method used previously for the one-center overlap integrals (equation 71) to give the general formula

$$q^{(m)}_{\alpha\beta} = \sum_{i=1}^{N_\alpha}\sum_{j=1}^{N_\beta} \frac{c_{\alpha_i} c_{\beta_j} (n_{\alpha_i} + n_{\beta_j} + m)!}{(\zeta_{\alpha_i} + \zeta_{\beta_j})^{n_{\alpha_i} + n_{\beta_j} + m + 1}} \tag{90}$$

Table VI gives values of the multipole moments (86) for nitrogen and oxygen calculated from this formula using the wavefunctions of tables I and IV. Table VII gives the corresponding values of the expansion coefficients c_{s_i} in equation (88).

TABLE VI

MULTIPOLE MOMENTS FOR THE $N-N^+$ AND $O-O^+$ INTERACTIONS (IN ATOMIC UNITS)

Species	q_0	q	d_1	d_2
$N-N^+$	0	2.18838	0.12094	1.28611
$O-O^+$	1.97413	0	0.10707	1.11493

TABLE VII

EXPANSION COEFFICIENTS c_{s_i} FOR THE WAVEFUNCTION ψ_s

Species	c_{s_1}	c_{s_2}	c_{s_i}	c_{s_3}	c_{s_4}	c_{s_5}
$N-N^+$	-5.33142	-0.37537		2.85277	8.55776	-9.94587
$O-O^+$	-6.15581	-0.13540		3.90076	11.20007	-13.36216

5. The Two-Center Overlap Integrals

Let us now turn to the evaluation of the two-center overlap integrals $S(\alpha, \beta)$ defined by equation (87). Substituting the form for the wavefunctions given by equations (16) and (17) into equation (87), we obtain

$$S(\alpha, \beta) = \sum_{i,j} c_{\alpha_i} c_{\beta_j} s_{n_{\alpha_i} \alpha, n_{\beta_j} \beta} (\zeta_{\alpha_i}, \zeta_{\beta_j}) \tag{91}$$

where the indices α and β indicate the angular dependence of the wavefunctions (i. e., either s, σ, π^+, or π^-) and the functions $s_{n\alpha, n\beta}$ represent the values of the overlap integral (87) for the simple unnormalized Slater wavefunctions

$$u^{(0)}_{n l m} = r^{n-1} e^{-\zeta r} Y_{l m}(\theta, \phi) \quad . \tag{92}$$

The elementary overlap integrals $s_{n\alpha, m\beta}$ which appear in equation (91) have been calculated by Roothaan[66] for all combinations of 1s, 2s, and 2p electrons. For the present calculation, it is convenient to write Roothaan's results in terms of the parameters

$$\begin{aligned} \rho_a &= \zeta_a R \\ \rho_b &= \zeta_b R \\ \mu &= \rho_a/\rho_b \\ \lambda &= 2/(\mu^2 - 1) \quad . \end{aligned} \tag{93}$$

With this notation, Roothaan's formulas for the elementary overlap integrals $s_{n\alpha, m\beta}$ become

$$s_{1s, 1s}(\zeta_a, \zeta_b) = \frac{1}{2} (\lambda^2 \mu/\zeta_b^3 \rho_b) [-2\lambda + \rho_b] e^{-\rho_b} +$$

$$+ \frac{1}{2} \lambda(\lambda + 2)(\mu/\zeta_a^3 \rho_a) [2(\lambda + 2) + \rho_a] e^{-\rho_a}$$

$$s_{1s, 2s}(\zeta_a, \zeta_b) = \frac{1}{2} (\lambda^2 \mu/\zeta_b^4 \rho_b) [2\lambda(3\lambda + 1) - 4\lambda \rho_b + \rho_b^2] e^{-\rho_b} +$$

$$+ \frac{1}{2} (\lambda + 2)^2 (\zeta_a^4 \rho_a)^{-1} [-2(\lambda + 2)(1 + 3\lambda) - (2\lambda + 1) \rho_a] e^{-\rho_a}$$

$$s_{2s,\,1s}(\zeta_a, \zeta_b) = \frac{1}{2}(\lambda^2/\zeta_b^4\ \rho_b)\,[-2\lambda(3\lambda+5)+(2\lambda+3)\rho_b]\,e^{-\rho_b} +$$

$$+ \frac{1}{2}\lambda(\lambda+2)(\mu/\zeta_a^4\ \rho_a)\,[2(\lambda+2)(3\lambda+5)+4(\lambda+2)\rho_a+\rho_a^2]\,e^{-\rho_a}$$

$$s_{2s,\,2s}(\zeta_a, \zeta_b) = \frac{1}{2}(\lambda^2/\zeta_b^5\ \rho_b)\,[2\lambda(12\lambda^2+24\lambda+5)-4\lambda(3\lambda+5)\rho_b+(2\lambda+3)\rho_b^2]\,e^{-\rho_b} +$$

$$- \frac{1}{2}(\lambda+2)^2(\zeta_a^5\ \rho_a)^{-1}\,[2(\lambda+2)(12\lambda^2+24\lambda+5)+4(\lambda+2)(3\lambda+1)\rho_a+(2\lambda+1)\rho_a^2]\,e^{-\rho_a}$$

$$s_{1s,\,2\sigma}(\zeta_a, \zeta_b) = \sqrt{3}\,(\lambda^2\,\mu/\zeta_b^4\ \rho_b^2)\,[6\lambda^2(1+\rho_b)-4\lambda\,\rho_b^2+\rho_b^3]\,e^{-\rho_b} +$$

$$- \sqrt{3}\ \lambda(\lambda+2)^2(\mu/\zeta_a^4\ \rho_a^2)\,[6(\lambda+2)(1+\rho_a)+2\rho_a^2]\,e^{-\rho_a}$$

$$s_{2s,\,2\sigma}(\zeta_a, \zeta_b) = \sqrt{3}\,(\lambda^2/\zeta_b^5\ \rho_b^2)\,[6\lambda^2(4\lambda+7)(1+\rho_b)-4\lambda(3\lambda+5)\rho_b^2+(2\lambda+3)\rho_b^3]\,e^{-\rho_b} +$$

$$- \sqrt{3}\,\lambda(\lambda+2)^2(\mu/\zeta_a^5\ \rho_a^2)\,[6(\lambda+2)(4\lambda+7)(1+\rho_a)+2(6\lambda+11)\rho_a^2+2\rho_a^3]\,e^{-\rho_a}$$

$$s_{2\pi,\,2\pi}(\zeta_a, \zeta_b) \equiv s_{2\pi^+,\,2\pi^+}(\zeta_a, \zeta_b) \equiv s_{2\pi^-,\,2\pi^-}(\zeta_a, \zeta_b)$$

$$= \frac{3}{2}(\lambda^3\ \mu/\zeta_b^5\ \rho_b^3)\,[24\lambda^2(1+\rho_b)-12\lambda\,\rho_b^2+2\rho_b^3]\,e^{-\rho_b} +$$

$$- \frac{3}{2}\lambda(\lambda+2)^2(\mu/\zeta_a^5\ \rho_a^3)\,[24(\lambda+2)^2(1+\rho_a)+12(\lambda+2)\rho_a^2+2\rho_a^3]\,e^{-\rho_a}$$

$$s_{2\sigma,\,2\sigma}(\zeta_a, \zeta_b) = -\frac{d}{dR}\,[R\,s_{2\pi,\,2\pi}(\zeta_a, \zeta_b)]$$

$$= \frac{3}{2}(\lambda^3\ \mu/\zeta_b^5\ \rho_b^3)\,[24\lambda^2(2+2\rho_b+\rho_b^2)-2(6\lambda+1)\rho_b^3+2\rho_b^4]\,e^{-\rho_b} +$$

$$- \frac{3}{2}\lambda(\lambda+2)^2(\mu/\zeta_a^5\ \rho_a^3)\,[24(\lambda+2)^2(2+2\rho_a+\rho_a^2)+2(6\lambda+11)\rho_a^3+2\rho_a^4]\,e^{-\rho_a}$$

In the special case $\zeta_a = \zeta_b$ the formulas (94a) for the overlap integrals all become indeterminate, and Roothaan gives special formulas for this case in the form

$$s_{1s,\,1s}(\zeta,\zeta) = (1/4\zeta^3)\left(1+\rho+\frac{1}{3}\rho^2\right)e^{-\rho}$$

$$s_{2s,\,2s}(\zeta,\zeta) = (3/4\zeta^5)\left(1+\rho+\frac{4}{9}\rho^2+\frac{1}{9}\rho^3+\frac{1}{45}\rho^4\right)e^{-\rho}$$

$$s_{2\pi,\,2\pi}(\zeta,\zeta) = (3/4\zeta^5)\left(1+\rho+\frac{2}{5}\rho^2+\frac{1}{15}\rho^3\right)e^{-\rho}$$

$$s_{2\sigma,\,2\sigma}(\zeta,\zeta) = -\frac{d}{dR}\left[R\, s_{2\sigma,\,2\sigma}(\zeta,\zeta)\right]$$

$$= (3/4\zeta^5)\left(-1-\rho-\frac{1}{5}\rho^2+\frac{2}{15}\rho^3+\frac{1}{15}\rho^4\right)e^{-\rho} \qquad (94b)$$

where, of course, $\rho = \rho_a = \rho_b$.

One notes that for all cases given in equation (94) the elementary overlap integrals are of the general form

$$s_{\alpha\beta}(\zeta_a,\zeta_b) = P_a(R)\,e^{-\zeta_a R} + P_b(R)\,e^{-\zeta_b R}$$

where P_a and P_b are polynominals in R with coefficients which depend on the parameters n, l, m, and ζ of the two wavefunctions. Thus the formula for $S(\alpha,\beta)$ obtained by substituting equation (94) into equation (91) will consist of a sum of terms each of which is proportional to a polynominal in R times one of the exponential factors $e^{-\zeta_{\alpha_i} R}$ or $e^{-\zeta_{\beta_j} R}$ occurring in the wavefunctions ψ_α and ψ_β (equations 16 and 17). For the approximation which we are using here, in which all terms of order $e^{-2\zeta R}$ are neglected, it will be consistent to also neglect all terms in $e^{-\zeta_{\alpha_i} R}$ for which the value

of ζ_{α_i} is greater than or equal to twice the minimum value of ζ_{α_i} occurring in the expansion. Since only atomic wavefunctions occur in equation (91), we see from table I that there will only be three values of ζ_{α_i} which satisfy this criterion, namely ζ_{p_1}, ζ_{p_2}, and ζ_{s_3}, so that only terms in these three exponentials need be retained in evaluating equation (91).

Using this approximation, we have evaluated the required overlap integrals $S(\alpha, \beta)$ for nitrogen and oxygen from equations (91) and (94) and the wavefunction parameters given in tables I and IV. The resulting formulas for the integrals are given explicitly in Appendix E, and are plotted as a function of R in figures 31 and 32.

6. The Two-Center Kinetic Energy Integral

The two-center kinetic energy integral

$$T(\alpha, \beta) = -\frac{1}{2} \int \psi^*_{\alpha A} \nabla^2 \psi_{\beta B} \, d\vec{r} \tag{95}$$

which occurs in the second term of equation (70) can be evaluated in the same way as the two-center overlap integral of equation (87). Introducing the elementary kinetic-energy integrals $t_{n\alpha, m\beta}$ between the unnormalized Slater wavefunctions (92), equation (95) can be expanded in the form

$$T(\alpha, \beta) = \sum_{i,j} c_{\alpha_i} c_{\beta_j} t_{n_{\alpha_i}\alpha, n_{\beta_j}\beta} (\zeta_{\alpha_i}, \zeta_{\beta_j}) \tag{96}$$

where the $t_{n\alpha, m\beta}$ are again obtained from Roothaan's work.

From equation (70) and table III, we see that only the values $T(2\sigma, 2\sigma)$ and $T(2\pi, 2\pi) \equiv T(2\pi^+, 2\pi^+) = T(2\pi^-, 2\pi^-)$ will be needed in the present calculation, so that we only require the elementary integrals $t_{2\pi, 2\pi}$ and $t_{2\sigma, 2\sigma}$. In the notation of equation (93), these integrals are found to be

$$t_{2\pi, 2\pi}(\zeta_a, \zeta_b) = -\frac{3}{2} (\lambda^3 \mu/\zeta_b^3 \rho_b^3) [12\lambda(\lambda+1)(1+\rho_b) - 2(3\lambda+2)\rho_b^2 + \rho_b^3] e^{-\rho_b} +$$

$$+ \frac{3}{2} \lambda(\lambda+2)^2 (\mu/\zeta_a^3 \rho_a^3) [12(\lambda+2)(\lambda+1)(1+\rho_a) + 2(3\lambda+4)\rho_a^2 + \rho_a^3] e^{-\rho_a}$$

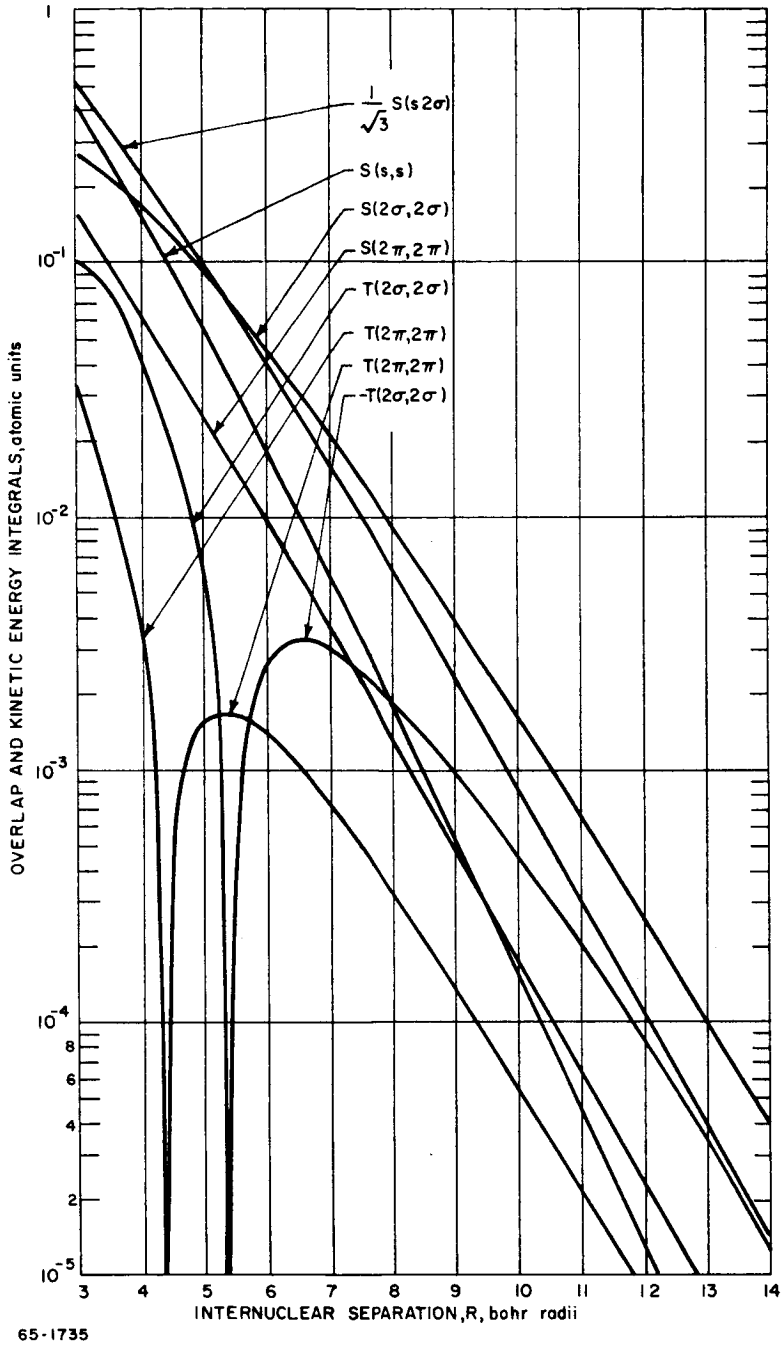

65-1735

Figure 31 TWO-CENTER OVERLAP AND KINETIC-ENERGY INTEGRALS FOR N-N^+

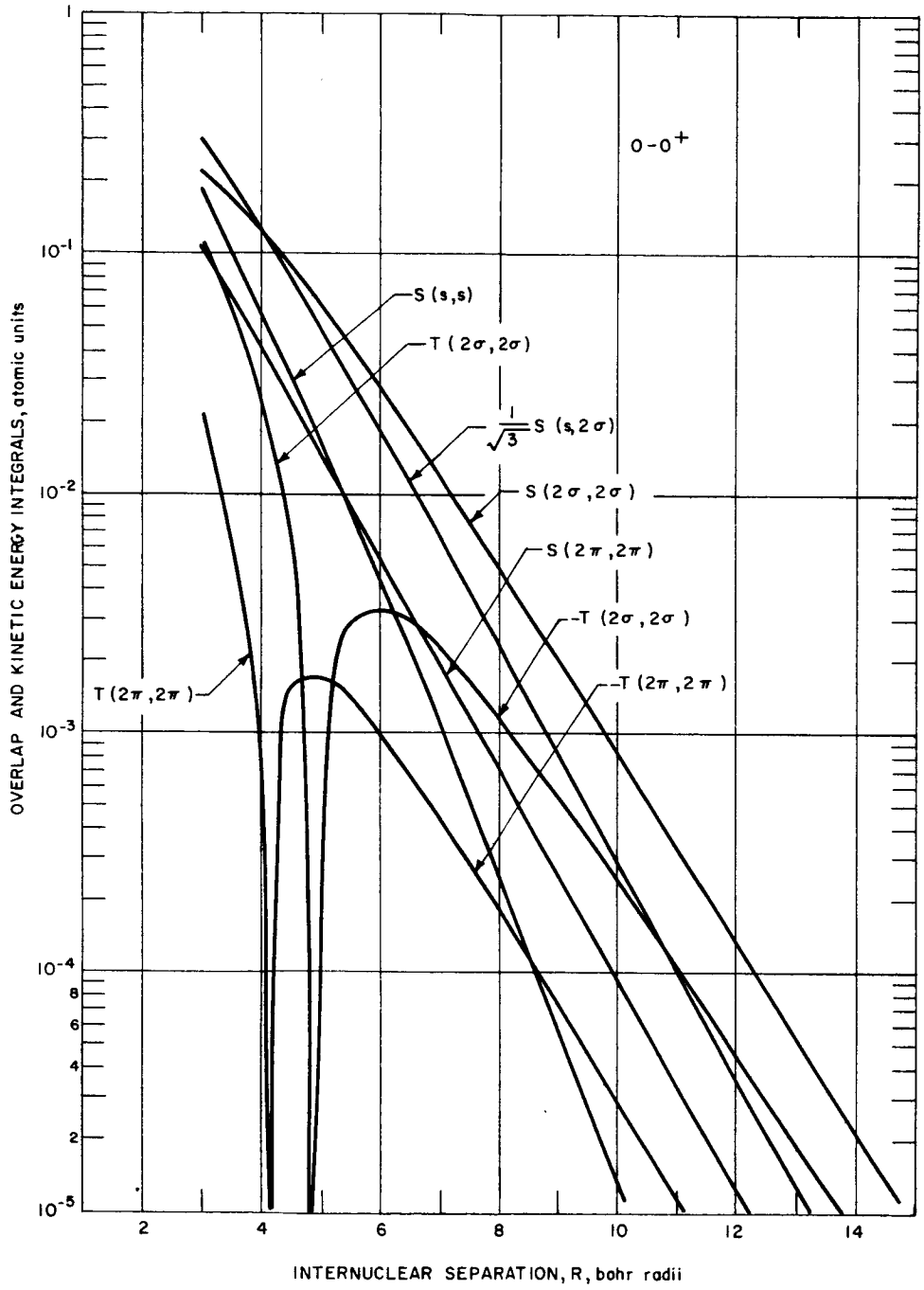

65-5595

Figure 32 TWO-CENTER OVERLAP AND KINETIC-ENERGY INTEGRALS FOR $0\text{-}0^+$

$$t_{2\sigma,\,2\sigma}(\zeta_a, \zeta_b) = -\frac{d}{dR}\left[R\, t_{2\pi,\,2\pi}(\zeta_a, \zeta_b)\right]$$

$$= -\frac{3}{2}(\lambda^3 \mu/\zeta_b^3 \rho_b^3)\left[12\lambda(\lambda+1)(2+2\rho_b+\rho_b^2) - (6\lambda+5)\rho_b^3 + \rho_b^4\right]e^{-\rho_b} +$$

$$+ \frac{3}{2}\lambda(\lambda+2)^2(\mu/\zeta_a^3 \rho_a^3)\left[12(\lambda+2)(\lambda+1)(2+2\rho_a+\rho_a^2) + (6\lambda+7)\rho_a^3 + \rho_a^4\right]e^{-\rho_a}$$

and for $\zeta_a \neq \zeta_b$ (97a)

$$t_{2\pi,\,2\pi}(\zeta, \zeta) = -(3/8\zeta^3)\left(-1 - \rho - \frac{4}{15}\rho^2 + \frac{1}{15}\rho^3\right) e^{-\rho}$$

$$t_{2\sigma,\,2\sigma}(\zeta, \zeta) = -\frac{d}{dR}\left[R\, t_{2\pi,\,2\pi}(\zeta, \zeta)\right]$$

$$= -(3/8\zeta^3)\left(1 + \rho - \frac{1}{5}\rho^2 - \frac{8}{15}\rho^3 + \frac{1}{15}\rho^4\right)e^{-\rho} \text{ for } \zeta_a = \zeta_b \qquad (97b)$$

Explicit formulas for the kinetic energy integrals $T(\alpha, \beta)$ have been calculated for nitrogen and oxygen from equations (96) and (97), using the same approximations as in the case of the overlap integrals $S(\alpha, \beta)$. These formulas are again given in Appendix E and are shown graphically in figure 31 and 32.

7. The Hybrid Integrals

The final two lines of equation (70) for the interaction potentials contain hybrid (or ionic) integrals of the general forms

$$L(\alpha, \gamma; \delta, \beta) \equiv \iint u_{\alpha A}^{+*}(1)\, u_{\beta B}^{*}(2)\, \frac{1}{r_{12}}\, u_{\gamma A}(1)\, u_{\delta A}(2)\, d\vec{r}_1\, d\vec{r}_2 \qquad (98a)$$

and

$$L^0(\delta, \beta) = \int u_{\beta B}^{*}(1)\, \frac{1}{r_{1A}}\, u_{\delta A}(1)\, d\vec{r}_1 \qquad (98b)$$

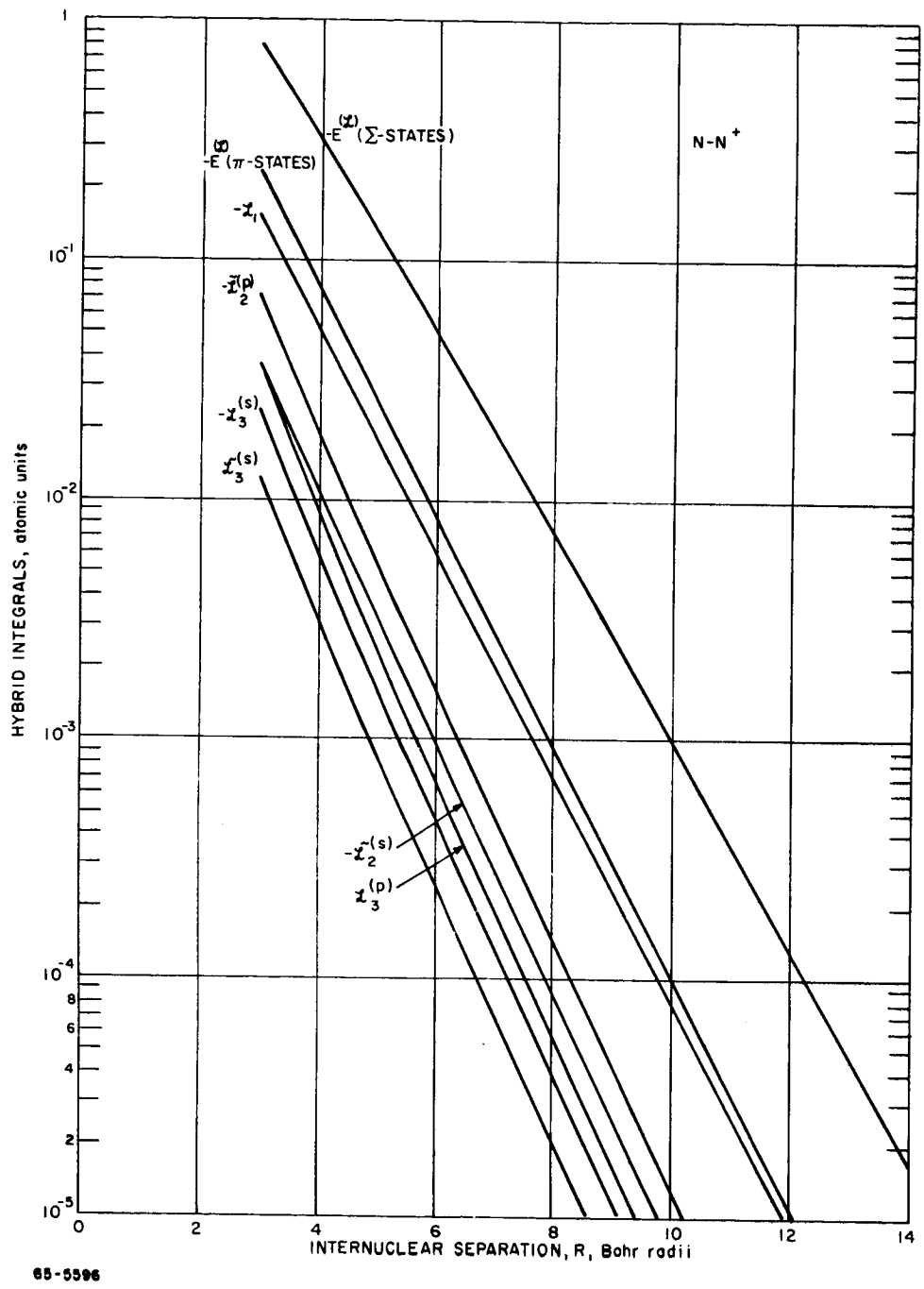

Figure 33 HYBRID INTEGRALS FOR N-N+

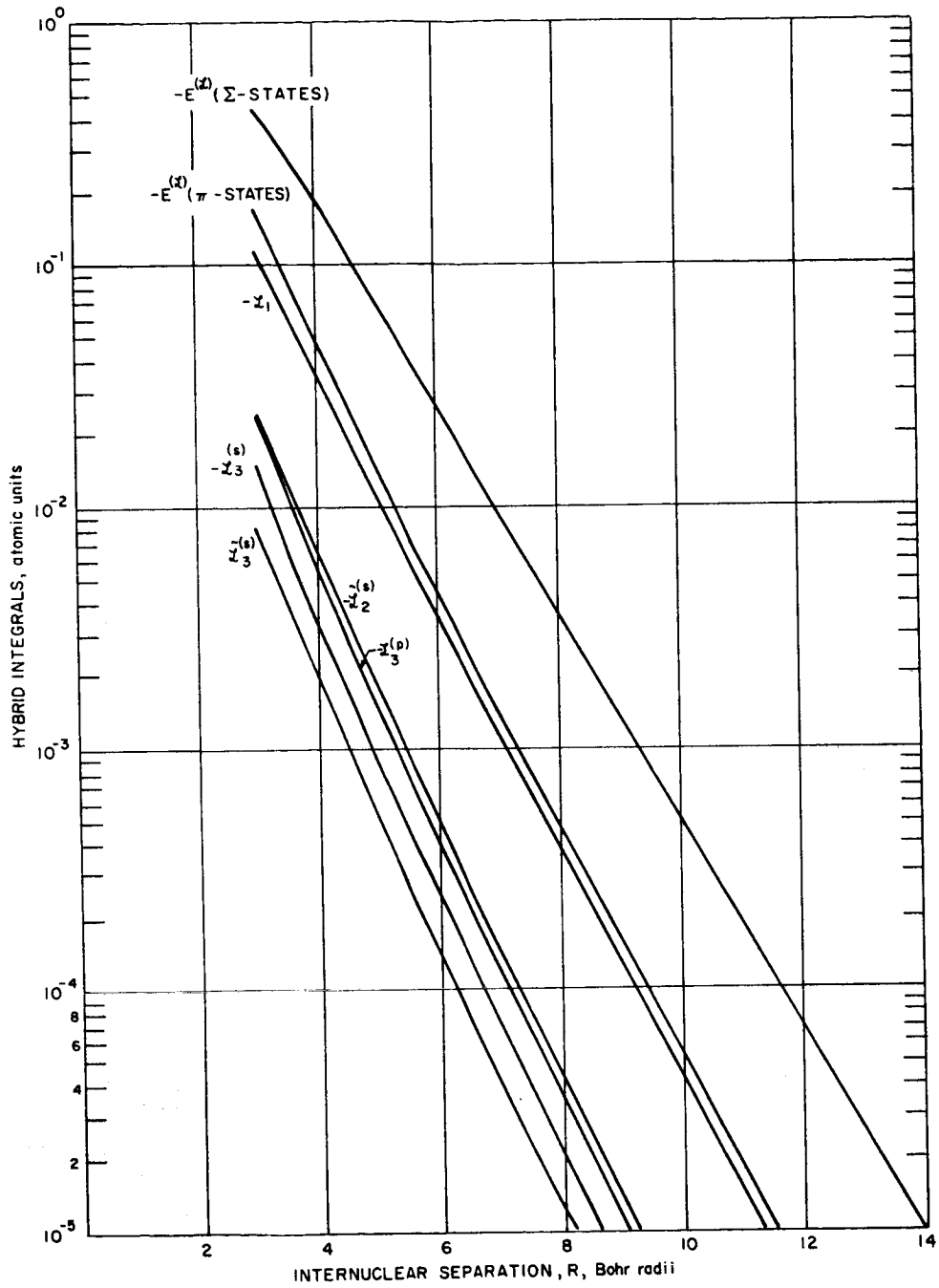

65-5597

Figure 34 HYBRID INTEGRALS FOR $0\text{-}0^+$

in which one electron is exchanged between the two nuclei, while the other electrons remain fixed. As in the case of the overlap and kinetic energy integrals, the first step in the evaluation of these integrals is to substitute the form of the wavefunctions (equations 1 and 2) into equation (98) to obtain the expansions

$$L(\alpha,\gamma;\delta,\beta) = \sum_{i,j,k,l} c^{+}_{\alpha_i}\, c_{\gamma_k}\, c_{\delta_l}\, c_{\beta_j}\, l_{n_{\alpha_i}\alpha,\, n_{\gamma_k}\gamma,\, n_{\delta_l}\delta,\, n_{\beta_j}\beta}\,(\zeta^{+}_{\alpha_i}, \zeta_{\gamma_k}; \zeta_{\delta_l}, \zeta_{\beta_j})$$

$$L^0(\delta,\beta) = \sum_{j,l} c_{\delta_l}\, c_{\beta_j}\, l^0_{n_{\delta_l}\delta,\, n_{\beta_j}\beta}\,(\zeta_{\delta_l}, \zeta_{\beta_j}) \tag{99}$$

where as before the functions l and l^0 represent the values of the hybrid integrals (98) for the unnormalized Slater wavefunctions (92). With the expansion (99), the last two lines of the expression (70) for the interaction energy take the form

$$E^{(L)} = -N \sum_{j=1}^{4} \sum_{l=1}^{4} c_{p_j}\, c_{p_l}\, F^{(0p)}(\zeta_{p_l}, \zeta_{p_j})$$

$$= \sum_{i=1}^{5} \sum_{k=1}^{5} \sum_{l=1}^{4} \sum_{j=1}^{4} (c^{+}_{1s_i}\, c_{1s_k} + c^{+}_{2s_i}\, c_{2s_k})\, c_{p_l}\, c_{p_j}$$

$$\times\, F^{(sp)}_{n_{s_i} n_{s_k}}(\zeta^{+}_{s_i}, \zeta_{s_k}, \zeta_{p_l}, \zeta_{p_j})$$

$$+ \sum_{i=1}^{4} \sum_{k=1}^{4} \sum_{l=1}^{4} \sum_{j=1}^{4} c^{+}_{p_i}\, c_{p_k}\, c_{p_l}\, c_{p_j}\, F^{(pp)}(\zeta^{+}_{p_i}, \zeta_{p_k}, \zeta_{p_l}, \zeta_{p_j}), \tag{100}$$

with the F-functions defined for the Π-states of the $N-N^{+}$ interaction by

$$F^{(0p)}(\zeta_a, \zeta_b) = 2\, l^0_{2\pi^-,\, 2\pi^-}(\zeta_a, \zeta_b)$$

$$F^{(sp)}_{ik}(\zeta', \zeta'', \zeta_a, \zeta_b) = 2[2 l_{is,\, ks,\, 2\pi^-,\, 2\pi^-}(\zeta', \zeta'', \zeta_a, \zeta_b) - l_{is,\, 2\pi^-,\, ks,\, 2\pi^-}(\zeta', \zeta_a, \zeta'', \zeta_b)]$$

$$F^{(pp)}(\zeta', \zeta'', \zeta_a, \zeta_b) = 2[l_{2\pi^+, 2\pi^+, 2\pi^-, 2\pi^-}(\zeta', \zeta'', \zeta_a, \zeta_b) + l_{2\sigma, 2\sigma, 2\pi^-, 2\pi^-}(\zeta', \zeta'', \zeta_a, \zeta_b)$$
$$- l_{2\pi^+ 2\pi^-, 2\pi^+, 2\pi^-}(\zeta', \zeta'', \zeta_a, \zeta_b) - l_{2\sigma, 2\pi^-, 2\sigma, 2\pi^-}(\zeta', \zeta'', \zeta_a, \zeta_b)] \quad (101a)$$

and for the Σ-states by

$$F^{(0p)}(\zeta_a, \zeta_b) = 2\, l^0_{2\sigma, 2\sigma}(\zeta_a, \zeta_b)$$

$$F^{(sp)}_{ik}(\zeta', \zeta'', \zeta_a, \zeta_b) = 2[2 l_{is, ks, 2\sigma, 2\sigma}(\zeta', \zeta'', \zeta_a, \zeta_b) - l_{is, 2\sigma, ks, 2\sigma}(\zeta', \zeta_a, \zeta'', \zeta_b)]$$

$$F^{(pp)}(\zeta', \zeta'', \zeta_a, \zeta_b) = 2[2 l_{2\pi^+, 2\pi^+, 2\sigma, 2\sigma}(\zeta', \zeta'', \zeta_a, \zeta_b) - 2 l_{2\pi^+, 2\sigma, 2\pi^+, 2\sigma}(\zeta', \zeta'', \zeta_a, \zeta_b)] \quad (101b)$$

The only change in equation (101) for the O-O^+ interaction is in the term $F^{(pp)}$ involving four 2 p-electrons, which for Π-states now becomes

$$F^{(pp)}(\zeta', \zeta'', \zeta_a, \zeta_b) = 2[l_{2\pi^+, 2\pi^+, 2\pi^+, 2\pi^+}(\zeta', \zeta'', \zeta_a, \zeta_b) + l_{2\sigma, 2\sigma, 2\pi^+, 2\pi^+}(\zeta', \zeta'', \zeta_a, \zeta_b)$$
$$+ l_{2\pi^-, 2\pi^-, 2\pi^+, 2\pi^+}(\zeta', \zeta'', \zeta_a, \zeta_b)] \quad (101c)$$

and for Σ-states becomes

$$F^{(pp)}(\zeta', \zeta'', \zeta_a, \zeta_b) = 2[2 l_{2\pi^+, 2\pi^+, 2\sigma, 2\sigma}(\zeta', \zeta'', \zeta_a, \zeta_b) + l_{2\sigma, 2\sigma, 2\sigma, 2\sigma}(\zeta', \zeta'', \zeta_a, \zeta_b)] \quad (101d)$$

Expressions for the elementary l-integrals occurring in equation (101) have been given by Roothaan[67] in terms of certain functions $C^{\gamma\delta\epsilon}_{\alpha\beta}$ defined by the relation

$$C^{\gamma\delta\epsilon}_{\alpha\beta}(\rho_a, \rho_b) = \left(\frac{1}{2}\rho_b\right)^{\alpha+\beta+\gamma+\delta+2\epsilon+1} \int_1^\infty d\xi \int_{-1}^1 d\eta\, e^{-\frac{1}{2}(\rho_a+\rho_b)\xi - \frac{1}{2}(\rho_a-\rho_b)\eta}$$

$$\times (\xi+\eta)^\alpha (\xi-\eta)^\beta (1+\xi\eta)^\gamma (1-\xi\eta)^\delta (\xi^2-1)^\epsilon (1-\eta^2)^\epsilon \quad (102)$$

Substituting Roothaan's expressions into equation (101) and simplifying the results, one obtains the F-functions for the Π-states in the form

$$F^{(0p)}(\zeta_a, \zeta_b) = \frac{3}{2}\frac{1}{\zeta_b^4} C^{001}_{01}(\rho_a, \rho_b)$$

$$F_{ij}^{(sp)}(\zeta_a', \zeta_a'', \zeta_a, \zeta_b) = \frac{3(i+j)!}{2^{i+j+1}} \frac{1}{\bar{\zeta}^{(i+j+1)} \zeta_b^4} C_{01}^{001}(\rho_a, \rho_b) + G_{ij}^{(sp)}(\zeta_a', \zeta_a'', \zeta_a, \zeta_b)$$

$$- \frac{(i+3)!}{2^{i+5}} \frac{1}{\tilde{\zeta}^{i+4} \zeta_b^{j+1}} C_{j-3,1}^{001}(\tilde{\rho}_a, \rho_b) - \tilde{G}_{ij}^{(sp)}(\zeta_a', \zeta_a'', \zeta_a, \zeta_b)$$

$$F^{(pp)}(\zeta_a', \zeta_a'', \zeta_a, \zeta_b) = \frac{9}{4} \frac{1}{\bar{\zeta}^5 \zeta_b^4} C_{01}^{001}(\rho_a, \rho_b) - \frac{27}{8} \frac{1}{\bar{\zeta}^7 \zeta_b^2} C_{-21}^{001}(\rho_a, \rho_b) + G^{(pp)}(\xi_a', \xi_a'', \xi_a, \xi_b)$$

for $N - N^+$

$$F^{(pp)}(\zeta_a', \zeta_a'', \zeta_a, \zeta_b) = \frac{27}{8} \frac{1}{\bar{\zeta}^5 \zeta_b^4} C_{01}^{001}(\rho_a, \rho_b) + \frac{3}{2} G_{22}^{(sp)}(\zeta_a', \zeta_a'', \zeta_a, \zeta_b) \qquad (103)$$

for $O - O^+$

where ρ_a and ρ_b are again given by equation (93) and we have introduced the notation

$$\tilde{\rho}_a = \zeta_a'' R$$

$$\rho_a^* = (\zeta_a + \zeta_a' + \zeta_a'') R$$

$$\bar{\zeta} = \frac{1}{2}(\zeta_a' + \zeta_a'')$$

$$\bar{\mu} = \bar{\zeta}/\zeta_b$$

$$\tilde{\zeta} = \frac{1}{2}(\zeta_a' + \zeta_a)$$

$$\tilde{\mu} = \tilde{\zeta}/\zeta_b \qquad (104)$$

Also, the G's in equation (103) are defined by

$$G_{11}^{(sp)}(\zeta_a', \zeta_a'', \zeta_a, \zeta_b) = -\frac{3}{4} (\bar{\zeta}^3 \zeta_b^4)^{-1} \left[C_{01}^{001} + \bar{\mu} C_{11}^{001}\right]$$

$$\tilde{G}_{11}^{(sp)}(\zeta_a', \zeta_a'', \zeta_a, \zeta_b) = \frac{3}{8} (\tilde{\zeta}^5 \zeta_b^2)^{-1} \left[C_{-21}^{001} + 2\tilde{\mu} C_{-11}^{001} + 2\tilde{\mu}^2 C_{01}^{001} + \tilde{\mu}^3 C_{11}^{001}\right]$$

$$G_{12}^{(sp)}(\zeta_a', \zeta_a'', \zeta_a, \zeta_b) = -\frac{3}{8}(\bar{\zeta}^4 \zeta_b^4)^{-1} \left[3C_{01}^{001} + 4\bar{\mu}\, C_{11}^{001} + 2\bar{\mu}^2\, C_{21}^{001}\right]$$

$$\tilde{G}_{12}^{(sp)}(\zeta_a', \zeta_a'', \zeta_a, \zeta_b) = -\frac{3}{8}(\tilde{\zeta}^5 \zeta_b^3)^{-1} \left[C_{-11}^{001} + \tilde{2}\mu\, C_{-11}^{001} + 2\tilde{\mu}^2\, C_{01}^{001} + \tilde{\mu}^3\, C_{11}^{001}\right]$$

$$G_{21}^{(sp)}(\zeta_a', \zeta_a'', \zeta_a, \zeta_b) = -\frac{3}{8}(\bar{\zeta}^4 \zeta_b^4)^{-1} \left[3C_{01}^{001} + 4\bar{\mu}\, C_{11}^{001} + 2\bar{\mu}^2\, C_{21}^{001}\right]$$

$$\tilde{G}_{21}^{(sp)}(\zeta_a', \zeta_a'', \zeta_a, \zeta_b) = -\frac{3}{16}(\tilde{\zeta}^6 \zeta_b^2)^{-1} \left[5C_{-21}^{001} + 10\tilde{\mu}\, C_{-11}^{001} + 10\tilde{\mu}^2\, C_{01}^{001} + 6\tilde{\mu}^3\, C_{11}^{001} + 2\tilde{\mu}^4\, C_{21}^{001}\right]$$

$$G_{22}^{(sp)}(\zeta_a', \zeta_a'', \zeta_a, \zeta_b) = -\frac{3}{8}(\bar{\zeta}^5 \zeta_b^4)^{-1} \left[6C_{01}^{001} + 9\bar{\mu}\, C_{11}^{001} + 6\bar{\mu}^2\, C_{21}^{001} + 2\bar{\mu}^3\, C_{31}^{001}\right]$$

$$\tilde{G}_{22}^{(sp)}(\zeta_a', \zeta_a'', \zeta_a, \zeta_b) = -\frac{3}{16}(\tilde{\zeta}^6 \zeta_b^3)^{-1} \left[5C_{-11}^{001} + 10\tilde{\mu}\, C_{01}^{001} + 10\tilde{\mu}^2\, C_{11}^{001} + 6\tilde{\mu}^3\, C_{21}^{001} + 2\tilde{\mu}^4\, C_{31}^{001}\right]$$

$$G^{(pp)}(\zeta_a', \zeta_a'', \zeta_a, \zeta_b) = \frac{9}{8}(\bar{\zeta}^7 \zeta_b^2) \left[3C_{-21}^{001} + 6\bar{\mu}\, C_{-11}^{001} + 4\bar{\mu}^2\, C_{01}^{001} + \bar{\mu}^3\, C_{11}^{001}\right] \qquad (105)$$

with the convention that in all cases $C_{\alpha\beta}^{\gamma\delta\epsilon}$ in equation (105) stands for $C_{\alpha\beta}^{\gamma\delta\epsilon}(\rho_a^*, \rho_b)$. The corresponding formulas for the Σ-states can be obtained from equation (103) simply by making the substitution

$$C_{\alpha\beta}^{001} \longrightarrow 2\, C_{\alpha\beta}^{110} \qquad (106)$$

everywhere in equations (103) and (105).

Equation (100) can now be simplified somewhat by summing the terms in equation (103) in $C_{01}(\rho_a, \rho_b)$ over the indices i and k. Making use of the normalization condition (equations 52 and 71), one finds that the contributions from $F^{(sp)}$ and $F^{(pp)}$ just cancel out N-1 of the N units of nuclear charge in equation (100), so that we are left with the integral $F^{(0p)}$ for a unit nuclear charge. Also, the terms in equation (103) in $C(\tilde{\rho}_a, \rho_b)$ can be summed over i and l by means of equations (86), (88), and (90), to give equation (100) in the form

$$E^{(L)} = L_1 + \tilde{L}_2^{(s)} + \tilde{L}_2^{(p)} + L_3^{(s)} + \tilde{L}_3^{(s)} + L_3^{(p)} \qquad (107)$$

where for Π-states

$$L_1 \equiv -\sum_{j=1}^{4}\sum_{l=1}^{4} c_{p_j}\, c_{p_l}\, (3/2\zeta_{p_j}^{4})\; C_{01}^{001}\; (\xi_{p_l} R,\ \zeta_{p_j} R)$$

$$\tilde{L}_2^{(s)} \equiv -\frac{1}{2}\sum_{j=1}^{4}\sum_{k=1}^{5} c_{s_k}\, c_{p_j}\, \zeta_{p_j}^{(-n_{s_k}-1)}\; C_{(-3+n_{s_k}),1}^{001}\; (\zeta_{s_k} R,\ \zeta_{p_j} R)$$

$$\tilde{L}_2^{(p)} \equiv -\frac{3}{5}\, q \sum_{j=1}^{4}\sum_{l=1}^{4} c_{p_l}\, c_{p_j}\, \zeta_{p_j}^{-2}\; C_{-2,1}^{001}\; (\zeta_{p_l} R,\ \zeta_{p_j} R)$$

$$L_3^{(s)} \equiv \sum_{i=1}^{5}\sum_{k=1}^{5}\sum_{l=1}^{4}\sum_{j=1}^{4} (c_{1s_i}^{+}\, c_{1s_k} + c_{2s_i}^{+}\, c_{2s_k})\, c_{p_l}\, c_{p_j}\, G_{n_{s_i} n_{s_k}}^{(sp)} (\zeta_{s_i}^{+}, \zeta_{s_k}, \zeta_{p_l}, \zeta_{p_j})$$

$$\tilde{L}_3^{(s)} \equiv \sum_{i=1}^{5}\sum_{k=1}^{5}\sum_{l=1}^{4}\sum_{j=1}^{4} (c_{1s_i}^{+}\, c_{1s_k} + c_{2s_i}^{+}\, c_{2s_k})\, c_{p_l}\, c_{p_j}\, \tilde{G}_{n_{s_i} n_{s_k}}^{(sp)} (\zeta_{s_i}^{+}, \zeta_{s_k}, \zeta_{p_l}, \zeta_{p_j}) \tag{108a}$$

for both nitrogen and oxygen, and

$$L_3^{(p)} \equiv \sum_{i=1}^{4}\sum_{k=1}^{4}\sum_{l=1}^{4}\sum_{j=1}^{4} c_{p_i}^{+}\, c_{p_k}\, c_{p_l}\, c_{p_j}\, G^{(pp)} (\zeta_{p_i}^{+}, \zeta_{p_k}, \zeta_{p_l}, \zeta_{p_j}) \quad \text{for } N-N^{+}$$

$$L_3^{(p)} \equiv \sum_{i=1}^{4}\sum_{k=1}^{4}\sum_{l=1}^{4}\sum_{j=1}^{4} \frac{3}{2}\, c_{p_i}^{+}\, c_{p_k}\, c_{p_l}\, c_{p_j}\, G_{22}^{(sp)} (\zeta_{p_i}^{+}, \zeta_{p_k}, \zeta_{p_l}, \zeta_{p_j}) \quad \text{for } O-O^{+} \tag{108b}$$

where the G-functions are defined by equation (105). The corresponding formulas for the Σ-states are again found by making the substitution (106) everywhere in equations (105) and (108).

A simple relationship between the values of $E^{(L)}$ for the Σ- and Π-states can be obtained by making use of the identity

$$\frac{d}{dR}\,[R\,C^{001}_{\alpha\beta}\,(\zeta_a R, \zeta_b R)] = -2\,C^{110}_{\alpha\beta}\,(\zeta_a R, \zeta_b R) \tag{109}$$

which is proved in Appendix F. Comparing this result with equation (106), we see that the value of $E^{(L)}$ for the Σ-states is obtained from the value for the Π-states simply by replacing $C^{001}_{\alpha\beta}$ by $-\frac{d}{dR}(R\,C^{001}_{\alpha\beta})$ wherever it occurs. From the form of equations (105), (107) and (108) for $E^{(L)}$, one sees that this substitution is equivalent to the formula

$$E^{(L)}_{\Sigma} = -\frac{d}{dR}\,(R\,E^{(L)}_{\Pi}) \tag{110}$$

where $E^{(L)}_{\Sigma}$ and $E^{(L)}_{\Pi}$ are of course the values of $E^{(L)}$ (equation 107) for the Σ- and Π-states respectively. We note that this same relationship (110) was also obtained previously between the overlap and kinetic energy integrals for the Σ- and Π-states.

In order to complete the evaluation of the hybrid term $E^{(L)}$ in the energy formula (70), it is necessary to know the values of the functions $C^{001}_{\alpha\beta}$ which occur in equations (105) and (108). The evaluation of these functions has been discussed at length by Roothaan[67, 68], who gives explicit formulas for the required C-functions having $\alpha \geq 0$ and recurrence relations by which the remaining functions with $\alpha < 0$ can be calculated. From his results, we obtain, after a good deal of algebra, the expressions for the required C-functions in the following form:

$$C^{001}_{-21}\,(\rho_a, \rho_b) = (2/\rho_b^3)\,[(\lambda^2 - 5\lambda - 30)(1 + \rho_b) - 2(\lambda + 6)\rho_b^2 - 2\rho_b^3]\,e^{-\rho_b} +$$

$$-(2\mu/\rho_a^3)(\lambda + 2)\,[(\lambda^2 - 5\lambda - 30)\lambda^{-1} + (\lambda - 5)\rho_a - \rho_a^2]\,e^{-\rho_a} +$$

$$+(2\mu/\rho_b^3)\,[(15 + 15\rho_b + 6\rho_b^2 + \rho_b^3)\,e^{-\rho_b}\,F(\rho_a, \rho_b) - (15 - 15\rho_b + 6\rho_b^2 - \rho_b^3)\,e^{\rho_b}\,G(\rho_a, \rho_b)]$$

$$C^{001}_{-11}\,(\rho_a, \rho_b) = (2\mu/\rho_b^3)\,\lambda[(2\lambda^2 - 5\lambda + 15)(1 + \rho_b) - 2(\lambda - 3)\rho_b^2 + \rho_b^3]\,e^{-\rho_b} +$$

$$-(2\mu/\rho_a^3)(\lambda + 2)\,[(2\lambda^2 - 5\lambda + 15)(\lambda + 2)\lambda^{-1} + (2\lambda^2 - \lambda + 5)\rho_a + \rho_a^2]\,e^{-\rho_a} +$$

$$+(2\mu/\rho_b^3)\,[-(15 + 15\rho_b + 6\rho_b^3 + \rho_b^3)\,e^{-\rho_b}\,F(\rho_a, \rho_b) + (15 - 15\rho_b + 6\rho_b - \rho_b^3)\,e^{\rho_b}\,G(\rho_a, \rho_b)]$$

$$C^{001}_{01}\,(\rho_a, \rho_b) = (2\lambda^2/\rho_b^3)\,[6\lambda^2(1 + \rho_b) - 4\lambda\rho_b^2 + \rho_b^3]\,e^{-\rho_b} +$$

$$-(4\mu\lambda^3/\rho_a^3)\,[3(\lambda + 2)(1 + \rho_a) + \rho_a^2]\,e^{-\rho_a}$$

$$C^{001}_{11}\,(\rho_a, \rho_b) = (4\mu\lambda^3/\rho_b^3)\,[12\lambda^2(1 + \rho_b) - 6\lambda\rho_b^2 + \rho_b^3]\,e^{-\rho_b}$$

$$-(4\lambda^3/\rho_b^3)\,[12(\lambda + 2)^2(1 + \rho_a) + 6(\lambda + 2)\rho_a^2 + \rho_a^3]\,e^{-\rho_a}$$

$$C_{21}^{001}(\rho_a,\rho_b) = (4\lambda^3/\rho_b^3)\,[12\lambda^2(5\lambda+9)(1+\rho_b) - 6\lambda(4\lambda+7)\rho_b^2 + (3\lambda+5)\rho_b^3]\,e^{-\rho_b} +$$
$$-(4\mu\lambda^4/\rho_a^3)\,[12(\lambda+2)(5\lambda+9)(1+\rho_a) + 6(6\lambda+11)\rho_a^2 + 9\rho_a^3 + \rho_a^4/(\lambda+2)]\,e^{-\rho_a}$$

$$C_{31}^{001}(\rho_a,\rho_b) = (12\mu\lambda^4/\rho_b^3)\,[60\lambda^2(2\lambda+3)(1+\rho_b) - 8\lambda(5\lambda+7)\rho_b^2 + (4\lambda+5)\rho_b^3]\,e^{-\rho_b} +$$
$$-(4\lambda^4/\rho_a^3)\,[180(\lambda+2)^2(2\lambda+3)(1+\rho_a) + 12(\lambda+2)(20\lambda+31)\rho_a^2 +$$
$$+ 3(24\lambda+43)\rho_a^3 + 12\rho_a^4 + \rho_a^5/(\lambda+2)]\,e^{-\rho_a} \qquad (111a)$$

where

$$F(\rho_a,\rho_b) = \mathrm{Ei}(-\rho_a+\rho_b) + \ln\left|\frac{u+1}{u-1}\right| \qquad (111b)$$

$$G(\rho_a,\rho_b) = \mathrm{Ei}(-\rho_a-\rho_b) \quad ,$$

$\mathrm{Ei}(x)$ is the usual exponential integral, and we have again used the notation of equation (93).

In the limiting case of $\rho_a = \rho_b$, the equations (111a) become indeterminate, so that one needs a special formula for the C-functions in this case. Taking the limit as $\rho_a \to \rho_b$, the formulas in this special case are found to be

$$C_{-21}^{001}(\rho,\rho) = (1/\rho^3)\,[-(60\rho+30\rho^2+7\rho^3) + 2(15+15\rho+6\rho^2+\rho^3)(\gamma+\ln 2\rho) +$$
$$-2(15-15\rho+6\rho^2-\rho^3)\,e^{2\rho}\,\mathrm{Ei}(-2\rho)]\,e^{-\rho}$$

$$C_{-11}^{001}(\rho,\rho) = (1/\rho^3)\left[\left(60\rho+30\rho^2+\frac{23}{3}\rho^3+\frac{2}{3}\rho^4\right) - 2(15+15\rho+6\rho^2+\rho^3)(\gamma+\ln 2\rho) +\right.$$
$$\left.+2(15-15\rho+6\rho^2-\rho^3)\,e^{2\rho}\,\mathrm{Ei}(-2\rho)\right]\,e^{-\rho}$$

$$C_{01}^{001}(\rho,\rho) = \left(\frac{1}{2}+\frac{1}{2}\rho+\frac{1}{6}\rho^2\right)\,e^{-\rho}$$

$$C_{11}^{001}(\rho,\rho) = \left(1+\rho+\frac{2}{5}\rho^2+\frac{1}{15}\rho^3\right)\,e^{-\rho}$$

$$C_{21}^{001}(\rho,\rho) = \left(\frac{5}{2}+\frac{5}{2}\rho+\frac{11}{10}\rho^2+\frac{4}{15}\rho^3+\frac{1}{30}\rho^4\right)\,e^{-\rho}$$

$$C_{31}^{001}(\rho,\rho) = \left(\frac{15}{2} + \frac{15}{2}\rho + \frac{7}{2}\rho^2 + \rho^3 + \frac{13}{70}\rho^4 + \frac{2}{105}\rho^5\right) e^{-\rho} \qquad (111c)$$

where $\gamma = 0.5772157$ is Euler's constant.

Equations (105), (107), (108), (110), and (111) provide an explicit formula for the contribution $E^{(L)}$ of the hybrid integrals to the interaction potentials (70). Examining these equations, we see that the first term in equation (107) will be a sum of exponentials times polynominals in R, of the same form as we found previously for the overlap and kinetic-energy integrals. The second and third terms will also be of this form, but in addition will contain a term involving exponential integrals and logarithms, as indicated in equations (111b) and (111c). Finally, in the approximation of neglecting multiple electron exchange which we are using here, we note that the last three terms in equation (107) can be simplified by neglecting terms of order $e^{-\rho_a^*}$. Since the exponential integrals in equation (111) are of this same order, they can also be neglected here, and the final terms in equation (107) thus reduce again to a sum of exponentials times polynominals in R.

Appendix E gives the final formulas used in the calculation of $E^{(L)}$ for the $N - N^+$ and $O - O^+$ systems. The formulas for the Π-states were obtained by evaluating the constants in equations (105), (107), (108), and (111) for the $N - N^+$ and $O - O^+$ wavefunctions given in tables I and IV, using a specially written digital computer program to perform the multiple sums occurring in equation (108). The formulas for the Σ-states were then obtained by direct differentiation of the corresponding Π-state formulas, according to equation (110).

G. THE $N - N^+$ AND $O - O^+$ INTERACTION POTENTIALS

In terms of the various molecular integrals defined in the previous section, equation (70) for the $N\text{-}N^+$ and $O\text{-}O^+$ interaction potentials can be written in the form*

$$E_{S,M_l} = \pm\, b_S D^2 \{(H_0' - H_0) S(2\pi, 2\pi) + T(2\pi, 2\pi) + E^{(Q)} + E^{(L)}\} \quad \text{for } \Pi\text{-states}$$

$$= \pm\, b_S D^2 \{(H_0' - H_0) S(2\sigma, 2\sigma) + T(2\sigma, 2\sigma) + E^{(Q)} + E^{(L)}\} \quad \text{for } \Sigma\text{-states} \qquad (112)$$

where b_S is given for $N\text{-}N^+$ and $O\text{-}O^+$ by equation (40), D^2 by equation (72), $H_0' - H_0$ by equation (79b), $E^{(Q)}$ by equation (89) and table VI, and the integrals S, T, and $E^{(L)}$ are given in Appendix E. Substituting all of these values into equation (112) we obtain the formulas for the interaction potentials in the relatively simple form

*We have omitted the Coulomb term $+ Q_0$ in equation (112), since it does not affect the calculated energy difference ΔE between the symmetric and antisymmetric states.

$$E_{S\Pi}(N-N^+) = \pm\, b_S \{[-0.00185726\, R^3 + 0.0095802\, R^2 + 0.052137\, R - 12.6978 + 165.603\, R^{-1}$$

$$- 667.901\, R^{-2} + 512.832\, R^{-3} - 399.45\, R^{-4} + 4481.2\, R^{-5} + 5934\, R^{-6}$$

$$+ 5480\, R^{-7} + 4600\, R^{-8} - 1.60632\, K_\pi^{N-N^+}(1.1937, R)]\; e^{-1.1937 R}$$

$$+ [-0.0711613\, R^3 + 0.093474\, R^2 + 0.368215\, R + 32.0694 + 552.170\, R^{-1}$$

$$+ 3265.71\, R^{-2} - 9787.06\, R^{-3} - 557011.8\, R^{-4} - 9646086\, R^{-5}$$

$$- 5637462\, R^{-6} - 7750\, R^{-7} - 4500\, R^{-8} - 9.24393\, K_\pi^{N-N^+}(1.7124, R)]\, e^{-1.7124 R}$$

$$+ [0.0272021\, R + 0.085343 - 7.06521\, R^{-1} - 2748.203\, R^{-2} + 9302.080\, R^{-3}$$

$$- 550549.1\, R^{-4} + 8970148\, R^{-5} + 5628504\, R^{-6}$$

$$+ 2.73535\, K_\pi^{N-N^+}(1.5937, R)]\, e^{-1.5937 R} \}$$

$$E_{S\Sigma}(N-N^+) = \pm\, b_S \{[-0.00221703\, R^4 + 0.0188652\, R^3 + 0.0238864\, R^2 - 15.3564\, R + 213.320$$

$$- 743.754\, R^{-1} - 860.183\, R^{-2} + 4968.22\, R^{-3} + 4164.32\, R^{-4} + 13135.3\, R^{-5}$$

$$+ 15364\, R^{-6} + 10960\, R^{-7} + 9200\, R^{-8} - 1.60632\, K_\sigma^{N-N^+}(1.1937, R)]\, e^{-1.1937 R}$$

$$+ [-0.121856\, R^4 + 0.444711\, R^3 + 0.274959\, R^2 + 54.2605\, R + 931.795$$

$$- 2535.48\, R^{-1} - 418735.4\, R^{-2} - 7366740\, R^{-3} - 5407925\, R^{-4} - 19297960\, R^{-5}$$

$$- 11278310\, R^{-6} - 15500\, R^{-7} - 9000\, R^{-8} - 9.24393\, K_\sigma^{N-N^+}(1.7124, R)]\, e^{-1.7124 R}$$

$$+ [0.0544040\, R - 16.5395 + 4023.903\, R^{-1} - 424848.1\, R^{-2} + 6850237\, R^{-3}$$

$$+ 3185553\, R^{-4} + 17940241\, R^{-5} + 11256974\, R^{-6}$$

$$+ 2.7353\, K_\sigma^{N-N^+}(1.5937, R)]\, e^{-1.5937 R} \}$$

$$E_{S\Pi}(O-O^+) = \pm\, b_S \{[-0.00056130\, R^3 + 0.0016559\, R^2 + 0.0122990\, R - 5.60514 + 50.2344\, R^{-1}$$

$$- 171.5977\, R^{-2} + 72.0091\, R^{-3} + 170.3118\, R^{-4} - 65.2992\, R^{-5} - 56.6047\, R^{-6}]\, e^{-1.1536 R}$$

$$+ [-0.140709\, R^3 + 0.131761\, R^2 + 0.552823\, R - 45.99086 + 926.7200\, R^{-1}$$

$$- 9925.986\, R^{-2} - 5725.950\, R^{-3} - 103.570\, R^{-4} + 96.620\, R^{-5} + 53.7973\, R^{-6}]\, e^{-1.7960 R}$$

$$+ [0.0424269\, R + 0.112885 + 23.44026\, R^{-1} + 10446.067\, R^{-2}$$

$$+ 5546.266\, R^{-3} + 39.7800\, R^{-4} + 3.67905\, K_\pi^{O-O^+}(1.8792, R)]\, e^{-1.8792 R} \}$$

$$
\begin{aligned}
E_{S\Sigma}(O-O^{+}) = \pm\ b_S \{ & [-0.00064753\, R^4 + 0.0041553\, R^3 + 0.00663520\, R^2 - 6.50061\, R + 63.5356 \\
& - 197.6218\, R^{-1} - 68.5730\, R^{-2} + 211.201\, R^{-3} + 549.519\, R^{-4} + 261.198\, R^{-5} \\
& + 226.419\, R^{-6}]\, e^{-1.1536 R} \\
& + [-0.252713\, R^4 + 0.79947\, R^3 + 0.476738\, R^2 - 84.7652\, R + 1718.5486 \\
& + 23102.954\, R^{-1} - 2924518.2\, R^{-2} + 68472725\, R^{-3} + 38130946\, R^{-4} \\
& - 386.480\, R^{-5} - 215.190\, R^{-6}]\, e^{-1.7960 R} \\
& + [0.0848538\, R + 43.82317 - 20335.954\, R^{-1} - 2904737.1\, R^{-2} \\
& - 71645814\, R^{-3} - 38131522\, R^{-4} + 3.67905\, K_{\sigma}^{O-O^{+}}(1.8792, R)]\, e^{-1.8792 R} \}
\end{aligned}
\tag{113}
$$

where all quantities are in atomic units and the functions K_π and K_σ are given by

$$
K_\pi(\zeta, R) = \sum_{j=1}^{4} \frac{c_{p_j}}{\zeta_{p_j}^3} [F_\pi(\zeta R, \zeta_{p_j} R) + F_\pi(\zeta R, -\zeta_{p_j} R)]
$$

$$
F_\pi(x, y) = \left(\frac{15}{y^3} + \frac{15}{y^2} + \frac{6}{y} + 1\right) e^{x-y}\, E(x, y)
$$

$$
K_\sigma(\zeta, R) = \sum_{j=1}^{4} \frac{c_{p_j}}{\zeta_{p_j}^3} [F_\sigma(\zeta R, \zeta_{p_j} R) + F_\sigma(\zeta R, -\zeta_{p_j} R)]
$$

$$
F_\sigma(x, y) = \left(\frac{30}{y^3} + \frac{30}{y^2} + \frac{15}{y} + 5 + y\right) e^{x-y}\, E(x, y)
$$

$$
\begin{aligned}
E(x, y) &= Ei(-x + y) \qquad \text{for } x \neq y \\
&= \ln(x + y) \qquad \text{for } x = y
\end{aligned}
\tag{114}
$$

where Ei (x) is the usual exponential integral, as defined for example by Roothaan,[67] and *ln* is the natural logarithm. The parameters c_{p_j} and ζ_{p_j} in equation (114) of course depend on the species considered, and are given for nitrogen and oxygen in table I.

The potential energy curves calculated from equation (113) for the $^2\Sigma$ and $^2\Pi$ states of N_2^+ and O_2^+ have been plotted in figures 35 and 36. The curves for the $^4\Sigma$ and $^4\Pi$ states are of course just twice the plotted points, and the curves for the $^6\Sigma$ and $^6\Pi$ states three times the plotted points.

One sees that in the range of energies which are important for charge exchange, about 10^{-2} ev, the calculated curves can be fitted very well (within about 5 percent) by a simple exponential function, $Ae^{-\alpha R}$, as shown by the solid lines in the figures. With this curvefit we obtain the following formulas for the potential curves at large internuclear separations R:*

For $N\text{-}N^+$

$$
\begin{aligned}
E &= \pm\ 40.8\, e^{-1.778R} \text{ ev for the } {}^2\Sigma^+_{g,u} \text{ states} \\
&= \pm\ 81.5\, e^{-1.778R} \text{ ev for the } {}^4\Sigma^+_{g,u} \text{ states} \\
&= \pm\ 122.3\, e^{-1.778R} \text{ ev for the } {}^6\Sigma^+_{g,u} \text{ states} \\
&= \pm\ 15.5\, e^{-2.026R} \text{ ev for the } {}^2\Pi_{g,u} \text{ states} \\
&= \pm\ 30.9\, e^{-2.026R} \text{ ev for the } {}^4\Pi_{g,u} \text{ states} \\
&= \pm\ 46.4\, e^{-2.026R} \text{ ev for the } {}^6\Pi_{g,u} \text{ states}
\end{aligned}
\tag{115a}
$$

and, for $O\text{-}O^+$

$$
\begin{aligned}
E &= \pm\ 33.2\, e^{-1.811R} \text{ ev for the } {}^2\Sigma^+_{g,u} \text{ states} \\
&= \pm\ 66.5\, e^{-1.811R} \text{ ev for the } {}^4\Sigma^+_{g,u} \text{ states} \\
&= \pm\ 99.7\, e^{-1.811R} \text{ ev for the } {}^6\Sigma^+_{g,u} \text{ states} \\
&= \pm\ 12.2\, e^{-2.055R} \text{ ev for the } {}^2\Pi_{g,u} \text{ states} \\
&= \pm\ 24.5\, e^{-2.055R} \text{ ev for the } {}^4\Pi_{g,u} \text{ states} \\
&= \pm\ 36.7\, e^{-2.055R} \text{ ev for the } {}^6\Pi_{g,u} \text{ states}
\end{aligned}
\tag{115b}
$$

where R is measured in Å.

*The actual potential curves at large separation of course contain a polarization term which has not been included in the present calculations, and which must therefore be added to equation (115) to obtain the true interaction potential at large internuclear separations. As discussed in section III.A however, it is expected that equation (115) should nevertheless give approximately correct values for the energy difference $\Delta E \equiv |E_g - E_u|$ between the symmetric and antisymmetric states.

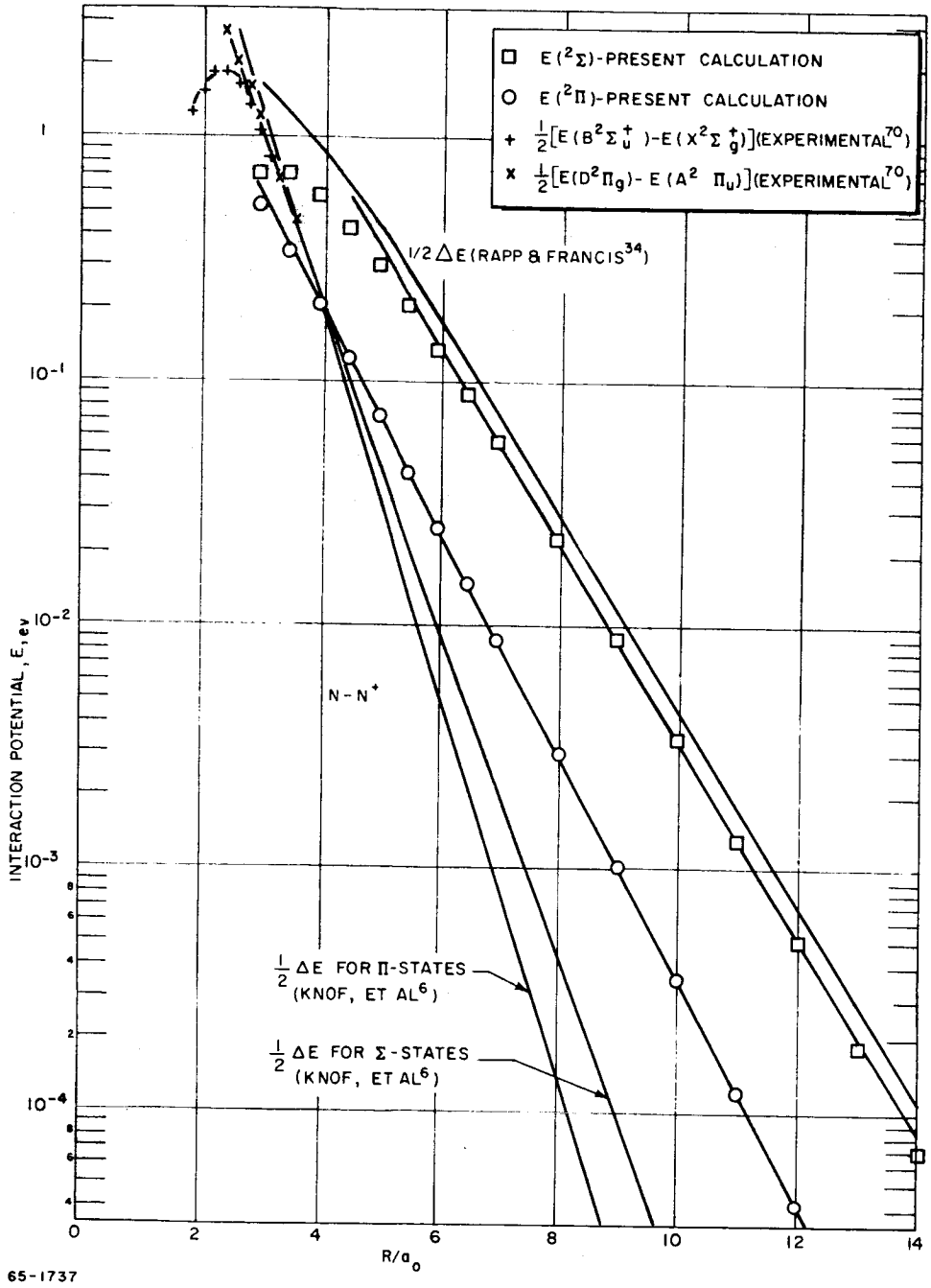

Figure 35 INTERACTION POTENTIALS BETWEEN GROUND-STATE N AND N^+

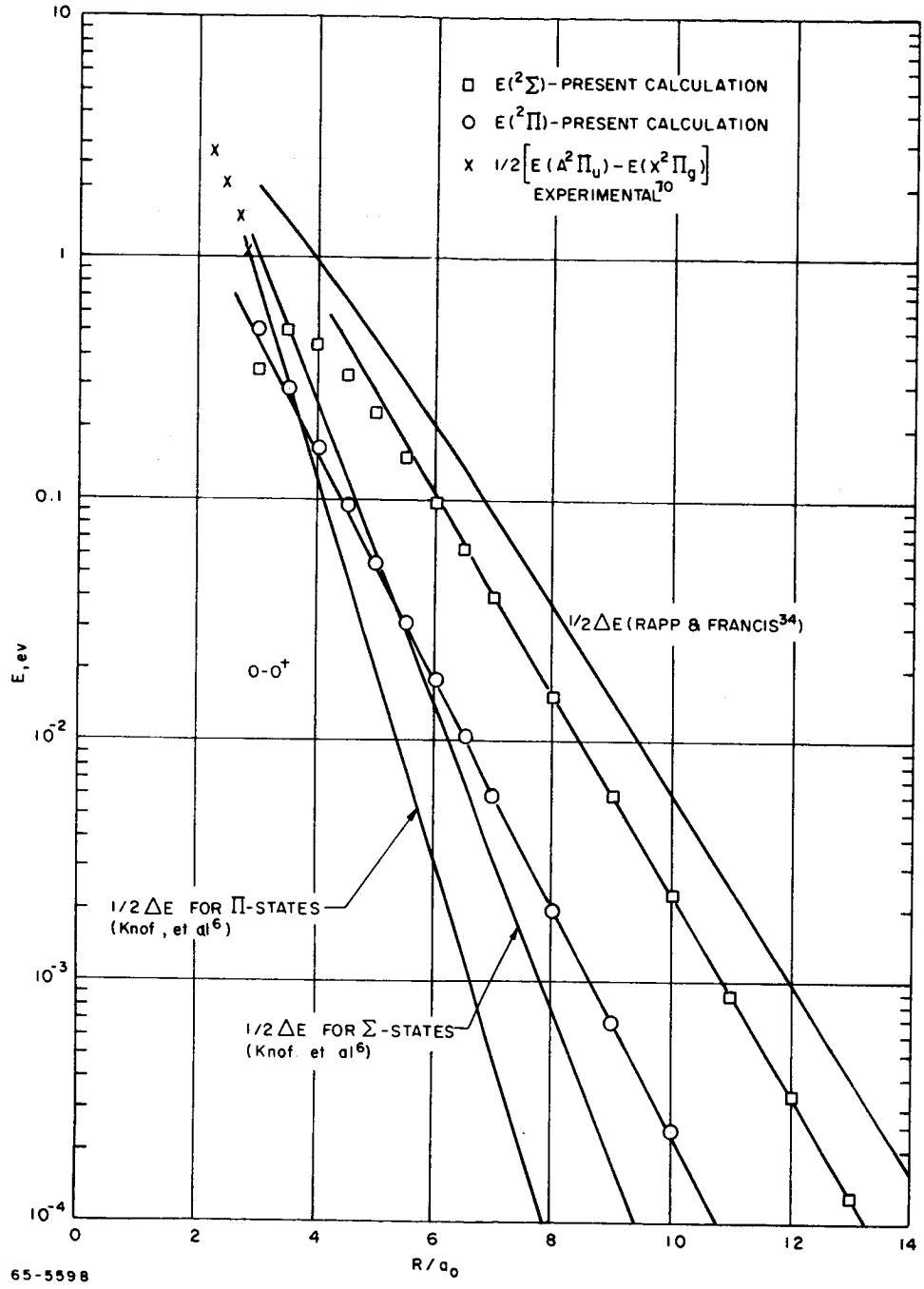

Figure 36 INTERACTION POTENTIALS BETWEEN GROUND-STATE O AND O^+

An interesting approximate relationship between the potentials for the Σ and Π-states may be obtained from our results, by noting that the condition

$$E_{\Sigma} \approx -\frac{d}{dR}(R E_{\Pi}) \tag{116}$$

is satisfied exactly by all terms in equation (112) for the interaction potentials, except for the Coulomb term $E^{(Q)}$ (equation 89). Since $E^{(Q)}$ turns out to be comparatively small, and in addition satisfies equation (116) approximately, one might except that (116) would also be approximately satisfied by the total interaction potential (112). For an exponential potential $E = Ae^{-\alpha R}$, this implies that the ratio $(E_{\Sigma}/E_{\Pi}) \approx (\alpha R-1)$, in good agreement with the numerical results shown in figures 35 and 36.

Estimates of the $N\text{-}N^+$ and $O\text{-}O^+$ interaction potentials at large internuclear separations have been made recently by Knof, Mason, and Vanderslice[6], by making use of approximate valence-bond arguments to extrapolate the observed spectroscopic potential curves to larger internuclear separations. The most direct comparison between their results and ours is provided by the predicted splitting $\Delta E = |E_g - E_u|$ between the symmetric and antisymmetric states. This comparison is shown in figures 35 and 36. We see that in the region of small separations, where the results of Knof, et al, are based directly on experimental data, the agreement with the present results is fairly good, but that the deviation between the two calculations becomes progressively greater at larger separations, so that, at the internuclear distances of importance for charge exchange, our results lie more than an order of magnitude above those of Knof, et al. Since our calculations are expected to be most accurate at larger internuclear separations, this would appear to indicate that the results of Knof, et al,[6] are too low at large values of R.

It is also of interest to compare the ratio of the energy splittings for the Σ- and Π-states calculated by Knof, et al, using Slater orbitals, with the approximate relationship (116) obtained in the present calculation. One sees from figures 35 and 36 that the ratio of the splittings obtained by Knof for $O\text{-}O^+$ is in reasonable agreement with equation (116), but that that obtained for $N\text{-}N^+$ is not. Since one would not expect the relationship (116) between the Σ and Π states to be greatly affected by the different wavefunctions used in the calculations, the observed difference for $N\text{-}N^+$ is rather surprising and would appear to indicate some inconsistency between the two calculations.

Figure 35 and 36 also show an approximate value of $\frac{1}{2}\Delta E$ for the $N\text{-}N^+$ and $O\text{-}O^+$ interactions calculated from a simple one-electron theory proposed by Rapp and Francis,[34] in which the potentials are given as a function of the ionization energy only. Since this theory assumes spherical symmetry, it of course gives only a single value of ΔE for each interaction, representing

some sort of an average over the six values which would be obtained in a correct treatment. From figures 35 and 36, we see that the potentials of Rapp and Francis have approximately the same slope as ours, but are perhaps about a factor of five higher.

In figures 35 and 36 we have also plotted the observed splitting between the $^2\Sigma$ and $^2\Pi$ states of N_2^+ and O_2^+ at small internuclear separations, as obtained from spectroscopic data.[70] Our calculations are not expected to be good at these small values of R; however, if our results are correct, the observed spectroscopic curves should merge into our results at larger internuclear separations. One sees that this is readily possible in the case of the $^2\Pi$ states, but that in the case of the $N\text{-}N^+$ $^2\Sigma$ states the observed curve would have to make a distinct bend in order to merge into our results at large R. This type of behavior might well be accounted for by interactions between the observed $B\,^2\Sigma_u^+$ and $C\,^2\Sigma_u^+$ states;[70] however, it does not appear possible to reach any definite conclusions on this point on the basis of presently available data.

In summary, our calculated interaction potentials appear to be reasonable on the basis of presently available evidence, but the data is too limited to permit definite conclusions to be reached as to their accuracy.

H. CHARGE EXCHANGE AND DIFFUSION CROSS SECTIONS FOR N^+ IN N AND O^+ IN O

The $N\text{-}N^+$ and $O\text{-}O^+$ interaction potentials calculated in the previous section (equation 115) can now be used in equations (13) and (14) to calculate the resonant charge-exchange cross sections Q_{ex} for these interactions. In these calculations we have made use of the simplified analysis given in reference 6, in which polarization is neglected and the atoms are assumed to move in straight-line trajectories. For an exponential potential difference $\Delta E = A e^{-\alpha R}$, reference 6 gives an asymptotic formula for the charge-exchange cross section in the parametric form[71, 72]

$$Q_{ex} = \frac{1}{2}\pi b_c^2 + \frac{\pi^3}{16\alpha^2}\left(\alpha b_c + 1 + \frac{1}{2\alpha b_c}\right) \tag{117a}$$

$$\hbar v = 2A\left(\frac{2b_c}{\pi\alpha}\right)^{1/2} e^{-\alpha b_c} \tag{117b}$$

where b_c is the critical impact parameter introduced in equation (15). Figure 37 shows a plot of

$$\alpha\sqrt{Q_{ex}} \quad \text{versus} \quad \log_{10}\left[(2\sqrt{2}\,A)/(\sqrt{\pi}\,\alpha\hbar v)\right],$$

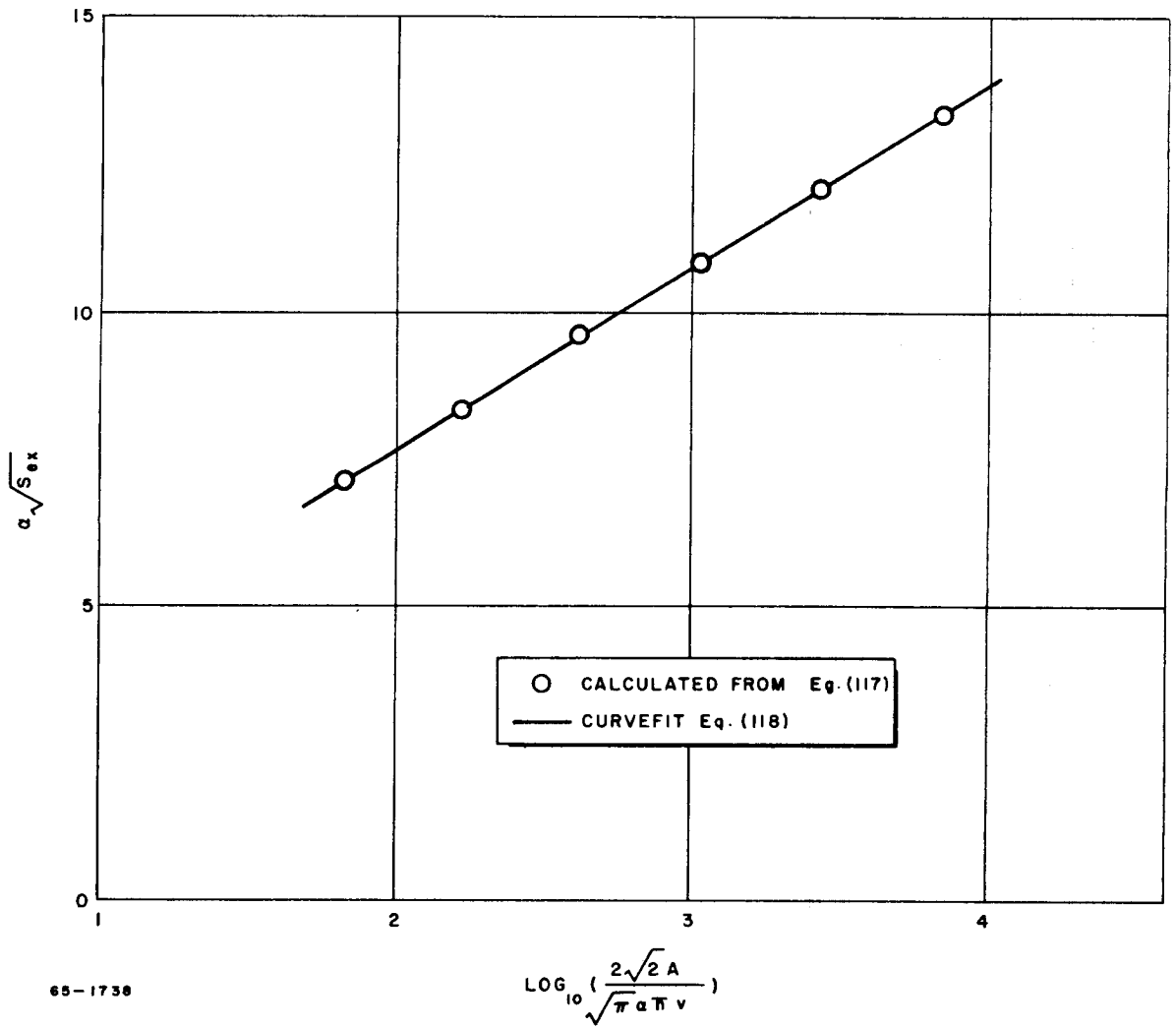

Figure 37 THEORETICAL RELATIONSHIP BETWEEN CHARGE-EXCHANGE CROSS SECTION AND COLLISION VELOCITY

as calculated from equation (117); one sees that the plotted points can be fit very well by the straight line

$$a\sqrt{Q_{ex}} = 1.48 + 3.09 \log_{10} [(2\sqrt{2}\, A)/(\sqrt{\pi}\, a\, \hbar v)] \quad \text{for } 7 \leq a\sqrt{Q_{ex}} \leq 14 \tag{118a}$$

or evaluating the constants,

$$a\sqrt{Q_{ex}} = 24.30 + 3.09 \log_{10} (A/a) - 3.09 \log_{10} v \tag{118b}$$

with v in cm/sec, A in ev and a in $\mathring{A}^{-1}$. Substituting the values of A and a from equation (115) into equation (118b) and averaging over the different states as described in reference 6, we obtain the desired charge-exchange cross sections in the form

$$\begin{aligned} Q_{ex} &= (15.3 - 1.60 \log_{10} v)^2 \ \mathring{A}^2 \\ &= (6.4 - 0.80 \log_{10} E)^2 \ \mathring{A}^2 \qquad \text{for } N - N^+ \\ Q_{ex} &= (14.9 - 1.57 \log_{10} v)^2 \ \mathring{A}^2 \\ &= (6.2 - 0.79 \log_{10} E)^2 \ \mathring{A}^2 \qquad \text{for } O - O^+ \end{aligned} \tag{119}$$

where E is the kinetic energy of the impinging ion in electron volts (in a coordinate system in which the atom is stationary).

The lower limit of validity of equation (119) is determined by the energy at which deviations from a straight-line trajectory become important in evaluating the integral in equation (13), while the upper limit is determined by the energy at which the error in the calculated Heitler-London interaction potentials (equation 115) begins to become significant. It is difficult to estimate these limits with any certainty; however, from figures 35 and 36 and equation (15) it appears that equation (119) should be most accurate in the range of energies 0.1 ev $\leq$ E $\leq$ 100 ev, but that extrapolation up to energies of perhaps 10^4 ev or more should be possible without too much loss of accuracy.

The values of Q_{ex} calculated from equation (119) are compared with other available data on these cross sections in figures 38 and 39. One sees that the various theoretical estimates of these cross sections are quite scattered, as would be expected from the potentials shown in figures 35 and 36, and that our results do not agree well with any of them. The only experimental data available on these cross sections is a recent crossed-beam measurement by Stebbings, et al[5] of the O-O^+ charge-exchange cross section for energies between 40 and 10^4 ev. The extrapolation of this data to lower energies is shown by the dashed line in figure 39, with the estimated experimental error of ±25% indicated by the vertical error bar. The good agreement shown in figure 39 between our results and this measurement is very encouaging; however agreement in a single case

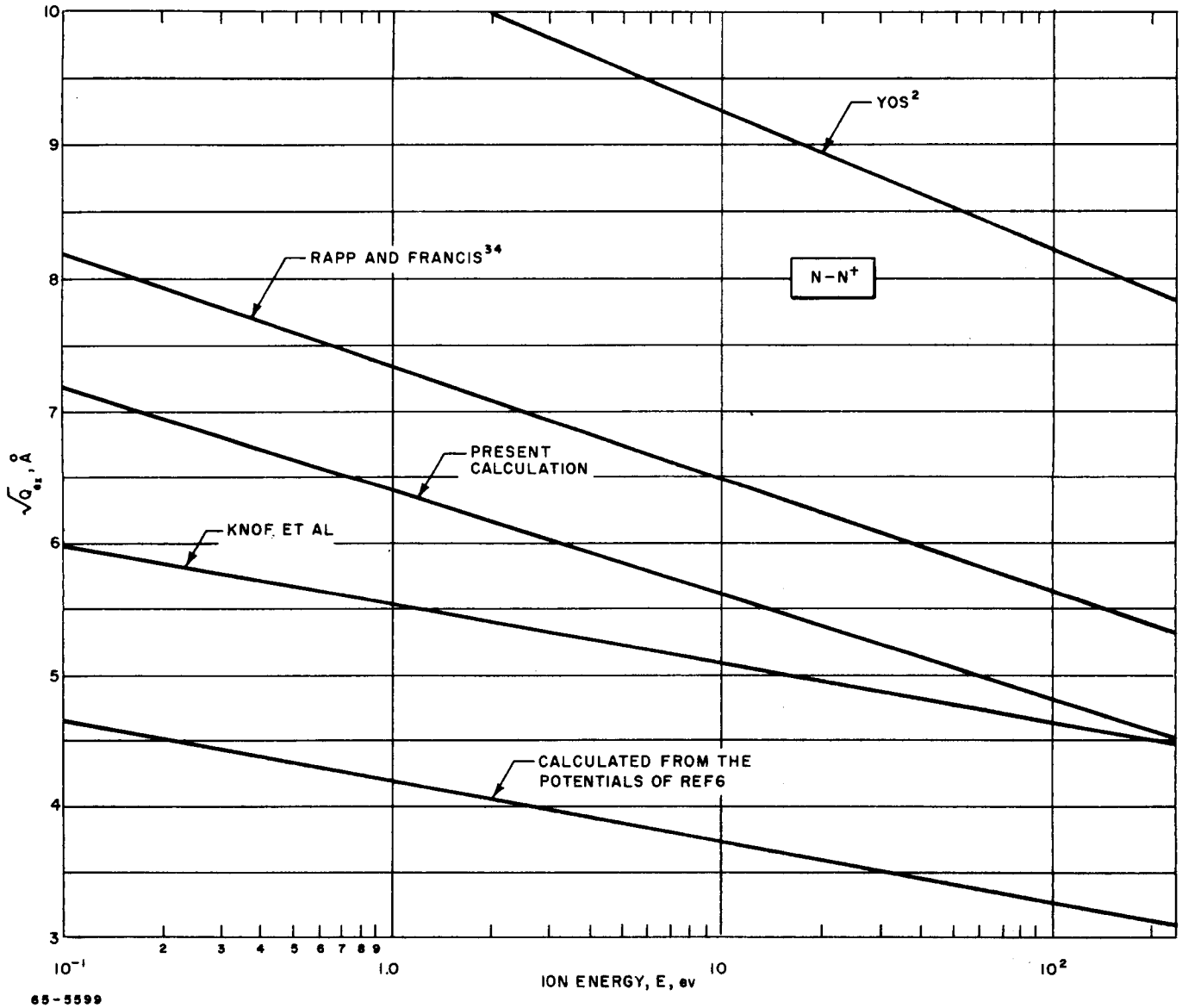

Figure 38 RESONANT CHARGE-EXCHANGE CROSS SECTION FOR N-N$^+$ COLLISIONS

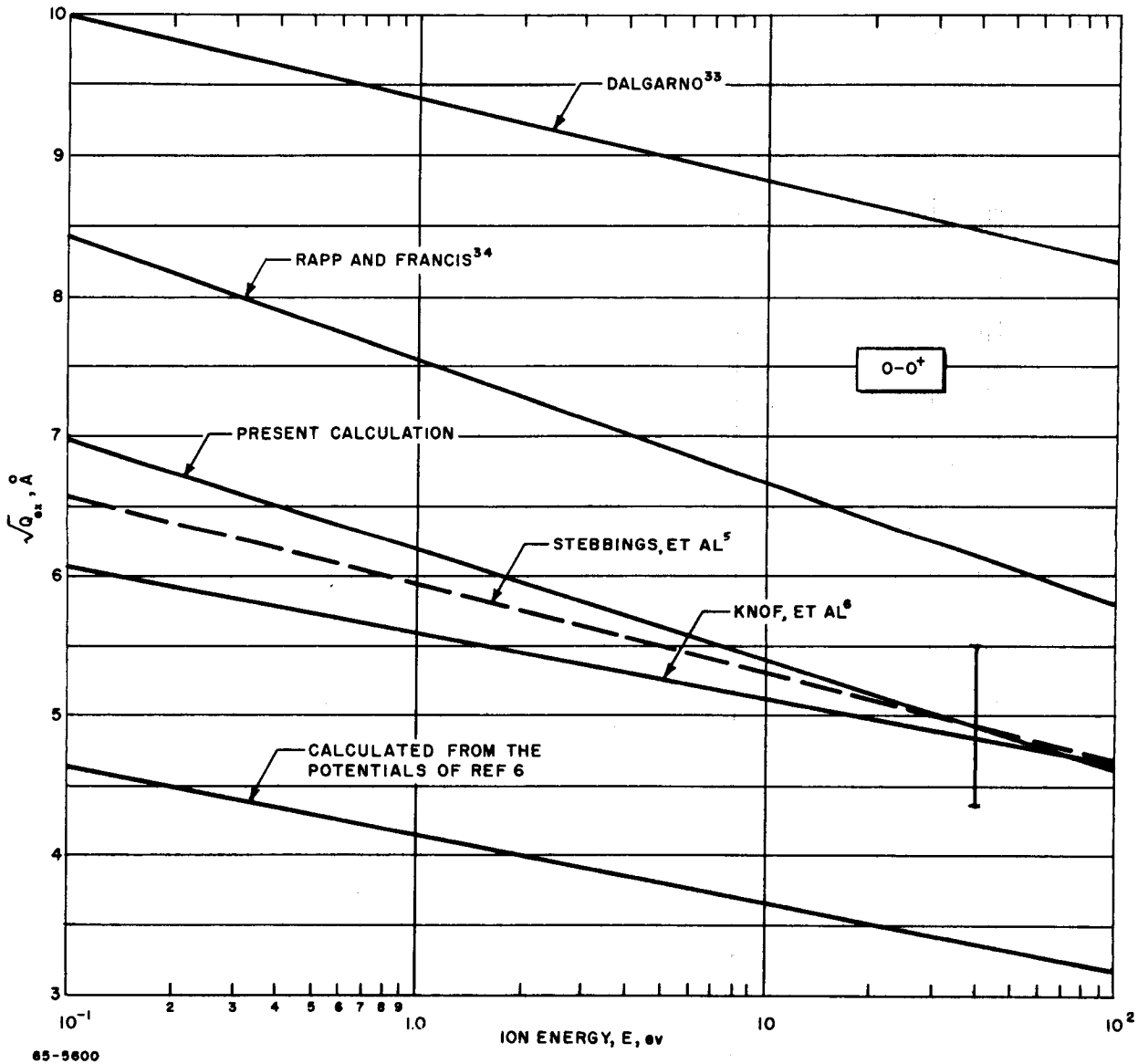

Figure 39 RESONANT CHARGE-EXCHANGE CROSS SECTION FOR O-O$^+$ COLLISIONS

could of course be accidental, and hence one should probably regard the charge-exchange cross sections calculated in the present work (equation 119) as somewhat tentative, until such time as a more extensive test of the theory can be obtained.

The important quantity for the determination of the transport properties of high temperature gases is the collision integral for diffusion $\bar{\Omega}^{(1,1)}$, which is here defined so that it would be equal to $\pi\sigma^2$ for rigid spheres of diamer σ. At high temperatures, the diffusion cross section is completely dominated by the charge-exchange effect and is equal to $2Q_{ex}$,[33, 71] so that the collision integral for diffusion becomes

$$\bar{\Omega}^{(1,1)} = (kT)^{-3} \int_0^\infty Q_{ex}\, E^2 \exp(-E/kT)\, dE \tag{120}$$

where k is Boltzmann's constant and T is the absolute temperature. This integral is easily evaluated for Q_{ex} given by equation (119) to yield

$$\bar{\Omega}^{(1,1)}_{N-N^+} = 2(9.1 - 0.80 \log_{10} T)^2 \ \mathring{A}^2$$

$$\bar{\Omega}^{(1,1)}_{O-O^+} = 2(8.8 - 0.79 \log_{10} T)^2 \ \mathring{A}^2 \tag{121}$$

for T in °K. These cross sections are plotted in figure 40, along with the corresponding quantities given by Knof, et al.[6]

Figure 40 also shows the effect of the polarization potential on the diffusion cross sections, as estimated in reference 6. We see that for temperatures above about 1000°K, polarization should have only a minor effect on the calculated diffusion cross sections $\bar{\Omega}^{(1,1)}$ so that the use of equation (120) for $\bar{\Omega}^{(1,1)}$ should be quite well justified in this temperature range.

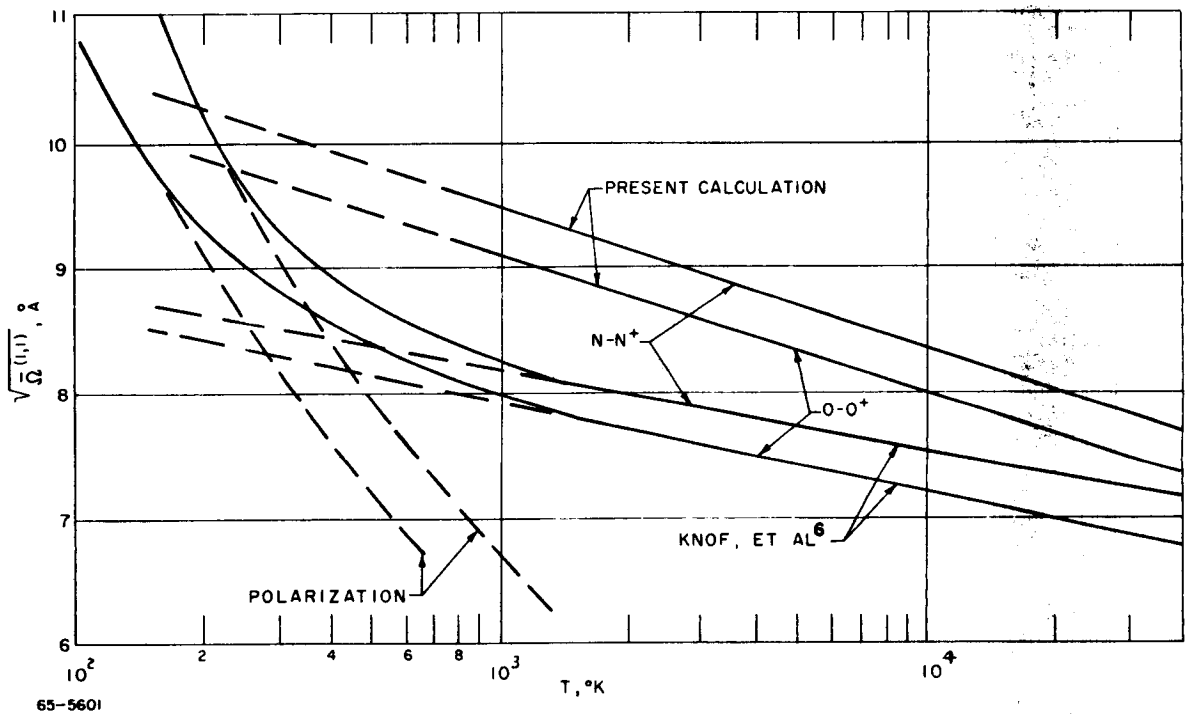

Figure 40 DIFFUSION COLLISION INTEGRALS FOR N^+ IN N AND O^+ IN O

IV. REFERENCES

1. Maecker, H., Zeit. Phys. 157, 1 (1959); 158, 392 (1960).

2. Yos, J.M., Avco/RAD, Transport Properties of Nitrogen, Hydrogen, Oxygen, and Air to 30,000°K, RAD-TM-63-7, March 1963.

3. Knopp, C.F., Doctoral Dissertation, Northwestern Univ. (1965).

4. Yos, J.M., Avco/RAD, unpublished calculations.

5. Stebbings, R.F., A.C.H. Smith, and H. Ehrhardt, J. Geophys. Research 69, 2349 (1964).

6. Knof, H., E.A. Mason, and J.T. Vanderslice, J. Chem. Phys. 40, 3548 (1964).

7. See, for example, W. Finkelnburg and H. Maecker, Electrische Bögen und Thermisches Plasma, Handbuch der Physik, Vol. 22, Springer-Verlag, Berlin, 1956, p. 254-444.

8. Pai, S.I., Viscous Flow Theory, D. van Nostrand Co., New York, 1956.

9. Drellishak, K., C. Knopp and A. Cambel, Technical Documentary Report No. AEDC-TDR-63-146, Arnold Engineering Development Center, Air Force Systems Command, U.S.A.F.

10. Drellishak, K., D. Aeschliman, and A. Cambel, Technical Documentary Report No. AEDC-TDR-64-12, Arnold Engineering Development Center, Air Force Systems Command, U.S.A.F.

11. Olsen, H.N., JQSRT 3, 59 (1963).

12. Solarski, J.E. and W.L. Wiese, Phys. Rev. 135, A1236 (1964).

13. Bates, D.R. and A. Damgaard, Phil. Trans. Roy. Soc. (London) A242, 101 (1949).

14. Moore, C.E., editor, Atomic Energy States, Bureau of Standards Circular 467, (1952).

15. Barr, W.L. JOSA 52, 885 (1962).

16. Amdur, I. and E.A. Mason, Phys. Fluids 1, 370 (1958).

17. Yos, J.M., Avco/RAD, unpublished calculation.

18. Pfender, E. and W. Bez, Proceedings, Fifth Inter. Conf. Ionization Phenomena in Gases, 897 (1961).

19. Sheindlin, A.E. and E.I. Asinovskii, Proceedings, Sixth Inter. Conf. Ionization Phenomena in Gases, 2, 379 (1963).

20. Maecker, H., Proceedings, Fifth Inter. Conf. Ionization Phenomena in Gases, 1793 (1961).

21. Samson, J.A.R., JOSA 54, 420 (1964).

22. Cann, G.L., Energy Transfer Processes in a Partially Ionized Gas, GALCIT Memo No. 61 (June 1961).

23. Barhorn, F., Zeit. Phys. 155, 42 (1959).

24. Maecker, H., The Properties of Nitrogen up to 15,000°K, AGARD Report No. 324 (September 1959).

25. Stewart, J.C. and K.D. Pyatt, Jr., Theoretical Study of Optical Properties, AFSWC-TR-61-71, Vol. III, Sept. 1961, p. 356.

26. Allen, R.A., A. Textoris, and J. Wilson, Measurements of the Free-Bound and Free-Free Continua of Nitrogen, Oxygen, and Air, JQSRT 5, 95 (1965).

27. Burgess, A. and M.J. Seaton, Rev. Mod. Phys. 30, 992 (1958).

28. Nicolet, M., Physics of the Upper Atmosphere, edited by J.A. Ratcliffe (Academic Press, N.Y., 1960), Chap. 2.

29. Dalgarno, A., J. Atmos. Terr. Phys. 12, 219 (1958).

30. Chamberlain, J.W., Physics of the Aurora and Airglow, (Academic Press, N.Y., 1961).

31. Pallone, A. and W. Van Tassel, Phys. Fluids 6, 983 (1963).

32. Holstein, T., J. Phys. Chem. 56, 832 (1952).

33. Dalgarno, A., Phil. Trans. Roy. Soc. London A250, 426 (1958).

34. Rapp, D., and W.E. Francis, J. Chem. Phys. 37, 2631 (1962).

35. Bates, D.R., H.S.W. Massey, and A.L. Stewart, Proc. Roy. Soc, A216, 437 (1953).

36. Gurnee, E.F., and J.L. Magee, J. Chem. Phys. 26, 1237 (1957).

37. Mason, E.A., J.T. Vanderslice, and J.M. Yos, Phys. Fluids 2, 688 (1959).

38. Hirschfelder, J.O., C.F. Curtiss, and R.B. Bird, Molecular Theory of Gases and Liquids, (Wiley, N.Y., 1954), Chap. 14.

39. Margenau, H. Phys. Rev. 55, 1000 (1939).

40. Heitler, W., and F. London, Zeit. Phys. 44, 455 (1927).

41. Pauling, L., and E.B. Wilson, Introduction to Quantum Mechanics (McGraw-Hill, N.Y., 1935), Chap. XII.

42. Rosen, P., J. Chem. Phys. 18, 1182 (1950).

43. Buckingham, R.A., and A. Dalgarno, Proc. Roy. Soc. (London) A 213, 327 (1952).

44. Bleick, W.E., and J.E. Mayer, J. Chem. Phys. 2, 252 (1934).

45. Kunimune, M., Prog. Theor. Phys. 5, 412 (1950).

46. Mulliken, R.S., Phys. Rev. 120, 1674 (1960).

47. Bates, D.R., K. Ledsham, and A.L. Stewart, Phil. Trans. Roy. Soc. (London) A216, 437 (1953).

48. Clementi, E., Tables of Atomic Functions, supplement to IBM J. Res. Dev. 9, (1965).

49. Slater, J.C., Quantum Theory of Atomic Structure, Vols. I and II (McGraw-Hill Book Company, Inc., New York, 1960).

50. Clementi, E., C.D.J. Roothaan, and M. Yoshimine, Phys. Rev. 127, 1618 (1962).

51. Clementi, E., J. Chem. Phys. 38, 996 (1963).

52. Roothaan, C.C.J., and P.S. Kelly, Phys. Rev. 131, 1177 (1963).

53. Sonnenschein, C.M., Analytic Hartree-Fock Wavefunctions for the 2p-Atoms, in Quarterly Progress Report No. 44 of the Solid-State and Molecular Theory Group, MIT (April 15, 1962).

APPENDIXES

54. Herzberg, G., Molecular Spectra and Molecular Structure I. Spectra of Diatomic Molecules, 2nd ed (D. Van Nostrand Company, Inc., New York, 1950), pp 212-218.

55. Herzberg, op. cit., pp. 315-322.

56. Section 20-7 of reference 49.

57. See, for example, R. Daudel, R. Lefebvre, and C. Moser, Quantum Chemistry, Methods and Applications (Interscience, N.Y. 1959).

58. Mulliken, R.S., J. Chem Phys. 37, 809 (1962).

59. See, for example, Section 43a of reference 41.

60. See, for example, Section 12-5 of reference 49.

61. Slater, J.C., Rev. Mod. Phys. 25, 199 (1953).

62. See for example, reference 36.

63. Section 13-3 of reference 49.

64. See for example, Chapter 12 of reference 49.

65. See, for example, the classification of molecular integrals given by M. Kotani, A. Amemiya, E. Ishiguro, and T. Kimura, Table of Molecular Integrals (Maruzen Co., Ltd., Tokyo (1955), pp 31-32.

66. Roothaan, C.C.J., J. Chem. Phys. 19, 1445 (1951).

67. Ruedenberg, K., C.C.J. Roothaan, and W. Jaunzemis, J. Chem. Phys. 24, 201 (1956).

68. Roothaan, C.C.J., J. Chem. Phys. 24, 947 (1956).

69. Wahl, A.C., P.E. Cade, and C.C.J. Roothaan, J. Chem. Phys. 41, 2578 (1964).

70. Gilmore, F.R., Potential Energy Curves for N_2, NO, O_2, and Corresponding Ions, Rand Corp., Memo RM-4034-PR (June 1964).

71. Dalgarno, A., and M.R.C. McDowell, Proc. Phys. Soc. (London) A69, 615 (1956).

72. Mason, E.A., and J.T. Vanderslice, J. Chem. Phys. 29, 361 (1958).

APPENDIX A

EXPLICIT SOLUTION OF THE ELENBAAS-HELLER ARC EQUATIONS FOR THE TRANSPORT PROPERTIES

One of the few methods presently available for obtaining experimental values of the electrical and thermal conductivities of gases at high temperature (~10,000°K) is the analysis of data obtained on a suitable, cylindrically symmetric electric arc (the "constricted" or "cascade" arc). This analysis is based on the Elenbaas-Heller model for the arc column, which assumes that the transport of energy out of the arc column is entirely due to radial heat conduction and optically thin radiation, and that all arc properties are independent of the axial coordinate. Thus the energy balance relation for the column is reduced to a single ordinary differential equation in the radial coordinate, r,

$$\sigma E^2 + \frac{1}{r}\frac{d}{dr}\left(r K \frac{dT}{dr}\right) - P_{rad} = 0 \qquad \text{(A-1)}$$

where T is the gas temperature, $\sigma = \sigma(T)$ and $K = K(T)$ are the electrical and thermal conductivities of the gas, $P_{rad} = P_{rad}(T)$ is the radiated power per unit volume, and E is the electric field strength in the axial direction (assumed constant). The total arc current I is given by the integrated Ohms's law for the column

$$I = 2\pi \int_0^R \sigma E r \, dr \qquad \text{(A-2)}$$

where R is the column radius.

A number of different numerical techniques have been given for inverting equations (A-1) and (A-2) to obtain transport property values from experimental arc data (references A1 to A4)*. In general these techniques are based on some sort of an iterative procedure in which an initial form is assumed for the properties $\sigma(T)$ and/or $K(T)$, equations (A-1) and (A-2) are solved using these assumed properties, and the results are compared with experiment. The property values are then adjusted and the process repeated until satisfactory agreement with experiment is obtained. Unfortunately this process generally tends to be quite laborious numerically, and the accuracy which can be obtained in the final property values is not clear. Further, the question of the existence and uniqueness of the solutions for the transport properties has never been studied, so that it is not known how much experimental information

*Also H. W. Emmons and K. Gopalakrishna, Hardard University (unpublished data).

is actually required to determine the transport properties uniquely, or whether the values which are derived from the above numerical analyses are the only ones which could account for the observed experimental data.

The present study is a beginning towards a more systematic treatment of the problem of deriving transport property values from electric arc data. We determine the amount of experimental information which is required to determine the properties σ and K uniquely as functions of T, and equations (A-1) and (A-2) are inverted to obtain explicit analytic formulas for these properties in terms of the measured data.

It must be pointed out, however, that this analysis is based upon the energy equation in the Elenbaas-Heller form (A-1), which assumes that the arc column is optically thin to its own thermal radiation. It has been demonstrated during the present program that the arc column, at least in argon and nitrogen, emits significant amounts of power at wavelengths in the far ultraviolet where the gas is relatively opaque. Neither the Elenbaas-Heller equation (A-1) nor the analysis presented in this appendix is accurately applicable to such arc columns. However, it might be possible to carry out an analysis similar to that presented here for the much more difficult problem of a cylindrical arc column with radiative transfer.

The quantities in equations (A-1) and (A-2) which are susceptible to direct experimental measurement are the arc current I, the electric field strength E, the radial temperature distribution $T(r)$, and the radiated power per unit volume $P_{rad}(T)$. Let us assume that these quantities have been measured for two different arc runs, 1 and 2, for all temperatures T greater than or equal to some temperature T_o, where T_o is such that the arc current flowing in regions with $T < T_o$ is negligible. (Ideally of course, T_o should be equal to the temperature of the tube wall confining the arc, but in practice, since the electrical conductivity drops off so sharply at the lower temperatures, it is not necessary to know the temperature distribution all the way out to the wall.) We wish to consider the problem of obtaining the unknown functions $\sigma(T)$ and $K(T)$ from the above experimental data. One obvious condition which must be satisifed by the experimental data in order for them to be consistent with equations (A-1) and (A-2) can be obtained from the energy balance on the column as a whole. Integrating equation (A-1) over the radial coordinate r and using equation (A-2) we obtain this balance in the form

$$-2\pi R K(T_o) \left.\frac{dT}{dr}\right|_{r=R} = E I - 2\pi \int_0^R P_{rad}\, r\, dr \qquad \text{(A-3)}$$

where R is now the radius at which $T = T_o$ and we have used the boundary condition that $\frac{dT}{dr} = 0$ at $r = 0$. All quantities in equation (A-3) are experimentally

measured except $K(T_o)$, so that for two different arc runs to be consistent they must given the same value of $K(T_o)$. This gives the simple condition

$$K(T_o) = \left.\frac{E\,I - 2\pi \int_0^R P_{rad}\, r\, dr}{-2\pi r \left.\frac{dT}{dr}\right|_R}\right|_{run\ 1} = \left.\frac{E\,I - 2\pi \int_0^R P_{rad}\, r\, dr}{-2\pi r \left.\frac{dT}{dr}\right|_R}\right|_{run\ 2} \qquad \text{(A-4)}$$

which must be satisfied by the experimental data for the two runs in order for them to be consistent with the Elenbaas-Heller model of the column (equations A-1 and A-2). We assume henceforth in our analysis that condition (A-4) is satisfied.

In order to solve equation (A-1) for the transport properties σ and K, it is convenient to treat T as the independent variable and to introduce the new dependent variable

$$\rho \equiv \rho(T) \equiv r\,E\ . \qquad \text{(A-5)}$$

Equation (A-1) may then be written in the equivalent form

$$\sigma + \frac{q}{\rho}\frac{d}{dT}(\rho K q) - \frac{P_{rad}}{E^2} = 0 \qquad \text{(A-6)}$$

where we have defined

$$q(T) \equiv -\frac{1}{E}\frac{dT}{dr} = -\frac{1}{d\rho/dT} \qquad \text{(A-7)}$$

Solving equation (A-6) for $\sigma(T)$ and combining the results for the two different arc runs gives

$$\sigma(T) = \frac{P_{rad}}{E_1^{\,2}} - \frac{q_1}{\rho_1}\frac{d}{dT}(\rho_1 q_1 K) = \frac{P_{rad}}{E_2^{\,2}} - \frac{q_2}{\rho_2}\frac{d}{dT}(\rho_2 q_2 K) \qquad \text{(A-8)}$$

where the subscripts 1 and 2 indicate the values for the two different runs, and the values for each run are evaluated at the radial position r, where the given value of T occurs for that run. Thus the data in equation (A-8) are evaluated at different radial coordinates for the two runs, but at the same temperature T. The gas properties σ, K and P_r in equation (A-8) are of course not subscripted, since they are the same function of T for both runs.

The last two members of equation (A-8) give a differential equation for K(T),

$$\frac{q_1}{\rho_1}\frac{d}{dT}(\rho_1 q_1 K) - \frac{q_2}{\rho_2}\frac{d}{dT}(\rho_2 q_2 K) = \left(\frac{1}{E_1^2} - \frac{1}{E_2^2}\right) P_{rad}$$

or, simplifying and making use of equation (A-7),

$$(q_1^2 - q_2^2)\frac{dK}{dT} + \left[\frac{q_1}{\rho_1}\frac{d}{dT}(\rho_1 q_1) - \frac{q_2}{\rho_2}\frac{d}{dT}(\rho_2 q_2)\right] K = \left(\frac{1}{E_1^2} - \frac{1}{E_2^2}\right) P_{rad}$$

$$(q_1^2 - q_2^2)\frac{dK}{dT} + \left[\frac{1}{2}\frac{d}{dT}(q_1^2 - q_2^2) - \left(\frac{q_1}{\rho_1} - \frac{q_2}{\rho_2}\right)\right] K = \left(\frac{1}{E_1^2} - \frac{1}{E_2^2}\right) P_{rad} \cdot \tag{A-9}$$

Equation (A-9) is an ordinary, first order, linear, inhomogenous, differential equation for K(T); it can be solved readily by elementary methods to give an explicit formula for the thermal conductivity K(T) in terms of the observed experimental data,

$$K(T) = K(T_o)\, y(T) + \left(\frac{1}{E_1^2} - \frac{1}{E_2^2}\right) y(T) \int_{T_o}^{T} \frac{P_{rad}(T')}{\Delta^2(T')\, y(T')}\, dT' \tag{A-10a}$$

where

$$\Delta(T) = \sqrt{q_1^2 - q_2^2} \tag{A-10b}$$

$$y(T) = \frac{\Delta(T_o)}{\Delta(T)} \exp\left[\int_{T_o}^{T} \frac{1}{\Delta^2}\left(\frac{q_1}{\rho_1} - \frac{q_2}{\rho_2}\right) dT'\right], \tag{A-10c}$$

and the integration constant $K(T_o)$ can be evaluated from equation (A-4). According to the theory of linear differential equations, the solution (A-10) is the only possible solution of equation (A-9) satisfying the boundary condition (A-4), so that it follows that the thermal conductivity is uniquely determined by the assumed experimental data.

The electrical conductivity σ can now be determined directly from equation (A-8), using the value of K(T) from equation (A-10). Eliminating dK/dT between equations (A-8) and (A-9) and simplifying the resulting expressions by the use of (A-7) and (A-10b) one obtains the formula for σ in the form

$$\sigma(T) = \frac{P_{rad}}{E_1^{\,2}} - q_1^{\,2}\,\frac{dK}{dT} - \frac{q_1 K}{\rho_1}\,\frac{d}{dT}\,(\rho_1\, q_1)$$

$$= \frac{1}{\Delta^2}\left[\left(\frac{q_1^{\,2}}{E_2^{\,2}} - \frac{q_2^{\,2}}{E_1^{\,2}}\right) P_{rad} + q_1^{\,2}\, q_2^{\,2}\left(\frac{1}{\rho_1\, q_1}\,\frac{d\,\rho_1\, q_1}{dT} - \frac{1}{\rho_2\, q_2}\,\frac{d\,\rho_2\, q_2}{dT}\right) K\right]$$

$$= \frac{1}{\Delta^2}\left[\left(q_1^{\,2}\, q_2^{\,2}\,\frac{d}{dT}\left(\ln\frac{\rho_1\, q_1}{\rho_2\, q_2}\right)\right) K + \left(\frac{q_1^{\,2}}{E_2^{\,2}} - \frac{q_2^{\,2}}{E_1^{\,2}}\right) P_{rad}\right] \qquad \text{(A-11)}$$

where the thermal conductivity $K = K(T)$ is given by equation (A-10). Since $K(T)$ is uniquely determined by the experimental data, it follows that the electrical conductivity $\sigma(T)$ is also. We thus conclude that if the Elenbaas-Heller model for the column (equations A-1 and A-2) is valid, then measurements of the arc currents I, electric field strengths E, and radial temperature distributions $T(r)$ for two different arc runs, together with a knowledge of the radiated power per unit volume P_{rad} as a function of temperature, are sufficient data to determine the electrical and thermal conductivities of the gas uniquely as a function of temperature, over the range of temperatures common to the two arc measurements.

Although equations (A-10) and (A-11) provide unique well-defined mathematical expressions for the electrical and thermal conductivities $\sigma(T)$ and $K(T)$ for any values of the experimental quantities E_1, I_1, $r_1(T)$, E_2, I_2, $r_2(T)$ and $P_{rad}(T)$, provided only that they satisfy the simple energy balance condition (A-4), these mathematical expressions do not always correspond to physically meaningful values of the transport properties; for example, one can readily find forms for the radial temperature distributions $T(r)$ which will yield negative, or even imaginary, values of σ and K when substituted into equations (A-10) and (A-11). Since the solutions (A-10) and (A-11) are unique, one concludes that such temperature distributions cannot actually occur in an arc satisfying the Elenbaas-Heller equations (A-1) and (A-2), and that if the experimentally measured data for an actual arc leads to physically meaningless results when substituted into equations (A-10) and (A-11), it indicates either that the data are in error or that the Elenbaas-Heller model is not applicable to the arc for which the data were obtained. Thus equations (A-10) and (A-11) can be used to provide a test of the validity of the Elenbaas-Heller model for a given arc facility. If data are available for only two arc runs this will be only a relatively crude test, since the arc would probably have to deviate rather strongly from the Elenbaas-Heller model in order to cause the calculated transport properties to actually go negative. However, if data are available for three or more arc runs then a more sensitive test for deviations from Elenbaas-Heller theory could of course be obtained by comparing the transport property values calculated for the different pairs of runs.

Equation (A-10) for the thermal conductivity K involves first derivatives of the measured temperature distributions, and equation (A-11) for the electrical conductivity σ involves second derivatives. Since the temperature distributions themselves are derived from the measured radiation intensities by inversion of the Abel integral, a procedure which is essentially equivalent to another differentiation, one sees that the quantities K and σ depend essentially on second and third derivatives, respectively, of the measured quantities; a great deal of refinement is thus required in the experimental measurements in order to obtain meaningful values of the transport properties σ and K. The measurements can be made very accurately, however, so that it does not appear that this degree of refinement is out of the question. (It should be pointed out that this difficulty is not peculiar to the present method of data analysis; any other scheme for obtaining σ and K from the experimental data is essentially equivalent to our equations (A-10) and (A-11) and suffers from the same difficulty. In particular, the difficulty of obtaining a smooth curve for $\sigma(T)$ from the experimental data has been known for a long time;[A1, A3] our equation (A-11) simply displays the reason for this difficulty more explicitly.) A further encouraging circumstance is that to obtain accurate values of the transport properties, it is not necessary to know the actual absolute temperatures with high accuracy, but merely the correspondence between points having the same temperature for the two arc runs. In fact, if $\theta = \theta(T)$ is some function of the temperature, such as, for example, the absolute intensity of some spectral line, then equation (A-1) can be written in the form

$$\sigma E^2 + \frac{1}{r}\frac{d}{dr}\left(r\,\lambda\,\frac{d\theta}{dr}\right) - P_{rad} = 0 \qquad \text{(A-12a)}$$

with

$$\lambda \equiv K\,\frac{dT}{d\theta} \qquad \text{(A-12b)}$$

and equations (A-2) and (A-12a) can be solved just as before to give $\sigma(\theta)$ and $\lambda(\theta)$ in terms of the radial distributions of θ and the radiated power P_{rad}.

The heat conduction potential $S \equiv \int^{T} K\,dT$ can then be found as a function of θ from the equation

$$S = \int^{\theta} K\,\frac{dT}{d\theta}\,d\theta = \int^{\theta} \lambda\,d\theta \quad . \qquad \text{(A-13)}$$

Thus, even without knowing the relation between θ and T, it is possible to find the important function $\sigma(S)$ which is required for calculating the arc characteristics. Further, one sees from equation (A-12b) that the error in the thermal

conductivity due to uncertainties in $\theta(T)$ is simply proportional to the error in $dT/d\theta$, so that $\theta(T)$ need not be known with particularly high accuracy in order to obtain satisfactory accuracy for σ and K (in actual practice, errors in $\theta(T)$ and $dT/d\theta$ seldom exceed a few percent.)

REFERENCES TO APPENDIX A

A1. Morris, J., G. Bach and J. Yos, Research on Radiation from Arc Heated Plasmas, Avco RAD-TR-64-10 (1964).

A2. Maecker, H., Z. Physik 157, 1 (1959); 158, 392 (1960).

A3. Schmitz, G., H. - J. Patt, L. Detloff and J. Uhlenbusch, Eine Methode Zur Bestimmung von Materialfunktionen Hochionisierter Gase aus der Temperaturverteilung und der Charakteristik von Lichtbogenentladung, Bericht fur das Bundesministerium fur Verteidigung, T II 5, Bonn (April 1963).

A4. Schmitz, G. and J. Uhlenbusch, Z. Naturforsch 18a, 772 (1963).

APPENDIX B

ANALYTIC CURVEFITS TO ARC TEMPERATURE DISTRIBUTIONS

All of the methods for determining transport properties from arc data by solving the Elenbaas-Heller equation require evaluation of derivatives of the radial temperature distribution $T(r)$. A graphical method for obtaining the first derivative, dT/dr, has been described in Section IIE. The present appendix discusses an alternative procedure, in which the points of the experimental temperature distribution, obtained by Abel inversion of the lateral integrated intensity data, are curvefitted by analytic functions, and the derivatives are obtained by differentiating the curvefit analytically.

For the two-run method (based upon the analysis presented in Appendix A), it is most convenient to fit the radius as a function of temperature, $r(T)$, rather than temperature as a function of radius, $T(r)$. It is known that at the axis ($r = 0$), the derivative $dT/dr = 0$ and the temperature is the experimental axis temperature, T_a. These features can be built into the curvefit by choosing a function of the form

$$r^2 = Q\,f(Q) \tag{B-1}$$

where

$$Q \equiv 1 - T/T_a \tag{B-2}$$

The following four-parameter* curvefits of the form (B-1) have been found useful for fitting argon arc-column temperature distributions:

Form 1:

$$r^2 = \begin{cases} \dfrac{Q}{C_2 + C_3\,Q^{C_4}} & \text{for } Q \le Q_m \\[2ex] \dfrac{C_4 - 1}{C_2\,C_4}\,Q_m & \text{for } Q > Q_m \end{cases} \tag{B-3}$$

where Q_m is given by

$$Q_m = \left[\frac{C_2}{C_3\,(C_4 - 1)}\right]^{1/C_4}$$

Form 2:

$$r^2 = Q\,(C_2 + C_3\,Q^{C_4}) \tag{B-4}$$

*The four parameters are, in each case, T_a, C_2, C_3, C_4.

$$\underline{\text{Form 3:}} \quad r^2 = \begin{cases} \dfrac{Q}{C_2 + C_3 e^{C_4 Q}} & \text{for } Q \le Q_m \\[2ex] \dfrac{C_4 Q_m - 1}{C_2 C_4} & Q_m \text{ for } Q > Q_m \end{cases} \tag{B-5}$$

where Q_m is the solution of

$$C_2 + C_3 (1 - C_4 Q_m) e^{C_4 Q_m} = 0$$

$$\underline{\text{Form 4:}} \quad r^2 = Q(C_2 + C_3 e^{-C_4 Q}) \tag{B-6}$$

The changes in form at $Q = Q_m$ in (B-3) and (B-5) prevent the distributions from turning back on themselves (predicting a fictitious region of negative dT/dr in which T would be a double-valued function of r). In each case, Q_m is the value of Q at which r reaches its maximum value.

Fitting the functions (B-3) to (B-6) to experimental data is best accomplished by plotting

$$U \equiv Q/r^2 \tag{B-7a}$$

and

$$V \equiv r^2/Q \tag{B-7b}$$

versus Q in various ways, the object being to obtain a plot in which the data points fall along a straight line to a close approximation. The slope and intercept of the line then determine two of the constants C_i. Table B-1 summarizes the cases which provide fits of the types (B-3) to (B-6). For the cases represented by the last four rows of this table, the parameter C_2 must be determined essentially by trial and error.

To minimize the labor of fitting experimental temperature distributions by this method, a computer program was written to calculate Q, U, and V and to prepare plots of the types listed in Table B-1 using the S-C 4020 automatic plotter.

The final fits obtained for the argon data are summarized in Table B-2. In some cases, the four-parameter analytic forms (B-3) to (B-6) are not sufficiently flexible to represent the data accurately over the full range. For this reason, two fits are given for each arc current (except 80 amps), one selected to fit the lower and the other the upper part of the temperature range covered by the experimental distributions.

No fits were made to the nitrogen data.

TABLE B-1

CORRESPONDENCE BETWEEN FORM OF CURVEFIT AND TYPE OF PLOT YIELDING A LINEAR CORRELATION OF THE DATA

Type of Plot	Form of Fit	Slope	Intercept (Q = 0)
U vs. Q	Form 1 with $C_4 = 1$	C_3	C_2
V vs. Q	Form 2 with $C_4 = 1$	C_3	C_2
$\log(U-C_2)$ vs. $\log Q$	Form 1	C_4	$\log C_3$
$\log(V-C_2)$ vs. $\log Q$	Form 2	C_4	$\log C_3$
$\ln(U-C_2)$ vs. Q	Form 3	C_4	$\ln C_3$
$\ln(V-C_2)$ vs. Q	Form 4	$-C_4$	$\ln C_3$

TABLE B-2

ANALYTIC CURVEFITS TO THE EXPERIMENTAL TEMPERATURE DISTRIBUTIONS IN ARGON

Arc Current (amp)	T_a (°K)	Temperature Range* (°K)	Form of fit	C_2	C_3	C_4	Max. Error in T (°K)
30	10905	9400-10905 8600- 9400	1 3	3.78 2.6	-1.667 0.389	1. 6.62	20 27
40	11546	9900-11546 9200- 9900	4 3	0.266 3.4	0.0518 0.0539	46. 12.16	9 71
50	12084	10600-12084 9600-10600	4 3	0.26 3.8	0. 0.00363	0. 21.1	18 44
60	12471	10800-12470 10000-10800	4 3	0.253 3.6	0.0797 0.0337	15.4 13.39	14 91
80	12880	10300-12880	4	0.23	0.239	10.88	16
100	13583	11500-13583 10700-11500	4 2	0.2 0.333	0.212 -0.447	7.78 1.	45 14

*The lower limit of temperatures for each arc current is set at a value lying between the third and fourth points of the Abel inversion, counting inward from the outer periphery of the arc column.

APPENDIX C

THE TWO-RUN METHOD OF ANALYZING WALL-STABILIZED ARC DATA TO OBTAIN TRANSPORT PROPERTIES

A procedure has been developed for analyzing arc data to obtain thermal conductivity and electrical conductivity, based upon the explicit solution of the "optically thin" Elenbaas-Heller equations (presented in appendix A). Since this procedure requires the use of data for two arc runs with different axial temperatures, it is briefly termed the "two-run method".

As pointed out in appendix A, the analysis presented there is based upon the energy equation in the form (A-1) which assumes that the arc column is optically thin to its own thermal radiation, while actual arc columns in argon and nitrogen have been found to be more or less opaque at least in some regions, to the substantial amounts of radiation emitted in the far ultraviolet. The two-run method was developed at a stage in the present program when the importance of vacuum ultraviolet radiation in wall-stabilized arc columns had not yet become apparent. In fact, the discrepancies established by applying the two-run method to the data for argon helped to stimulate the reexamination of assumptions which led to realization of the significance of far ultraviolet radiation. Even though the two-run method in its existing form is not accurately applicable to argon and nitrogen arc columns at atmospheric pressure, it is summarized in the present appendix to document the discrepancies found in the argon data. Also, the method might be applicable to arc columns in other gases or at lower pressures.

In this technique of data analysis, the thermal conductivity is calculated as a function of temperature using equation (A-10) of appendix A, and the electrical conductivity using equation (A-11). The derivatives of the temperature distributions for the two runs, which determine the quantities q_1, q_2, Δ^2, and $d[\ln(\rho_1 q_1/\rho_2 q_2)]/dT$, are evaluated by differentiating analytical curvefits to the temperature distributions, such as those discussed in Appendix B. The smoothing of the experimental temperature data provided by this use of analytical distribution functions also makes programming of the numerical integrations in (A-10) more convenient.

The radiative power loss per unit volume, $P_{rad}(T)$, is also represented by an analytical curvefit. In the analysis of the argon data, the function

$$\log_{10} P_{rad} = A_1 T - A_2 - \frac{1}{2}\left[A_1 (T - T_i) + \sqrt{A_1^2 (T - T_i)^2 + A_3}\right] \qquad \text{(C-1)}$$

with

$A_1 = 7.37 \times 10^{-4}$

$A_2 = 5.67$

$T_i = 13030$

$A_3 = 0.7396$

was used to approximate the measured radiative power loss in the infrared, visible, and near ultraviolet spectral regions. This equation gives P_{rad} in w/cm^3 with T in °K.

In equation (A-10a), the quantity $K(T_o)$ represents the thermal conductivity of the gas at the temperature T_o at which the two-run calculation is started. This quantity is not provided by the two-run method, but must be obtained by some other means. In the two-run calculations for argon, reported in section IIE, $K(T_o)$ was obtained from the experimental data using the measured-current energy balance method, also discussed in that section.

A number of test cases have been run to verify the correctness of the program for the two-run method, and to investigate the sensitivity of the method to errors in the input data.

1. Simplified Analytical Solution

For a fictitious gas with the properties

$$K = AT \tag{C-2a}$$

$$P_{rad} = \text{constant} \tag{C-2b}$$

$$\sigma = \text{constant} \tag{C-2c}$$

the Elenbaas-Heller equation (A-1) has the simple analytical solution

$$r^2 = \frac{2A\,T_a^2}{\sigma E^2 - P_{rad}} \left[1 - \left(\frac{T}{T_a} \right)^2 \right] \tag{C-3}$$

where T_a denotes the axial temperature. Moreover, if T_m denotes the temperature at the outer boundary of the column, the total current for this model is given by

$$I = \frac{2\pi A \sigma E (T_a^2 - T_m^2)}{\sigma E^2 - P_{rad}} \tag{C-4}$$

The program for the two-run method was applied to three cases of this simplified model. The results agreed with the assumed analytical properties (C-2a), (C-2c) exactly to within the four-figure accuracy permitted by the output format of the program.

2. Numerical Solutions of the Elenbaas-Heller Equation for Argon

The program for the two-run method has also been applied to numerical solutions of the Elenbaas-Heller equation for argon, computed using a program (1289C) already available at Avco RAD. The temperature distributions computed by 1289C for the four cases summarized in table C-1 were curvefitted using the techniques described in appendix B. These curvefits, which were accurate to within 10°K in the range from 10,000 to 12,000°K, were used in the two-run calculations. The thermal conductivities obtained by the two-run method from these data agreed with the values assumed in the 1289C calculations to within about 10 percent, as shown in figure C-1. The electrical conductivities obtained (figure C-2) showed similar accuracy through most of the temperature range considered, but scattered widely near the lowest temperature used (10,000°K).

3. Sensitivity Studies

A few other test calculations were carried out, in which the two-run method was applied to "data" from numerical solutions of the Elenbaas-Heller equation, in order to study the sensitivity of the method to errors in input data. This investigation was not sufficiently comprehensive to establish the sensitivity to all input quantities in all regimes, but did provide the following indications:

a. In regions where the temperature gradient is very large (i.e., in the peripheral region of the arc column), the two-run method is extremely sensitive to errors in the shape of the temperature distribution.

b. The method becomes more sensitive to errors as the difference in axis temperature between the two runs decreases.

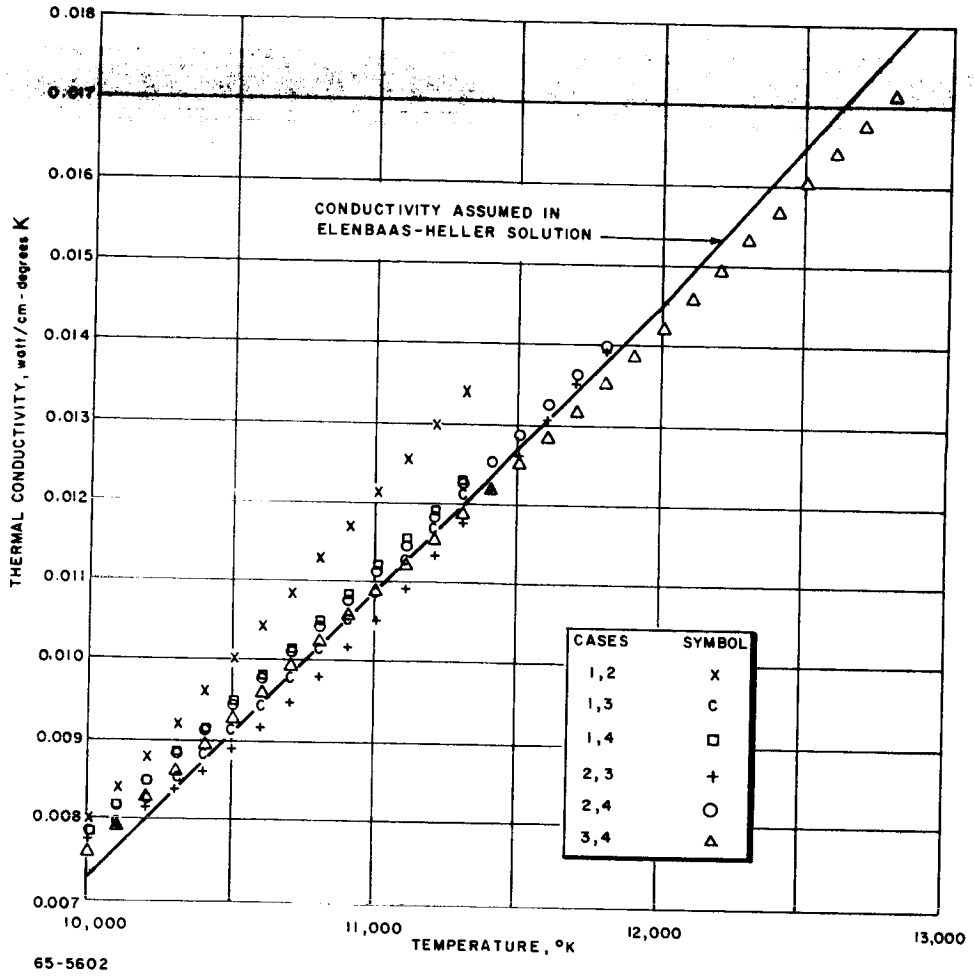

Figure C-1 THERMAL CONDUCTIVITY CALCULATED BY THE TWO-RUN METHOD FROM NUMERICAL SOLUTIONS OF THE ELENBAAS-HELLER EQUATION

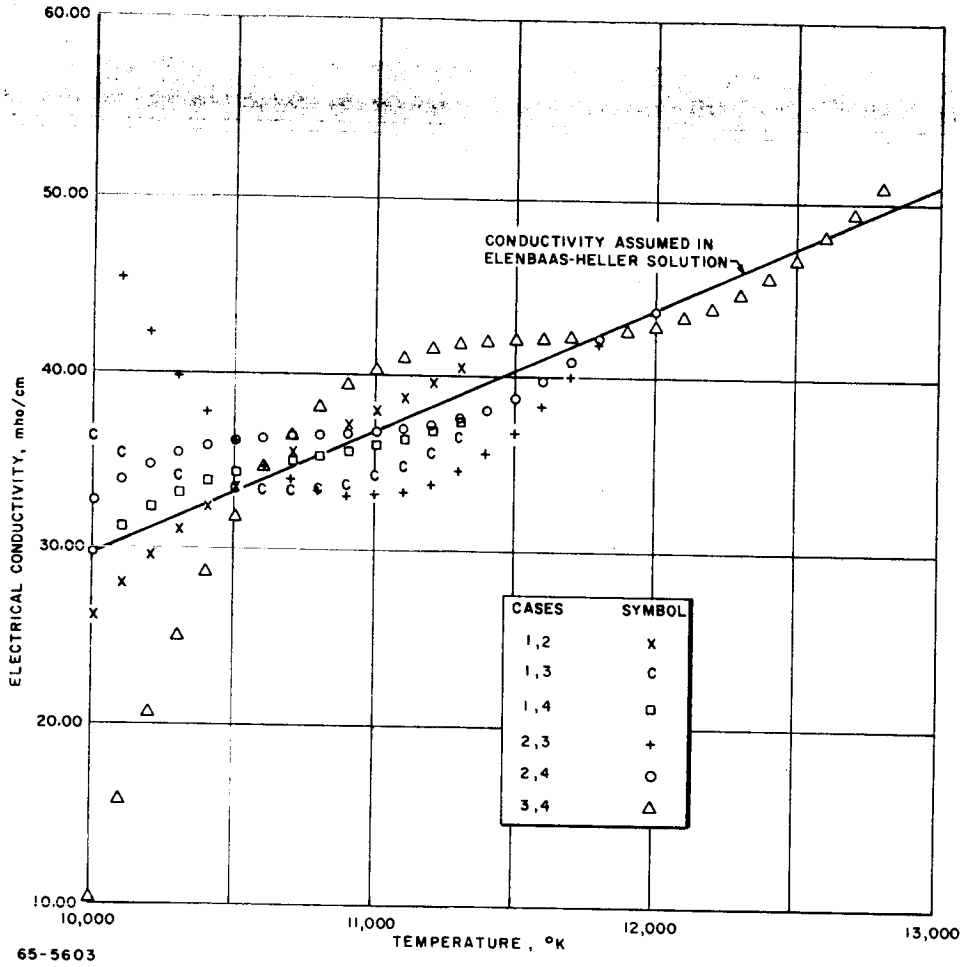

Figure C-2 ELECTRICAL CONDUCTIVITY CALCULATED BY THE TWO-RUN METHOD FROM NUMERICAL SOLUTIONS OF THE ELENBAAS-HELLER EQUATION

TABLE C-1

SUMMARY OF CASES FOR TEST OF THE TWO-RUN METHOD ON NUMERICAL SOLUTIONS OF THE ELENBAAS-HELLER EQUATION

Case No.	Axial Temperature (°K)	Current (amp)	Voltage Gradient (V/cm)	Column Radius (cm)
1	11500	32.58	10	0.2271
2	12000	41.94	10	0.2385
3	13000	83.75	10	0.2907
4	15000	44.09	25	0.1174

APPENDIX D

THE EFFECT OF PAIRED ELECTRONS ON THE SPIN DEPENDENCE OF THE POTENTIALS

In this appendix we wish to show that for a general permutation τ in which no electron is exchanged between the atom and ion, or in which only one electron is exchanged, the quantities $a_S(\tau)$ and $b_S(\tau)$ defined in eq. (36) can be factored into a permutation dependent part and a spin dependent part, as stated in the text. We first note that since the orbital part of the wavefunction $U(\vec{r})$ (eq. 32) is not affected by interchanging two paired electrons, the spin function $\alpha(i)\,\beta(j)$ for any two paired electrons in eq. (32) can be replaced by the new function

$$(i, j) \equiv \frac{1}{2}\,[\alpha(i)\,\beta(j) - \alpha(j)\,\beta(i)] \tag{D-1}$$

without changing the value of the matrix elements (35). With this transformation, one sees that the spin functions g_{M_S} in eq. (38a) can all be written in the general form

$$g_{M_S}(1, \ldots, n) = h_{M_S}(1, \ldots, m)\,(m+1, m+2) \ldots (n-1, n) \tag{D-2}$$

where n is the total number of electrons in the atom or ion, m is the number of unpaired electrons, and the function h_{M_S} is totally symmetric with respect to permutations of the m unpaired electrons in its argument. With the form (D-2) for the spin functions, it is possible to carry out the sum over spins in eq. (36) explicitly for the paired electrons by using the following identities, which are readily derived from the usual orthonormality properties of the one-electron spin functions α and β:

$$(i, j) = -(j, i)$$

$$\sum_{i,j} (i, j)(i, j) = \frac{1}{2} \tag{D-3}$$

$$\sum_{i,j} (i, j)(i, k)\,H(j, k, l_1, \ldots, l_n) = H(k, k, l_1, \ldots, l_n)$$

where the sums are over the spins of the indicated electrons, and it is assumed that each term in the factor H contains either the factor $\alpha(j)$ or $\beta(j)$. When eq. (D-3) is applied to perform the summations in eq. (36), we note that it is not necessary to place any restrictions on the form of the function H, since

from the form of the wavefunctions one sees that each term under the summation in eq. (36) consists of a product of spin functions in which each electron under consideration occurs exactly twice, and hence the assumed form of H is obtained automatically.

Equations (D-2) and (D-3) may now be applied to evaluate the spin-factor $a_S(\tau)$ for a general permutation τ in which no electron is exchanged between the atom and ion. For this case, equations (21) and (23) may be combined to yield the equation.

$$a_S(\tau) = \sum_{M_1, M_2, M_3, M_4} C(M_1, M_2; S, M_S)\, C(M_3, M_4; S, M_S)$$

$$\cdot \left[\sum_{1,\ldots,N} g_{M_1}(1,\ldots,N)\, g_{M_3}(\tau'_1,\ldots,\tau'_N) \right] \left[\sum_{1,\ldots,N-1} g^{+}_{M_2}(1,\ldots,N-1)\, g^{+}_{M_4}(\tau''_1,\ldots,\tau''_{N-1}) \right] \tag{D-4}$$

where τ' and τ'' are arbitrary permutations of the integers 1 through N and 1 through N − 1 respectively. For the spin functions g_{M_S} of eq. (D-2), we see that each of the factors in the square brackets in equation (D-4) will be of the general form

$$\sum_{1,\ldots,n} [h_{M_i}(1,\ldots,m)(m+1, m+2)\ldots(n-1, n)]$$

$$\cdot [h_{M_j}(\tau_1,\ldots,\tau_m)(\tau_{m+1}, \tau_{m+2})\ldots(\tau_{n-1}, \tau_n)] \tag{D-5}$$

where τ is some permutation of the integers 1 through n. Now, if any of the integers $\tau_{m+1}, \tau_{m+2}, \ldots, \tau_n$ is equal to any of the integers m+1 through n, then we see that eq. (D-3) may be applied to eliminate two electrons and two of the functions (i, j) (eq. D-1) from the expression (D-5), to yield a reduced expression of the form

$$A(\tau) \sum_{1,\ldots,n-2} [h_{M_i}(1,\ldots,m)(m+1, m+2)\ldots(n-3, n-2)]$$

$$\cdot [h_{M_j}(\tau'_1,\ldots,\tau'_m)(\tau'_{m+1}, \tau'_{m+2})\ldots(\tau'_{n-3}, \tau'_{n-2})] \tag{D-5'}$$

where $A(\tau)$ is a constant depending only on the permutation τ, τ' is some new permutation of the integers 1 through $n-2$, and it is important to note that each of the remaining electrons 1 through $n-2$ in (D-5') occurs once in the first bracket and once in the second. The reduced expression (D-5') is thus of the same form as the original expression (D-5), but with two fewer electrons. This process of reduction may evidently be repeated until one arrives at an expression of the form (D-5') in which there is no electron which is paired in both the first bracket and the second bracket. There are then two possibilities; either there are no paired electrons left at all, in which case, because of the assumed symmetry of the functions h_{M_S} with respect to electron permutations, equation (D-5') can be put in the form

$$A(\tau) \sum_{1,\ldots,m} h_{M_i}(1,\ldots,m)\, h_{M_j}(1,\ldots,m), \tag{D-6}$$

or else there are two electrons, say $m+1$ and $m+2$, which are paired with each other in the first bracket and unpaired in the second. In this latter case however, we note that the pairing function (D-1) is antisymmetric in the electron coordinates whereas the unpaired electrons are assumed to be symmetric, so that the expression (D-5') vanishes from symmetry considerations. Thus we see that for this case also the expression (D-5') can be written in the form (D-6) by taking the coefficient $A(\tau)$ in (D-6) equal to zero. It thus follows that for spinfunctions of the form (D-2) in which the unpaired electrons are completely symmetric, the expression (D-5) can always be reduced to the form (D-6) in which the dependence on the permutation τ is contained entirely in the first factor $A(\tau)$ and the dependence on spin entirely in the second factor. Substituting this result into eq. (D-4), we obtain the expression for $a_S(\tau)$ in the form

$$a_S(\tau) = A(\tau')\, A^+(\tau'') \sum_{M_1, M_2, M_3, M_4} C(M_1, M_2; S, M_S)\, C(M_3, M_4; S, M_S)$$

$$\cdot \left[\sum_{1,\ldots,m} h_{M_1}(1,\ldots,m)\, h_{M_3}(1,\ldots,m) \right] \left[\sum_{1,\ldots,m^+} h^+_{M_2}(1,\ldots,m^+)\, h^+_{M_4}(1,\ldots,m^+) \right] \tag{D-7}$$

in which the first factor $A(\tau')\, A^+(\tau'')$ contains the entire dependence on the permutation τ and the second factor contains the entire spin dependence. Eq. (D-7) thus demonstrates the desired factorization of the function $a_s(\tau)$ into permutation and spin dependent parts, and in addition provides an explicit formula for the spin dependence of the potentials in terms of the spin functions h_{M_S} and the Clebsch-Gordan coefficients. One readily verifies from eqs. (34) and (38) that this formula is equivalent to the formula (39) given in the text, as it should be.

We now turn to the case in which a single electron is transferred from the atom to the ion, and attempt to evaluate the function $b_S(\tau)$. For this case, eqs. (34) and (36) give the expression for $b_S(\tau)$ in the form

$$b_S(\tau) = \sum_{M_1, M_2, M_3, M_4} C(M_1, M_2; S, M_S)\, C(M_3, M_4; S, M_S)$$

$$\cdot \sum_N \left[\sum_{1,\ldots,N-1} g^+_{M_4}(1,\ldots,N-1)\, g_{M_1}(\tau_1',\ldots,\tau_N') \right] \left[\sum_{1,\ldots,N-1} g^+_{M_2}(1,\ldots,N-1)\, g_{M_3}(\tau_1'',\ldots,\tau_N'') \right] \tag{D-8}$$

where τ' and τ'' again represent two arbitrary permutations of the integers 1 through N. The spin functions (D-2) may now be substituted into eq. (D-8) and the resulting expresssions reduced by the same methods as in the case of the expression (D-5) above. One finds that there are different cases according to the relative number of unpaired electrons in the atom and ion. Since the atom contains one more electron than the ion and the number of paired electrons must always be even, the difference $m - m^+$ between the number of unpaired electrons in the atom and ion must be odd. Applying the methods which were used previously in the reduction of expression (D-5), one finds readily that for the various possible values, $m - m^+$, the quantity

$$\chi_\tau(N) \equiv \sum_{1,\ldots,N-1} g^+_{M_i}(1,\ldots,N-1)\, g_{M_j}(\tau_1,\ldots,\tau_N) \tag{D-9}$$

which occurs in eq. (D-8) must reduce to the following forms:

$$\chi_\tau(N) = 0 \qquad \text{for} \qquad |m - m^+| \geq 3$$

$$\chi_\tau(N) = A(\tau) \sum_{1,\ldots,m^+} h^+_{M_i}(1,\ldots,m^+)\, h_{M_j}(1,\ldots,m^+, N) \qquad \text{for} \quad m - m^+ = 1 \tag{D-10}$$

$$\chi_\tau(N) = A(\tau) \sum_{1,\ldots,m^+} h^+_{M_i}(1,\ldots,m^+)\, h_{M_j}(1,\ldots,m)\,(m^+, N) \qquad \text{for} \quad m - m^+ = -1$$

Substituting eq. (D-10) into (D-8) and using eq. (D-3) to perform the sum over the remaining electron pair in the case $m - m^+ = -1$, we obtain the expressions for $b_S(\tau)$ in the form

$$b_S(\tau) = 0 \qquad \text{for } |m - m^+| \geq 3$$

$$b_S(\tau) = A(\tau')\,A(\tau'') \sum_{M_1, M_2, M_3, M_4} C(M_1, M_2; S, M_S)\, C(M_3, M_4; S, M_S)$$

$$\cdot \sum_N \left[\sum_{1, \ldots, m^+} h^+_{M_4}(1, \ldots, m^+)\, h_{M_1}(1, \ldots, m^+, N) \right]$$

$$\cdot \left[\sum_{1, \ldots m^+} h^+_{M_2}(1, \ldots, m^+)\, h_{M_3}(1, \ldots, m^+, N) \right] \qquad \text{for } m - m^+ = 1$$

$$b_S(\tau) = \frac{1}{4} A(\tau')A(\tau'') \sum_{M_1, M_2, M_3, M_4} C(M_1, M_2; S, M_S)\, C(M_3, M_4; S, M_s) \tag{D-11}$$

$$\cdot \sum_N \left[\sum_{1, \ldots, m} h^+_{M_4}(1, \ldots, m, N)\, h_{M_1}(1, \ldots, m) \right] \left[\sum_{1, \ldots, m} h^+_{M_2}(1, \ldots, m, N)\, h_{M_3}(1, \ldots, m) \right] \text{for } m - m^+ = -1$$

The desired factorization of $b_S(\tau)$ is thus obtained in all cases, as we wished to show. Again, the expression for the spin dependence given by eq. (D-11) is readily shown to be equivalent to that given by eq. (39) of the text.

APPENDIX E

EXPLICIT FORMULAS FOR THE TWO-CENTER OVERLAP, KINETIC ENERGY, AND HYBRID INTEGRALS FOR N-N$^+$ AND O-O$^+$

This appendix presents explicit formulas for the two-center overlap integrals $S(\alpha, \beta)$, the two-center kinetic energy intergrals $T(\alpha, \alpha)$, and the hybrid integrals L for the N–N$^+$ and O–O$^+$ systems. These formulas were calculated from the general expression for these integrals given in section III. F of the main text, using the wavefunction parameters for nitrogen and oxygen given in tables I and IV. Specifically, the overlap integrals $S(\alpha,\beta)$ were calculated from eqs. (91) and (94) of the text, the kinetic energy integrals $T(\alpha, \alpha)$ from eqs. (96) and (97), the hybrid integrals L and $E^{(L)}$ for the Π-states from eqs. (105), (107), (108), and (111), and finally the hybrid integrals $E^{(L)}$ for the Σ-states were calculated from eq. (110) and the previously calculated values of $E^{(L)}$ for the Π-states.

For N–N$^+$ the resulting formulas for the integrals in atomic units were:

$$S(s, s) = (0.0851093\, R^4 + 0.267018\, R^3 + 0.670184\, R^2 + 27.3827\, R + - 125.167 + 228.678\, R^{-1})\, e^{-1.5937\, R}$$

$$\frac{1}{\sqrt{3}} S(s, 2\sigma) = (42.1232\, R - 539.138 + 2330.64\, R^{-1} + 1952.45\, R^{-2})\, e^{-1.1937\, R}$$

$$- (4244.351\, R + 221032.9 + 3830864\, R^{-1} + 2237131\, R^{-2})\, e^{-1.7124\, R}$$

$$+ (4389.286\, R - 218677.3 + 3562457 R^{-1} + 2235337\, R^{-2})\, e^{-1.5937 R}$$

$$S(2\pi, 2\pi) = (0.0100219\, R^3 + 0.0503739\, R^2 + 0.105499\, R + 28.4690 + - 262.928\, R^{-1} + 828.636\, R^{-2} + 694.174\, R^{-3})\, e^{-1.1937\, R} +$$

$$+ (0.0783714\, R^3 + 0.274602\, R^2 + 0.400903\, R - 12.0709 + - 284.209\, R^{-1} - 1161.60\, R^{-2} - 678.347\, R^{-3})\, e^{-1.7124\, R}$$

$$S(2\sigma, 2\sigma) = - \frac{d}{dR} [R\, S(2\pi, 2\pi)]$$

$$= (0.0119631\, R^4 + 0.0200438\, R^3 - 0.0251870\, R^2 + 33.7724\, R +$$

$$- 342.326 + 989.143\, R^{-1} + 11657.27\, R^{-2} + 1388.35\, R^{-3})\, e^{-1.1937\, R}$$

$$+ (0.134203\, R^4 + 0.156743\, R^3 - 0.137301\, R^2 - 21.4720\, R - 474.609 +$$

$$- 1989.12\, R^{-1} - 2323.20\, R^{-2} - 1356.69\, R^{-3})\, e^{-1.7124\, R}$$

$$T(2\pi, 2\pi) = (-0.00714020\, R^3 + 0.0239263\, R^2 + 0.0751638\, R - 20.1571 +$$

$$+ 255.082\, R^{-1} - 904.227\, R^{-2} - 757.500\, R^{-3})\, e^{-1.1937\, R}$$

$$+ (-0.114905\, R^3 + 0.268406\, R^2 + 0.587787\, R + 18.3843 +$$

$$+ 374.553\, R^{-1} + 1216.408\, R^{-2} + 710.353\, R^{-3})\, e^{-1.7124\, R}$$

$$T(2\sigma, 2\sigma) = - \frac{d}{dR}[RT(2\pi, 2\pi)]$$

$$= (-0.00852326\, R^4 + 0.0571216\, R^3 + 0.0179447\, R^2 - 24.2119\, R +$$

$$+ 324.648 - 1079.38\, R^{-1} - 1808.45\, R^{-2} - 1515.00\, R^{-3}) \times e^{-1.1937\, R} +$$

$$+ (-0.196763\, R^4 + 0.919240\, R^3 + 0.201304\, R^2 + 30.3057\, R +$$

$$+ 623.000 + 2082.98\, R^{-1} + 2432.42\, R^{-2} + 1420.71\, R^{-3}) \times e^{-1.7124\, R}$$

$$L_1 = (-0.050110\, R^2 - 0.125936\, R - 6.72215 + 10.6530\, R^{-1} +$$

$$+ 40.0715\, R^{-2} + 35.5692\, R^{-3})\, e^{-1.1937 R} +$$

$$- (0.391859\, R^2 + 0.686510\, R + 9.96301 + 34.8898\, R^{-1} +$$

$$+ 51.8177\, R^{-2} + 30.2603\, R^{-3})\, e^{-1.7124\, R}$$

for Π – states

$$\tilde{L}_2^{(s)} = (-1.66934 + 6.91528\, R^{-1} - 14.7032\, R^{-2} - 12.3173\, R^{-3})\, e^{-1.1937\, R}$$

$$+ (18.7899 + 374.3309\, R^{-1} + 3114.823\, R^{-2} + 1818.981\, R^{-3})\, e^{-1.7124\, R}$$

$$+ [-7.59189\, R^{-1} - 2875.303\, R^{-2} - 1783.395\, R^{-3}$$

$$+ 2.85277\, K_\pi(1.5937, R)]\, e^{-1.5937\, R}$$

for Π – states

$\tilde{L}_2^{(p)}$ $[-0.08038 + 8.2110\,R^{-1} + 15.0997\,R^{-2} - 3.6371\,R^{-3}$

$-1.67527\,K_\pi(1.1937, R)]\,e^{-1.1937\,R}$

$+ [10.0396 + 21.7380\,R^{-1} + 13.6039\,R^{-2} - 57.3906\,R^{-3}$

$- 9.64074\,K_\pi(1.7124, R)]\,e^{-1.7124\,R}$ for Π – states

$L_3^{(s)}$ $= [-0.530302 + 0.308247\,R^{-1} - 0.066899\,R^{-2} - 0.056043\,R^{-3}]\,e^{-1.1937\,R}$

$+ [-2.58473 + 2.36511\,R^{-1} - 0.811604\,R^{-2} - 0.473957\,R^{-3}]\,e^{-1.7124\,R}$

for Π – states

$\tilde{L}_3^{(s)}$ $= [0.291307 - 0.233250\,R^{-1} - 0.032966\,R^{-2} - 0.027616\,R^{-3}]\,e^{-1.1937\,R}$

$+ [1.48587 - 1.50057\,R^{-1} + 0.531236\,R^{-2} + 0.310229\,R^{-3}]\,e^{-1.7124\,R}$

for Π – states

$L_3^{(p)}$ $= [0.747603 - 0.168883\,R^{-1} + 0.022669\,R^{-2} + 0.018990\,R^{-3}]\,e^{-1.1937\,R}$

$+ [3.23298 - 1.16355\,R^{-1} + 0.252947\,R^{-2} + 0.147715\,R^{-3}]\,e^{-1.7124\,R}$

for Π – states

$E^{(L)}$ $= [-0.050110\,R^2 - 0.125936\,R - 7.96326 + 25.6853\,R^{-1} +$

$+ 40.3908\,R^{-2} + 17.5501\,R^{-3} - 1.67527\,K_\pi(1.1937, R)]\,e^{-1.1937\,R}$

$+ [-0.391859\,R^2 - 0.686510\,R + 21.0006 + 360.0880\,R^{-1}$

$+ 3096.581\,R^{-2} + 1731.265\,R^{-3} - 9.6407\,K_\pi(1.7124, R)]\,e^{-1.7124\,R}$

$+ [-7.59189\,R^{-1} - 2875.303\,R^{-2} - 1783.395\,R^{-3} + 2.85277\,K_\pi(1.5937, R)]\,e^{-1.5937\,R}$

for Π – states

$E^{(L)}$ $= [-0.059816\,R^3 - 9.33351\,R + 38.6238 + 48.214\,R^{-1}$

$+ 61.340\,R^{-2} + 35.099\,R^{-3} - 1.67527\,K_\sigma(1.1937, R)]\,e^{-1.1937\,R}$

$+ [0.671019\,R^3 + 37.3345\,R + 596.970 + 5268.34\,R^{-1} +$

$$+ 6041.202\, R^{-2} + 3462.531\, R^{-3} - 9.64074\, K_\sigma (1.7124, R)]\, e^{-1.7124\, R}$$

$$- [12.0992 + 4582.370\, R^{-1} + 5717.5000\, R^{-2} +$$

$$+ 3566.790\, R^{-3} - 2.85277\, K_\sigma (1.5937, R)]\, e^{-1.5937 R}$$

for Σ – states,

where the functions K_π and K_σ are defined by equation (114).

The corresponding formulas for $0\text{–}0^+$ were:

$$S(s, s) = [0.134951\, R^4 + 0.359064\, R^3 + 0.764290\, R^2 + 22.7643\, R$$

$$- 84.4620 + 126.532\, R^{-1}]\, e^{-1.8792\, R}$$

$$\frac{1}{\sqrt{3}} S(s, 2\sigma) = [5.27234\, R - 32.5516 + 68.5735\, R^{-1} + 59.4431\, R^{-2}]\, e^{-1.1536\, R}$$

$$+ [21698.33\, R - 1539709.4 + 36305670\, R^{-1} + 20214738\, R^{-2}]\, e^{-1.7960\, R}$$

$$+ [- 21180.46\, R - 1550985.5 - 37987572\, R^{-1} - 20214757\, R^{-2}]\, e^{-1.8792\, R}$$

$$S(2\pi, 2\pi) = [0.00274369\, R^3 + 0.0142702\, R^2 + 0.0309254\, R + 10.20009$$

$$- 72.3595\, R^{-1} + 175.354\, R^{-2} + 152.006\, R^{-3}]\, e^{-1.1536\, R}$$

$$+ [0.128133\, R^3 + 0.428062\, R^2 + 0.595854\, R + 0.340741 - 87.7763\, R^{-1}$$

$$- 259.463\, R^{-2} - 144.467\, R^{-3}]\, e^{-1.7960\, R}$$

$$S(2\sigma, 2\sigma) = [0.00316512\, R^4 + 0.00548738\, R^3 - 0.0071351\, R^2 + 11.7050\, R - 93.6740$$

$$+ 202.288\, R^{-1} + 350.708\, R^{-2} + 304.012\, R^{-3}]\, e^{-1.1536\, R}$$

$$+ [0.230127\, R^4 + 0.256266\, R^3 - 0.214031\, R^2 - 0.579738\, R - 157.987$$

$$- 465.995\, R^{-1} - 518.925\, R^{-2} - 288.934\, R^{-3}]\, e^{-1.7960\, R}$$

$$T(2\pi, 2\pi) = [-0.00182564\,R^3 + 0.00633022\,R^2 + 0.0205777\,R - 6.75143$$
$$+ 71.6196\,R^{-1} - 200.154\,R^{-2} - 173.504\,R^{-3}]\,e^{-1.1536\,R}$$
$$+ [-0.206654\,R^3 + 0.460254\,R^2 + 0.960999\,R + 0.520605 + 141.599\,R^{-1}$$
$$+ 260.817\,R^{-2} + 145.221\,R^{-3}]\,e^{-1.7960\,R}$$

$$T(2\sigma, 2\sigma) = [-0.00210606\,R^4 + 0.0146051\,R^3 + 0.00474767\,R^2 - 7.82960\,R + 89.3718$$
$$- 230.897\,R^{-1} - 400.308\,R^{-2} - 347.007\,R^{-3}]\,e^{-1.1536\,R}$$
$$+ [-0.371151\,R^4 + 1.65323\,R^3 + 0.345191\,R^2 - 0.955755\,R + 253.790$$
$$+ 468.428\,R^{-1} + 521.634\,R^{-2} + 290.442\,R^{-3}]\,e^{-1.7960\,R}$$

$$L_1 = [-0.0137184\,R^2 - 0.0356755\,R - 2.87940 + 2.69394\,R^{-1}$$
$$+ 13.0071\,R^{-2} + 11.2752\,R^{-3}]\,e^{-1.1536\,R}$$
$$+ [-0.640666\,R^2 - 1.070155\,R - 7.16992 - 13.0924\,R^{-1} - 16.2419\,R^{-2}$$
$$- 9.04335\,R^{-3}]\,e^{-1.7960\,R}$$

for Π – states

$$\tilde{L}_2^{(s)} = [-0.48635 + 1.00299\,R^{-1} - 1.03559\,R^{-2} - 0.89770\,R^{-3}]\,e^{-1.1536\,R}$$
$$+ [-37.1786 + 888.4960\,R^{-1} - 10563.174\,R^{-2} - 5881.500\,R^{-3}]\,e^{-1.7960\,R}$$
$$+ [24.59807\,R^{-1} + 11067.987\,R^{-2} + 5908.653\,R^{-3} + 3.900762\,K_\pi(1.8792, R)]\,e^{-1.8792\,R}$$

for Π – states

$$\tilde{L}_2^{(p)} = 0$$

$$L_3^{(s)} = [-0.204512 + 0.083756\,R^{-1} - 0.012999\,R^{-2} - 0.011268\,R^{-3}]\,e^{-1.1536\,R}$$
$$+ [-2.59444 + 1.81212\,R^{-1} - 0.48113\,R^{-2} - 0.26789\,R^{-3}]\,e^{-1.7960\,R}$$

for Π – states

$$\tilde{L}_3^{(s)} = [0.11711 - 0.055855\,R^{-1} + 0.008662\,R^{-2} + 0.007509\,R^{-3}]\,e^{-1.1536\,R}$$

$$+ [1.52536 - 1.21066\,R^{-1} + 0.32395\,R^{-2} + 0.18037\,R^{-3}]\,e^{-1.7960\,R}$$

for Π – states

$$L_3^{(p)} = [-0.342771 + 0.175055\,R^{-1} - 0.023805\,R^{-2} - 0.020636\,R^{-3}]\,e^{-1.1536\,R}$$

$$+ [-4.56353 + 4.15762\,R^{-1} - 1.02108\,R^{-2} - 0.56853\,R^{-3}]\,e^{-1.7960\,R}$$

for Π – states

$$E^{(L)} = [-0.0137184\,R^2 - 0.0356755\,R - 3.79593 + 3.89989\,R^{-1} + 11.9434\,R^{-2}$$

$$+ 10.3531\,R^{-3}]\,e^{-1.1536\,R}$$

$$+ [-0.640666\,R^2 - 1.070155\,R - 49.98108 + 880.1627\,R^{-1}$$

$$- 10580.594\,R^{-2} - 5891.199\,R^{-3}]\,e^{-1.7960\,R}$$

$$+ [24.59807\,R^{-1} + 11067.987\,R^{-2} + 5908.653\,R^{-3} + 3.900762\,K_\pi(1.8792, R)]\,e^{-1.8792\,R}$$

for Π – states

$$E^{(L)} = [-0.0158255\,R^3 - 4.30763\,R + 8.29484 + 13.7779\,R^{-1} + 23.8867\,R^{-2} + 20.7062\,R^{-3}]\,e^{-1.1536\,R}$$

$$+ [-1.15064\,R^3 - 88.6253\,R + 1639.5549 - 19002.747\,R^{-1} - 21161.188\,R^{-2}$$

$$- 11782.398\,R^{-3}]\,e^{-1.7960\,R}$$

$$+ [39.30943 + 20798.961\,R^{-1} + 22135.974\,R^{-2} + 11817.306\,R^{-3}$$

$$+ 3.900762\,K_\sigma(1.8792, R)]\,e^{-1.8792\,R}$$

for Σ – states

APPENDIX F

A RELATION AMONG THE FUNCTIONS $C^{\gamma\delta\epsilon}_{\alpha\beta}$

In this appendix we wish to derive a useful relationship between the functions $C^{\gamma\delta\epsilon}_{\alpha\beta}$ defined in eq. (102) and their derivatives. Differentiating eq. (102) with respect to R, we find that:

$$\frac{2}{\partial R}\left[R\, C^{\gamma\delta\epsilon}_{\alpha\beta}\,(\zeta_a R, \zeta_b R)\right] = (\alpha + \beta + \gamma + \delta + 2\epsilon + 2)\, C^{\gamma\delta\epsilon}_{\alpha\beta}\,(\rho_a, \rho_b)$$

$$- (\rho_b/2)^{\alpha+\beta+\gamma+\delta+2\epsilon+1} \int_1^\infty d\xi \int_{-1}^{1} d\eta \left[-\frac{1}{2}(\rho_a+\rho_b)\,\xi - \frac{1}{2}(\rho_a-\rho_b)\,\eta\right]$$

$$\times\, e^{-\frac{1}{2}(\rho_a+\rho_b)\xi - \frac{1}{2}(\rho_a-\rho_b)\eta} (\xi+\eta)^{\alpha}(\xi-\eta)^{\beta}(1+\xi\eta)^{\gamma}(1-\xi\eta)^{\delta}(\xi^2-1)^{\epsilon}(1-\eta^2)^{\epsilon} \qquad \text{(F-1)}$$

where we have introduced the notation

$$\rho_a = \zeta_a R$$

$$\rho_b = \zeta_b R \qquad \text{(F-2)}$$

on the right-hand-side of eq. (F-1). The factor in the square brackets in eq. (F-1) may now be eliminated by dividing it into two terms and integrating each term separately by parts using the factors $dv \equiv \exp\left[-\frac{1}{2}(\rho_a+\rho_b)\xi\right] d\xi$ and $dv \equiv \exp\left[-\frac{1}{2}(\rho_a-\rho_b)\,\eta\right] d\eta$ respectively in the parts integrations. Substituting for $C^{\gamma\delta\epsilon}_{\alpha\beta}$ from eq. (102) and integrating by parts as indicated above, eq. (F-1) becomes:

$$\frac{\partial}{\partial R}\left[R\, C^{\gamma\delta\epsilon}_{\alpha\beta}\,(\xi_a R, \zeta_b R)\right] = (\rho_b/2)^{\alpha+\beta+\gamma+\delta+2\epsilon+1} \int_1^\infty d\xi \int_{-1}^{1} d\eta$$

$$\times\, e^{-\frac{1}{2}(\rho_a+\rho_b)\xi - \frac{1}{2}(\rho_a-\rho_b)\eta} (\xi+\eta)^{\alpha}(\xi-\eta)^{\beta}(1+\xi\eta)^{\gamma}(1-\xi\eta)^{\delta}(\xi^2-1)^{\epsilon}(1-\eta^2)^{\epsilon}$$

$$\times \left\{[\alpha + \beta + \gamma + \delta + 2\epsilon + 2] - \left[1 + \frac{\alpha\xi}{\xi+\eta} + \frac{\beta\xi}{\xi-\eta} + \frac{\gamma\xi\eta}{1+\xi\eta} - \frac{\delta\xi\eta}{1-\xi\eta} + \frac{2\epsilon\xi^2}{\xi^2-1}\right]\right.$$

$$- \left[1 + \frac{\alpha\eta}{\xi+\eta} - \frac{\beta\eta}{\xi-\eta} + \frac{\gamma\xi\eta}{1+\xi\eta} - \frac{\delta\xi\eta}{1-\xi\eta} - \frac{2\epsilon\eta^2}{1-\eta^2} \right] \Bigg\}$$

$$= (\rho_b/2)^{\alpha+\beta+\gamma+\delta+2\epsilon+1} \int_1^\infty d\xi \int_{-1}^{1} d\eta$$

$$\times e^{-\frac{1}{2}(\rho_a-\rho_b)\xi - \frac{1}{2}(\rho_a-\rho_b)\eta} (\xi+\eta)^\alpha (\xi-\eta)^\beta (1+\xi\eta)^\gamma (1-\xi\eta)^\delta (\xi^2-1)^\epsilon (1-\eta^2)^\epsilon$$

$$\times \left\{ \gamma \left(\frac{1-\xi\eta}{1+\xi\eta} \right) + \delta \left(\frac{1+\xi\eta}{1-\xi\eta} \right) - 2\epsilon \frac{(1-\xi\eta)(1+\xi\eta)}{(\xi^2-1)(1-\eta^2)} \right\} \qquad \epsilon \geq 1$$

The right-hand side of this equation may now be expressed in terms of C-functions by the use of equation (102) to yield the general relationship:

$$\frac{\partial}{\partial R} \left[R\, C_{\alpha\beta}^{\gamma\delta\epsilon} (\zeta_a R, \zeta_b R) \right] = \gamma\, C_{\alpha\beta}^{\gamma-1,\delta+1,\epsilon} (\rho_a, \rho_b) + \delta\, C_{\alpha\beta}^{\gamma+1,\delta-1,\epsilon} (\rho_a, \rho_b)$$

$$- 2\epsilon\, C_{\alpha\beta}^{\gamma+1,\delta+1,\epsilon-1} (\rho_a, \rho_b) \qquad \text{for } \epsilon \geq 1 \qquad \text{(F-3)}$$

The desired identity (109) can now be obtained by setting $\gamma = \delta = 0$ and $\epsilon = 1$ in eq. (F-3).